Author/s:
van As, Dean Joseph

Title:
The Synthesis and α-Functionalisation of Amines via Visible Light Mediated Catalysis

Date:
2020

Persistent Link:
https://hdl.handle.net/11343/265877

The Synthesis and α-Functionalisation of Amines via Visible Light Mediated Catalysis

Dean van As

Orchid ID : 0000-0002-9224-8382

Submitted in total fulfilment of the requirements of the Degree of Doctor of Philosophy

October 2020

School of Chemistry
The University of Melbourne

Declaration

I certify that the thesis comprises of the original work that I conducted throughout this PhD and acknowledgment has been made in the text to any other material used or any work conducted in collaboration with others. The thesis is less than 100,000 words in length.

Dean van As *October 2020*

Abstract

The ubiquity of amines in pharmaceutical, agrochemical and advanced materials has incentivised modern synthetic chemists to develop novel and innovative methods for their synthesis and functionalisation. Specifically, the direct α-C-H functionalisation of aliphatic amines represents one such transformation which demands further development and improvement of current methodology. Visible-light mediated catalysis has presented a powerful platform to facilitate this transformation, with several pathways established to achieve the α-functionalisation of amines.

This thesis is an exploration of the visible-light mediated functionalisation of aliphatic amines. Specifically, it explores the formal α-functionalisation of amines via the generation of α-amino radicals as key intermediates and investigates subsequent pathways of reactivity. The methodologies developed have been applied to the synthesis of biologically relevant amine scaffolds. Upon optimisation, continuous flow protocols were established to enhance the photochemical reaction conditions.

Chapter 1 summarises the protocols for the α-functionalisation of amines. A brief history of this transformation is explored, highlighting several methodologies and is accompanied by a critical evaluation of their benefits and limitations. The concept and principles of photoredox catalysis are introduced and notable examples examined within the context of photocatalytic protocols for amine α-functionalisation. Finally, flow chemistry is presented detailing its advantages with emphasis towards photoredox catalysis.

Chapter 2 establishes a visible-light mediated transfer hydrogenation of diarylmethimines. This process makes use of the single electron reduction of imines to engender α-amino radicals with triethylamine functioning as both a sacrificial reductant

and hydrogen source. The developed conditions enabled the synthesis of a series of diarylmethamines to be synthesised with excellent chemoselectivity. A plausible mechanism was established, highlighting the dual role of triethylamine. Flow engineering enabled this procedure to be efficiently scaled to synthetically useful quantities with retention of the chemoselectivity established in batch.

Chapter 3 details the development of the decarboxylative α-alkylation of fused heterocyclic amines. This process engages fused heterocyclic amines and *N*-hydroxy phthalimide esters as radical surrogates to simultaneously establish both α-amino and alkyl radicals. Upon *in situ* generation of α-amino and alkyl radicals, radical-radical coupling produces the desired α-alkylated amine. The addition of co-reductant, diphenylamine is believed to facilitate a second mechanistic pathway that proceeds concurrently and improves the efficiency of this transformation. A flow protocol established more favourable reaction conditions, enabling conjugation of a variety of biologically active derivatives in typically good yields.

Chapter 4 introduces the concept of the tandem photocatalytic cycle revealing that *in situ* generation of a highly reducing iridium species establishes an effective pathway for single electron reduction of energy demanding substrates. This chapter further extends the knowledge of the tandem photoredox cycle, applying this mechanism towards the radical-radical coupling of α-amino and alkyl radicals. Accessing a highly reducing species enabled the single electron reduction of energy demanding alkyl halides; substrates previously difficult to access. This chapter further investigates the tandem photocatalytic cycle and establishes an alternative protocol for α-amino sp^3 C-C bond formation.

Acknowledgements

First and foremost, I would like to thank Dr. Anastasios “Tash” Polyzos, he has been an amazing supervisor throughout out my PhD and is a mentor I strive to emulate. Over the course of my PhD, Tash has always been there for guidance, encouragement, and support. Whether it be a suggestion of how to undertake an issue in the lab, helping improve my writing skills, or motivating me when I am down; Tash has always been there for me. I have found this PhD to be incredibly challenging and I could not have gotten through this without him, he has been an outstanding supervisor; I will fondly remember the group lunches and the late night whisky sessions, they have been some of the greatest memories (or absence of) throughout this period.

I would next like to mention, Tash’s “lieutenants”, the post-doctoral researchers present throughout this period, these include Dr. Milena Czyz, Dr. Martin Brzozowski, Dr. Geethi Weragoda and Dr. Tim Connell. These individuals have been able to guide our ever-growing research group split over The University of Melbourne and CSIRO when Tash has been otherwise disposed with his many commitments. These individuals have been an incredible source of guidance, support, knowledge and have helped me to overcome any challenges.

I would also like to extend this thank you towards the guidance of my advisory panel: co-supervisor Dr. Wallace Wong, Prof. Mark Rizzacasa and Dr. Georgina Such. I would also like to further broaden this towards all the technical staff who have taken the time to help and train me. They have been there beyond formal meetings and training, but they have welcomed me to chat and discuss whenever needed.

They say a group is only as good as its students (well I do), and I will say the Polyzos research group has been world class, from discussing new ideas to music choice and all

the jokes in between. I would like to specifically thank soon to be Dr. Nenad Micic who I shared an office with throughout this time, as well as the other PhD students: Tyra Horngren, Xiaocong 'Nero' Guan and José Forni. I would further like to thank Rowan Pilkington, Mitch Taylor, Nikolai Rossouw, Edward Phung, Addina Hakim, Mohammed Alhajji, Theerada Seehamongkol and industry affiliate Dr. Christian Gunawam. If it weren't for this team as well as the many visiting students this PhD would not have been achieved or been anywhere near as memorable, I have cherished all the support they have given me and still do, I have come to think of them as a second family.

I come to thanking my actual family now, for all the support they have given me over this period, they have helped support and encourage me, and I hope that I have made them proud. This includes my mum and dad: Debbie and Brett, as well as my brother, Trevor and his wife Luci, and all extended family, particularly, Dr. Valerie Sands and Prof. Bob Stewart, all of whom have given me so much encouragement. Without my family none of this would be possible.

I would like to extend the thank you towards my other groups of friends, such as: those also in the chemistry department who have also undertaken research studies, the 'Brotherhood of the Travelling Pants', the 'K-9s' group and all the friends I have made at Mettler Toledo in my period working there and my roommate Ana-Maria. I would like to thank Dr. Alice Ying who has given me a tremendous amount of support and motivation. I would like to thank any friends I have missed and especially my dog Lumi, he has been the most supportive (and fluffy) friend I can have. My friends have always been there when the stress of this PhD and everything surrounding has overtaken me and have been invaluable.

Finally, and most importantly I would like to thank the University of Melbourne, and the School of Chemistry for supporting me and providing me the opportunity and funding to conduct the research that I will present to you.

Table of Contents

Abbreviations

A	Acceptor molecule
Ar	Aryl
BHT	Butylated hydroxytoluene
BNAH	1-Benzyl-1,4-dihydronicotinamide
Boc	*tert*-Butyloxycarbonyl
BuLi	Butyl lithium
CAN	Cerium ammonium nitrate
CDC	Cross dehydrogenative coupling
CFL	Compact fluorescent lamp
CV	Cyclic voltammetry
4CZIPN	2,4,5,6-tetra(carbazol-9-yl)benzene-1,3-dicarbonitrile
D	Donor molecule
DIPEA	*N*,*N*-Diisopropylethylamine
DABCO	1,4-diazabicyclo[2.2. 2]octane
DCE	Dichloroethane
DCM	Dichloromethane
DMA	Dimethylacetamide
DMF	Dimethylformamide
DMSO	Dimethylsulfoxide

DPE	Diphenylethene
dtbbpy	4,4′-di-tert-butyl-2,2′-dipyridyl
E	Electrophile
EB	Erythrosine B
Equiv.	Equivalents
Et	Ethyl
EtOAc	Ethyl acetate
EWG	Electron withdrawing group
FTIR	Fourier-transform infrared spectroscopy
h	Hour(s)
HFIP	Hexafluoroisopropanol
$HNPh_2$	Diphenylamine
HOMO	Highest occupied molecular orbital
HRMS	High Resolution Mass Spectroscopy
*i*Pr	Isopropyl group
*i*PrOH	Isopropanol
ISC	Intersystem crossing
$[Ir(ppy)_3]$	Tris[2-phenylpyridinato-C2,N]iridium(III)

$[Ir(ppy)_2(dtbbpy)]PF_6$	[4,4′-Bis(1,1-dimethylethyl)-2,2′-bipyridine-N1,N1′]bis[2-(2-pyridinyl-N)phenyl-C]iridium(III) hexafluorophosphate
$[Ir((dF)ppy)_2(dtbbpy)]PF_6$	[4,4′-*Bis*(1,1-dimethylethyl)-2,2′-bipyridine-*N*1,*N*1′]*bis*[3,difluoro-2-[5-(trifluoromethyl)-2-pyridinyl-*N*]phenyl-C]Iridium(III) hexafluorophosphate
KOAc	Potassium acetate
$KOAcF_3$	Potassium trifluoroacetate
K_q	Quenching rate constant
$La(OTf)_3$	Lanthanum(III) trifluoromethanesulfonate
LED	Light emitting diode
LiOAc	Lithium acetate
LUMO	Lowest unoccupied molecular orbital
Me	Methyl
MeCN	Acetonitrile
MLTC	Metal-ligand charge transfer
Mol	mole(s)
Min	Minute(s)
MS	Mass Spectroscopy
NADH	Nicotinamide adenine dinucleotide + hydrogen
NaOAc	Sodium acetate

NBS	*N*-Bromosuccinimide
NHC	*N*-Heterocyclic carbene
NHP ester	*N*-Hydroxyphthalimide ester
NMP	*N*-Methyl-2-pyrrolidone
NMR	Nuclear magnetic resonance spectroscopy
Nu	Nucleophile
OMe	Methoxy
OPh	Phenoxy
PC	Photocatalyst
PCET	Proton coupled electron transfer
PFA	Perfluoroalkoxy alkanes
Ph	Phenyl
PMP	*para*-Methoxyphenyl
ppy	2-Phenylpyridine
PTFE	Polytetrafluoroethylene
RBF	Round bottom flask
rt	Room temperature
$[Ru(bpy)_3]Cl_2$	Tris(bipyridine)ruthenium(II) chloride
SCE	Saturated calomel electrode
SET	Sigle electron transfer

t-Bu	*tert*-Butyl group
t-BuOH	*tert*-Butyl alcohol
TEA	Triethylamine
TEMPO	(2,2,6,6-Tetramethylpiperidin-1-yl)oxyl
TFA	Trifluoroacetic acid
TFE	Trifluoroethanol
THF	Tetrahydrofuran
THIQ	Tetrahydroisoquinoline
Tosyl	Toluenesulfonyl
UV	Ultraviolet light

List of Figures

List of Tables

3.10: Concentration screen for the decarboxylative α-alkylation of THIQ in flow.

3.1: Equivalents of diphenylamine for the decarboxylative α-alkylation of THIQ in flow.

4.1: Solvent screen for the α-alkylation of THIQ.

4.2: Control reactions for the α-alkylation of THIQ.

4.3: Equivalents of alkyl iodide screen.

4.4: Bases screened for the α-alkylation of THIQ.

4.5: Optimization of the tandem photocatalytic α-alkylation of THIQ in flow.

List of Awards

- Melbourne Research Scholarship, 2016, from The University of Melbourne
- T. W. Healy Travel Award, 2018, from The University of Melbourne
- G. I. Feutrill Award, 2018, from The University of Melbourne
- Study and Travel Abroad Scholarships, 2018, from The University of Melbourne

List of Publications

- van As, D.; Connell, T.; Brzozowski, M.; Scully, A.; Polyzos. A. Photocatalytic and Chemoselective Transfer Hydrogenation of Diarylimines in Batch and Continuous Flow. *Org. Lett*. **2018**, *20*, (4), 905-908

- Pilkington, R. L.; Rossouw, N. P.; van As, D.; Polyzos, A. A Chemoselective and Scalable Transfer Hydrogenation of Aryl Imines by Rapid Continuous Flow Photoredox Catalysis. *CHIMIA*, **2019**, 73, (10), 823-827

- van As, D.; Polyzos, A. The Visible Light Mediated Decarboxylative α-Alkylation of Tetrahydroisoquinolines via Batch and Flow Methods (provisional tittle) (***In preparation***)

- van As, D.; Czyz, M.; Polyzos, A. Direct C-H Functionalization of Tetrahydroisoquinolines via Radical-Radical Coupling Enabled by The Redox Neutral Tandem Photoredox Catalysis (***Submitted to Org. Lett.***)

List of Presentations

- 44th Annual Synthesis Symposium, The University of Melbourne 2019 (Poster)
- Australian Flow Chemistry Symposium (AFCS19), Melbourne 2019 (Poster)
- Departmental Seminar, The University of Melbourne, 2019 (Oral)
- Organic 18, The University of Western Australia, Perth, 2018 (Poster)
- 43rd Annual Synthesis Symposium, The University of Melbourne, 2018 (Oral)
- 22nd International Conference on Organic Synthesis (ICOS-22), Florence, Italy, 2018 (Poster)
- RACI National Centenary Conference, Melbourne, 2017 (Poster)
- ACS on campus one day event at Bio21, The University of Melbourne 2017 (Poster)
- 42nd Annual Synthesis Symposium, The University of Melbourne 2017 (Poster)

Chapter 1: Introduction

1.1.1 Amines

Amine containing molecular architectures are ubiquitous structural motifs in pharmaceuticals, agrochemicals, natural products, materials science and fine chemicals.[1-6] Particularly amines are of utmost importance in the pharmaceutical industry with 88% of the top selling 200 small molecule drugs in 2018 containing a nitrogen based functionality[7] (figure 1.1). Due to their prevalence, the development of new approaches towards the synthesis and functionalisation of amines has remained an ongoing focus in modern synthetic chemistry.[8-9]

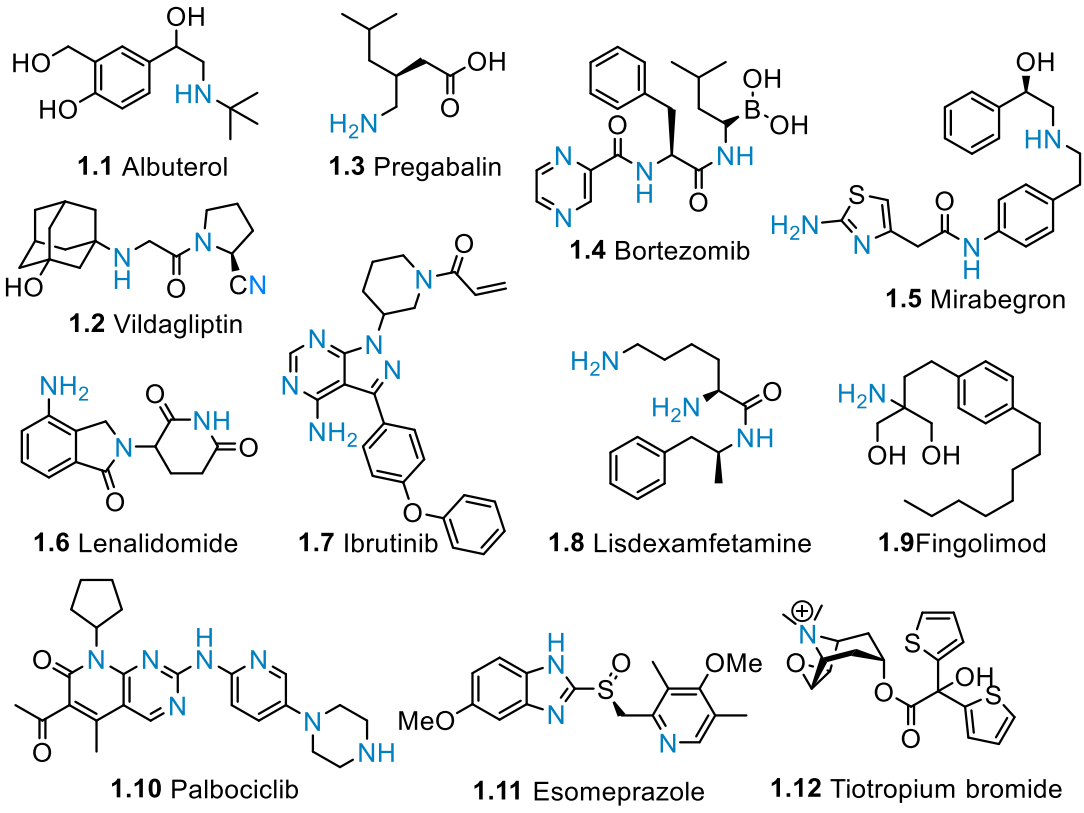

Figure 1.1: A selection of pharmaceuticals which incorporate amines and related derivatives.

The ubiquity of amines in drug design has meant that synthetic efforts in academic and industrial laboratories have focussed on their synthesis and functionalisation.[10] Specifically: amidation, reductive amination, heterocycle formation, *N*-arylation and alkylation and *N*-*tert*-butyloxycarbonyl (Boc) deprotection represent 6 out of 7 of the most performed transformations by GSK, Pfizer, and Astra Zeneca in 2008.[11] The significance of amines has necessitated a persistent demand for the development of innovative methodologies to enable their efficient and straightforward synthesis.[5-6, 12-14]

The α-functionalisation of amines exemplifies one such transformation, enabling an expeditious route to biologically active molecules (figure 1.2).[15-18] Traditional approaches for the α-functionalisation of amines are limited with respect to their reaction conditions and chemoselectivity, hence there is an ongoing demand to establish new protocols that are mild, efficient and selective.

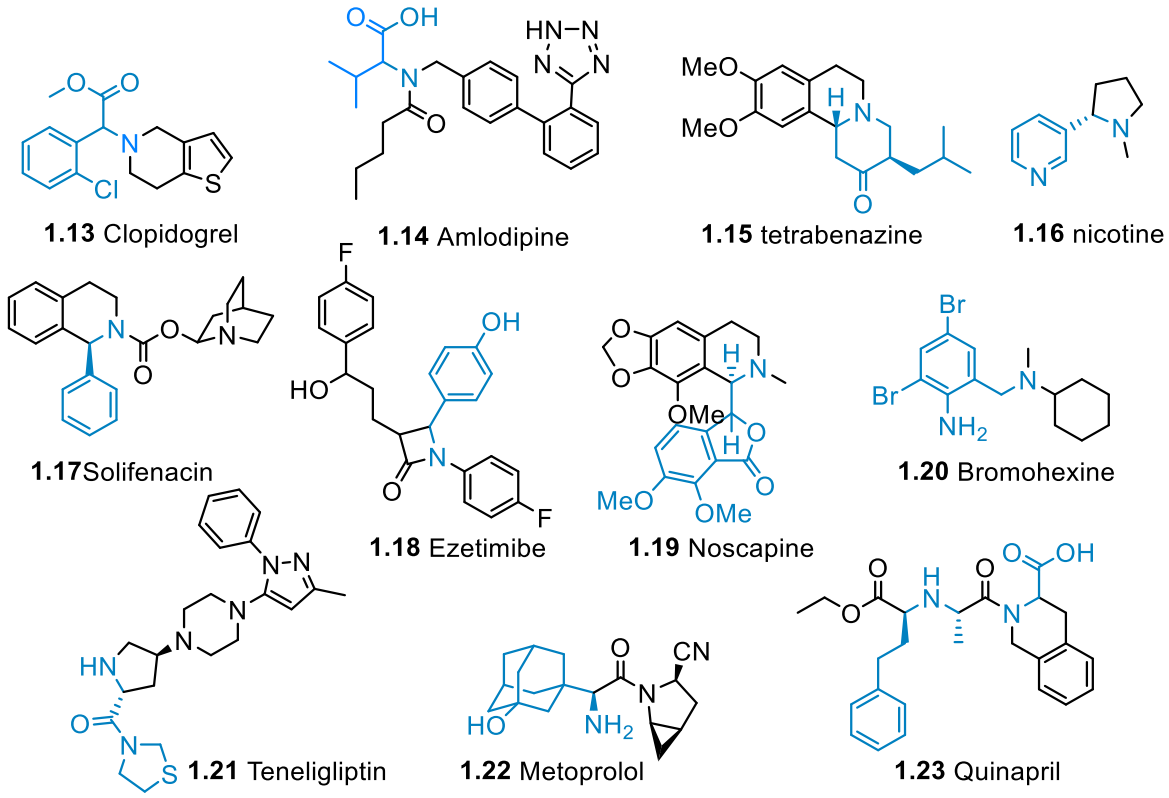

Figure 1.2: A selection of biologically active compounds accessible via the α-functionalisation of amines.

1.2 α-Functionalisation of Amines

1.2.1 α-Functionalisation via Lithiation

The use of organolithium reagents to install a carbon-carbon or carbon-heteroatom bond, α to an amine is well established. Strongly basic organolithium reagents (Pka ≈ 50 for *n*-BuLi) can deprotonate the α-C-H bond of an amine revealing nucleophilic anion, **1.25**. Once deprotonated the anionic intermediate undergoes subsequent nucleophilic attack with an electrophile, furnishing the α-functionalised product (**1.26**).[19-21] α-Functionalisation via this procedure has been extensively explored with asymmetric alkylation accessible via a chiral surrogate[22-23] and the synthesis natural products have been reported.[24] Lithiation of the α-position via highly alkaline and nucleophilic organo-lithium reagents represent harsh reaction conditions, presenting issues with selectivity and functional group tolerance. Employing a nucleophilic intermediate limits reactivity toward electrophilic reagents; while utilising pyrophoric reagents presents a substantial safety hazard,[25-26] imparting a desire to explore other pathways.

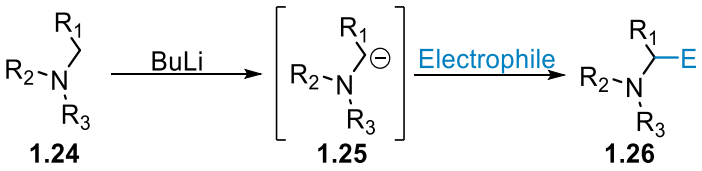

Figure 1.3: α-Functionalisation of amines via lithiation subsequent nucleophilic attack.

1.2.2 α-Functionalisation via Cross Dehydrogenative Coupling

Cross dehydrogenative coupling (CDC) reactions have also emerged as a potent method for amine α-functionalisation. This robust methodology proceeds via the oxidation of an amine to its corresponding electrophilic iminium intermediate **1.28**. The newly formed

iminium is then intercepted by a nucleophilic reagent delivering the α-functionalised product (**1.29**).[27-30] Iminium formation has been exploited via a number of oxidative pathways namely the addition of chemical oxidants[31-33] and transition metal catalysis[31, 34-36]; while electrochemical[37] and thermal[38-39] oxidation have also been achieved. In addition, an extensive array of pronucleophilic species have been utilised to intercept **1.28**.[34, 40-41] CDC reactivity complements the use of organolithium reagents however, is limited through the use of nucleophilic reagents and method for oxidative iminium formation.

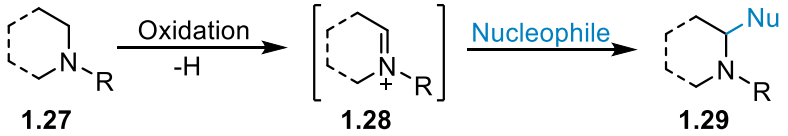

Figure 1.4: General scheme of CDC reaction.

1.2.3 α-functionalisation via Transition metal Catalysed C-H Activation

Over the last decade α-functionalisation has been achieved via transition metal catalysed C-H activation. This technique involves the oxidative addition of a transition metal[42-45] into the α-C-H bond facilitated by a directing group. Use of a directing group allows arrangement of the catalyst, facilitating the oxidative addition to a precise C-H bond, enabling highly selective transformations.[15] Subsequent transmetallation of the catalyst facilitates reductive elimination, affording the α-functionalised product (figure 1.5).[46] Transition metal catalysed C-H activation remains a pathway still in its infancy, with several challenges to overcome including: the necessity of a directing group to obtain selectivity and an undesired β-hydride elimination pathway.

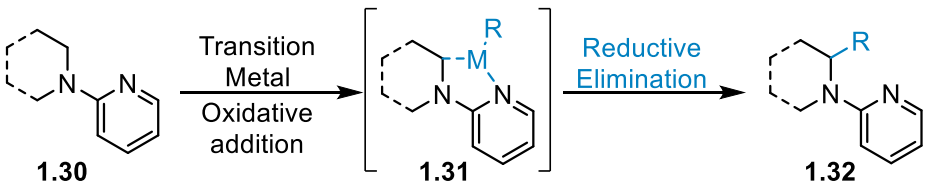

Figure 1.5: General figure for C-H activation of amines with transition metal catalysis.

1.2.4 Radical Approaches Towards α-Functionalisation

Radical approaches have enabled the α-functionalisation of amines, proceeding via an α-amino radical intermediate. Several groups have utilised traditional radical methodology, enacting tin hydrides in combination with radical initiators to instigate the formation of an α-amino radical with subsequent α-functionalisation.[47-51] The α-amino radical (**1.34**) represents a highly useful intermediate due its stabilised and nucleophilic nature,[52] which enables a variety of transformations. Traditional radical approaches are limited via the use of high temperatures, explosive initiators, and stoichiometric quantities of toxic tin hydrides. Alternatives to tin hydrides such as: thiophenol,[50] silanes[53-55] and UV light[56-57] have been reported. Employing UV light has addressed several limitations however such an approach is constrained through irradiation with a highly oxidising light source.[58] More recently, visible-light mediated catalysis has provided an effective pathway for radical generation under mild conditions.

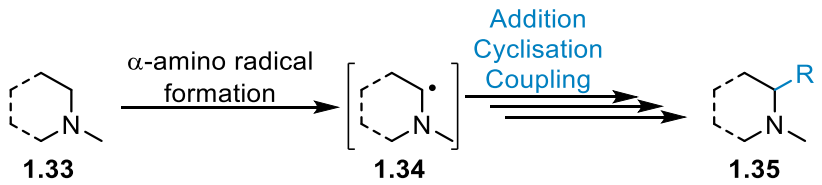

Figure 1.6: α-functionalisation of amines via a radical pathway.

1.3 Visible Light Mediated Catalysis

In 1912 Giacomo Ciamician recognised that sunlight could be harnessed as an abundant and renewable energy source to enact chemical transformations.[59] Over the last decade photoredox catalysis has realised this, utilising visible light to enable mild radical formation, inspiring a renaissance in synthetic radical chemistry.[60] Photoredox catalysis harnesses catalytic quantities of a chromophore to absorb light and convert photons into chemical energy through successive single electron transfer events.[61-66] Conceptually, photoredox catalysis is initiated via the absorption of a photon by a chromophore/photocatalyst, promoting an electron to a singlet excited state whereby consequent intersystem crossing generates a long-lived triplet species (**1.37**). The excitonic nature of **1.37**, permits this species to act as both an oxidant or reductant, either via donation of an electron from the E_g orbitals or accepting an electron into the T_{2g} orbital. If an electron is donated (oxidation of catalyst) to an acceptor molecule, photocatalyst **1.36** can be consequently regenerated through single electron reduction by a donor molecule, instilling further reactivity; this process is known as an oxidative quenching cycle. Alternatively, if triplet **1.37** is reduced, consequent donation of an electron from the catalyst to an acceptor molecule enables regeneration of the photocatalyst's ground state which is known as a reductive quenching cycle. Photoredox chemistry represents a green methodology to generate radicals, this is accomplished at ambient temperatures in the absence of explosive initiators, toxic tin hydrides or oxidising UV light.[63] Photoredox chemistry further expands upon traditional radical chemistry enabling both a single electron oxidation and reduction to be achieved in a reaction mixture.

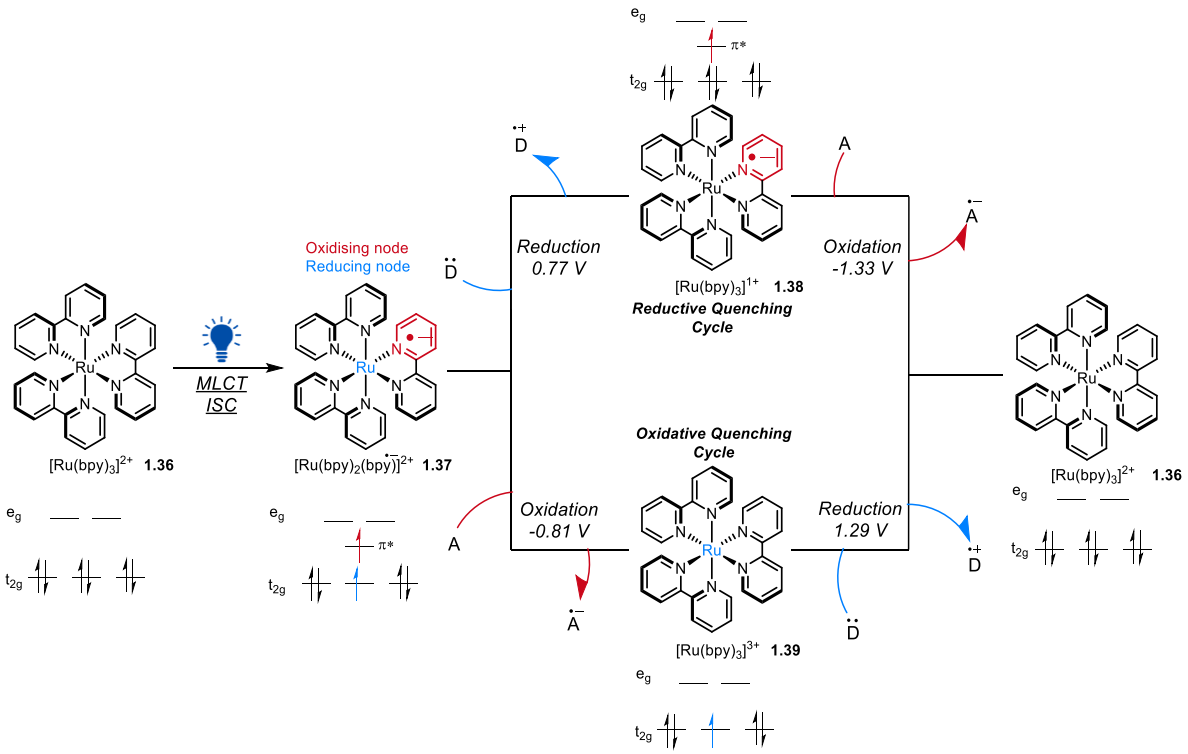

Figure 1.7: Fundamental mechanism of photoredox catalysis.

A plethora of chromophores have been utilised as photocatalysts throughout the literature. The most widespread photocatalysts involve polypyridyl ruthenium and iridium octahedral complexes. Other photoactive transition metal complexes based on copper[67-69], chromium[70-72], cerium,[73-76] iron,[77-79] zinc,[80-81] gold[82-83] and palladium[84-86] have been used. In addition, organic chromophores encompassing structural motifs, such as: eosin Y,[87] fluorescein,[88-89] rose Bengal,[90-92] rhodamines,[93-94] acrdinium[95-96] and polycarbazoles[97-98] among many others[99] have also appeared throughout literature. The structural properties of the chromophore greatly influence the photophysical and electrochemical properties of the photocatalyst via alteration of the HOMO-LUMO energy gap. A selection of photocatalysts, their structures and redox properties (against SCE) can be highlighted in figure 1.8 below.

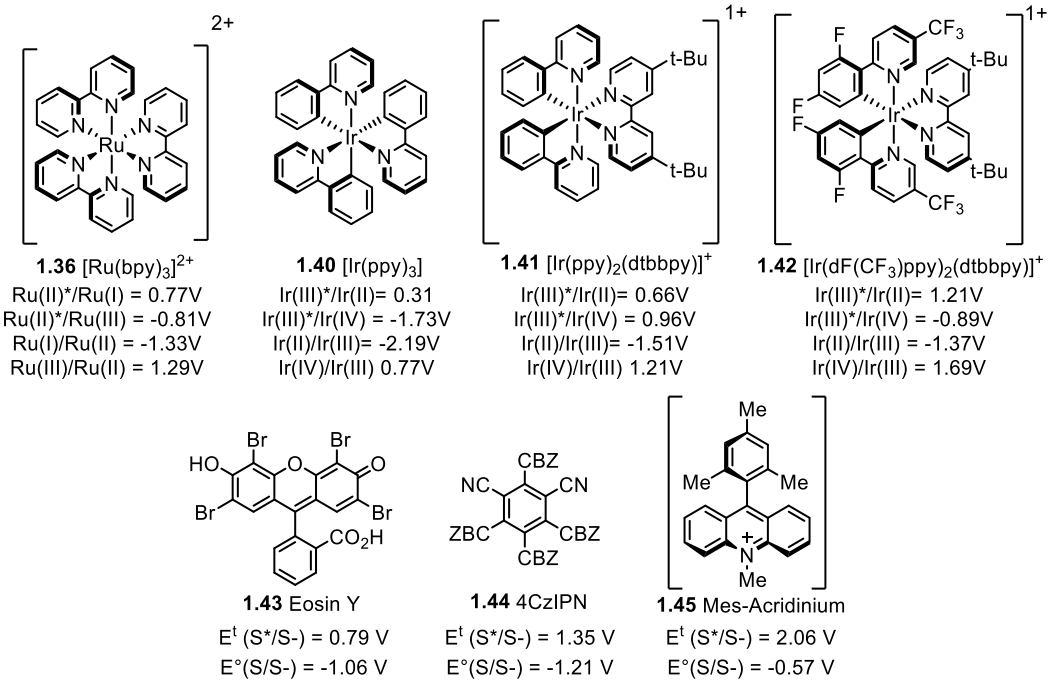

Figure 1.8: A selection of reported photocatalysts and their redox potentials.

1.3.1 Early Examples of Visible-Light Mediated Catalysis

Photoredox catalysis was established in 1978 when Kellogg *et al.* disclosed the photo-mediated reduction of sulfonium ions to the corresponding thioethers and ketones in the presence of NADH analogues, 1,4-dihydropyridines.[100] Kellogg observed reactivity by irradiating the reaction mixture however noted accelerated reaction rates in the presence of a dye. Utilising $[Ru(bpy)_3]Cl_2$, Kellogg observed the complete reduction of sulfonium (**1.46**) to acetophenone in quantitative yields which extended towards the corresponding ammonium and phosphonium salts. As summarised in figure 1.9, Kellogg hypothesised that this process proceeds when the triplet state of $[Ru(bpy)_3]Cl_2$ oxidises a trace amount of Hantzsch ester (**1.49**) generating a reducing Ru(I) species, which undergoes single electron reduction with **1.46** to the corresponding α-carbonyl radical (**1.47'**) and thioether **1.48**. **1.47'** undergoes hydrogen abstraction with another molecule of Hantzsch ester

furnishing acetophenone (**1.47**), while the radical 1,4-dihydropyridine is further oxidised, facilitating regeneration of the Ru(I) species, prompting a catalytic cycle.[101]

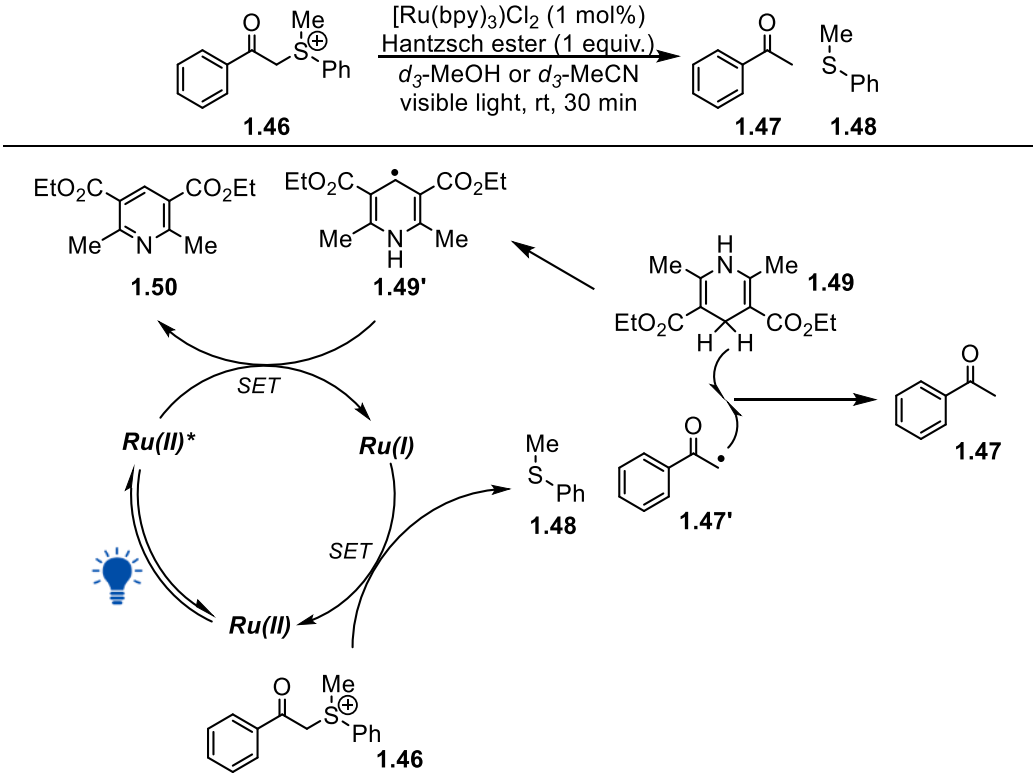

Figure 1.9: Kellogg's visible light mediated reduction of sulfonium ions.

Kellogg's reports initiated the photoredox field, and were followed by several publications utilising similar chromophore-1,4-dihydropyridine systems to reduce a variety of substrates including benzyl bromides,[102-103] phenacylhalides,[104-105] electron deficient olefins,[106] and the desulfation of β-keto sulfones.[107-108] In 1984 Cano-Yelo and Deronzier demonstrated the facile reduction of aryl diazonium salts in the presence of $[Ru(bpy)_3]Cl_2$ when conducting a photomediated Pschorr reaction for the synthesis of phenanthrolines.[109] This report realised the potential of diazonium salts as radical surrogates, allowing the first intramolecular cyclisation via a visible light mediated catalytic process. Inspired by this cyclisation, Cano-Yelo utilised diazonium salts as

sacrificial oxidants enabling the photooxidation of benzyl alcohols.[110] Okada exploited *N*-hydroxyphthalimide (NHP) esters to undergo decarboxylative fragmentation upon single electron reduction generating alkyl radicals.[111] Upon alkyl radical formation, Okada demonstrated 1,2-radical addition into a selection of Michael acceptors. This transformation was the first intermolecular photoredox reaction reported. Okada further expanded this methodology towards a decarboxylative approach for generating C-S[112] and C-H[113] bonds.

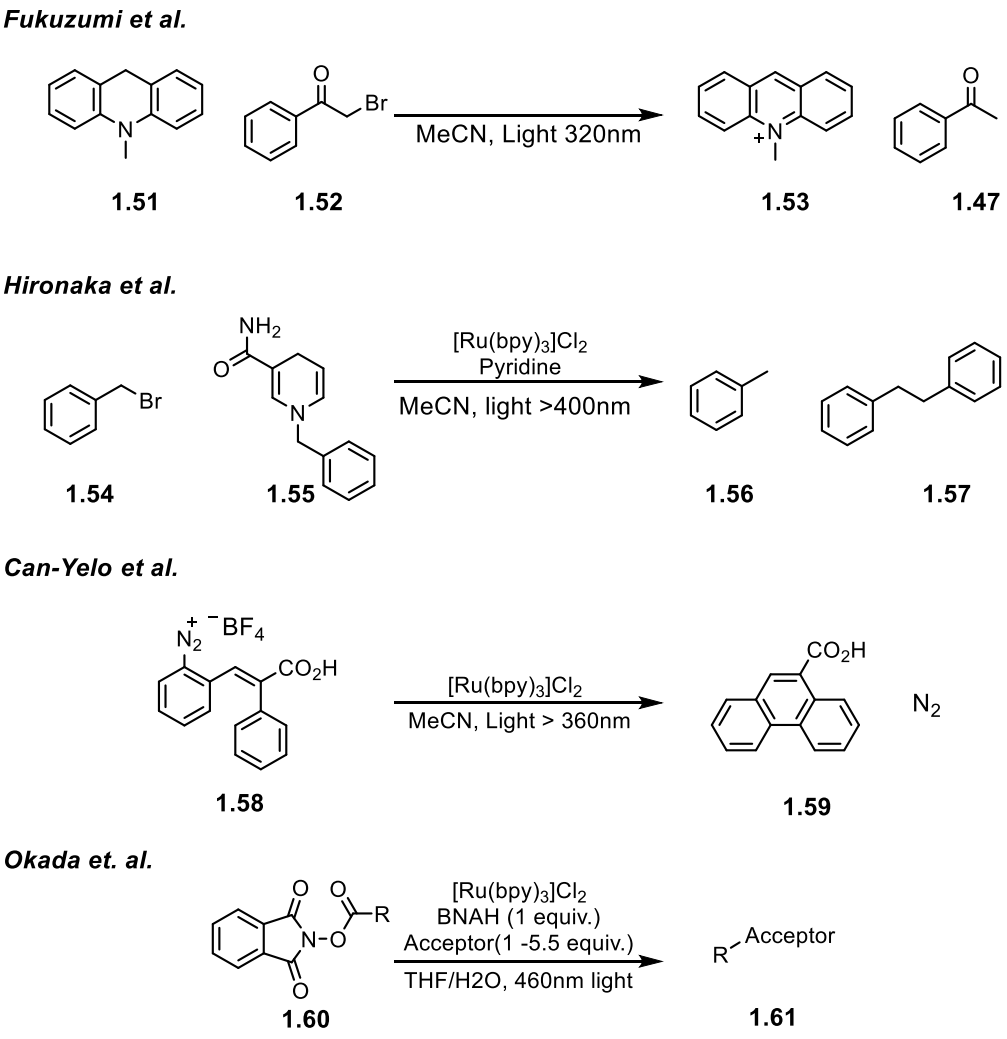

Figure 1.10: Some early examples of photoredox catalysis.

1.3.2 Modern Photoredox Catalysis

Despite early advances, photoredox catalysis was not widely adopted by the synthetic community until 2008 when seminal works by the Yoon, MacMillan and Stephenson laboratories were published, inspiring a renaissance in the field. In 2008 Yoon *et al.* reported the formal [2+2] cycloaddition of bis-enones, in the presence of $[Ru(bpy)_3]Cl_2$, sacrificial reductant DIPEA and $LiBF_4$ to stimulate single electron reduction of enone **1.62**.[114] Upon excitation, Yoon hypothesised a reductive quenching cycle in which triplet $[Ru(bpy)_3]Cl_2$ is reduced by DIPEA instilling a highly reducing Ru(I) species. Catalyst regeneration is achieved via the subsequent single electron reduction of a lithium coordinated α,β-unsaturated ketone to radical **1.64**. Intramolecular radical cyclization proceeds via Michael addition to the adjacent enone, with consequent intramolecular radical addition constructing both a 4 and 5 membered ring in one step and engendering the desired [2+2] cycloaddition adduct **1.63**. Yoon's conditions effectively enabled the intramolecular and intermolecular cycloaddition of a variety of symmetrical and unsymmetrical bis(enones).

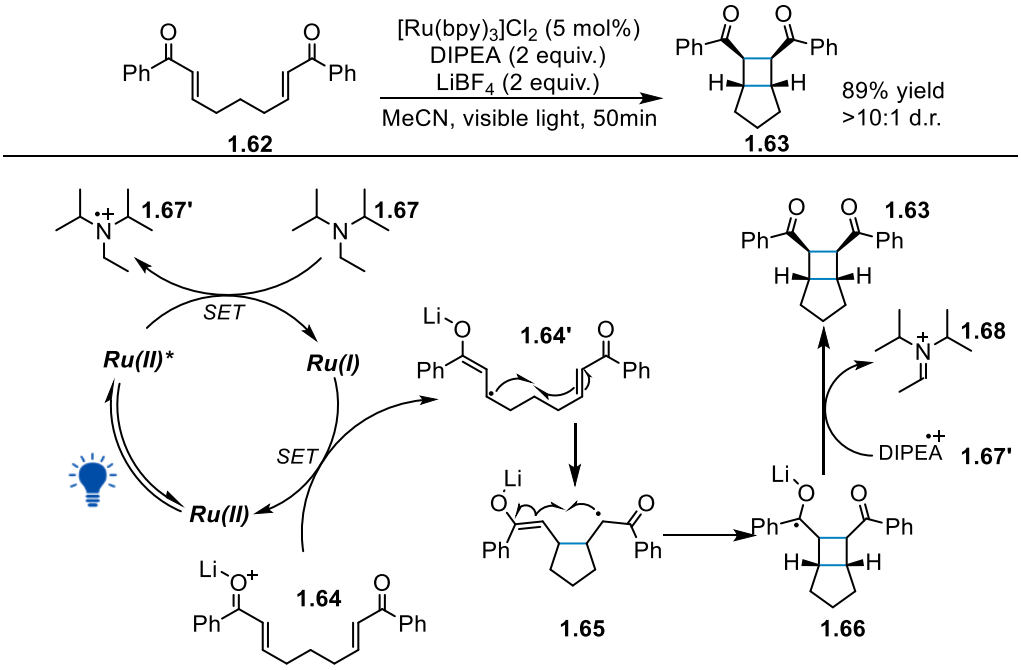

Figure 1.11: Yoon's photoredox mediated [2+2] cyclization of bis(enones).

Nicewicz and MacMillan merged photoredox catalysis with organocatalysis when pursuing the enantioselective α-alkylation of aldehydes utilising activated alkyl bromides.[115] They hypothesised the *in situ* generation of intermediate **1.73** via condensation between an aldehyde (**1.70**) and chiral amine **1.72**, engendering an iminium intermediate with consequent rearrangement to chiral ene-amine **1.74**. Upon irradiation of $[Ru(bpy)_3]Cl_2$, reductive cleavage of the activated C-Br bond of **1.69** transpires with subsequent enantioselective intermolecular conjugate addition to the chiral ene-amine yielding an α-amino radical (**1.75**). Further single electron oxidation produces **1.76** and regenerates the photocatalyst, subsequent hydrolysis of the iminium selectively yields the desired adduct (**1.71**). Utilisation of asymmetric amine, **1.72** enabled Nicewicz and MacMillan to enact enantiofacial control of radical addition to the α-keto radical, facilitating enatioselective control. Nicewicz and McMillan's protocol represents the first instance of dual catalysis of photoredox merged with organocatalysis, enabling the asymmetric alkylation of a variety of aldehydes and activated bromides in excellent yields and enantiomeric excesses. Since this initial report, many laboratories have merged photoredox catalysis with other catalytic methods accessing previously unattainable transformations.[116-120]

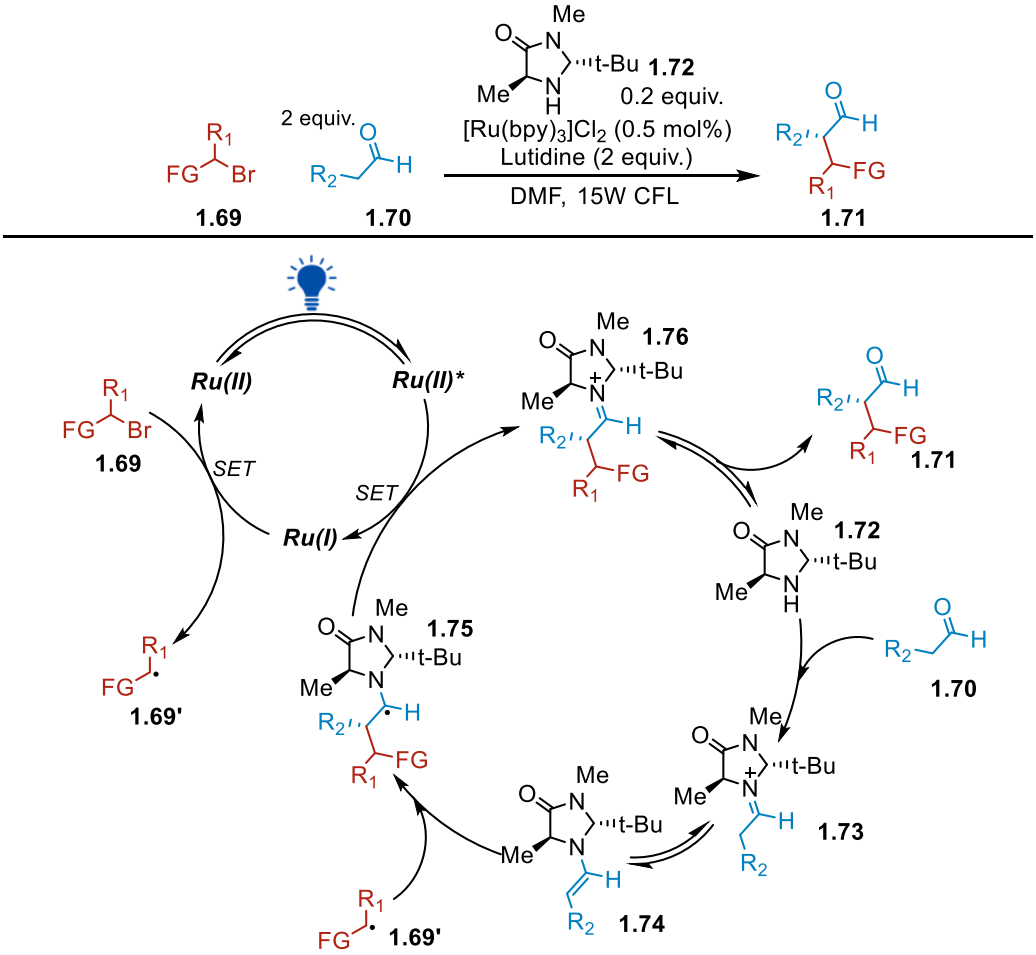

Figure 1.12: Visible-light mediated enantioselective α-alkylation of aldehydes via merging photoredox and organocatalysis.

DeClue and Falvey simultaneously developed protocols for the photocatalytic deprotection of carboxylic acids via the reductive cleavage of picolinium esters. DeClue *et al.* hypothesised that single electron reduction could deprotect picolinium functionalised decanoic acid (**1.77**) generating micellular structures as the reaction proceeds.[121] Borak and Falvey noted that that 2-cyanopicolinium esters could be reductively cleaved in the presence of $[Ru(bpy)_3]^{2+}$ and ascorbic acid which fulfills a dual role of sacrificial reductant and hydrogen source.[122] These procedures represent the first visible light mediated photocatalytic deprotections in the literature.

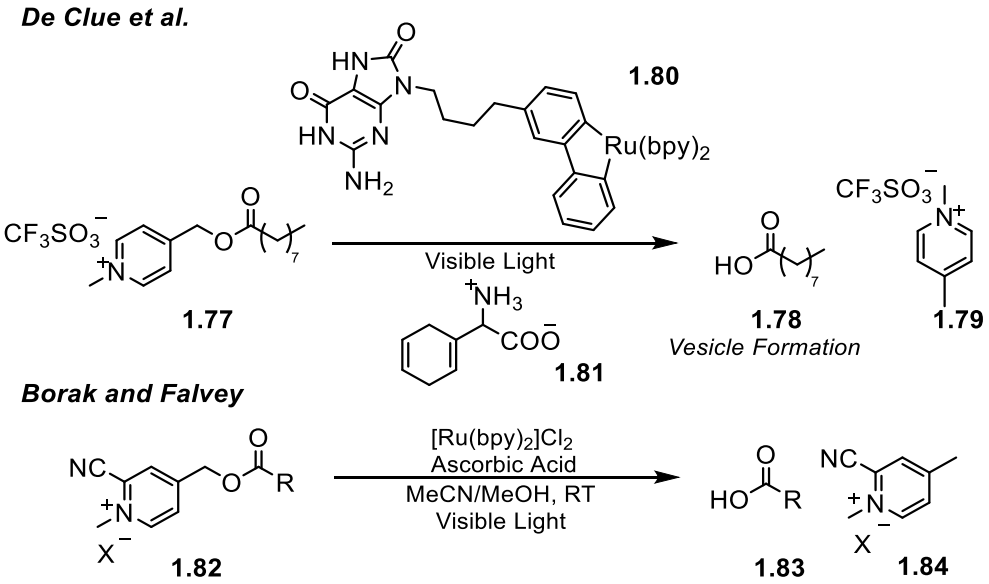

Figure 1.13: Visible-light mediated deprotection of carboxylic acids.

The next breakthrough in photoredox chemistry came from the Stephenson group, when they re-elaborated on Fukuzumi's[104] visible-light mediated proto-dehalogenation of activated halogens.[123] Stephenson observed that in the presence of a COOH:DIPEA azeotrope, photocatalyst $[Ru(bpy)_3]Cl_2$ achieves the photoreductive cleavage of activated carbon-halogen bonds[123]. Conceptually similar to Fukuzumi, Stephenson proposed a reductive quenching cycle in which triplet $[Ru(bpy)_3]Cl_2$ is reduced by DIPEA, with the corresponding Ru(I) species achieving single electron reduction, cleaving the C-Br bond of the activated alkyl halide, engendering alkyl radical **1.85'** and regenerating the photocatalyst. The newly formed alkyl radical (**1.85'**) undergoes hydrogen abstraction from the DIPEA:COOH azotrope attaining the formally protodehalogenated product **1.86**. This seminal work exhibited selectivity as the reduction of activated alkyl bromides was achieved in the presence of other unactivated halide species. Substitution of DIPEA for d_{15}-TEA observed deuterium incorporation into the product, revealing that the sacrificial amine is the major source of hydrogen in this reaction.

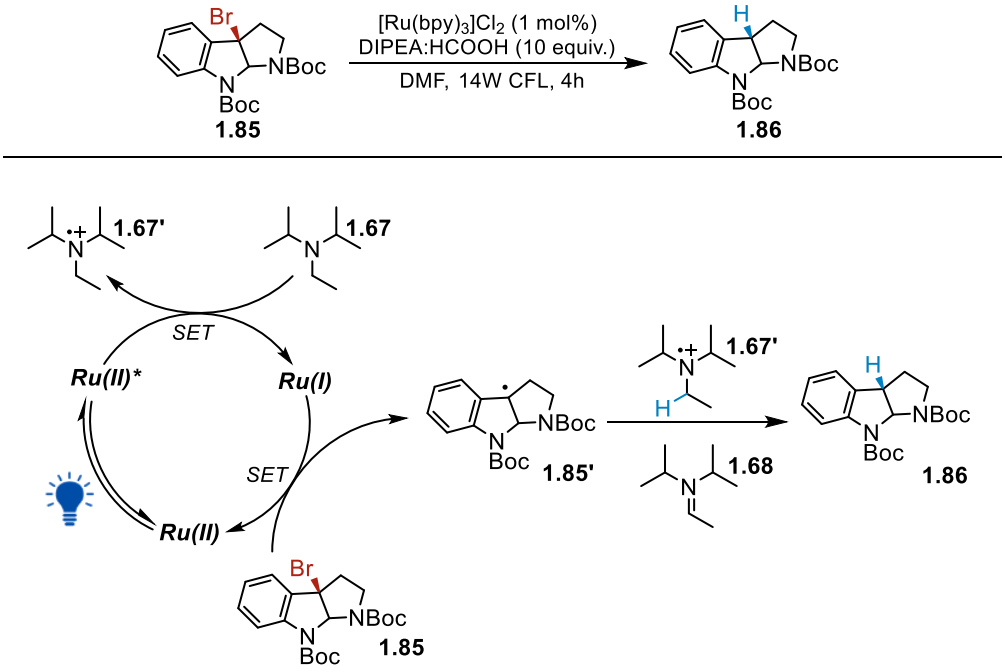

Figure 1.14: Visible-light mediated protodehalogenation of alkyl halides.

Stephenson expanded this synthetic methodology via development of a visible light mediated intramolecular radical cyclisation.[124] Driven by the same conceptual mechanism as protodehalogenation, prior to hydrogen abstraction, the alkyl radical of **1.87** undergoes intramolecular 1,2-radical addition to an alkene or alkyne functionality. The cyclised radical then experiences hydrogen abstraction from oxidised TEA, achieving cyclised product **1.88**. Stephenson observed that less activated halides required the substitution of $[Ru(bpy)_3]Cl_2$ for more reducing $[Ir(ppy)_2(dtbbpy)]PF_6$. Since these initial reports Stephenson has also accessed unactivated alkyl, aryl and vinyl halides by employing highly reducing photocatalyst $[Ir(ppy)_3]$.[125] In addition, Stephenson has conducted the intramolecular cyclisation between electron poor α-bromo malonates and electron rich indoles/pyrroles enabling the synthesis of biologically active polycyclic products.[126]

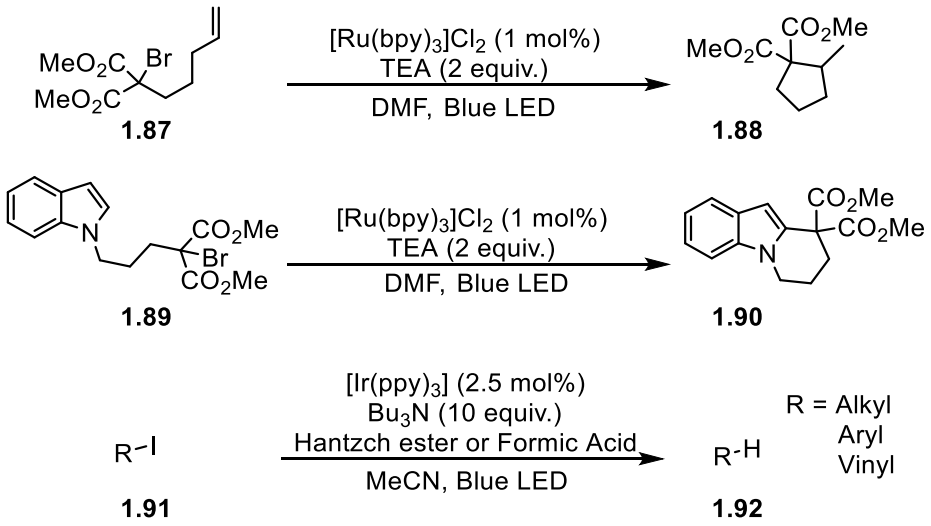

Figure 1.15: Expansions of Stephenson's protodehalogenation methodology.

Since these seminal publications, the field of photoredox catalysis has flourished with an immense and diverse array of methodology.[61, 63, 66, 99, 120] The synthesis and functionalisation of amine derivatives has recently witnessed major advances with the application of photoredox catalysis.

1.4 Visible-Light Mediated Functionalisation of Amines via Iminium Formation

Photoredox catalysis has accessed several pathways to facilitate the α-functionalisation of amines. This is typically achieved via an oxidative pathway, in which single electron oxidation of an amine produces a nitrogen radical cation (**1.94**) with subsequent reactivity allowing modification of the α-C-H bond (figure 1.16). Upon formation of the nitrogen radical cation, a variety of pathways can proceed, predominantly these include the formation of an iminium ion or an α-amino radical intermediate.

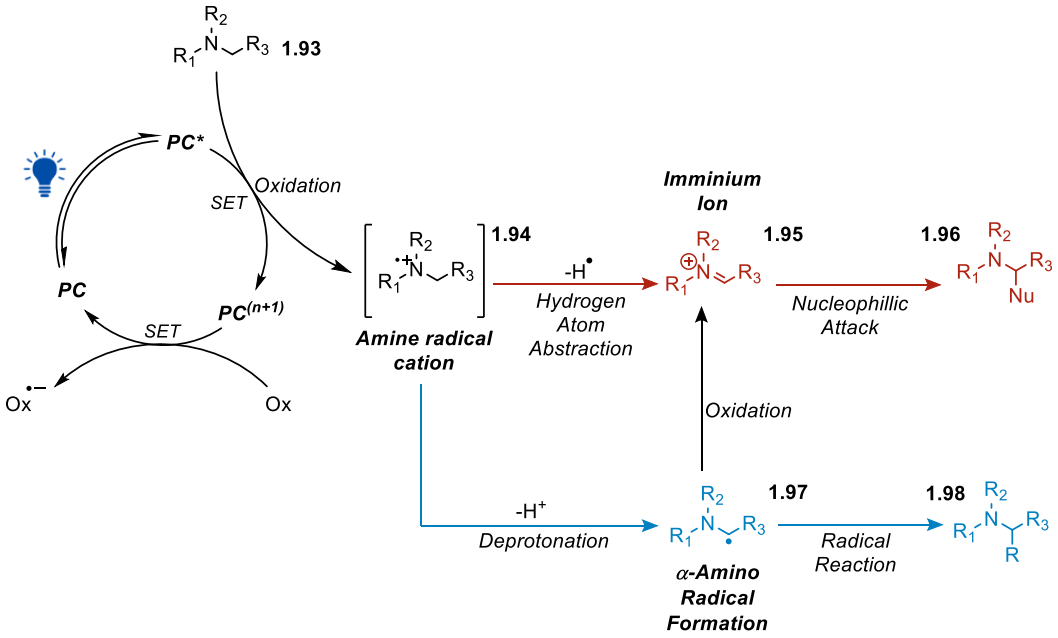

Figure 1.16: Photo-oxidative pathways of amine radical cations.

The α-hydrogen of an nitrogen radical cation **1.94** is a highly reactive species, susceptible to both hydrogen atom abstraction and deprotonation.[127] Abstraction of the α-hydrogen represents a valuable hydrogen source,[123-124] however this process has been targeted for its iminium by-product. Iminium **1.95** represents a desirable reactive intermediate susceptible towards nucleophilic attack from a wide variety of pronucleophiles,[127-128] furnishing the α-functionalised product. Photoredox mediated iminium ion formation represents synonymous reactivity to CDC reaction, exemplifying a green pathway towards the oxidation step.

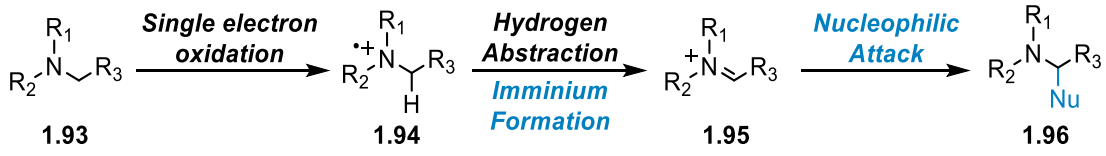

Figure 1.17: Formation of the iminium intermediate and nucleophilic attack.

This process was initially postulated by Giannotti and Whitten in 1980 when a wet solution of triethylamine was irradiated in the presence of $[Ru(bpy)_3]Cl_2$.[129] Upon irradiation, acetaldehyde was detected with postulation that this formation proceeds via

the oxidative formation of an iminium, with subsequent hydrolysis inducing acetaldehyde formation.

In 2010, Stephenson *et al.* harnessed the concept of visible light mediated iminium formation, reporting the photoredox catalysed Aza-Henry coupling between nitroalkanes and tetrahydroisoquinolines (THIQ).[130] Stephenson's methodology employed $[Ir(ppy)_2(dtbbpy)]PF_6$ as a photocatalyst in which upon irradiation induces the single electron oxidation of THIQ (**1.99**) to radical cation **1.99'**. It is proposed that consequent regeneration of the photocatalyst is achieved via either the single electron reduction of atmospheric O_2 to triplet oxygen (**1.102**) or the reduction of nitromethane to its radical anion. Either of these reduced species are then proposed to abstract the highly labile α-hydrogen atom of **1.99'** instilling iminium **1.101**. Subsequent nucleophilic attack from **1.103** to iminium **1.101** furnishes the desired α-functionalised tetrahydroisoquinoline (**1.100**). Stephenson's procedure allowed the efficient Aza-Henry coupling of a variety of THIQ derivatives and nitromethane in excellent yields. In the absence of oxygen, reactivity was observed at a decreased rate, highlighting that diatomic oxygen is primarily responsible for turning over the photocatalyst, while nitromethane fulfills this role to a lesser extent. Stephenson also noted that the presence of oxygen hindered catalytic turnover due to the formation of an undesired amide product, therefore Stephenson *et al.* later developed conditions under an inert atmosphere. Under N_2 and in the presence of sacrificial oxidant, bromotrichloromethane, a clean reaction was achieved with an accelerated 3 hour reaction time.[131]

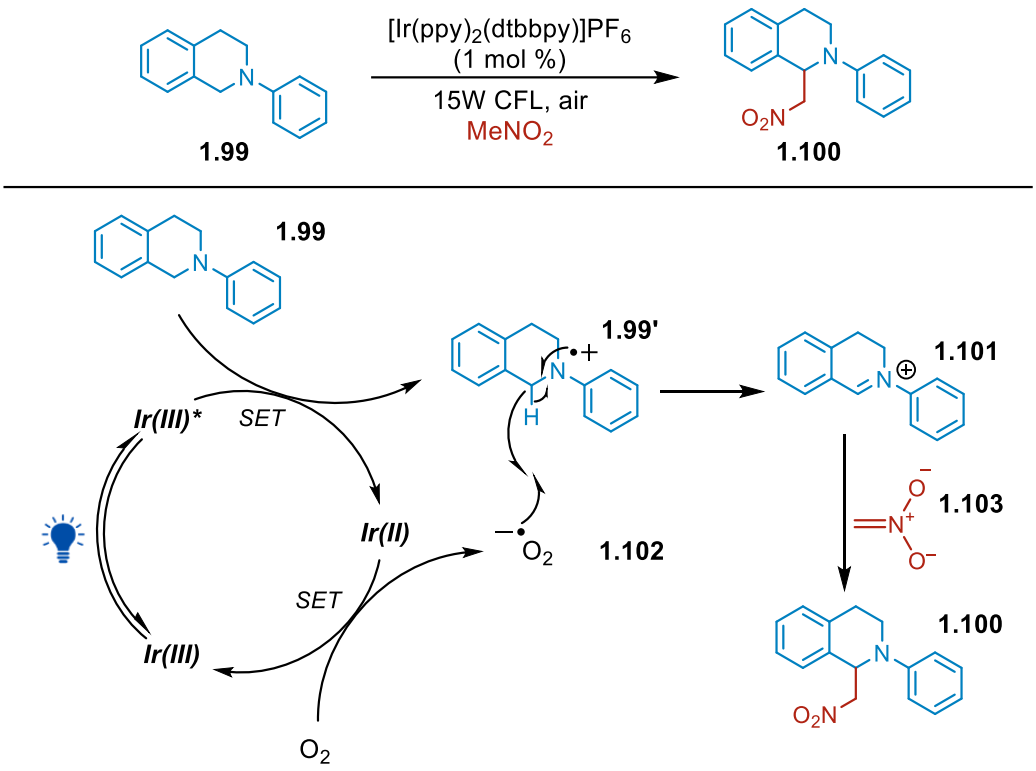

Figure 1.18: Stephenson's visible light induced Aza-Henry reaction.

This seminal publication spurred extensive interest in the visible-light mediated formation of iminium intermediates, with a variety of studies being published on this topic. Further studies have concerned: broadening the scope towards other hard nucleophiles beyond nitro alkanes,[91, 131-137] use of an organic photocatalyst,[90, 132, 138-139] detailed mechanistic studies[140] and transferring this methodology to a flow protocol.[141]

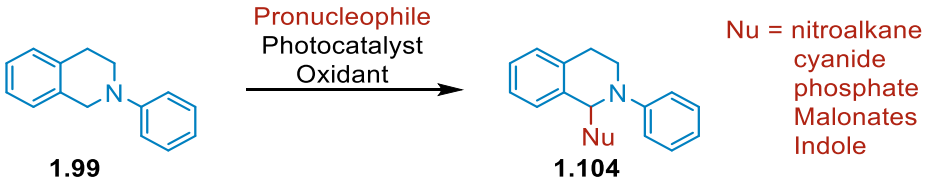

Figure 1.19: Advancements on the photocatalytic CDC reaction.

With the interception of an iminium by hard nucleophiles having been thoroughly explored, Rueping *et al.* pursued the α-functionalisation of THIQ derivatives incorporating soft nucleophiles by merging photoredox and Lewis Base catalysis (figure 20).[142] The addition of catalytic quantities of L-proline enabled condensation and formation of enamine derivative **1.107** from the corresponding ketones and aldehydes.

Nucleophilic attack by **1.107** to an *in situ* generated iminium species (**1.101**) followed by consequent hydrolysis engenders the desired α,β-ketoamine (**1.106**). Due to rapid iminium formation, a 5W light source was employed to modulate the rates of iminium and enamine formation. Zhu *et al.* achieved analogous reactivity, exploiting a photoactive gold complex which enhanced the efficiency of ketone substrates with extended alkyl chains.[82] DiRocco and Rovis exploited a chiral *N*-Heterocyclic carbene (NHC) for the formation of the ene-amine intermediate.[143] Condensation between an NHC complex and aldehyde confers a chiral acyl anion, locking the conformation for enantiofacial controlled nucleophilic addition into the THIQ iminium species, subsequent hydrolysis reveals the asymmetric α-acylated THIQ derivative.

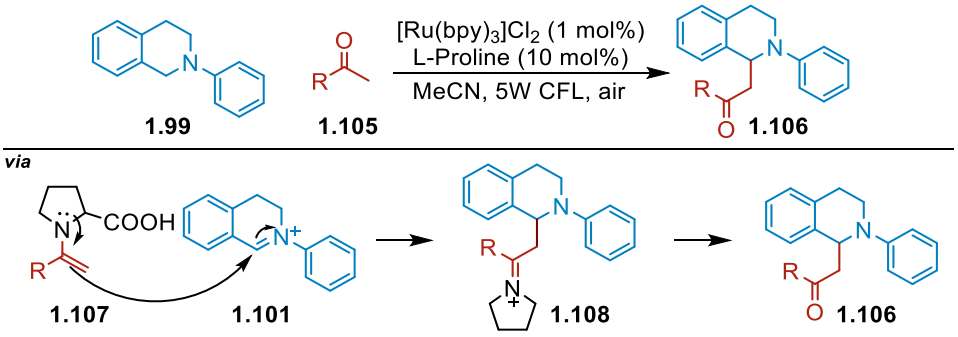

Figure 1.20: Rueping's synthesis of 1,2-amino ketones via nucleophilic addition of an ene-amine to a THIQ derived iminium.

Substitution of the *N*-phenyl substituent on THIQ with a methyl ester or methyl diester induces further deprotonation adjacent to the iminium, with consequent formation of an azomethine ylide (**1.117**). Xiao[144] and Rueping[145] simultaneously developed procedures utilising this intermediate to access 1,3-dipolar cycloadditions, establishing a light induced protocol for the synthesis of a variety of functionalised fused heterocyclic pyrroles and pyrrolidines, as summarised in figure 1.21.

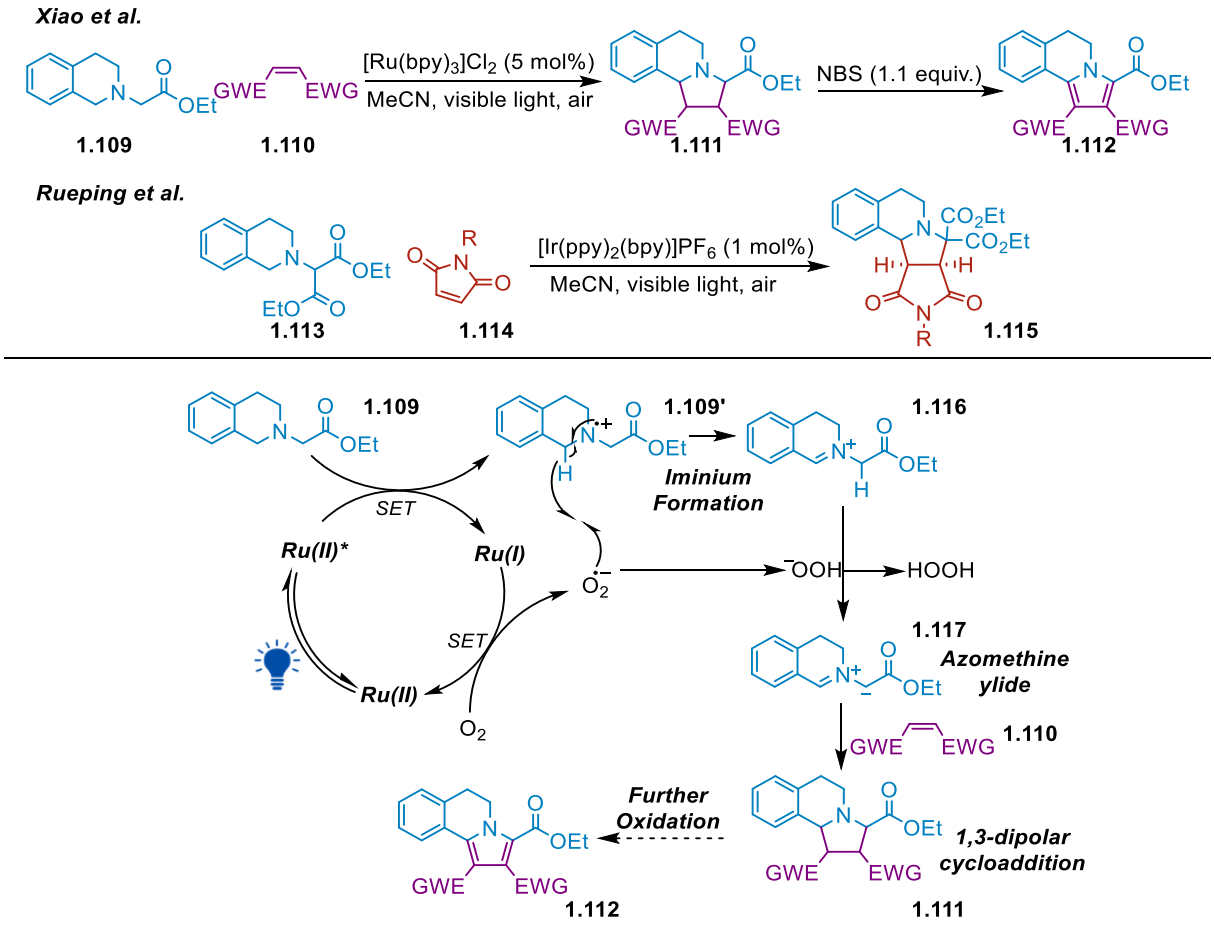

Figure 1.21: Xiao and Rueping's photocatalytic 1,3-dipolar cycloadditions.

Visible light mediated iminium formation is a well-established procedure, widely exploiting THIQ derivatives as an effective workhorse substrate. Other structural frameworks have been employed and encompass amino acids,[146] pyrrolidines/piperidine,[147-149] amides[150-151] and dihydroquinoxalin.[152] Expansion of the nucleophile scope has enabled a broad variety of different bonds to be constructed including sp^3 C-C.[132] C-O,[153-154] C-N[154-155] and C-P[132-133] bonds α to an amine

1.5 Visible-Light Mediated Functionalisation of Amines via α-Amino Radicals

1.5.1 Oxidative Approaches for the Visible Light Mediated α-Functionalisation of Amines

Another pathway accessible from the nitrogen radical cation is the formation of an α-amino radical. Deprotonation at the acidic α-position of **1.94** and subsequent 1,2-electron rearrangement engenders a reactive α-amino radical intermediate (**1.97**).[127] Accessing an α-amino radical permits a nucleophilic radical pathway in contrast to ionic electrophilic reactivity observed via an iminium species. In comparison to its iminium counterpart, the chemistry surrounding α-amino radicals has been considerably less explored.

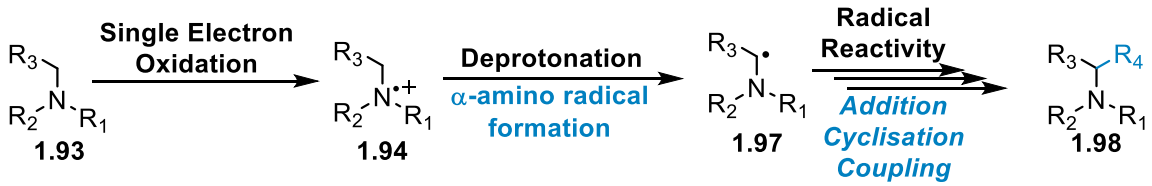

Figure 1.22: Generation of α-amino radical via photoredox catalysis.

The initial inception of α-amino radical generation via photocatalytic methods occurred when MacMillan *et al.* published the serendipitous α-arylation of amines.[156] Enabled via high throughput screening, MacMillan hypothesised an oxidative quenching cycle in which triplet [$Ir(ppy)_3$] induces single electron reduction of an electron deficient *para*-substituted benzonitrile forging **1.118'**. Photocatalyst regeneration is achieved via the single electron oxidation of an amine, with deprotonation of the α-position in the presence of sodium acetate instilling α-amino radical **1.97**. Radical-radical coupling by the two

radical species and subsequent rearomatisation via expulsion of the nitrile functionality imparts the desired α-arylated amine (**1.119**).

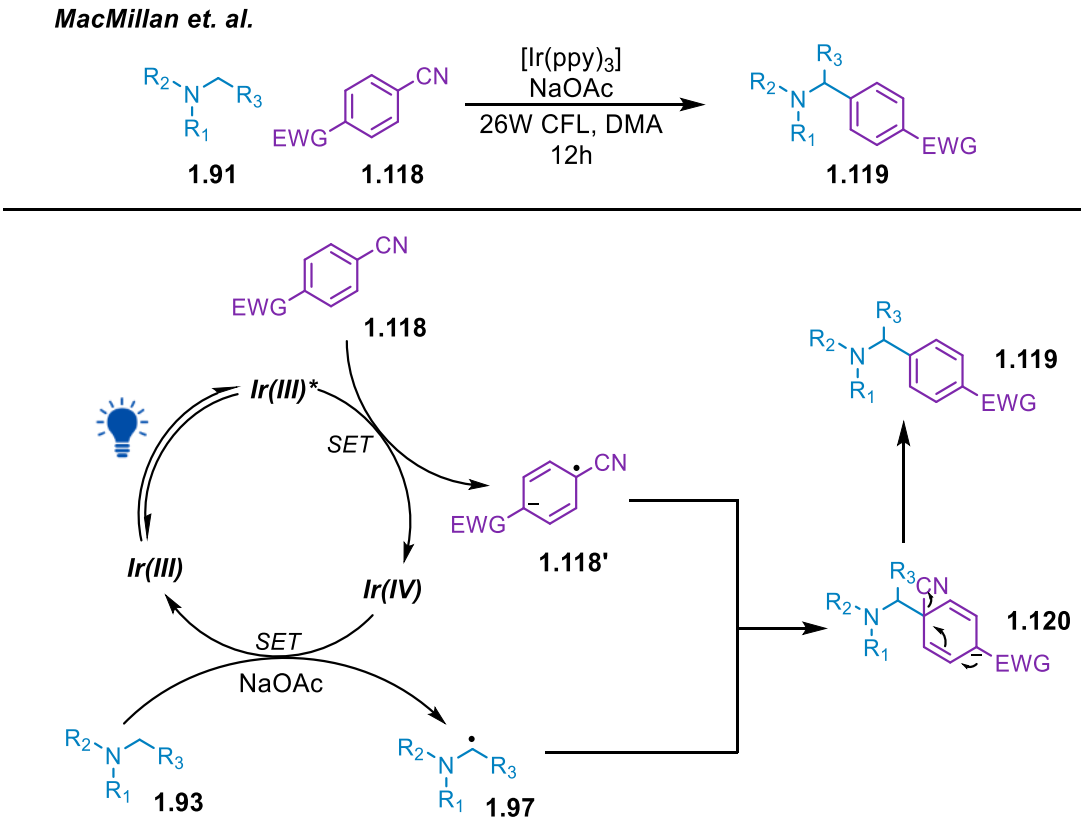

Figure 1.23: MacMillan's visible light mediated α-arylation of amines via radical-radical coupling.

MacMillan's report paved way for Pandey and Reiser *et al.* when they demonstrated the nucleophilic nature of α-amino radicals via the intermolecular radical Michael addition between THIQ derivatives and electron deficient alkenes.[157] Conceptually Reiser *et al.* propose that upon irradiation of a photocatalyst (either $[Ru(bpy)_3]Cl_2$ or $[Ir(ppy)_2(dtbby)]PF_6$) with blue LED's, the triplet state is reduced by **1.99**, generating nitrogen radical cation (**1.99'**). Upon deprotonation of the α-position, **1.99'** rearranges to the nucleophilic α-amino radical **1.123** and consequent intermolecular 1,2-radical addition with methyl vinyl ketone produces radical **1.124**. Regeneration of the photocatalyst is achieved via the reduction of **1.124** to its anionic counterpart, subsequent protonation constructs the α-functionalised adduct (**1.122**). The existence of the α-amino

radical was investigated via two control reactions, initially this reaction was conducted in the absence of the Michael acceptor, revealing homocoupled THIQ **1.125**. Dimerization occurred due to the absence of an alternative reactive species, inducing homocoupling of **1.123**. Conducting the reaction in the presence of oxygen revealed substantial quantities of amide **1.126**, thought to have occurred via coupling of the α-amino radical with of singlet oxygen.

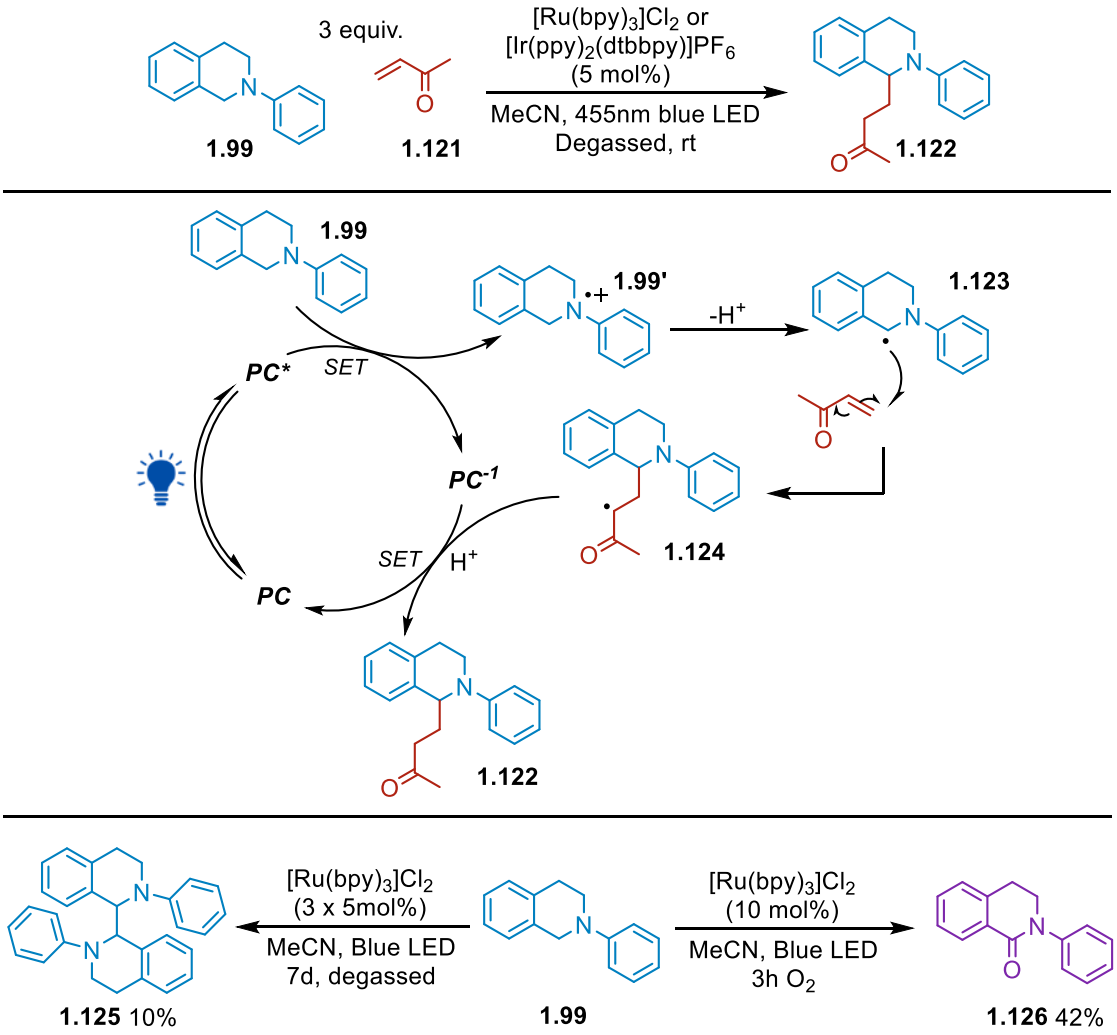

Figure 1.24: Pandey and Reiser's intermolecular 1,2 radical addition between THIQ and electron deficient alkenes.

Yoon *et al.* independently developed conditions for the photocatalytic intermolecular 1,2-radical addition between THIQ and electron deficient alkenes, this process was improved via the addition of a Brønsted acid (figure 1.25).[158] The addition of Brønsted acid,

trifluoroacetic acid allowed accelerated reaction times and enhanced yields. Yoon hypothesised the addition of trifluoroacetic acid protonates the Michael acceptor's carbonyl conferring enone **1.127**, a further electron deficient species. The activated enone intermediate (**1.127**) facilitates the addition of the α-amino radical (**1.123**) and hence enhances this process in contrast to Reiser *et al*.

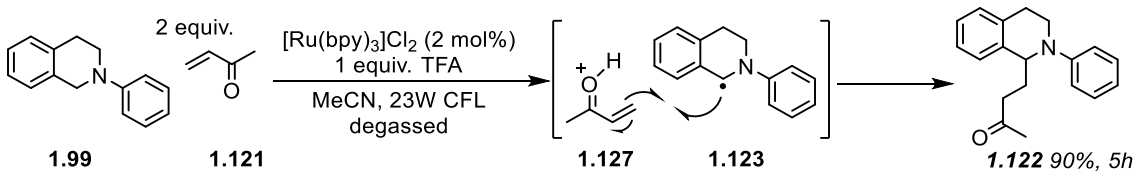

Figure 1.25: Yoon's Brønsted acid mediated intermolecular 1,2-radical addition.

Nishibayashi expanded the scope of this transformation towards a variety of aniline derivatives.[159] Proceeding via the same general mechanism as Reiser and Yoon, photocatalyst $[Ir(ppy)_2(dtbbpy)]PF_6$ was utilised to facilitate the generation of an α-amino radical with ensuing 1,2-intermolecular radical addition to highly electron deficient acceptors bearing two electron withdrawing groups. Nishibayashi noted that solvent choice was critical to the reaction's success, with NMP permitting success while no product was observed by utilising common polar solvents such as MeCN or MeOH. To determine whether this process occurs via a radical pathway, Nishibayashi conducted a control experiment in which cyclopropyl functionalised radical acceptor **1.132** was submitted to the developed the reaction conditions. Under these conditions, the ring opened product (**1.134**) was observed in 64% yield, consistent with the hypothesised radical pathway.

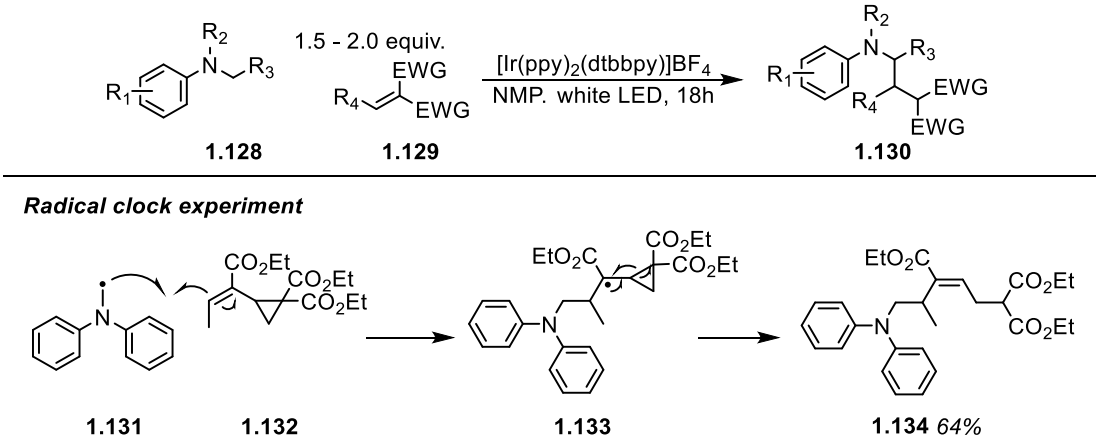

Figure 1.26: Nishibayashi's visible-light mediated intermolecular 1,2-radical addition.

Since these initial reports, a variety of methodologies have been developed via incorporation of α-amino radicals as key intermediates. These transformations include: other intermolecular radical additions,[160-163] cyclisations[144, 163] and radical-radical coupling.[164-169]

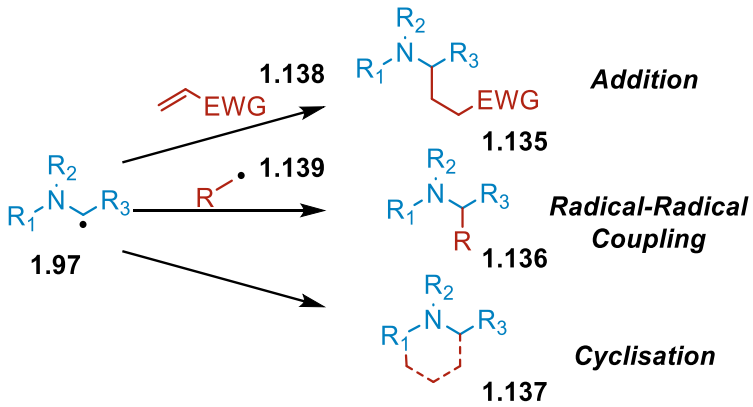

Figure 1.27: Reactivity pathways of an α-amino radical.

α-Amino radicals have been accessed by other protocols beyond direct oxidation of an amine substrate. This includes utilisation of substrates susceptible to degradation to the α-amino radical under photocatalytic conditions. α-amino radicals have been accessed from precursors including amino acids,[160, 167, 170-172] NHP esters[111, 173] and α-silyl amines.[174-175] This protocol has broadened the scope of substrates available for accessing α-amino radicals, while bypassing direct oxidation of the amine enables substrates with higher oxidation potentials to be utilised. In the presence of base, amino acids photo

oxidatively decarboxylate to the corresponding α-amino radicals, while further functionalisation of the carboxylic acid moiety to an NHP ester provides a reductive approach towards α-amino radical formation.

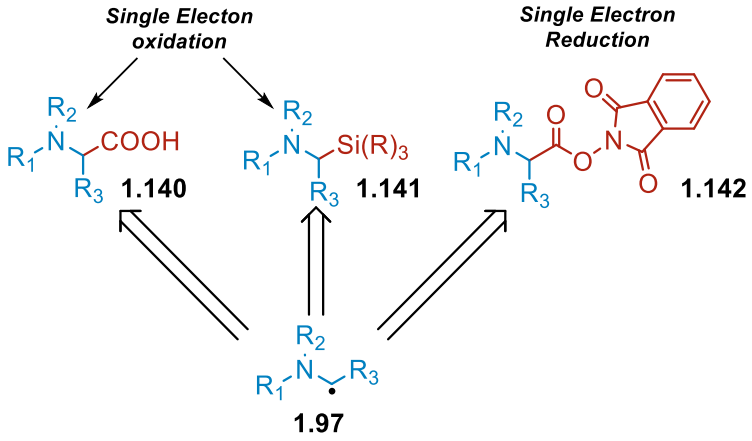

Figure 128: Generation of α-amino radicals via precursor substrates.

1.5.2 Reductive Approaches for the Visible Light Mediated α-Functionalisation of Amines

Another reductive technique to engage α-amino radicals involves the single electron reduction of imines.[176] Harnessing a reductive pathway enables the controlled synthesis of α-amino radicals from imines, further broadening the scope of compatible coupling partners. However, in contrast to an oxidative pathway, reductive α-amino radical formation has been seldom explored, due to the energy demanding reduction potential of the imine, hindering its access (approximately -2.0V vs SCE[176]).

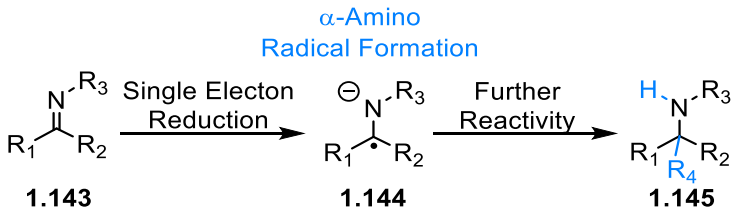

Figure 1.29: Photoreductive generation of an α-amino radical.

Hager and MacMillan first described the reductive generation of α-amino radicals with photoredox catalysis reporting the synthesis of 1,2-amino ethers through coupling *N*-aryl

Schiff bases and benzyl ethers.[177] As highlighted in figure 1.30, MacMillan proposes that a proton coupled electron transfer (PCET) process between triplet $[Ir(ppy)_2(dtbbpy)]PF_6$ and lithium acetate simultaneously oxidises and deprotonates methyl thioglycolate to thiol radical **1.149'**. Radical **1.149'** subsequently abstracts an α-ether hydrogen of **1.147** producing **1.147'**. Hager and Macmillan stipulate that the photocatalyst is regenerated via the single electron reduction of *N*-aryl imine **1.146** to the corresponding α-amino radical (**1.146'**). Radical-radical coupling is then hypothesised to assemble the desired 1,2-aminoether (**1.148**).

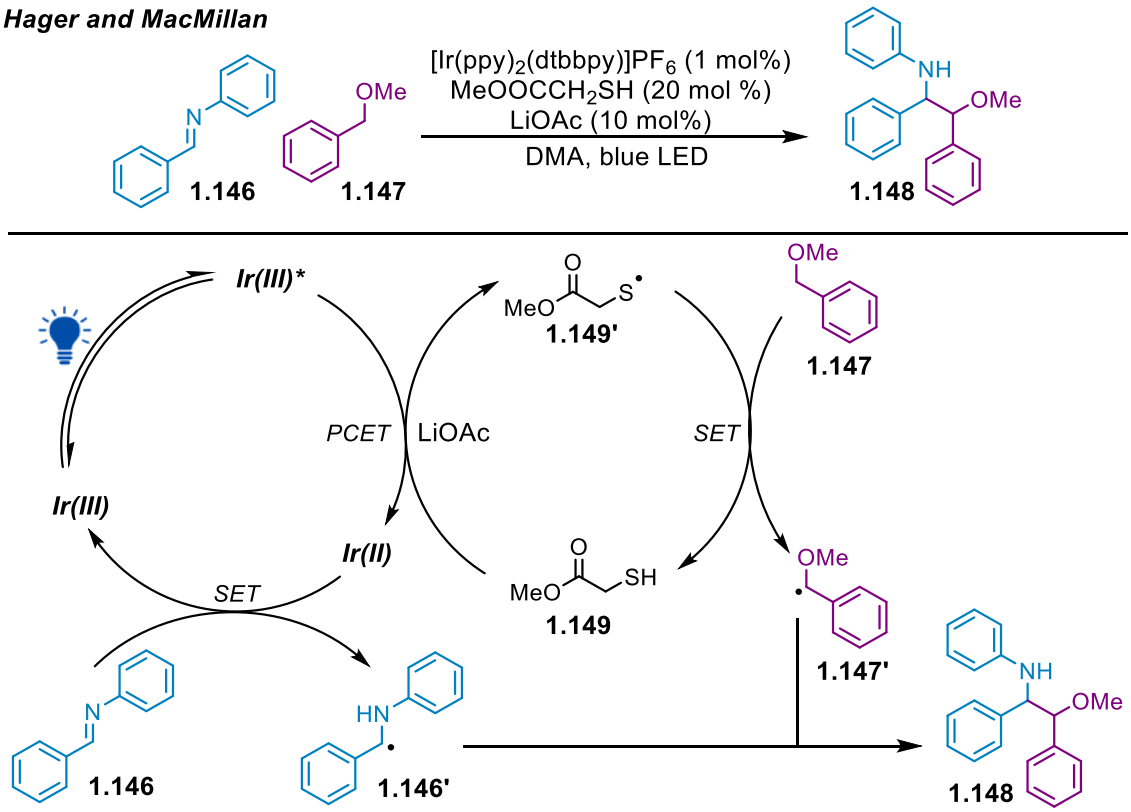

Figure 1.30: The first report of the reductive generation of α-amino radicals from imines- MacMillans synthesis of 1,2-aminoethers.

Hager and MacMillan's report paved the way for Rueping's reductive coupling of ketones, aldehydes and *N*-Benzyl Schiff bases.[178] Rueping proposed that upon irradiation, triplet $[Ir(II)(F(CF_3)ppy)_2(bpy)]$ is reductively quenched by tributylamine, imparting

1.152' and a highly reducing Ir(III) species. To overcome the energy demanding barrier of single electron reduction, Reuping hypothesises that PCET between [Ir(III)(F(CF_3)ppy)$_2$(bpy)], **1.152'** and **1.150** is achieved via either a 2-center-3-electron intermediate (**1.153**) or hydrogen bonding with an ammonium salt (**1.154**) - reducing the imines reduction potential. The activation of the imine promotes subsequent single electron reduction, regenerating the photocatalyst and furnishing α-amino radical **1.150'**. The α-amino radical proceeds to dimerize, conferring the reductively coupled product. Rueping was able to access a broad scope of substrates encompassing ketones, aldehydes and Schiff bases via this methodology.

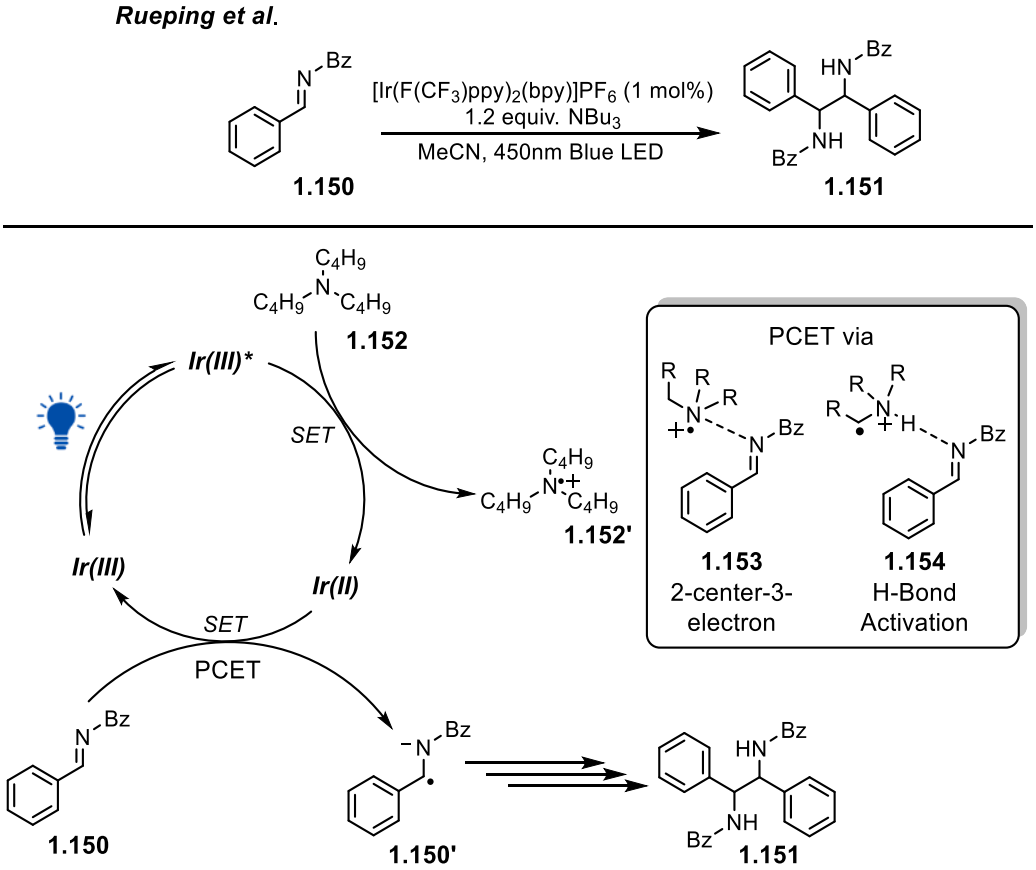

Figure 1.31: Rueping's visible light mediated reductive coupling of imines.

Rueping's report provided insight into the reductive pathway of α-amino radical formation and has inspired several research groups to similarly utilise imines for the α-functionalisation of amines. Further transformations have included: nucleophilic radical

additions,[179-181] radical-radical coupling,[182-184] reductive amination[185-187] and has further been applied towards enantioselective C-C bond formation.[182, 188]

1.6 Photoredox Chemistry Enabled by Flow

Photoredox catalysis is typically limited when processing larger quantities, primarily due to the strong absorption coefficient of the photocatalyst, inhibiting transmittance of light throughout a reaction vessel.[189] The Beer-Lambert-Bouger law dictates that the photocatalyst absorbs the majority of light irradiating a reaction vessel within the first few millimetres of the reaction vessel with the amount of light transmitted through a solution decaying via an exponential function with path length (figure 1.32). This corresponds to an uneven absorbance of light throughout a solution, hence, photoredox processes are typically constrained with larger reaction vessels. Flow chemistry has been utilised to enable the efficient processing of large scale photoredox reactions.

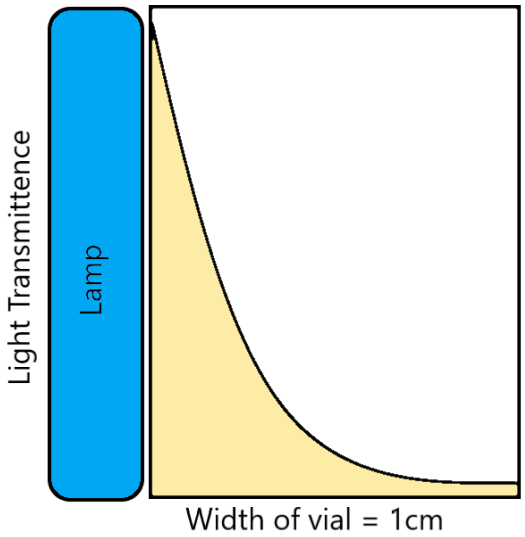

Figure 1.32: Transmittance of light through a photocatalytic reaction.

Flow chemistry is characterised by the continuous pumping of two or more reagents into a flow reactor where they mix, inducing reactivity.[190] Substitution of the reaction vessel from glassware to narrow tubing confers several advantages including: improved heat

transfer, efficient mixing and the ability to conduct reactions under pressure – permitting utilisation of pressurised gaseous reagents and simultaneously enabling temperatures beyond the typical solvent boiling point.[190-191] These benefits improve the robustness of chemical reactions, resulting in enhanced yields and reduced reaction times. Scaling processes via a flow protocol allows for an increased throughput while allowing enhanced safety due to the reduced quantity of hazardous intermediates generated at a given point.[190-191] Utilisation of flow methodology has enabled improved safety of highly exothermic processes and intermediates such as organolithium[192] and diazomethane[193] reagents, while high pressures of toxic and flammable gases such as carbon monoxide can also be accessed with ease.[194]

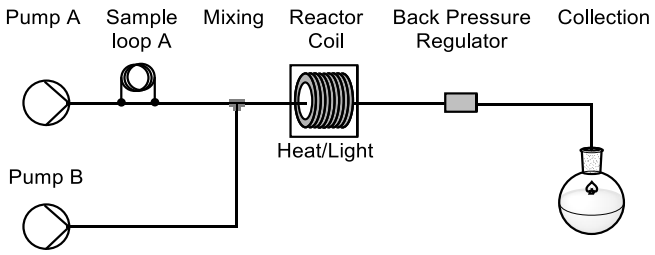

Figure 1.33: Basic configuration of a flow reaction.

Due to the poor attenuation of photons in a reaction flask, photoredox chemistry greatly suffers when processing larger volumes. By substituting glassware for narrow tubing, an increased surface area to volume ratio is obtained- enhancing the reaction's potential for photon absorption. The application of flow engineering to photoredox catalysis has profoundly enhanced its efficiency, enabling reduced reaction times and increased reaction yields while conferring the ability to scale these processes.

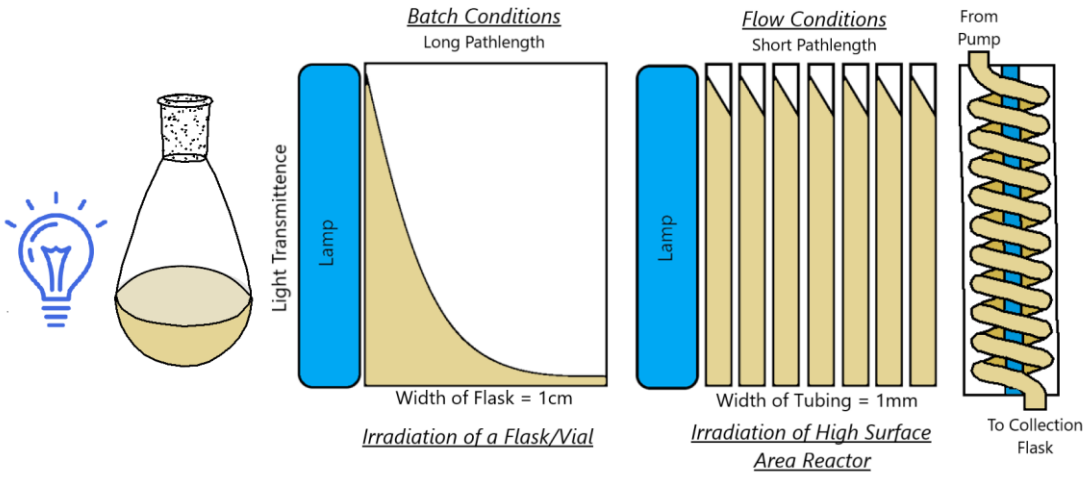

Figure 1.34: Transmittance of light through a batch reactor vs. flow reactor.

The first application of flow chemistry towards photoredox chemistry was in 2012 when Seeberger's laboratory transferred 4 previously established reactions to flow protocols.[195] The reactions optimised for flow included: the reduction of phenyl azides to the corresponding aniline,[196] the protodehalogenation of α-chloro esters,[123] the visible-light induced ring-opening of chalcone-α,β-epoxide[197] and the bromination of alcohols.[198] Seeberger noted that transferring these methodologies to a flow protocol conferred several improvements including: increased reaction scale, rapid reaction times (less than 30 minutes), lower photocatalyst loadings and in specific reactions, the absence of co-reagents. Seeberger demonstrated the synthetic potential of flow processing in photoredox chemistry and foresaw the potential impact it would have on synthetic chemistry.

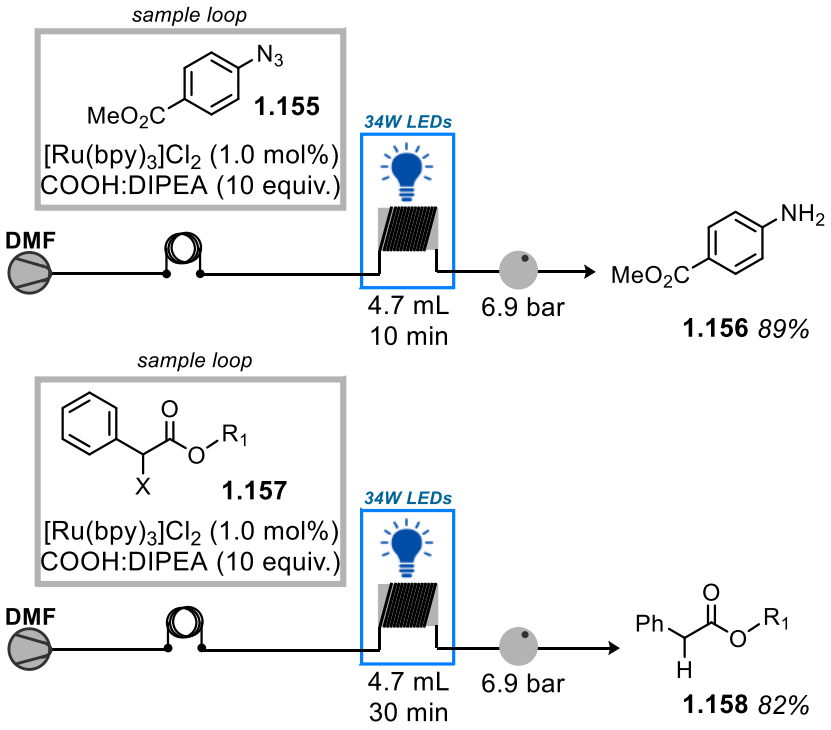

Figure 1.35: Representative examples of Seeberger's optimisation of photoredox processes from batch to flow processing.

Concurrently, a collaboration between the Jamison and Stephenson groups hypothesised the potential benefits flow chemistry could impart on photocatalytic processes.[199] They postulated that the slower reaction rates observed by photoredox processes at increased scales were influenced by the inefficient attenuation of light throughout a reaction (imparted by the Beer-Lambert-Bouger law). To determine whether flow processing would negate this issue, Stephenson and Jamison adapted the photooxidative iminium generation of THIQ in the presence of bromotrichloromethane[131] for a flow setup. An in-house built flow reactor involving coiled transparent polytetrafluoroethylene (PTFE) tubing wrapped around two test tubes corresponding to a 479 µL volume was utilised for this optimisation. Complete iminium formation was observed at a residence time of 0.5 minutes. This intermediate was then intercepted through the addition of a variety of pronucleophiles producing the α-alkylated product in excellent yields. This rapid reactivity allowed the facile scale up of this process to gram scale, enabling a 5.75 mmol

h^{-1} throughput via flow in contrast to 0.24 mmol h^{-1} in batch. Jamison and Stephenson highlighted the potential to further increase the throughput of this process by increasing the internal volume of the flow reactor to enable the efficient scaling of photochemical reactions. At this point, a series of other visible light mediated processes were transferred to flow, all demonstrating similar improvements.

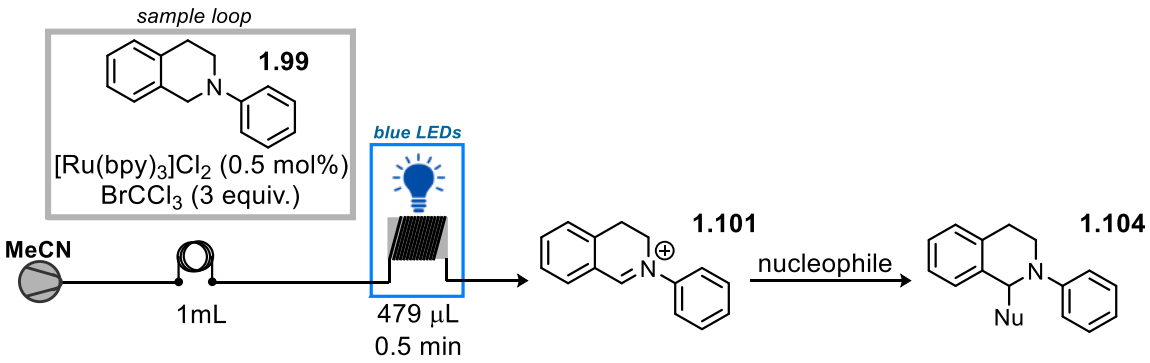

Figure 1.36: Formation of an imminium via flow and its consequent inteception with a nucleophile.

Concurrently to Seeberger, Jamison and Stephenson, the Gagné laboratory was independently exploring the application of flow methodology towards photoredox chemistry. Gagné *et al.* investigated the intermolecular coupling between α-bromo glycosides (**1.159**) and α,β unsaturated aldehydes (**1.160**).[200] Gagné observed that when decreasing the reactor size from a 25mL round bottom flask to an NMR tube (5mm internal diameter) that the turnover frequency of reaction was enhanced from 3.5 to 70 h^1 which was attributed to the reaction vessel's increased surface area to volume ratio. Gagné *et al.* further extended this principle by utilizing a flow system with tubing of 1.6 mm internal diameter. Again, Gagné noted that the increase of surface area to volume ratio improved turnover frequencies (120 h^{-1}), highlighting that the improved photon attenuation achieved via flow benefits the reaction conditions. Gagné further functionalised glycoside (**1.161**) to produce a variety of biologically relevant C-linked glycoconjugates.

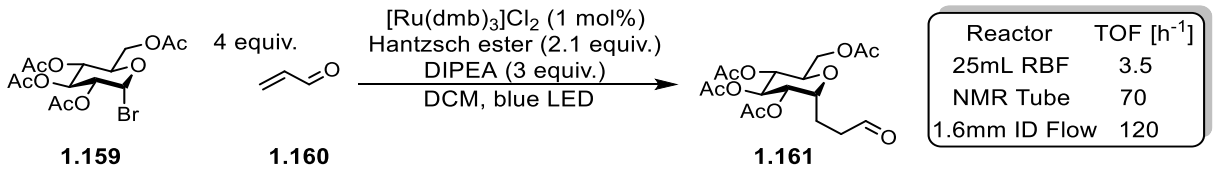

Figure 1.37: The visible light mediated functionalisation of bromine functionalised glycoside.

Flow chemistry has been well received by the photoredox community with many publications utilising the methodology to facilitate and enhance photoredox processes.[201] Flow engineering has also enabled gaseous reagents such as CO[202] and CO_2[203] to be easily incorporated into photoredox reactions. The enhanced processing capabilities that flow provides have benefitted photoredox processes immensely, facilitating scaling and enabling more favourable reaction conditions.

1.7 Aim

The primary objective of this thesis is to develop new protocols for the synthesis and α-functionalisation of aliphatic amines via visible-light mediated photoredox catalysis. Each methodology established makes use of the photocatalytic generation of α-amino radicals via oxidative and reductive pathways, then exploits their reactivity to access new reaction pathways. Upon optimisation of a new catalytic method, further enhancement of the conditions will be accomplished via flow chemistry. This thesis is presented as three chapters, each detailing a novel photochemical methodology; these include:

- The photocatalytic and chemoselective transfer hydrogenation of diarylimines.
- The decarboxylative α-alkylation of fused heterocyclic amines via a radical-radical coupling approach.
- The radical-radical coupling between fused heterocyclic amines and unactivated alkyl halides, achieved by accessing a tandem photocatalytic cycle.

1.8 Bibliography

1. Taylor, R. D.; MacCoss, M.; Lawson, A. D. G., *J. Med. Chem.* **2014,** *57* (14), 5845-5859.
2. Mirvakili, S. M.; Hunter, I. W., *Adv. Mater.* **2017,** *29* (4), 1604734.
3. Lawrence, S. A., *Amines: synthesis, properties and applications*. Cambridge University Press: 2004.
4. Evans, P. D., Biogenic Amines in the Insect Nervous System. In *Adv In Insect Phys*, Berridge, M. J.; Treherne, J. E.; Wigglesworth, V. B., Eds. Academic Press: 1980; Vol. 15, pp 317-473.
5. Downing, R. S.; Kunkeler, P. J.; van Bekkum, H., *Catal. Today* **1997,** *37* (2), 121-136.
6. Smith, T. A., *Food Chem.* **1981,** *6* (3), 169-200.
7. McGrath, N. A.; Brichacek, M.; Njardarson, J. T., *J. Chem. Educ.* **2010,** *87* (12), 1348-1349.
8. Kurti, L.; Czakó, B., *Strategic applications of named reactions in organic synthesis*. Elsevier: 2005.
9. Mundy, B. P.; Ellerd, M. G.; Favaloro, F. G., *Name Reactions and Reagents in Organic Synthesis*. John Wiley & Sons: 2005.
10. Carey, J. S.; Laffan, D.; Thomson, C.; Williams, M. T., *Org. Biomol. Chem.* **2006,** *4* (12), 2337-2347.
11. Brown, D. G.; Boström, J., *J. Med. Chem.* **2016,** *59* (10), 4443-4458.
12. Pelckmans, M.; Renders, T.; Van de Vyver, S.; Sels, B. F., *Green Chem.* **2017,** *19* (22), 5303-5331.
13. Li, B.; Sortais, J.-B.; Darcel, C., *RSC Adv.* **2016,** *6* (62), 57603-57625.
14. Omprakash Rathi, J.; Subray Shankarling, G., *ChemistrySelect* **2020,** *5* (23), 6861-6893.
15. Mitchell, E. A.; Peschiulli, A.; Lefevre, N.; Meerpoel, L.; Maes, B. U. W., *Chem. Eur. J.* **2012,** *18* (33), 10092-10142.
16. Qin, Y.; Lv, J.; Luo, S., *Tetrahedron Lett.* **2014,** *55* (2), 551-558.
17. Shang, M.; Chan, J. Z.; Cao, M.; Chang, Y.; Wang, Q.; Cook, B.; Torker, S.; Wasa, M., *J. Am. Chem. Soc.* **2018,** *140* (33), 10593-10601.
18. Cheng, M.-X.; Yang, S.-D., *Synlett* **2017,** *28* (02), 159-174.
19. Chen, W.; Ma, L.; Paul, A.; Seidel, D., *Nat. Chem.* **2018,** *10* (2), 165-169.
20. Hoppe, D.; Hense, T., *Angew. Chem. Int. Ed.* **1997,** *36* (21), 2282-2316.
21. Beak, P.; Basu, A.; Gallagher, D. J.; Park, Y. S.; Thayumanavan, S., *Acc. Chem. Res.* **1996,** *29* (11), 552-560.
22. McGrath, M. J.; Bilke, J. L.; O'Brien, P., *Chem. Commun.* **2006,** (24), 2607-2609.
23. Dearden, M. J.; Firkin, C. R.; Hermet, J.-P. R.; O'Brien, P., *J. Am. Chem. Soc.* **2002,** *124* (40), 11870-11871.
24. Barker, G.; McGrath, J. L.; Klapars, A.; Stead, D.; Zhou, G.; Campos, K. R.; O'Brien, P., *J. Org. Chem.* **2011,** *76* (15), 5936-5953.
25. Schwindeman, J. A.; Woltermann, C. J.; Letchford, R. J., *J Chem Health Saf* **2002,** *9* (3), 6-11.
26. Gau, M. R.; Zdilla, M. J., *JoVE* **2016,** (117), e54705.
27. Li, C.-J., *Acc. Chem. Res.* **2009,** *42* (2), 335-344.
28. Scheuermann, C. J., *Chem. Asian J.* **2010,** *5* (3), 436-451.
29. Girard, S. A.; Knauber, T.; Li, C.-J., *Angew. Chem. Int. Ed.* **2014,** *53* (1), 74-100.

30. Huang, C.-Y.; Kang, H.; Li, J.; Li, C.-J., *J. Org. Chem.* **2019,** *84* (20), 12705-12721.
31. Xu, X.; Li, X., *Org. Lett.* **2009,** *11* (4), 1027-1029.
32. Shu, X.-Z.; Xia, X.-F.; Yang, Y.-F.; Ji, K.-G.; Liu, X.-Y.; Liang, Y.-M., *J. Org. Chem.* **2009,** *74* (19), 7464-7469.
33. Tanoue, A.; Yoo, W.-J.; Kobayashi, S., *Org. Lett.* **2014,** *16* (9), 2346-2349.
34. Brzozowski, M.; Forni, J. A.; Paul Savage, G.; Polyzos, A., *Chem. Commun.* **2015,** *51* (2), 334-337.
35. Richter, H.; García Mancheño, O., *Eur. J. Org. Chem* **2010,** *2010* (23), 4460-4467.
36. Zhang, W.; Yang, S.; Shen, Z., *Adv. Synth. Catal.* **2016,** *358* (15), 2392-2397.
37. Shankaraiah, N.; Pilli, R. A.; Santos, L. S., *Tetrahedron Lett.* **2008,** *49* (34), 5098-5100.
38. Zhang, C.; De, C. K.; Mal, R.; Seidel, D., *J. Am. Chem. Soc.* **2008,** *130* (2), 416-417.
39. Zhang, C.; Murarka, S.; Seidel, D., *J. Org. Chem.* **2009,** *74* (1), 419-422.
40. Zhao, L.; Li, C.-J., *Angew. Chem. Int. Ed.* **2008,** *47* (37), 7075-7078.
41. Chao-Jun, L.; Zhiping, L., *Pure Appl. Chem.* **2006,** *78* (5), 935-945.
42. Pastine, S. J.; Gribkov, D. V.; Sames, D., *J. Am. Chem. Soc.* **2006,** *128* (44), 14220-14221.
43. Chen, L.; Yang, Y.; Liu, L.; Gao, Q.; Xu, S., *J. Am. Chem. Soc.* **2020,** *142* (28), 12062-12068.
44. Chu, J.-H.; Huang, H.-P.; Hsu, W.-T.; Chen, S.-T.; Wu, M.-J., *Organometallics* **2014,** *33* (5), 1190-1204.
45. Prokopcová, H.; Bergman, S. D.; Aelvoet, K.; Smout, V.; Herrebout, W.; Van der Veken, B.; Meerpoel, L.; Maes, B. U. W., *Chem. Eur. J.* **2010,** *16* (44), 13063-13067.
46. Sambiagio, C.; Schönbauer, D.; Blieck, R.; Dao-Huy, T.; Pototschnig, G.; Schaaf, P.; Wiesinger, T.; Zia, M. F.; Wencel-Delord, J.; Besset, T.; Maes, B. U. W.; Schnürch, M., *Chem. Soc. Rev.* **2018,** *47* (17), 6603-6743.
47. Hiller, K. O.; Asmus, K. D., *J. Phys. Chem.* **1983,** *87* (19), 3682-3688.
48. Citterio, A.; Gentile, A.; Minisci, F.; Serravalle, M.; Ventura, S., *J. Org. Chem.* **1984,** *49* (18), 3364-3367.
49. Wood, M. E.; Bissiriou, S.; Lowe, C.; Norrish, A. M.; Sénéchal, K.; Windeatt, K. M.; Coles, S. J.; Hursthouse, M. B., *Org. Biomol. Chem.* **2010,** *8* (20), 4653-4665.
50. Dénès, F.; Beaufils, F.; Renaud, P., *Org. Lett.* **2007,** *9* (21), 4375-4378.
51. Chowdhry, M. I.; Horton, P. N.; Hursthouse, M. B.; Wood, M. E., *Tetrahedron Lett.* **2009,** *50* (26), 3400-3403.
52. De Vleeschouwer, F.; Van Speybroeck, V.; Waroquier, M.; Geerlings, P.; De Proft, F., *Org. Lett.* **2007,** *9* (14), 2721-2724.
53. Jackl, M. K.; Kreituss, I.; Bode, J. W., *Org. Lett.* **2016,** *18* (8), 1713-1715.
54. Chatgilialoglu, C., *Organosilanes in radical chemistry*. John Wiley & Sons: 2004.
55. Studer, A.; Amrein, S., *Angew. Chem. Int. Ed.* **2000,** *39* (17), 3080-3082.
56. Balta, D. K.; Arsu, N.; Yagci, Y.; Jockusch, S.; Turro, N. J., *Macromolecules* **2007,** *40* (12), 4138-4141.
57. Campos, P. J.; Arranz, J.; Rodríguez, M. A., *Tetrahedron* **2000,** *56* (37), 7285-7289.
58. Ortega, M.; Rodríguez, M. A.; Campos, P. J., *Tetrahedron* **2005,** *61* (49), 11686-11691.
59. Ciamician, G., *Science* **1912,** *36* (926), 385-394.
60. Stephenson, C. R. J.; Yoon, T., *Acc. Chem. Res.* **2016,** *49* (10), 2059-2060.

61. Narayanam, J. M. R.; Stephenson, C. R. J., *Chem. Soc. Rev.* **2011,** *40* (1), 102-113.
62. Xuan, J.; Xiao, W.-J., *Angew. Chem. Int. Ed.* **2012,** *51* (28), 6828-6838.
63. Shaw, M. H.; Twilton, J.; MacMillan, D. W. C., *J. Org. Chem.* **2016,** *81* (16), 6898-6926.
64. Jain, A.; Ameta, C., *Kinet. Catal.* **2020,** *61* (2), 242-268.
65. Reckenthäler, M.; Griesbeck, A. G., *Adv. Synth. Catal.* **2013,** *355* (14-15), 2727-2744.
66. Filip, T., *Phys. Sci. Rev.* **2019,** *5* (4), 171.
67. Paria, S.; Reiser, O., *ChemCatChem* **2014,** *6* (9), 2477-2483.
68. Hernandez-Perez, A. C.; Collins, S. K., *Acc. Chem. Res.* **2016,** *49* (8), 1557-1565.
69. Nicholls, T. P.; Bissember, A. C., *Tetrahedron Lett.* **2019,** *60* (32), 150883.
70. Stevenson, S. M.; Shores, M. P.; Ferreira, E. M., *Angew. Chem. Int. Ed.* **2015,** *54* (22), 6506-6510.
71. Higgins, R. F.; Fatur, S. M.; Shepard, S. G.; Stevenson, S. M.; Boston, D. J.; Ferreira, E. M.; Damrauer, N. H.; Rappé, A. K.; Shores, M. P., *J. Am. Chem. Soc.* **2016,** *138* (16), 5451-5464.
72. Otto, S.; Nauth, A. M.; Ermilov, E.; Scholz, N.; Friedrich, A.; Resch-Genger, U.; Lochbrunner, S.; Opatz, T.; Heinze, K., *ChemPhotoChem* **2017,** *1* (8), 344-349.
73. Qiao, Y.; Yang, Q.; Schelter, E. J., *Angew. Chem. Int. Ed.* **2018,** *57* (34), 10999-11003.
74. Hu, A.; Guo, J.-J.; Pan, H.; Tang, H.; Gao, Z.; Zuo, Z., *J. Am. Chem. Soc.* **2018,** *140* (5), 1612-1616.
75. Yin, H.; Jin, Y.; Hertzog, J. E.; Mullane, K. C.; Carroll, P. J.; Manor, B. C.; Anna, J. M.; Schelter, E. J., *J. Am. Chem. Soc.* **2016,** *138* (50), 16266-16273.
76. Hu, A.; Guo, J.-J.; Pan, H.; Zuo, Z., *Science* **2018,** *361* (6403), 668-672.
77. Zhang, J.; Campolo, D.; Dumur, F.; Xiao, P.; Fouassier, J. P.; Gigmes, D.; Lalevée, J., *J. Chem. Soc., Perkin Trans. 2* **2015,** *53* (1), 42-49.
78. Xu, R.; Cai, C., *Chem. Commun.* **2019,** *55* (30), 4383-4386.
79. Kumar, P.; Singh, G.; Tripathi, D.; Jain, S. L., *RSC Adv.* **2014,** *4* (92), 50331-50337.
80. Rybicka-Jasińska, K.; Shan, W.; Zawada, K.; Kadish, K. M.; Gryko, D., *J. Am. Chem. Soc.* **2016,** *138* (47), 15451-15458.
81. Shanmugam, S.; Xu, J.; Boyer, C., *J. Am. Chem. Soc.* **2015,** *137* (28), 9174-9185.
82. Xue, Q.; Xie, J.; Jin, H.; Cheng, Y.; Zhu, C., *Org. Biomol. Chem.* **2013,** *11* (10), 1606-1609.
83. Xie, J.; Shi, S.; Zhang, T.; Mehrkens, N.; Rudolph, M.; Hashmi, A. S. K., *Angew. Chem. Int. Ed.* **2015,** *54* (20), 6046-6050.
84. Zhou, W.-J.; Cao, G.-M.; Shen, G.; Zhu, X.-Y.; Gui, Y.-Y.; Ye, J.-H.; Sun, L.; Liao, L.-L.; Li, J.; Yu, D.-G., *Angew. Chem. Int. Ed.* **2017,** *56* (49), 15683-15687.
85. Czyz, M. L.; Weragoda, G. K.; Horngren, T. H.; Connell, T. U.; Gomez, D.; O'Hair, R. A. J.; Polyzos, A., *Chem. Sci.* **2020,** *11* (9), 2455-2463.
86. Hsu, Y.-C.; Wang, V. C. C.; Au-Yeung, K.-C.; Tsai, C.-Y.; Chang, C.-C.; Lin, B.-C.; Chan, Y.-T.; Hsu, C.-P.; Yap, G. P. A.; Jurca, T.; Ong, T.-G., *Angew. Chem. Int. Ed.* **2018,** *57* (17), 4622-4626.
87. Hari, D. P.; Konig, B., *Chem. Commun.* **2014,** *50* (51), 6688-6699.
88. Guo, W.; Lu, L. Q.; Wang, Y.; Wang, Y. N.; Chen, J. R.; Xiao, W. J., *Angew. Chem.* **2015,** *127* (7), 2293-2297.
89. Chen, L.; Chao, C. S.; Pan, Y.; Dong, S.; Teo, Y. C.; Wang, J.; Tan, C.-H., *Org. Biomol. Chem.* **2013,** *11* (35), 5922-5925.

90. Pan, Y.; Wang, S.; Kee, C. W.; Dubuisson, E.; Yang, Y.; Loh, K. P.; Tan, C.-H., *Green Chem.* **2011,** *13* (12), 3341-3344.
91. Pan, Y.; Kee, C. W.; Chen, L.; Tan, C.-H., *Green Chem.* **2011,** *13* (10), 2682-2685.
92. Kumar, G.; Verma, S.; Ansari, A.; Khan, N.-u. H.; Kureshy, R. I., *Catal. Commun.* **2017,** *99*, 94-99.
93. Zhang, J.-J.; Cheng, Y.-B.; Duan, X.-H., *Chin. J. Chem.* **2017,** *35* (3), 311-315.
94. Ghosh, I.; König, B., *Angew. Chem. Int. Ed.* **2016,** *55* (27), 7676-7679.
95. Perkowski, A. J.; Nicewicz, D. A., *J. Am. Chem. Soc.* **2013,** *135* (28), 10334-10337.
96. McManus, J. B.; Onuska, N. P. R.; Nicewicz, D. A., *J. Am. Chem. Soc.* **2018,** *140* (29), 9056-9060.
97. Luo, J.; Zhang, J., *ACS Catal.* **2016,** *6* (2), 873-877.
98. Shang, T.-Y.; Lu, L.-H.; Cao, Z.; Liu, Y.; He, W.-M.; Yu, B., *Chem. Commun.* **2019,** *55* (38), 5408-5419.
99. Romero, N. A.; Nicewicz, D. A., *Chem. Rev.* **2016,** *116* (17), 10075-10166.
100. Hedstrand, D. M.; Kruizinga, W. H.; Kellogg, R. M., *Tetrahedron Lett.* **1978,** *19* (14), 1255-1258.
101. Van Bergen, T. J.; Hedstrand, D. M.; Kruizinga, W. H.; Kellogg, R. M., *J. Org. Chem.* **1979,** *44* (26), 4953-4962.
102. Fukuzumi, S.; Hironaka, K.; Tanaka, T., *Chem. Lett.* **1982,** *11* (10), 1583-1586.
103. Hironaka, K.; Fukuzumi, S.; Tanaka, T., *J. Chem. Soc., Perkin Trans. 2* **1984,** *13* (10), 1705-1709.
104. Fukuzumi, S.; Mochizuki, S.; Tanaka, T., *J. Phys. Chem.* **1990,** *94* (2), 722-726.
105. Fukuzumi, S.; Mochizuki, S.; Tanaka, T., *J. Chem. Soc., Perkin Trans. 2* **1989,** *18* (10), 1583-1589.
106. Pac, C.; Ihama, M.; Yasuda, M.; Miyauchi, Y.; Sakurai, H., *J. Am. Chem. Soc.* **1981,** *103* (21), 6495-6497.
107. Nakamura, K.; Fujii, M.; Mekata, H.; Oka, S.; Ohno, A., *Chem. Lett.* **1986,** *15* (1), 87-88.
108. Fujii, M.; Nakamura, K.; Mekata, H.; Oka, S.; Ohno, A., *Bull. Chem. Soc. Jpn.* **1988,** *61* (2), 495-500.
109. Cano-Yelo, H.; Deronzier, A., *J. Chem. Soc., Perkin Trans. 2* **1984,** (6), 1093-1098.
110. Cano-Yelo, H.; Deronzier, A., *Tetrahedron Lett.* **1984,** *25* (48), 5517-5520.
111. Okada, K.; Okamoto, K.; Morita, N.; Okubo, K.; Oda, M., *J. Am. Chem. Soc.* **1991,** *113* (24), 9401-9402.
112. Okada, K.; Okubo, K.; Morita, N.; Oda, M., *Chem. Lett.* **1993,** *22* (12), 2021-2024.
113. Okada, K.; Okubo, K.; Morita, N.; Oda, M., *Tetrahedron Lett.* **1992,** *33* (48), 7377-7380.
114. Ischay, M. A.; Anzovino, M. E.; Du, J.; Yoon, T. P., *J. Am. Chem. Soc.* **2008,** *130* (39), 12886-12887.
115. Nicewicz, D. A.; MacMillan, D. W. C., *Science* **2008,** *322* (5898), 77-80.
116. Nagib, D. A.; Scott, M. E.; MacMillan, D. W. C., *J. Am. Chem. Soc.* **2009,** *131* (31), 10875-10877.
117. Koike, T.; Akita, M., *Chem. Lett.* **2009,** *38* (2), 166-167.
118. Hopkinson, M. N.; Sahoo, B.; Li, J.-L.; Glorius, F., *Chem. Eur. J.* **2014,** *20* (14), 3874-3886.

119. Gui, Y.-Y.; Sun, L.; Lu, Z.-P.; Yu, D.-G., *Org. Chem. Front.* **2016,** *3* (4), 522-526.
120. Zhang, H.-H.; Chen, H.; Zhu, C.; Yu, S., *Sci. China Chem.* **2020,** *63* (5), 637-647.
121. DeClue, M. S.; Monnard, P.-A.; Bailey, J. A.; Maurer, S. E.; Collis, G. E.; Ziock, H.-J.; Rasmussen, S.; Boncella, J. M., *J. Am. Chem. Soc.* **2009,** *131* (3), 931-933.
122. Borak, J. B.; Falvey, D. E., *J. Org. Chem.* **2009,** *74* (10), 3894-3899.
123. Narayanam, J. M. R.; Tucker, J. W.; Stephenson, C. R. J., *J. Am. Chem. Soc.* **2009,** *131* (25), 8756-8757.
124. Tucker, J. W.; Nguyen, J. D.; Narayanam, J. M. R.; Krabbe, S. W.; Stephenson, C. R. J., *Chem. Commun.* **2010,** *46* (27), 4985-4987.
125. Nguyen, J. D.; D'Amato, E. M.; Narayanam, J. M.; Stephenson, C. R., *Nat. Chem.* **2012,** *4* (10), 854-859.
126. Tucker, J. W.; Narayanam, J. M. R.; Krabbe, S. W.; Stephenson, C. R. J., *Org. Lett.* **2010,** *12* (2), 368-371.
127. Hu, J.; Wang, J.; Nguyen, T. H.; Zheng, N., *Beilstein J. Org. Chem.* **2013,** *9*, 1977-2001.
128. Shi, L.; Xia, W., *Chem. Soc. Rev.* **2012,** *41* (23), 7687-7697.
129. DeLaive, P. J.; Foreman, T. K.; Giannotti, C.; Whitten, D. G., *J. Am. Chem. Soc.* **1980,** *102* (17), 5627-5631.
130. Condie, A. G.; González-Gómez, J. C.; Stephenson, C. R. J., *J. Am. Chem. Soc.* **2010,** *132* (5), 1464-1465.
131. Freeman, D. B.; Furst, L.; Condie, A. G.; Stephenson, C. R. J., *Org. Lett.* **2012,** *14* (1), 94-97.
132. Hari, D. P.; König, B., *Org. Lett.* **2011,** *13* (15), 3852-3855.
133. Rueping, M.; Zhu, S.; Koenigs, R. M., *Chem. Commun.* **2011,** *47* (30), 8679-8681.
134. Rueping, M.; Zhu, S.; Koenigs, R. M., *Chem. Commun.* **2011,** *47* (47), 12709-12711.
135. Jia, Z.; Yang, Q.; Zhang, L.; Luo, S., *ACS Catal.* **2019,** *9* (4), 3589-3594.
136. He, Y.-H.; Xiang, Y.; Yang, D.-C.; Guan, Z., *Green Chem.* **2016,** *18* (19), 5325-5330.
137. To, W.-P.; Tong, G. S.-M.; Lu, W.; Ma, C.; Liu, J.; Chow, A. L.-F.; Che, C.-M., *Angew. Chem. Int. Ed.* **2012,** *51* (11), 2654-2657.
138. Liu, Q.; Li, Y.-N.; Zhang, H.-H.; Chen, B.; Tung, C.-H.; Wu, L.-Z., *Chem. Eur. J.* **2012,** *18* (2), 620-627.
139. Möhlmann, L.; Baar, M.; Rieß, J.; Antonietti, M.; Wang, X.; Blechert, S., *Adv. Synth. Catal.* **2012,** *354* (10), 1909-1913.
140. Bartling, H.; Eisenhofer, A.; König, B.; Gschwind, R. M., *J. Am. Chem. Soc.* **2016,** *138* (36), 11860-11871.
141. Neumann, M.; Zeitler, K., *Org. Lett.* **2012,** *14* (11), 2658-2661.
142. Rueping, M.; Vila, C.; Koenigs, R. M.; Poscharny, K.; Fabry, D. C., *Chem. Commun.* **2011,** *47* (8), 2360-2362.
143. DiRocco, D. A.; Rovis, T., *J. Am. Chem. Soc.* **2012,** *134* (19), 8094-8097.
144. Zou, Y.-Q.; Lu, L.-Q.; Fu, L.; Chang, N.-J.; Rong, J.; Chen, J.-R.; Xiao, W.-J., *Angew. Chem. Int. Ed.* **2011,** *50* (31), 7171-7175.
145. Rueping, M.; Leonori, D.; Poisson, T., *Chem. Commun.* **2011,** *47* (34), 9615-9617.
146. Li, S.; Yang, X.; Wang, Y.; Zhou, H.; Zhang, B.; Huang, G.; Zhang, Y.; Li, Y., *Adv. Synth. Catal.* **2018,** *360* (22), 4452-4456.
147. Benimana, S. E.; Cromwell, N. E.; Meer, H. N.; Marvin, C. C., *Tetrahedron Lett.* **2016,** *57* (46), 5062-5064.

148. Muralirajan, K.; Kancherla, R.; Rueping, M., *Angew. Chem. Int. Ed.* **2018,** *57* (45), 14787-14791.
149. Yilmaz, O.; Oderinde, M. S.; Emmert, M. H., *J. Org. Chem.* **2018,** *83* (18), 11089-11100.
150. Chen, H.; Fan, W.; Yuan, X.-A.; Yu, S., *Nat. Commun.* **2019,** *10* (1), 4743.
151. Chu, J. C. K.; Rovis, T., *Nature* **2016,** *539* (7628), 272-275.
152. Akula, P. S.; Hong, B.-C.; Lee, G.-H., *RSC Adv.* **2018,** *8* (35), 19580-19584.
153. Mathis, C. L.; Gist, B. M.; Frederickson, C. K.; Midkiff, K. M.; Marvin, C. C., *Tetrahedron Lett.* **2013,** *54* (16), 2101-2104.
154. Xuan, J.; Feng, Z.-J.; Duan, S.-W.; Xiao, W.-J., *RSC Adv.* **2012,** *2* (10), 4065-4068.
155. Xuan, J.; Cheng, Y.; An, J.; Lu, L.-Q.; Zhang, X.-X.; Xiao, W.-J., *Chem. Commun.* **2011,** *47* (29), 8337-8339.
156. McNally, A.; Prier, C. K.; MacMillan, D. W. C., *Science* **2011,** *334* (6059), 1114-1117.
157. Kohls, P.; Jadhav, D.; Pandey, G.; Reiser, O., *Org. Lett.* **2012,** *14* (3), 672-675.
158. Ruiz Espelt, L.; Wiensch, E. M.; Yoon, T. P., *J. Org. Chem.* **2013,** *78* (8), 4107-4114.
159. Miyake, Y.; Nakajima, K.; Nishibayashi, Y., *J. Am. Chem. Soc.* **2012,** *134* (7), 3338-3341.
160. Kölmel, D. K.; Loach, R. P.; Knauber, T.; Flanagan, M. E., *ChemMedChem* **2018,** *13* (20), 2159-2165.
161. Ashley, M. A.; Yamauchi, C.; Chu, J. C. K.; Otsuka, S.; Yorimitsu, H.; Rovis, T., *Angew. Chem. Int. Ed.* **2019,** *58* (12), 4002-4006.
162. Cai, S.; Zhao, X.; Wang, X.; Liu, Q.; Li, Z.; Wang, D. Z., *Angew. Chem. Int. Ed.* **2012,** *51* (32), 8050-8053.
163. Zhu, S.; Das, A.; Bui, L.; Zhou, H.; Curran, D. P.; Rueping, M., *J. Am. Chem. Soc.* **2013,** *135* (5), 1823-1829.
164. Pandey, G.; Tiwari, S. K.; Singh, B., *Tetrahedron Lett.* **2016,** *57* (40), 4480-4483.
165. Xie, J.; Yu, J.; Rudolph, M.; Rominger, F.; Hashmi, A. S. K., *Angew. Chem. Int. Ed.* **2016,** *55* (32), 9416-9421.
166. Xuan, J.; Zeng, T. T.; Feng, Z. J.; Deng, Q. H.; Chen, J. R.; Lu, L. Q.; Xiao, W. J.; Alper, H., *Angew. Chem.* **2015,** *127* (5), 1645-1648.
167. Zuo, Z.; MacMillan, D. W. C., *J. Am. Chem. Soc.* **2014,** *136* (14), 5257-5260.
168. Walker, M. M.; Koronkiewicz, B.; Chen, S.; Houk, K. N.; Mayer, J. M.; Ellman, J. A., *J. Am. Chem. Soc.* **2020,** *142* (18), 8194-8202.
169. Miyake, Y.; Nakajima, K.; Nishibayashi, Y., *Chem. Euro. J.* **2012,** *18* (51), 16473-16477.
170. Li, J.; Kong, M.; Qiao, B.; Lee, R.; Zhao, X.; Jiang, Z., *Nat. Commun.* **2018,** *9* (1), 2445.
171. Yin, Y.; Dai, Y.; Jia, H.; Li, J.; Bu, L.; Qiao, B.; Zhao, X.; Jiang, Z., *J. Am. Chem. Soc.* **2018,** *140* (19), 6083-6087.
172. Millet, A.; Lefebvre, Q.; Rueping, M., *Chem. Eur. J.* **2016,** *22* (38), 13464-13468.
173. Pratsch, G.; Lackner, G. L.; Overman, L. E., *J. Org. Chem.* **2015,** *80* (12), 6025-6036.
174. Miyake, Y.; Ashida, Y.; Nakajima, K.; Nishibayashi, Y., *Chem. Commun.* **2012,** *48* (55), 6966-6968.
175. Nakajima, K.; Kitagawa, M.; Ashida, Y.; Miyake, Y.; Nishibayashi, Y., *Chem. Commun.* **2014,** *50* (64), 8900-8903.

176. Leitch, J. A.; Rossolini, T.; Rogova, T.; Maitland, J. A. P.; Dixon, D. J., *ACS Catal.* **2020,** *10* (3), 2009-2025.
177. Hager, D.; Macmillan, D. W. C., *J. Am. Chem. Soc.* **2014,** *136* (49), 16986-16989.
178. Nakajima, M.; Fava, E.; Loescher, S.; Jiang, Z.; Rueping, M., *Angew. Chem. Int. Ed.* **2015,** *54* (30), 8828-8832.
179. Leitch, J. A.; Fuentes de Arriba, Angel L.; Tan, J.; Hoff, O.; Martínez, C. M.; Dixon, D. J., *Chem. Sci.* **2018,** *9* (32), 6653-6658.
180. Rossolini, T.; Leitch, J. A.; Grainger, R.; Dixon, D. J., *Org. Lett.* **2018,** *20* (21), 6794-6798.
181. Lee, K. N.; Lei, Z.; Ngai, M. Y., *J. Am. Chem. Soc.* **2017,** *139* (14), 5003-5006.
182. Uraguchi, D.; Kinoshita, N.; Kizu, T.; Ooi, T., *J. Am. Chem. Soc.* **2015,** *137* (43), 13768-13771.
183. Fava, E.; Millet, A.; Nakajima, M.; Loescher, S.; Rueping, M., *Angew. Chem. Int. Ed.* **2016,** *55* (23), 6776-6779.
184. Patel, N. R.; Kelly, C. B.; Siegenfeld, A. P.; Molander, G. A., *ACS Catal.* **2017,** *7* (3), 1766-1770.
185. Alam, R.; Molander, G. A., *Org. Lett.* **2018,** *20* (9), 2680-2684.
186. Rong, J.; Seeberger, P. H.; Gilmore, K., *Org. Lett.* **2018,** *20* (13), 4081-4085.
187. Guo, X.; Okamoto, Y.; Schreier, M. R.; Ward, T. R.; Wenger, O. S., *Eur. J. Org. Chem* **2019,** *2020* (10), 1288-1293.
188. Cao, K.; Tan, S. M.; Lee, R.; Yang, S.; Jia, H.; Zhao, X.; Qiao, B.; Jiang, Z., *J. Am. Chem. Soc.* **2019,** *141* (13), 5437-5443.
189. Gilmore, K.; Seeberger, P. H., *Chem. Rec.* **2014,** *14* (3), 410-418.
190. Plutschack, M. B.; Pieber, B.; Gilmore, K.; Seeberger, P. H., *Chem. Rev.* **2017,** *117* (18), 11796-11893.
191. Wegner, J.; Ceylan, S.; Kirschning, A., *Adv. Synth. Catal.* **2012,** *354* (1), 17-57.
192. Moon, S.-Y.; Jung, S.-H.; Bin Kim, U.; Kim, W.-S., *RSC Adv.* **2015,** *5* (97), 79385-79390.
193. Rossi, E.; Woehl, P.; Maggini, M., *Org. Process Res. Dev.* **2012,** *16* (5), 1146-1149.
194. Koos, P.; Gross, U.; Polyzos, A.; O'Brien, M.; Baxendale, I.; Ley, S. V., *Org. Biomol. Chem.* **2011,** *9* (20), 6903-6908.
195. Bou-Hamdan, F. R.; Seeberger, P. H., *Chem. Sci.* **2012,** *3* (5), 1612-1616.
196. Chen, Y.; Kamlet, A. S.; Steinman, J. B.; Liu, D. R., *Nat. Chem.* **2011,** *3* (2), 146-153.
197. Larraufie, M.-H.; Pellet, R.; Fensterbank, L.; Goddard, J.-P.; Lacôte, E.; Malacria, M.; Ollivier, C., *Angew. Chem. Int. Ed.* **2011,** *50* (19), 4463-4466.
198. Dai, C.; Narayanam, J. M. R.; Stephenson, C. R. J., *Nat. Chem.* **2011,** *3* (2), 140-145.
199. Tucker, J. W.; Zhang, Y.; Jamison, T. F.; Stephenson, C. R. J., *Angew. Chem. Int. Ed.* **2012,** *51* (17), 4144-4147.
200. Andrews, R. S.; Becker, J. J.; Gagné, M. R., *Angew. Chem. Int. Ed.* **2012,** *51* (17), 4140-4143.
201. Straathof, N. J. W.; Noël, T., Accelerating visible-light photoredox catalysis in continuous-flow reactors. In *Visible Light Photocatalysis in Organic Chemistry*, Wiley: 2018; pp 389-413.
202. Micic, N.; Polyzos, A., *Org. Lett.* **2018,** *20* (15), 4663-4666.
203. Seo, H.; Katcher, M. H.; Jamison, T. F., *Nat. Chem.* **2017,** *9* (5), 453-456.

Chapter 2: The Photocatalytic and Chemoselective Transfer Hydrogenation of Diarylimines

2.1 Introduction

The photooxidative generation of α-amino radicals provides an efficient route to the corresponding α-functionalised adducts.[1] However, this method of α-amino radical generation is accompanied by overoxidation generating a cationic iminium intermediate, limiting reactivity to nucleophilic attack from pronucleophiles. Despite this limitation, photo-oxidatively generated α-amino radical reactivity has been successfully developed (including nucleophilic radical addition[2-5] and radical-radical coupling[6-10]), however undesired iminium formation remains challenging. To address this, imines have recently been harnessed as α-amino radical precursors via a photoreductive pathway. This process provides a controlled pathway for the α-functionalisation of amines; avoiding the undesired cationic iminium pathway (figure 2.1). Comparatively, the photoreductive pathway is seldom explored in contrast to its photooxidative counterpart; this is likely due to the demanding reduction potential of imines (approximately -2.0 V vs SCE).

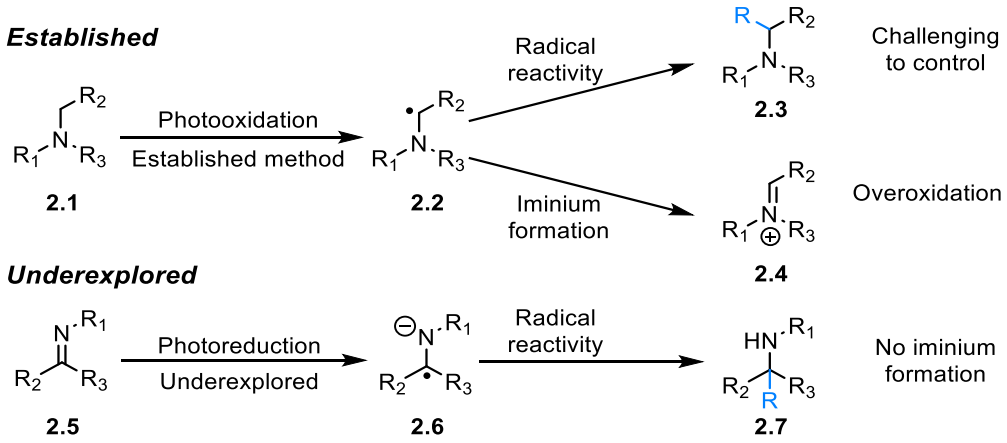

Figure 2.1: Generation of α-amino radicals via photooxidative and photoreductive methods.

2.1.1 The Photoreductive Formation of C-C Bonds

The photoreductive pathway has been harnessed to furnish carbon-carbon bond formation; first described in 2014 by Hager and MacMillan who synthesised 1,2-aminoethers, by coupling benzylic α-oxo radicals acquired from benzyl ethers (**2.9**) with α-amino radicals derived from *N*-aryl Schiff bases (**2.8**) (Figure 2.2).[11] Central to this approach is the reduction of the triplet excited state of photocatalyst $[Ir(III)(ppy)_2(dtbbpy)]PF_6$ via proton coupled electron transfer (PCET) with methyl thioglycolate; achieving simultaneous oxidation and deprotonation of methyl thioglycolate by the triplet photocatalyst and LiOAc, engendering thiol radical (**2.11'**). The reduced Ir(II) species is restored to its ground state via the single electron reduction of an *N*-aryl Schiff base (**2.8**) to the corresponding α-amino radical (**2.8'**). Abstraction of the α-hydrogen from a benzyl ether (**2.9**) by methyl thioglycolate radical (**2.11'**) furnishes the corresponding ketyl radical (**2.9'**); consequent radical-radical coupling furnishes the desired 1,2-amino-ether (**2.10**). Due to the difference in oxidation potentials, MacMillan highlights the need to harness PCET between methyl thioglycolate ($E_{1/2}$ = 0.85 V vs. SCE) and triplet $[Ir(ppy)_2(dtbbpy)]PF_6$ ($E_{1/2}$ = 0.66V vs. SCE) to stimulate initial oxidation, while the greater mismatch in reduction potential between *N*-aryl imines ($E_{1/2}$ = -1.98V vs SCE) and $[Ir(II)(ppy)_2(dtbbpy)]PF_6$ ($E_{1/2}$ = -1.51V vs. SCE) is not addressed. Stern-Volmer quenching demonstrates energy transfer between the excited state photocatalyst and the thiol in the presence of $N(Bu)_4OAc$, while minute interaction was observed directly with the imine. Hager and MacMillan's synthesis of 1,2-aminoethers represents the first report of the photoreductive pathway to generate α-amino radicals.

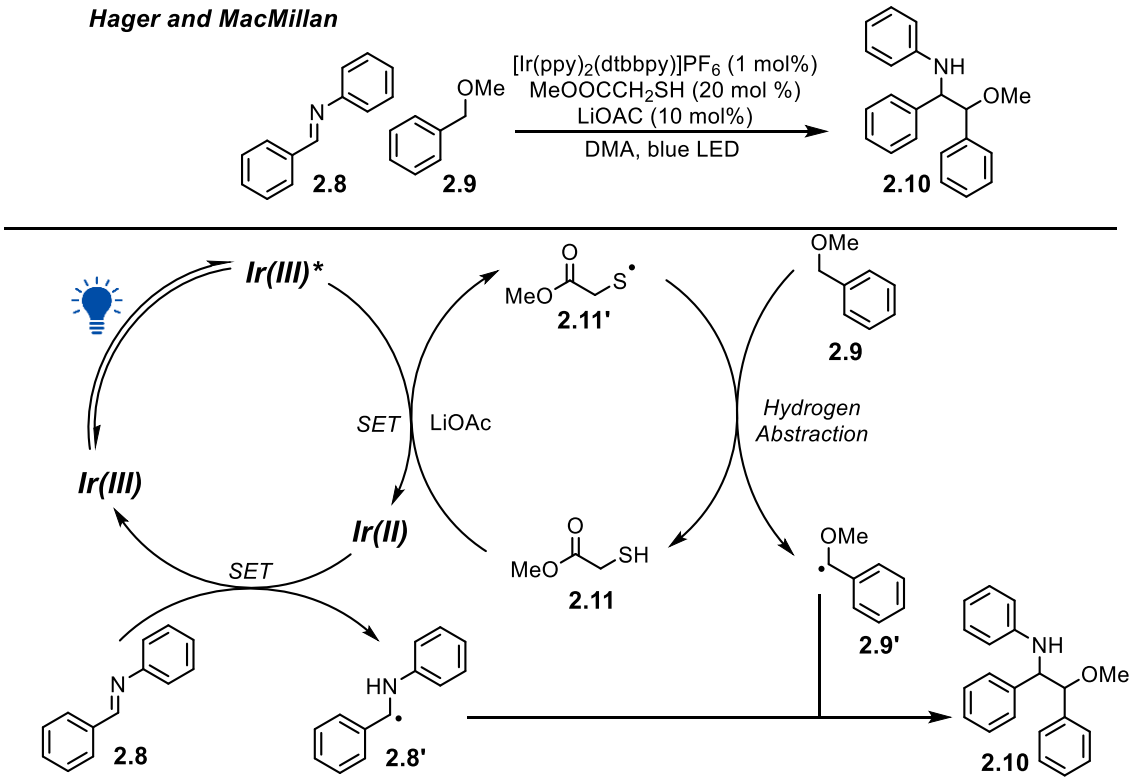

Figure 2.2: Hager and MacMillan's synthesis of 1,2-aminoethers via a photoreductive approach.

In 2015, Rueping's seminal publication described the reductive pinacol coupling of ketones, aldehydes and Schiff bases.[12] Rueping harnessed PCET to efficiently generate α-amino and ketyl radicals via a photoreductive pathway (figure 2.3). This process proceeds via the initial oxidation of tributylamine by triplet [Ir(III)(F(CF_3)ppy)$_2$(bpy)]PF_6 to generate a highly reducing Ir(II) species ($E_{1/2}$ = -1.69V vs. SCE), with consequent photoreductive α-amino radical generation from **2.12**, facilitated by PCET between the photocatalyst, imine and the tributylamine aminal radical. Rueping proposes that PCET activates the Schiff base via interaction with aminyl radical (**2.14'**) forming either a 2-center-3-electron intermediate (**2.15**) or hydrogen bonding with an ammonium salt (**2.16**). Both intermediates, **2.15** and **2.16** are hypothesised to decrease the imine's reduction potential, allowing single electron transfer with [Ir(II)(F(CF_3)ppy)$_2$(bpy)] and subsequently affording α-amino radical (**2.12'**) (Figure 2.3). Upon formation of α-amino radical **2.12'**, radical-radical dimerization bestows the corresponding aza-pinacol 1,2-

diamine product (**2.13**). A broad substrate scope was reported, encompassing imines, aldehydes and ketones. Rueping's proposal of PCET addresses the mismatch in reduction potential between unactivated imines and photocatalyst, with activation via intermediates **2.15** or **2.16** allowing the photoreductive generation of α-amino/ketyl radicals.

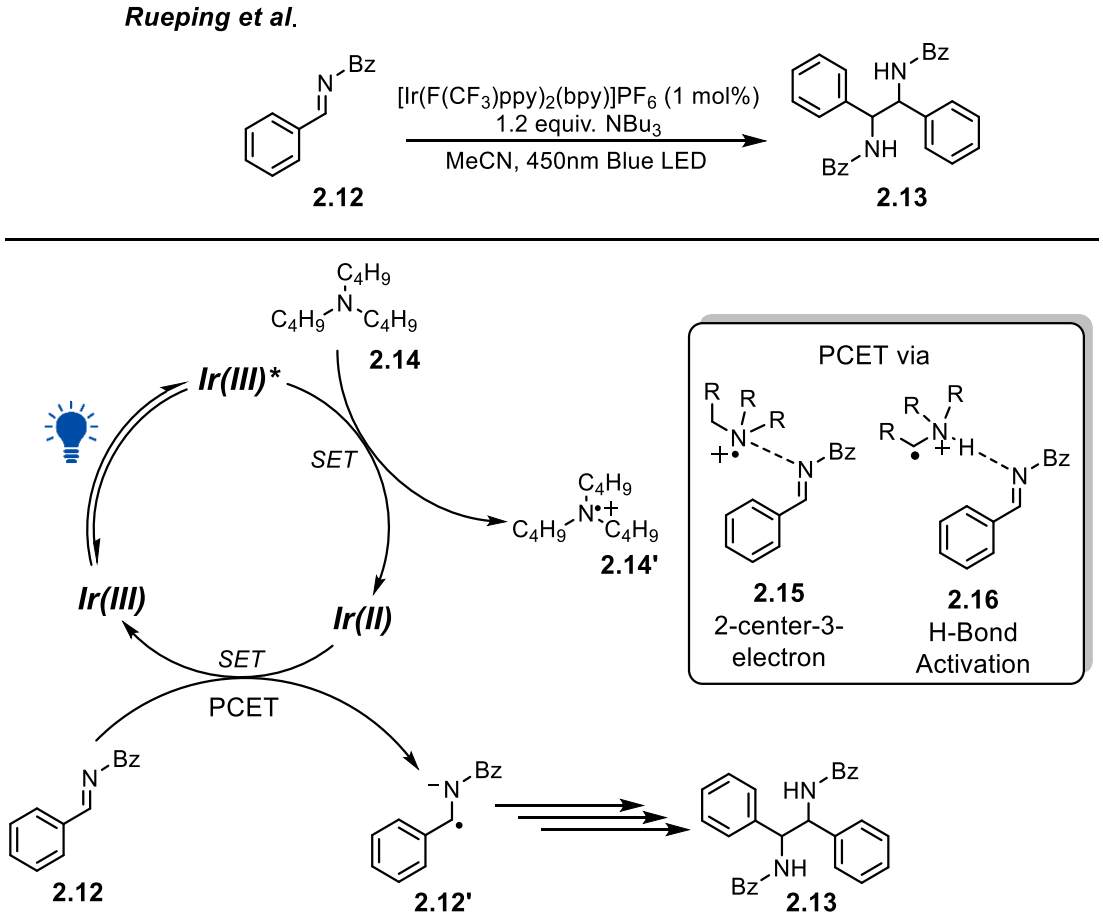

Figure 2.3: Rueping *et al.* light mediated aza-pinnacol coupling of *N*-benzyl aldimines via PCET.

The synthesis of unsymmetrical 1,2-diamines via photoredox catalysis was independently developed by both the Ooi[13] and Rueping[14] laboratories; each method involved the cross coupling of two distinct α-amino radicals generated by the photooxidation of an amine and photoreduction of an imine (figure 2.4). The addition of a chiral P-spiro arylaminophosphonium barfate (**2.20**) salt promoted the enantioselective coupling of *N*-sulfonyl protected imines (**2.17**) and diphenylmethylamines (**2.18**), merging Brønsted acid[15-19] and photoredox catalysis. Ooi *et al.* proposed that upon irradiation, triplet

[Ir(III)(ppy)$_2$(bpy)] oxidises diarylmethamine **2.18** with subsequent formation of an α-amino radical. [Ir(II)(ppy)$_2$(bpy)] is returned to its original state via the single electron reduction of a chiral Brønsted acid complexed sulfonyl-aldimine (**2.27**), generating a second α-amino radical (**2.23**). The two α-amino radicals undergo enatiofacial radical-radical coupling generating chiral 1,2-diamines with excellent stereo-control (figure 2.4), demonstrating excellent yields and enantiomeric excesses (85-97% ee). Ooi *et al.* were able to further expand this protocol by utilising α-silylamines as oxidative radical precurrsors.[20] In 2016, Rueping disclosed a conceptually similar protocol for the synthesis of unsymmetrical 1,2-diamines exploiting unactivated *N*-aryl Schiff bases and dimethylanilines also proceeding via a radial-radical coupling pathway in good yields.[14] This methodology was extended to the reductive coupling of benzaldehyde derivatives with dimethylanilines generating 1,2-aminoalcohols. Addition of electrofugal groups achieved the defunctionalized cross-coupled product, while α-esterimines conferred amino acid derivatives.

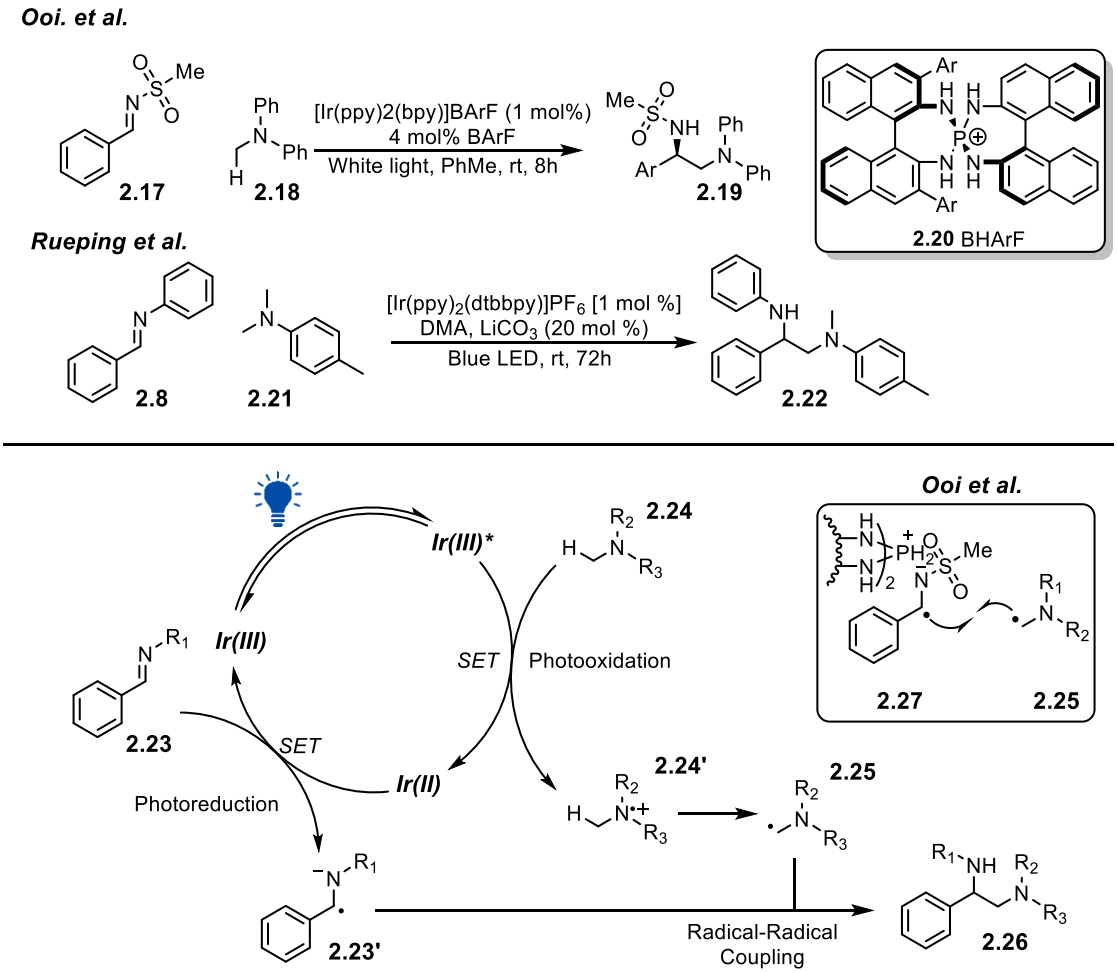

Figure 2.4: Ooi and Rueping's light mediated synthesis of unsymmetrical 1,2-diamines.

Several groups then reported the intermolecular 1,2-addition of α-amino radicals derived from imines into electron deficient alkene systems. Qi and Chen reported the α-allylation of imines, engaging PCET to generate an α-amino radical via a photoreductive pathway.[21] In the presence of an activated allyl sulphone, the nucleophilic α-amino radical undergoes intermolecular radical addition into the electron deficient alkene, ejecting the sulphone, furnishing the corresponding allyl amine. In the absence of a sulphone leaving group, the Michael addition product was obtained, enabled via hydrogen abstraction from Hantzch ester terminating potential chain propagation. Dixon et al. simultaneously developed the reductive allylation of Schiff bases, with *in situ* condensation facilitating aldimine formation while utilising organic dye, Eosin Y as a photocatalyst.[22] Dixon further

extended this methodology by exchanging the sulphone leaving group for a Boc-protected amine. Following intermolecular radical addition to the electron deficient alkene, the corresponding α-amino-α-ester radical abstracts hydrogen from the oxidised Hantzch ester, yielding a 1,3-diamine.[23] Dixon also reported a reverse polarity Povarov cyclisation, which upon intermolecular radical addition to an electron deficient alkene by an α-amino radical, intramolecular cyclisation accesses a highly reducing radical anion. Subsequent reduction of a Schiff base by the radical anion furnishes the tetrahydroquinoline and α-amino radical propagating the reaction.[24] In 2017, Ngai reported a formal Giese reaction between Schiff bases and vinyl-pyridines.[25] Upon photoreductive α-amino radical formation facilitated by PCET, Lewis acid activation of the electron rich vinyl-pyridine biases the electron density facilitating conjugate addition to proceed, furnishing 1,3-amio-pyridine motif (**2.35**).

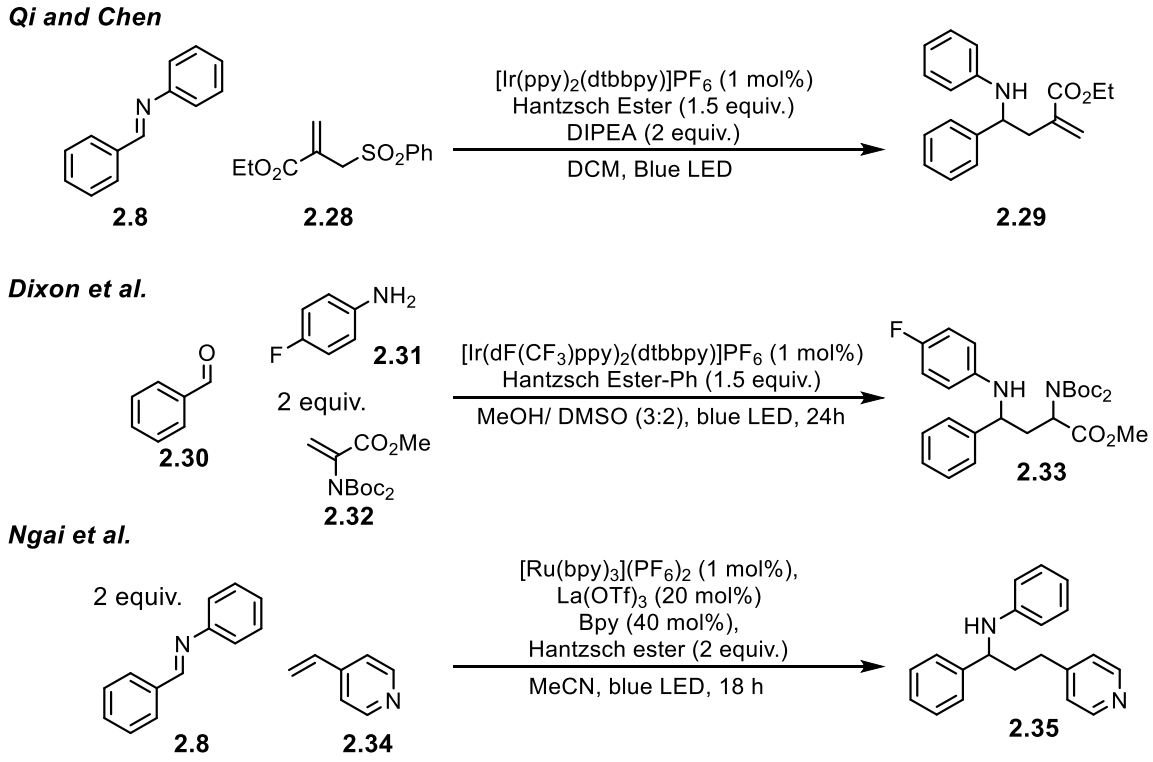

Figure 2.5: Radical addition of α-amino radicals generated via a photoreductive pathway into π-systems.

Both Molander and Yu disclosed methodologies for the reductive alkylation of imines. Molander *et al*. reported the visible light mediated reductive-alkylation of sulfonyl imines.[26] This procedure occurs via single electron oxidation of an alkyl bis(catecholato)silicates-Diisopropylamine salt (**2.36**) by the triplet state of 4CZIPN, generating an alkyl radical species (figure 2.6). Two viable reaction pathways are then proposed; Firstly, the single electron reduction of an *N*-sulfonyl Schiff base (**2.17**) which furnishes an α-amino radical with subsequent radical-radical coupling yielding the α-alkylated amine. Alternatively, intermolecular radical 1,2-addition into the imine generates an aminyl radical with subsequent reduction by the photocatalyst and protonation on workup. Molander demonstrates a broad substrate scope attaining typically good yields and chemoselectivity, while showing applicability to gram scale processing. Via a mechanistically synonymous pathway, Zhang and Yu reported the reductive benzylation of *N*-phenyl aldimines and ketimines utilising 4-benzyl-1,4-dihydropyridines (**2.38**) as an oxidant and benzyl radical precursor[27] (figure 2.6). The appearance of the aza-pinacol product in the crude ^{1}H NMR lead Yu *et al.* to conclude that photoreductive generation of an α-amino radical with subsequent radical-radical coupling is the major pathway. In 2017 Xia *et al.* described the reductive arylation of imines achieved by radical-radical coupling between an imine and 1,4-dicyanobenzene.[28] This protocol utilises two catalytic cycles in which both an imine and 1,4-dicyanobenzene are reduced with consequent radical-radical coupling furnishing the α-arylated product. This protocol allowed the synthesis of an α-tertiary amine by submitting ketimines to the developed conditions.

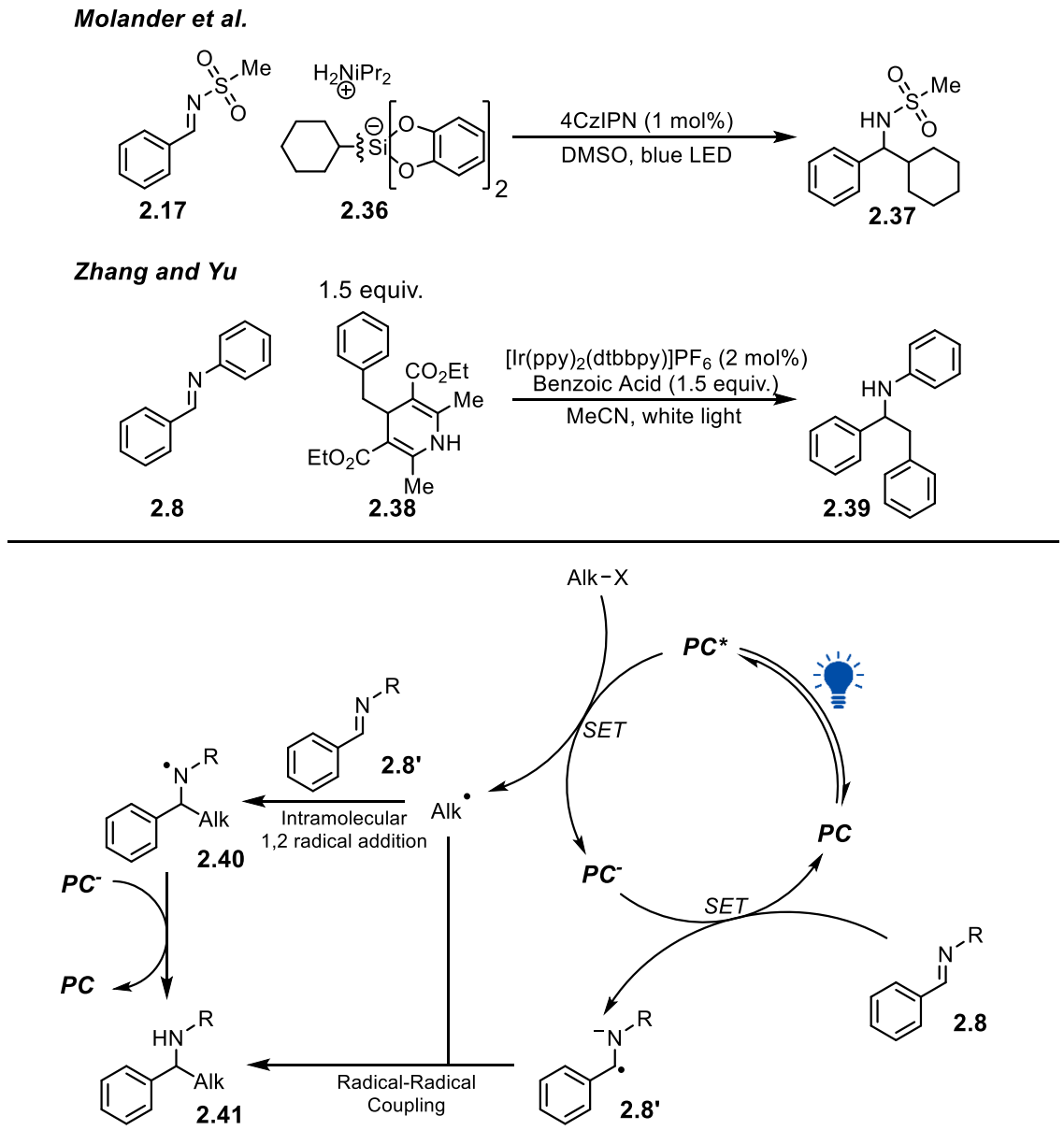

Figure 2.6: General mechanism for the reductive alkylation of imines reported by Molander *et al.* and Zhang *et al.*

2.1.2 Formation of C-H Bonds

Recently, the Polyzos group disclosed a visible-light catalysed Pictet-Spengler reaction of **2.42** utilising photocatalyst [Ir(ppy)$_3$] and DIPEA as a sacrificial reductant (Figure 2.7).[29-30] Single electron reduction of aryl iodide **2.42** facilitates intramolecular radical addition into the imine forming tetrahydroisoquinoline **2.43**. However, competitive single electron reduction of the imine was also observed (figure 2.7) furnishing α-amino radical

2.42* with subsequent hydrogen atom abstraction from the labile α-hydrogens of oxidised DIPEA yielding amine (**2.44**). Competitive reduction was attributed to the similarity of reduction potentials between imines and aryl iodides (-2.06V vs. SCE for iodide and -2.20V vs. SCE for imine). The competitive reduction of the imine was to my knowledge the first example of a visible-light induced transfer hydrogenation of an imine.

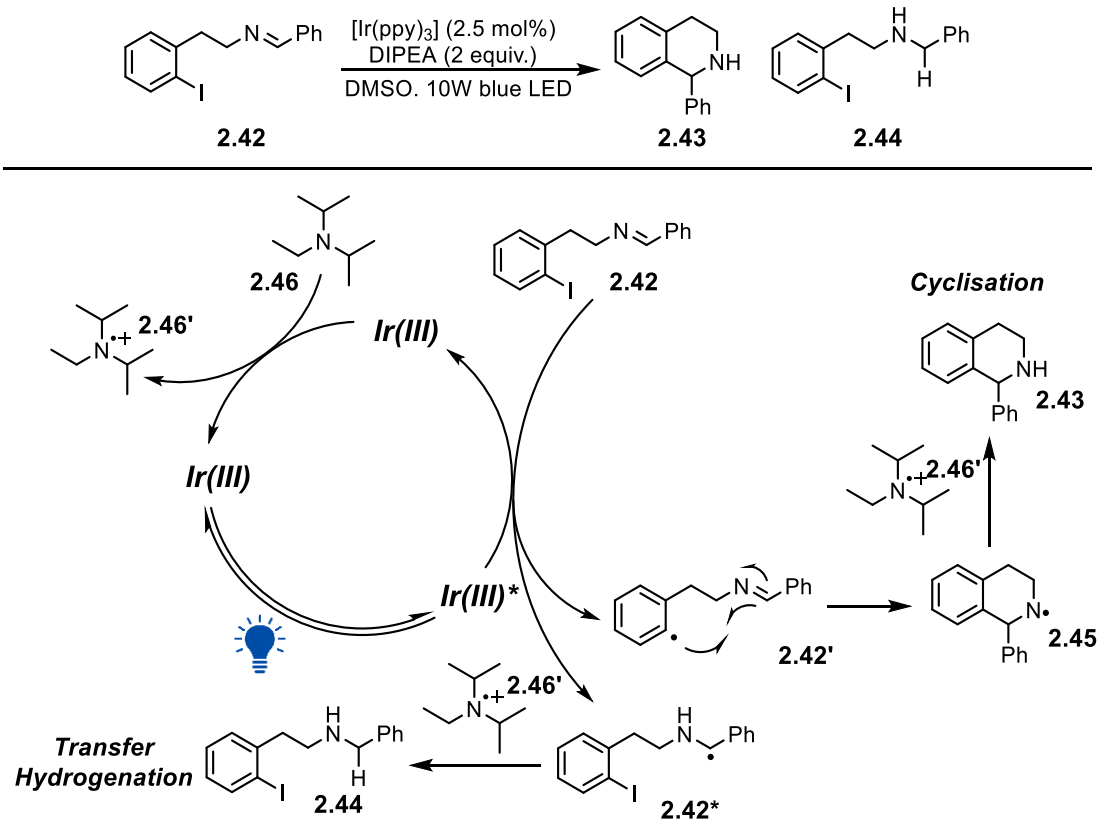

Figure 2.7: Visible light catalysed Pictet-Spengler cyclization developed by the Polyzos group.

Reductive amination is one of the most widely adopted techniques for the synthesis of amines in the pharmaceutical industry,[31-32] hence the reduction of imines has been thoroughly explored. Traditional procedures for the reduction of imines involve metal hydride reductions and catalytic hydrogenation; these methodologies are limited,[32-33] necessitating stoichiometric quantities of reagents or high temperatures and high

pressures of hydrogen gas which requires specialised equipment and represents a safety hazard. Transfer hydrogenation substitutes hydrogen gas for alternative hydrogen sources (formic acid[34], Hantzsch ester[35-36] or isopropanol[37]), and is able to achieve the mild, catalytic and facile reduction of imines; however chemoselectivity for imine reduction in the presence of other reducible functional groups remains challenging. There is a prerogative for synthetic chemists to continuously develop mild and chemoselective methods for the hydrogenation of imines, this has been highlighted through its heavy representation in the literature.[38-44] Photoredox catalysis could provide an alternative pathway to achieve this tranformation. The unexpected reduction of imine **2.42** inspired further exploration of this pathway to develop methodology specifically targeting the chemoselective transfer hydrogenation of imines.

2.2 Project Aims

2.2.1 Project Proposal

The aim of this project is to develop a photoreductive transfer hydrogenation of imines to furnish the corresponding amine products. Key to this approach is the photoreductive generation of α-amino radicals with subsequent interception of this intermediate with a hydrogen source, similarly to that previously observed in the Polyzos group. The developed protocol will allow the mild and chemoselective synthesis of amines enabled by visible light, the first reported in this important class of reaction.

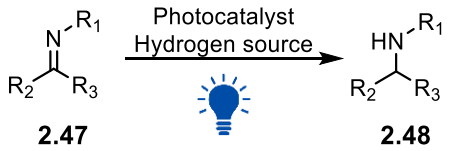

Figure 2.8: General scheme for the visible light mediated transfer hydrogenation of imine.

This unexplored transformation provides the potential to establish a new and mild approach for the synthesis of amine derivatives; a transformation at the forefront of chemical research, with a constant demand for improvements.[38-44]

2.2.2 Reaction Design

The proposed reaction mechanism is shown in figure 2.9. This transformation is hypothesised to proceed via irradiation of the photocatalyst to its triplet state followed by oxidation of a tertiary amine (**2.49**) generating a highly reducing species (**PC**-) and an aminium radical (**2.49'**). It is posited that simple tertiary amines can act as mild reductants ($E_{1/2}$ = 0.6-0.8V) while the *in situ* generated aminium radical facilitates PCET undergoing facile hydrogen atom transfer (BDE= ≈ 42kcal/mol). PCET between **2.50**, aminium

radical **2.49'** and the reduced photocatalyst (**PC**-) regenerates the photocatalyst's ground state (**PC**) as well as an α-amino radical (**2.50'**).[12] I hypothesize that α-amino radical **2.50'** abstracts a proton from the aminium radical cation bestowing the desired amine. Diaryl-ketimines were selected as synthetic targets as the benzhydrylamine products represent key structural motifs in δ opioid receptor agonists,[45] dopamine transporter ligands, [46-47] and histamine H_1 antagonists.[48,49]

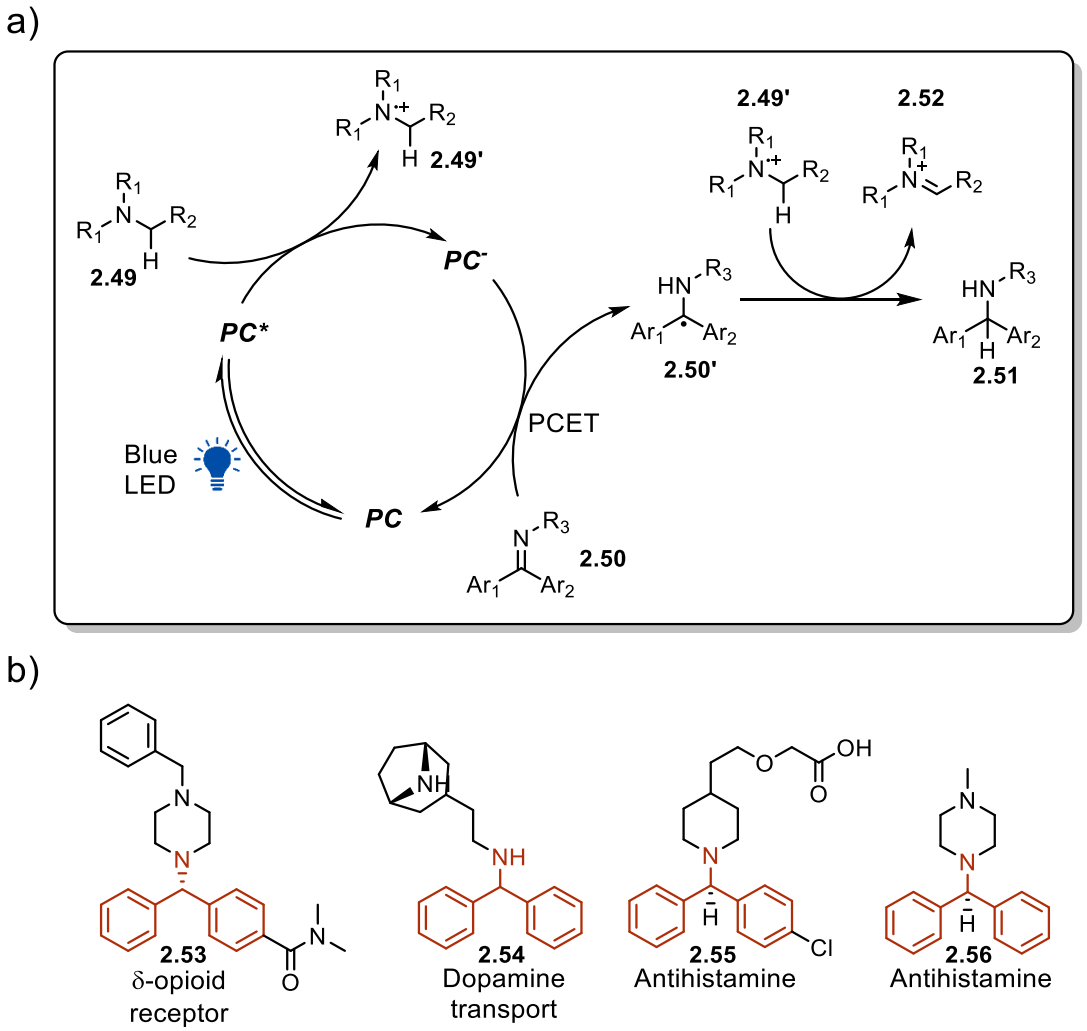

Figure 2.9: a) Proposed mechanism for the visible light mediated transfer hydrogenation of imines b) Structures of biologically relevant benzhydrylamines.

2.3 Reaction Optimisation

With a mechanistic hypothesis developed, the investigation began by screening a range of photocatalysts based on the redox potentials of the reduced oxidation state required for the single electron reduction of imine **2.57**. Initially, 5 equivalents of TEA (which fulfills the role of both sacrificial reductant and H-donor) and DMF as solvent were arbitrarily chosen as initial conditions to screen

Table 2.1: Photocatalyst screen for transfer hydrogenation of diarylimines.

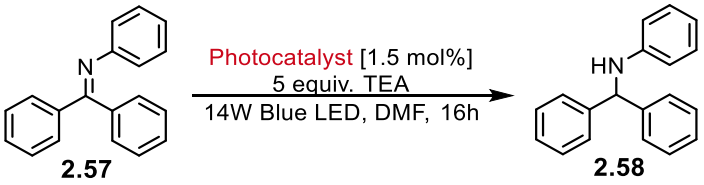

2.57 **2.58**

Entry	Photocatalyst	Photocatalyst Reduction Potential (V vs. SCE)	Yield 2.58 (%)*
1	$[Ru(bpy)_3]Cl_2$	-1.33	39
2	$[Ir(ppy)_3]$	-1.73	25
3	$[Ir(dF(CF_3)ppy)_2(dtbbpy)]PF_6$	-1.37	52
4	$[Ir(ppy)_2(dtbby)]PF_6$	-1.51	98
5	Eosin Y	-1.06	25
6	Fluorescein	-1.27	26

**yield measured via ^{1}H NMR spectroscopy against 2,5-dimethylfuran as internal standard*

The catalysts screened, their corresponding reduction potentials and yields of benzhydrylamine **2.58** are summarised in Table 2.1. In the presence of $[Ru(bpy)_3]Cl_2$, a 39% yield of **2.58** was observed via ^{1}H NMR spectroscopy, utilising 2,5-dimethylfuran as internal standard. The highly reducing $[Ir(ppy)_3]$ proceeded to give **2.58** in 25% yield, this was rationalised by the low oxidation potential of triplet $[Ir(ppy)_3]$ ($E_{1/2}$ = 0.31V vs. SCE), hindering the oxidation of TEA and thus access to the highly reducing $[Ir(ppy)_3]$ species as unfavourable. Heteroleptic iridium photocatalyst, $[Ir(ppy)_2(dtbbpy)]PF_6$ ($E_{1/2}$ = -1.51V Vs. SCE) gave a quantitative yield, while its fluorinated counterpart, $[Ir(dFCF_3ppy)_2(dtbbpy)]PF_6$ ($E_{1/2}$ = -1.37V vs. SCE) obtained modest yields of 52%. Further optimisation proceeded with $[Ir(ppy)_2(dtbbpy)]PF_6$. Two organic dyes, Eosin Y

and Fluorescein also were investigated, each affording benzhydrylamine **2.58** in 25% and 26% yield, respectively. The lower yields were attributed to the excited states of the organophotocatalysts being mild oxidants ($E_{1/2}$= 0.79 and 0.78V vs. SCE respectively) allowing TEA oxidation, however the reduced photocatalysts are not reducing enough to achieve efficient photoreduction of **2.58** ($E_{1/2}$ = -1.06 and -1.27V vs. SCE respectively vs. approximately $E_{1/2}$ = -2.0 V vs. SCE of an imine).

Table 2.2: Amine screening for the transfer hydrogenation of diarylimines.

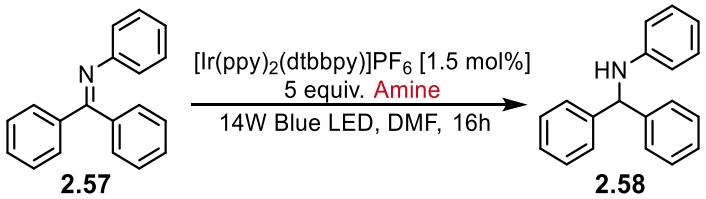

2.57 **2.58**

Entry	Amine	Yield 2.58 (%)*
1	TEA	>98
2	i-Pr_2NEt	96
3	$N(Bu)_3$	>98
4	$N(EtOH)_3$	>98

**yield measured via ^{1}H NMR spectroscopy against 2,5-dimethylfuran as internal standard*

A series of tertiary amines were screened to determine applicability to the reaction. As shown in table 2.2, TEA, DIPEA, $N(Bu)_3$ and $N(EtOH)_3$ (table 2.2 entries 1-4) all attained quantitative yields of benzhydrylamine **2.58**. TEA was continued for optimisation due to its cheap and readily available nature coupled with its low boiling point (bp = 89 °C) allowing for straightforward removal upon completion of reaction.

Table 2.3: Stoichiometry screening of TEA for the transfer hydrogenation of diarylimines.

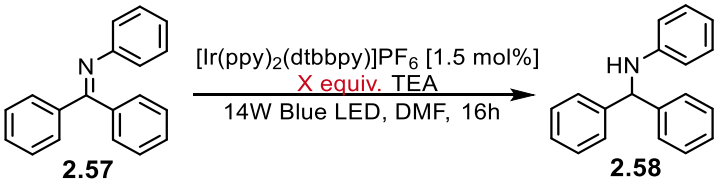

2.57 2.58

Entry	Equivalents of TEA	Yield 2.58 (%)*
1	1	38
2	2	78
3	5	>98
4	10	>98
5	20	90

**yield measured via ^{1}H NMR spectroscopy against 2,5-dimethylfuran as internal standard*

Next, the stoichiometry of TEA was examined. As shown in Table 2.3, 1 equivalent of triethylamine reduced the yield to 38%, while 2 equivalents allowed 78% yield. Increasing to 10 equivalents did not affect the yield of **2.58**, while 20 equivalents decreased the yield slightly to 90%. Optimisation was continued with 5 equivalents of TEA.

Table 2.4: Solvent screen for the transfer hydrogenation of diarylimines.

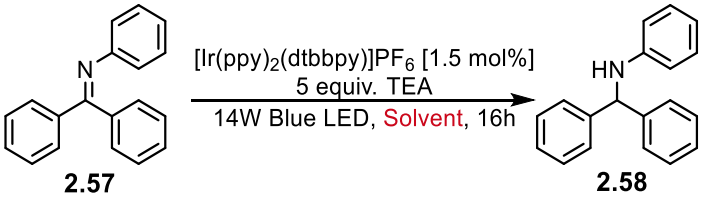

2.57 2.58

Entry	Solvent	Yield 2.58 (%)*
1	DMF	>97
2	DMSO	93
3	MeCN	>98
4	*i*PrOH	>98
5	THF	76
6	PhMe	55
7	H_2O	15
8	$CHCl_3$	N.P.
9	$H_3C(CH_2)_5CH_3$	N.P.

**yield measured via ^{1}H NMR spectroscopy against 2,5-dimethylfuran as internal standard*

Next, a solvent screen was performed (Table 2.4), typically polar organic solvents generated **2.58** in excellent to quantitative yields, with DMSO, MeCN, and *i*-PrOH all achieving yields >90%. A reduction in solvent polarity (Table 2.4, entries 5-6) afforded

amine **2.58** in moderate yields of 76% and 55% for THF and toluene respectively; this was rationalised due to a kinetic-solvent effect leading to decreased solvation and destabilisation of the aminium and α-amino radicals in less polar solvents.[50] Low reactivity was observed in water with **2.58** obtained in 15% yield despite the heterogeneous conditions of this mixture. The reaction did not proceed with CH_3Cl or heptane (table 2.4, Entries 8-9). Further optimisation was continued with MeCN.

Table 2.5: Control reactions for the transfer hydrogenation of diarylimines.

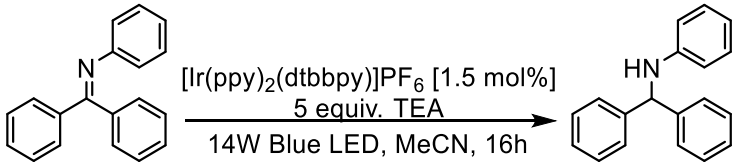

2.57 **2.58**

Entry	Deviation from conditions	Yield 2.58 (%)*
1	No Light	0%
2	No catalyst	3%
3	No TEA	0%
4	Substitution of TEA for $HNPh_2$	0%
5	3 hour reaction time	>98%

**yield measured via ^1H NMR spectroscopy against 2,5-dimethylfuran as internal standard*

A selection of control reactions were conducted to probe the reaction mechanism. In the absence of light or triethylamine no reaction occurred, suggesting a photocatalytic cycle dependent on added triethylamine.

In the absence of $[Ir(ppy)_2(dtbbpy)]PF_6$, trace amounts of **2.58** was detected, this is attributed to the absorption of blue light by **2.57**. It is postulated that upon excitation **2.57** generates an iminyl triplet state di-radical, similar to benzophenone.[51-52] The iminyl di-radical may abstract a proton from triethylamine forming trace amounts of the product as shown in figure 2.10.

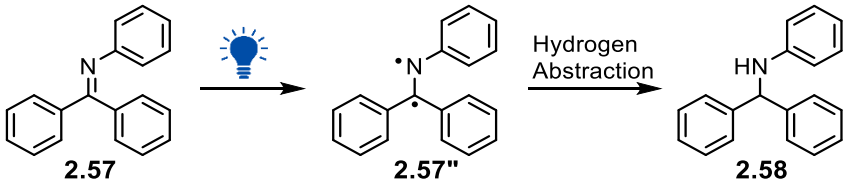

Figure 2.10: Possible mechanism for reduction in the absence of photocatalyst.

TEA was substituted for diphenylamine, an amine devoid of abstractable α-hydrogens. No reaction proceeded, highlighting the necessity of labile α-hydrogens of the sacrificial reductant. Finally, a time-course reaction was conducted to determine the time required to achieve full conversion of **2.57** to **2.58**. The progress of the reduction was monitored with ^{1}H NMR analysis via abstraction of a 0.1mL sample of the reaction mixture taken at 10-minute intervals. It was noted that the reduction of **2.57** to **2.58** was complete over approximately 1 hour of irradiation. A 3-hour reaction time was applied to ensure future substrates with slower reduction rates proceed to completion.

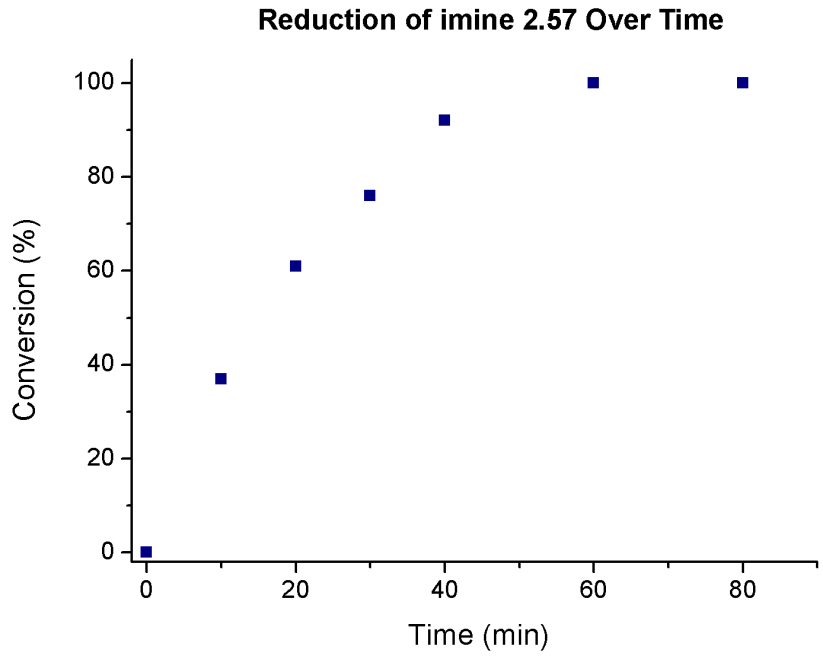

yield measured via ^{1}H NMR spectroscopy monitoring integration of the starting material compared to product
0.1mL samples were taken from the reaction mixture at 10 minute increments and tested via ^{1}H NMR

Figure 2.11: Time course study for the transfer hydrogenation of imine 2.57

Following completion of the time course experiments, the reaction was considered optimised. The optimised conditions were: imine **2.57** (0.45 mmol), 5 equivalents of TEA and 1.5 mol% of $[Ir(ppy)_2(dtbbpy)]PF_6$ in acetonitrile (5mL) under 14W blue LED irradiation for 3 hours (Figure 2.12).

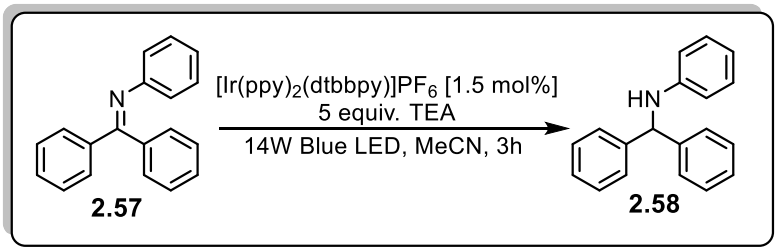

Figure 2.12: Optimized reaction conditions for the visible light mediated transfer hydrogenation of imines

2.4 Scope of Reaction

The generality of the optimised conditions was examined against a series of imines. A range of *N*-aryl-diarylketimines were synthesised, initially with a variety of substituents on the *N*-phenyl ring and diaryl-ketimine allowing exploration of the chemoselectivity of the developed reaction. Substitution of *N*-Phenyl and the diaryl-ketimine core for alkyl derivatives were then screened to determine the generality of the developed reaction.

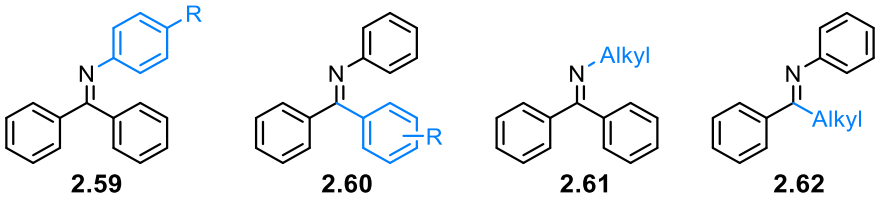

Figure 2.13: Positions of functionalisation for imine substrate scope.

Electron donating groups on the *N*-phenyl ring resulted in excellent isolated yields, this included alkyl groups, halides, ethers and free alcohols (substrates **2.64b,c,d,g,h,I,j**).

Electron withdrawing groups including nitriles, trifluoromethyl, esters and ketones (substrates **2.64e,f,k,j**) were also well tolerated, achieving good to excellent yields (Figure 2.14).

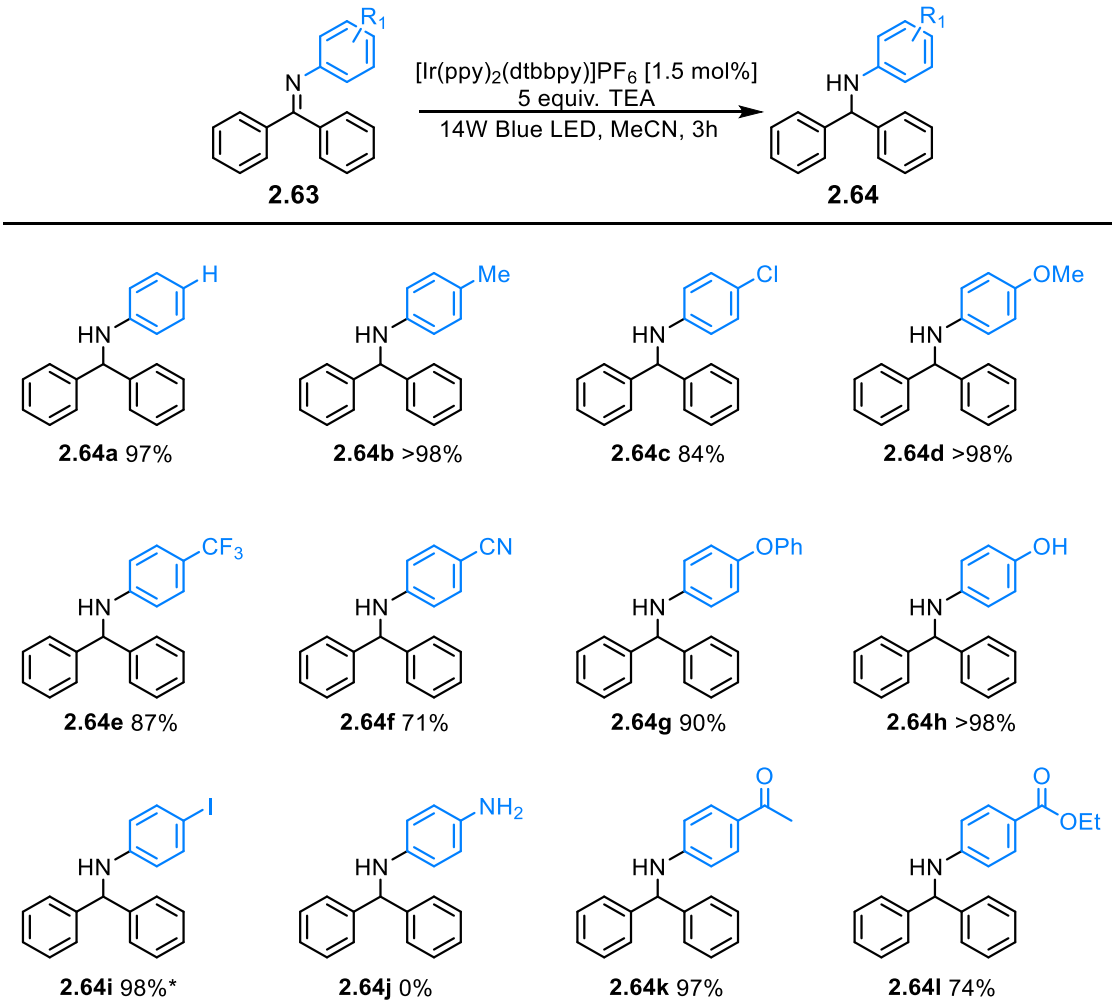

Figure 2.14: Scope of *N*-aryl substituents.

The developed conditions displayed remarkable chemoselectivity with imines **2.63k**,**l**,**f** all containing functionalities sensitive to reductive conditions. The reduction of imine **2.63k** is specifically highlighted as selective hydrogenation of imines in the presence of ketones is challenging. The methodology developed observed no selectivity issues in the presence of carbonyls, esters or nitrile moieties, however free amines inhibited reactivity with no reaction observed for **2.63j**; it is hypothesised that competitive oxidation over triethylamine inhibits this reaction.

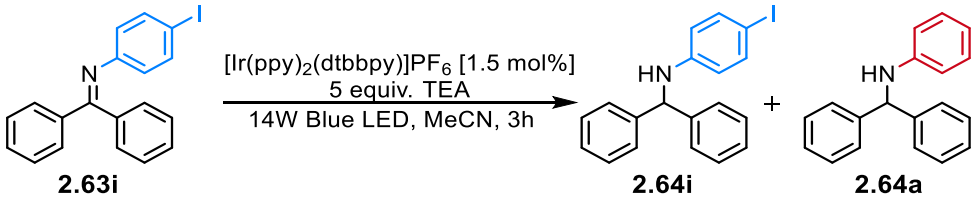

Figure 2.15: Competitive reduction between imines and aryl iodides.

Competitive reduction of an aryl iodide was observed for substrate **2.63i**, with the hydrodehalogenated product **2.64a** observed in the reaction mixture. This was anticipated due to the comparable reduction potential of aryl iodides ($E_{1/2}$ = -1.7 to -2.2 V vs. SCE) and imines ($E_{1/2}$ = -2.0V vs. SCE). The hydrodehalogenation of aryl iodides by photoredox catalysts is a well-established process.[53-57]

2.4.1 Time-Course Study of the Hydrodehalogenation of Iodo-Substituted Imines

The reduction of imine **2.63i** was monitored via ^{1}H NMR spectroscopy to determine whether hydrogenation could be achieved selectively over protodehalogenation. This was conducted in an NMR tube (5 mm diameter) proceeding on a 0.2 reaction scale (0.09mmol **2.63i**). The reaction was conducted in d_3-MeCN and a ^{1}H NMR spectrum was measured at 5-minute intervals. This process was rapid, achieving complete hydrogenation within 5 minutes with approximately 8% hydrodehalogenation, rapid reactivity was accounted for via the increased surface area to volume ratio of an NMR tube compared to reaction vial. Extended irradiation resulted in further hydrodehalogenation (figure 2.16). A reaction time of 4 minutes and 45 seconds enabled full conversion to **2.64i** and enabled 98% isolated yield.

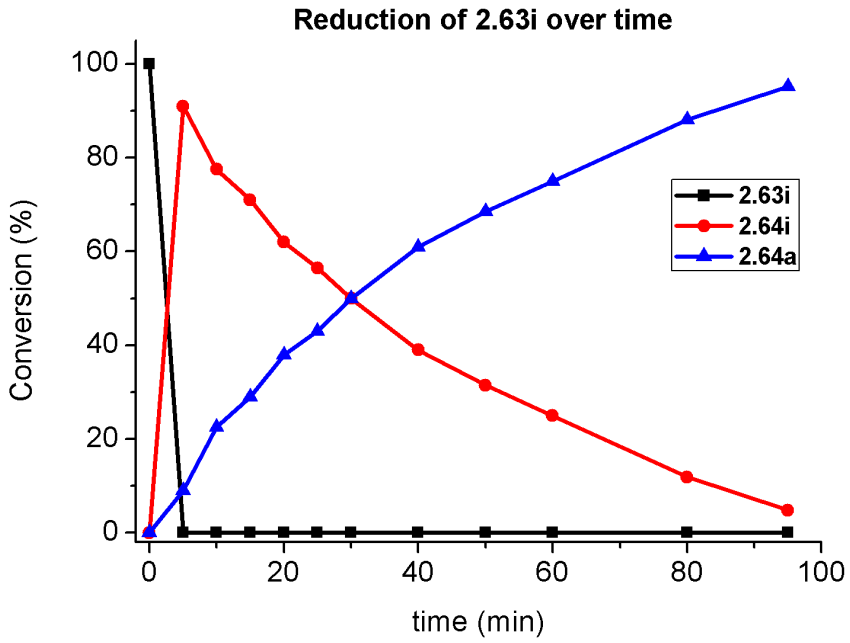

Figure 2.16: time course of the reduction of 2.63i.

Imines with substitution on the diaryl-ketimine core were synthesised and subjected to the optimized conditions. The reduction proceeds unhindered when methyl, chloro and methoxy groups were substituted in the *para*-position of a phenyl ring (substrates **2.63m**, **2.63o**, **2.63q**), achieving excellent yields. No reaction was observed for **2.63r**, as the presence of a *para*-nitro group could incite preferential electron transfer to the electron deficient aryl ring. Substitution of a phenyl ring for a 2-pyridine heterocycle achieved an excellent yield of **2.64s** (97%), while fusion of the diarylmethimine structure, allowed reduction of polycyclic fluorene **2.63u** in 95%. The products synthesised here are chiral, however there was no effort to measure or control enantioselectivity as this is beyond the scope this project. The yields reported for compounds **2.64m-2.64u** are racemic mixtures. Substitution of *N*-phenyl for a *para*-methoxyphenyl (PMP) protecting group was applicable, with **2.64n,p,t** isolated in excellent yields. Addition of a PMP protecting group allows the possibility of subsequent deprotection to the free amine with the addition

of reagents including cerium ammonium nitrate (CAN),[58-59] phenyl iodoacetate,[60] periodic acid[61] or trichloroisocyanuric acid.[61]

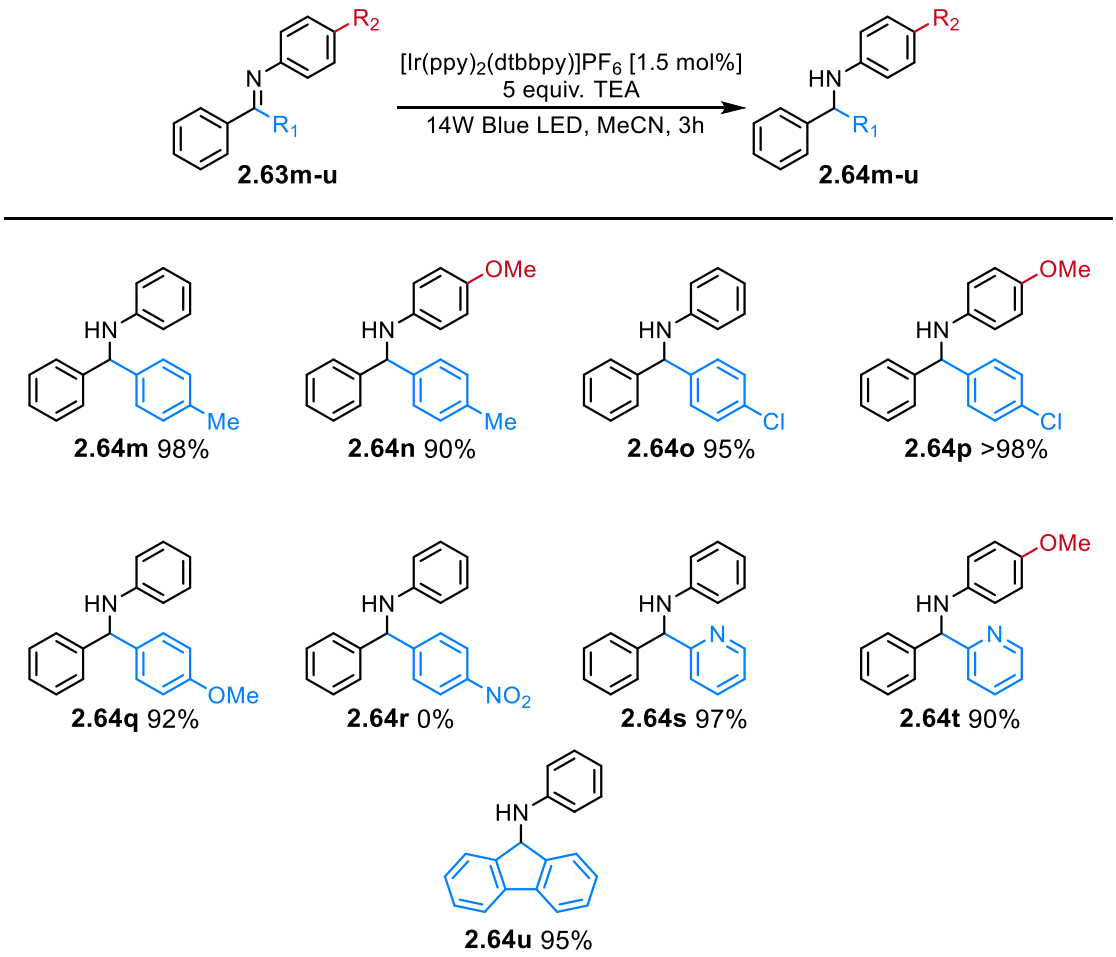

Figure 2.17: Scope of substitution on the diaryl-ketimine core.

N-alkyl diphenyl-ketimines were well tolerated, three examples were demonstrated, incorporating a benzyl protected imine (**2.63v**), *N*-allylimine (**2.63w**) and *N*-hexylimine (**2.63x**). These all showed efficient reduction, proceeding in high yields. Notably, self-cyclization or alkene reduction was not observed for **2.63w** with the allyl-substituted amine obtained exclusively.

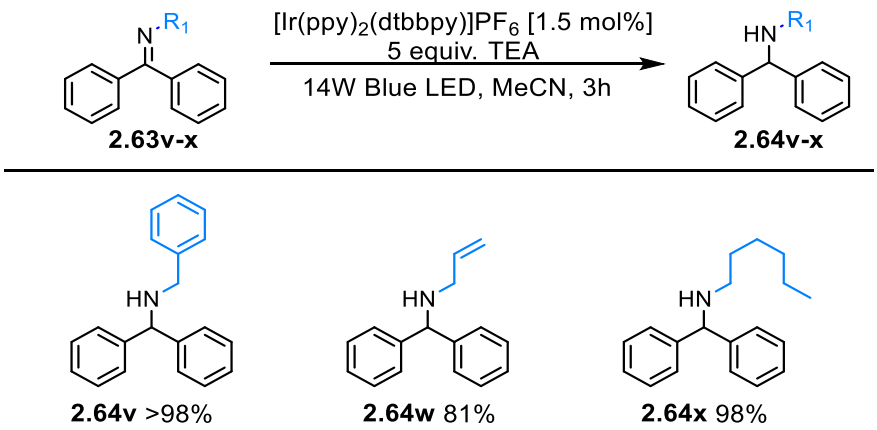

Figure 2.18: Scope of *N*-alkyl substitution.

To determine the generality of the reaction, a series of *N*-1-alkyl,1-arylmethimines were submitted for reduction using the standard reactions conditions. As shown in Figure 2.19, these imines were generally incompatible with the reaction. Reduction of the acetophenone derived imine (**2.65a)** to the expected amine was not observed and starting material was recovered. Furthermore, a reduction of **2.65e** and **2.65f** was not observed. The crude ^{1}H NMR revealed that Schiff base **2.65d** underwent a reductive aza-pinacol coupling.[12] Approximately 30% conversion was observed with imines **2.65b** and **2.65c**, however these results were not consistently reproducible.

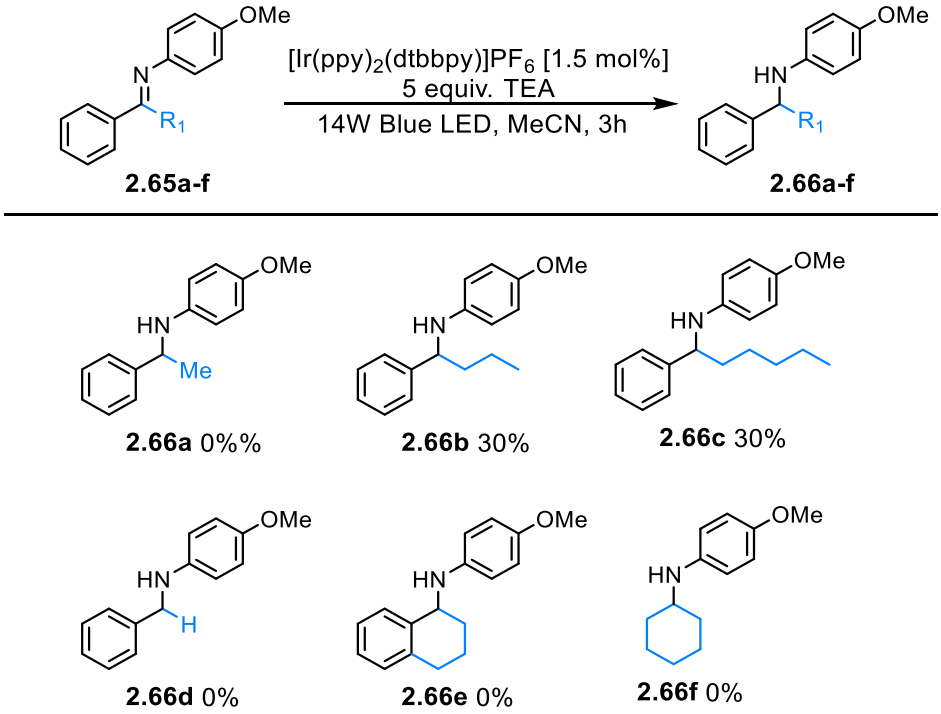

Figure 2.19: Scope of substitution on the benzophenone core.

2.5 Mechanistic Studies

Attention was then turned towards investigating the proposed reaction mechanism. The mechanistic studies conducted included fluorescence quenching, transient absorption spectroscopy, radical trapping studies and deuterium labelling as summarised in Figure 2.20.

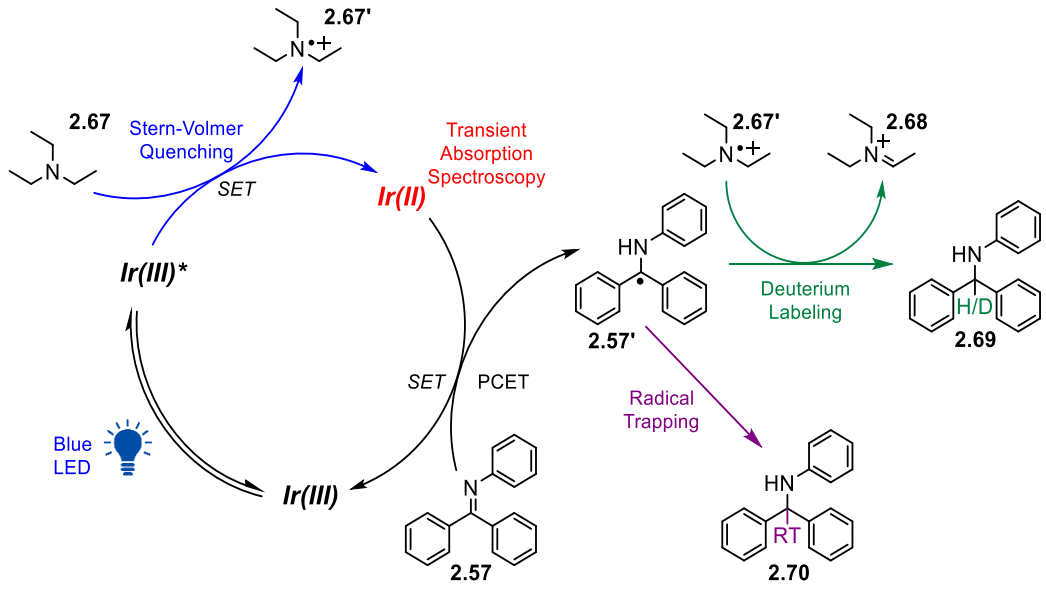

Figure 2.20: Summary of mechanistic studies conducted.

2.5.1 Emission Quenching Experiments

Upon excitation of a chromophore, a radiative decay pathway allows emission (via fluorescence or phosphorescence) of a photon to regenerate the ground state. The addition of a quencher can intercept the chromophore prior to emission, achieving energy/electron transfer, providing a non-radiative pathway, reducing the intensity of chromophore emission.[62] The extent of chromophore emission quenching is concentration dependant and can be modelled with the equation $\mathbf{I_o/I = 1 + k_q\tau[M]}$ where I_o is the initial emission, I is the emission with quencher present, k_q is the quenching constant and τ is the lifetime

of chromophore emission.[63] The quenching of a chromophore can be plotted via a Stern-Volmer plot, with I_o/I plotted against concentration of quencher revealing an ideal straight line with a gradient of $k_q\tau$.

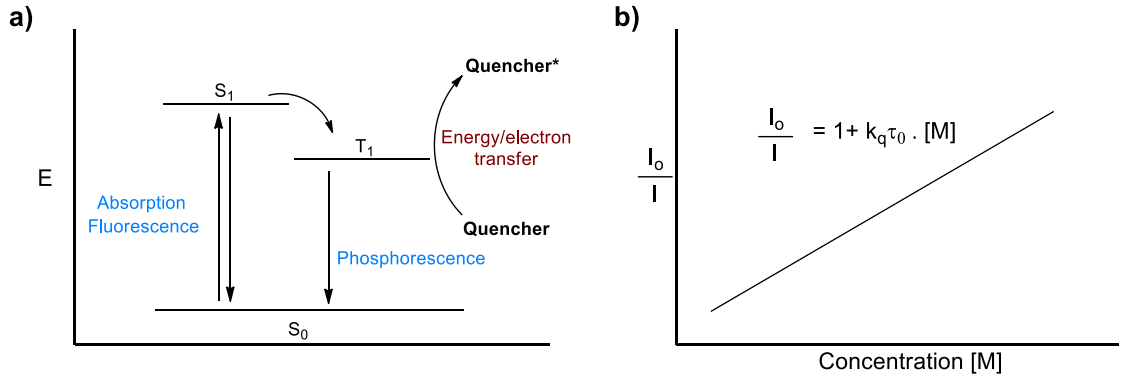

Figure 2.21: Description of Stern-Volmer quenching a) Quenching of a chromophore b) A representative Stern-Volmer plot.

Stern-Volmer quenching is an invaluable technique to probe photoredox systems, as quenching with the addition of reagents can indicate electron/energy transfer, validating whether a reaction likely proceeds via an oxidative or reductive quenching cycle, while the value of k_q can allow insight into the rate of energy/electron transfer.[62] Stern-Volmer quenching experiments were conducted with $[Ir(ppy)_2(dtbbpy)]PF_6$ [100µM] and either **2.57** or TEA to determine which species interacts with the photocatalyst's triplet excited state (figure 2.22). It was observed that the addition of imine **2.57** to a 100µM solution of $[Ir(ppy)_2(dtbbpy)]PF_6$ gave no change in emission, however addition of TEA resulted in concentration dependent emission quenching (figure 2.22a). In the presence of TEA, $[Ir(ppy)_2(dtbbpy)]PF_6$ observed incredibly rapid quenching with a k_q calculated to be 1.589×10^9 $mol^{-1}s^{-1}$ (assuming τ of $[Ir(ppy)_2(dtbbpy)]PF_6$ is 570ns). Interaction between triplet state of $[Ir(ppy)_2(dtbby)]PF_6$ and triethylamine agrees with the proposed mechanism of a reductive quenching cycle.

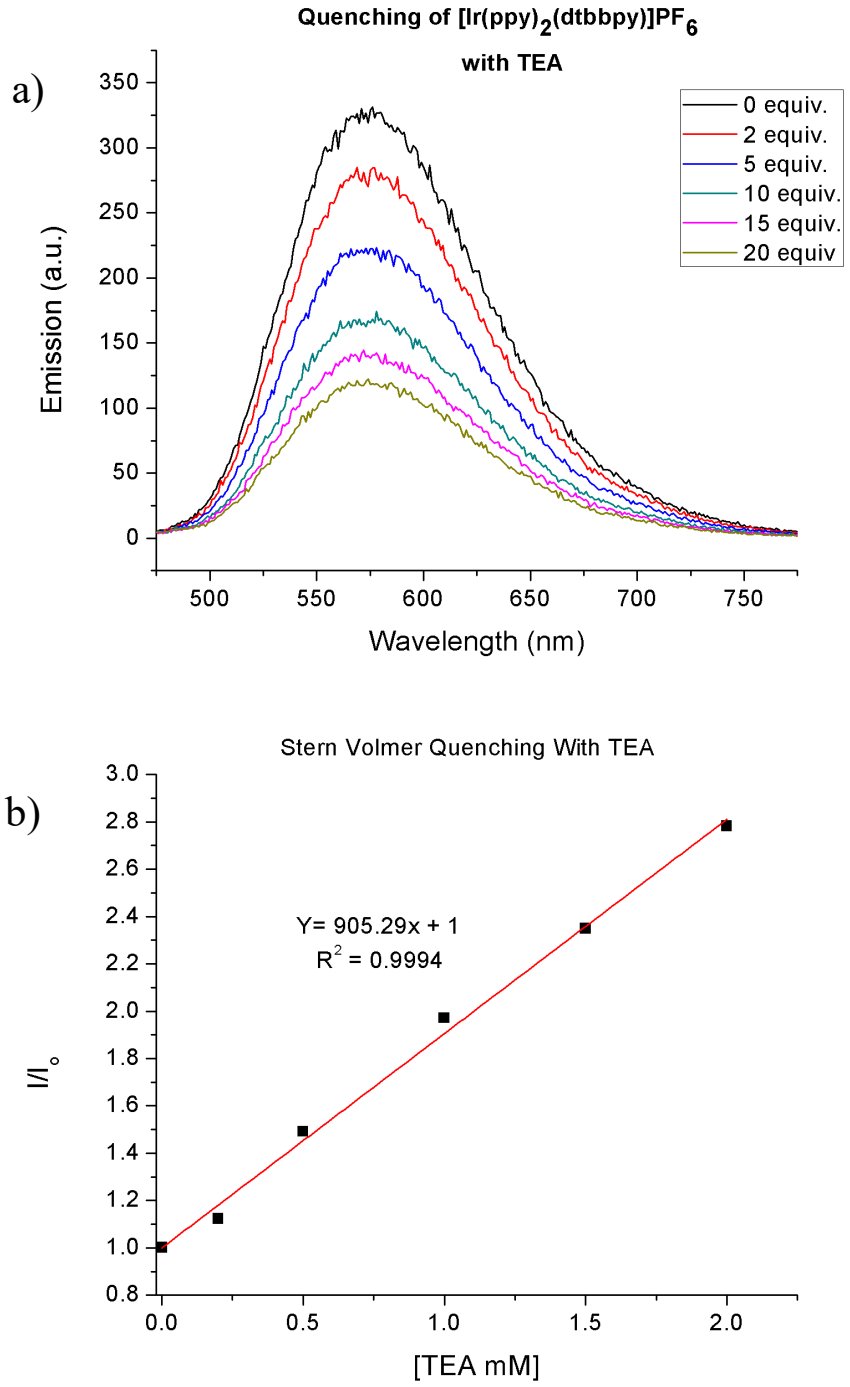

Figure 2.22: Quenching experiments (a) Excitation quenching in the presence of triethylamine (b) Stern-Volmer plot of quenching with triethylamine. Excitation wavelength measure was that of the Blue LED used in reaction (449nm).

2.5.2 Transient Absorption Spectroscopy

Transient absorption spectroscopy is a technique used to probe the electronic and structural characteristics of short-lived excited states of photoactive molecules.[62, 64-65] Transient absorption measures changes in the absorption/transmittance of a material over time via ultra-fast pump-probe irradiation. Upon absorption of a pump pulse, further exploration of a chromophore's absorption properties can be studied via irradiation by a probe pulse. Transient absorption spectroscopy allows measurement of photophysical properties with ultra-fast time resolutions ranging between microseconds to attoseconds. To further elucidate the triplet exited state of $[Ir(ppy)_2(dtbbpy)]PF_6$ and the nature of its quenching by TEA, transient absorption studies were conducted in collaboration with Dr. Tim Connell (RMIT). The differential absorption spectrum of $[Ir(ppy)_2(dtbbpy)]PF_6$ displayed strong bands at 380, 480 and 800nm (figure 2.23a), closely resembling other heteroleptic Ir(III) compounds containing bypyridine-based ligands[66]. Watts et al. assigned similar species as a triplet metal-to-ligand charge transfer (^{3}MLCT) in which the an electron is transferred from the triplet iridium centre to the bipyridine ligand[66]. It is assumed that with similar transient absorption spectra to that measured by Watts *et al*. that the same process is occurring (i.e. ^{3}MLCT from triplet iridium to the dtbbpy ligand). The decay profile of the absorption band at 380nm was determined to have a half-life decay of 0.58 µs. In the presence of triethylamine, the decay profile at 380nm was altered drastically, with a much shorter lifetime of decay, as well as the formation of a continuously absorbing signal that does not decay throughout the timescale of measurement (100µs) was observed (figure 2.23b). The extensively long lived species that is generated in the presence of triethylamine is a separate, chemically distinct species from $[Ir(IV)(ppy)_2(dtbbpy)]^-$ and believed to be the reduced photocatalyst $[Ir(III)(ppy)_2(dtbbpy^{\cdot -})]$. This result is consistent with the mechanistic hypothesis in

which upon excitation $[Ir(ppy)_2(dtbbpy)]PF_6$ is reduced in the presence of triethylamine to form a highly reducing species that subsequently reduces imine **2.57**.

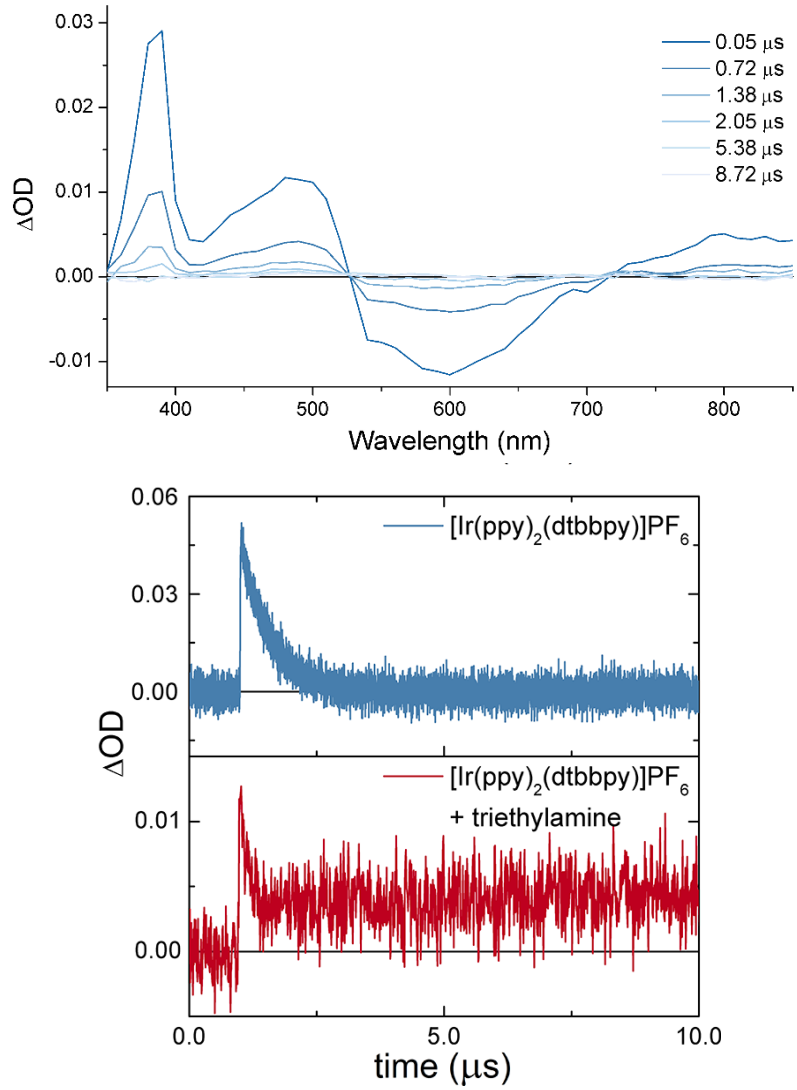

Figure 2.23: Transient absorption experiments (a) Differential absorption spectrum of $Ir(ppy)_2(dtbbpy)PF_6$ (b) Decay profiles of $[Ir(ppy)_2(dtbbpy)]PF_6$ in the absence and presence of triethylamine.

2.5.3 Radical Trapping Studies

To further confirm single electron reduction and the formation of an α-amino radical on **2.57**, radical traps were added to the reaction mixture. Three radical traps were screened to intercept the α-amino radical intermediate, these included: butylated hydroxytoluene (BHT), diphenylethene (DPE) and (2,2,6,6-tetramethylpiperidin-1-yl)oxyl (TEMPO). 1

and 5 equivalents of each radical trap were added to the optimised conditions. Unfortunately trapping the α-amino radical proved elusive and was not observed by ^{1}H NMR spectroscopy or mass spectroscopy. It is hypothesised that the α-amino radical was not trapped due the steric bulk of the trapping agents which hindered radical-radical coupling, while favourable hydrogen abstraction furnishes benzhydrylamine **2.58**. It was hypothesised that deuterated triethylamine could be employed to trap the α-amino radical, isolating the α-deuterated product.

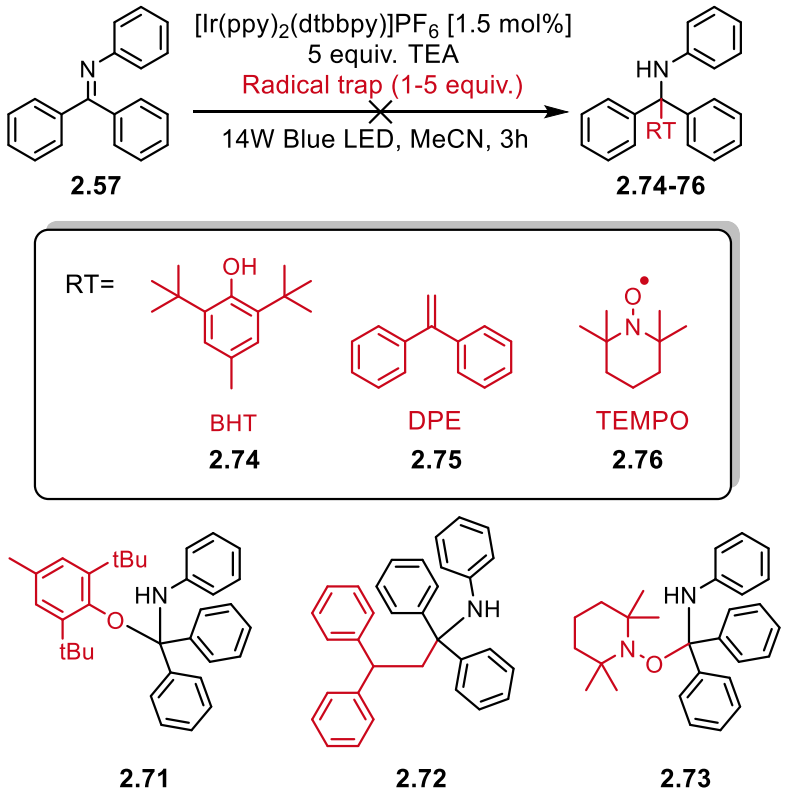

Figure 2.24: Radical trapping experiments.

2.5.4 Deuterium Labelling Studies

Deuterium labelling experiments were undertaken to determine the origin of hydrogen in this reaction and confirm the presence of an α-amino radical. Triethylamine was substituted for triethyl-d_{15}-amine, analysis of the crude ^{1}H NMR spectrum revealed a

reduction in integration of the diphenylmethane hydrogen peak. ^{1}H NMR analysis revealed 75% deuterium incorporation (figure 2.26), identifying the hydrogen source while simultaneously confirming the presence of the α-amino radical. Addition of d_3-MeCN in the presence of hydrogenated triethylamine was also screened to verify that solvent is not functioning as a hydrogen source. Utilising deuterated solvent showed no incorporation, confirming that triethylamine is the hydrogen source in this reaction.

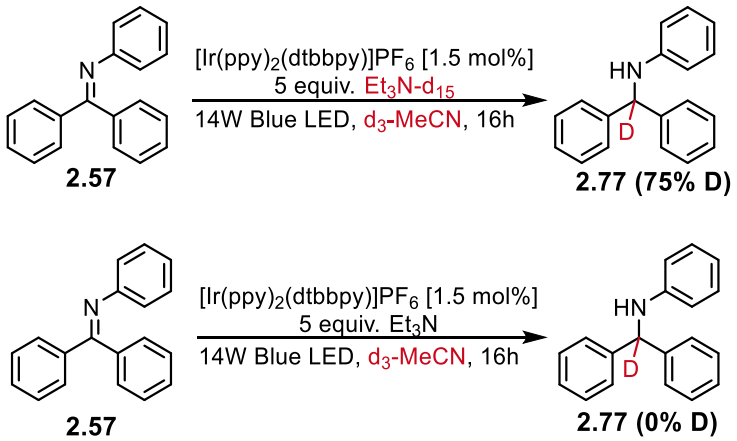

Figure 2.25: Deuterium labelling experiments.

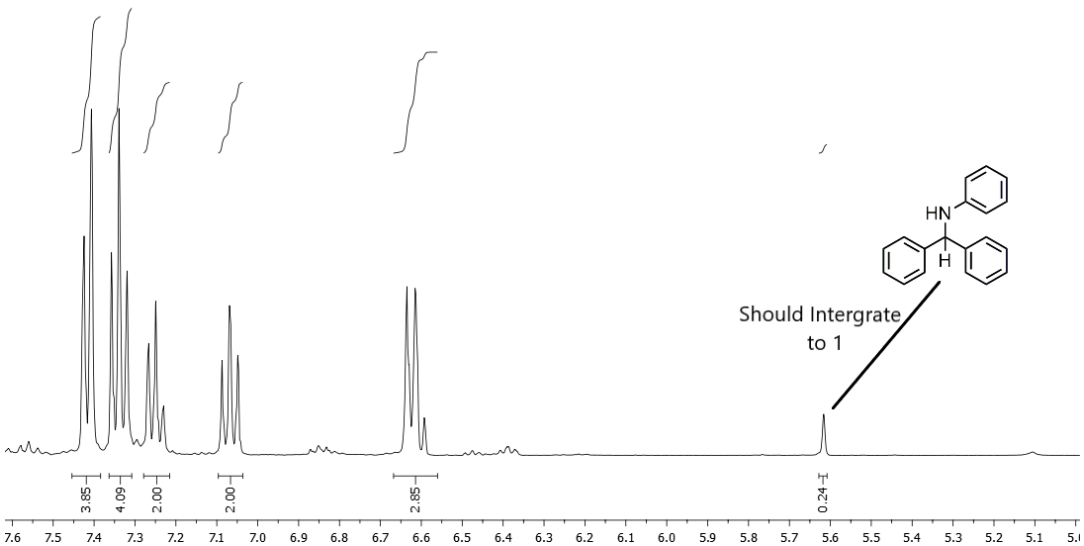

Figure 2.26: Crude ^{1}H NMR of the deuterium labelling experiments with Et_3N-d_{15}.

2.6 Application of the Method to Continuous Flow Processing

2.6.1 Optimisation for Flow Processing

To enhance processing and scalability of this method, the development of a flow protocol was investigated. Optimisation proceeded utilising a commercially available Syrris Asia pump fitted with a 1mL sample loop and a 5mL bespoke photoreactor coil and with a 40 PSI back-pressure regulator were utilised for optimization (figure 2.27).

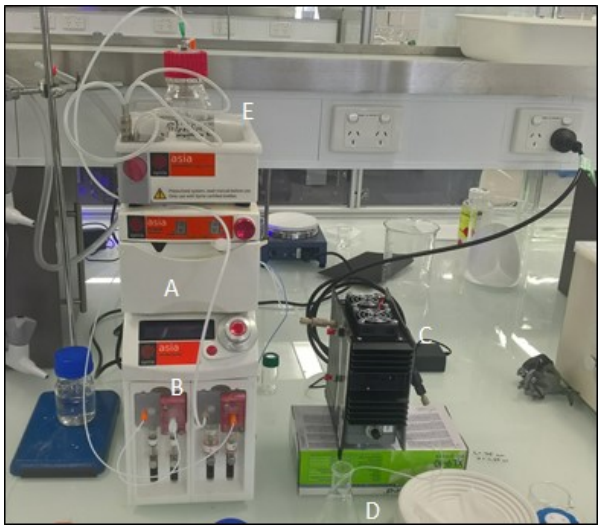

Figure 2.27: Experimental setup for the transfer hydrogenation in flow (A) Sample loop (B) Syringe pump (C) Illuminated photoreactor (D) collection flask (E) Solvent reservoir.

Table 2.6: Optimisation of the visibile-light mediated transfer hydrogenation of diarylimines in flow.

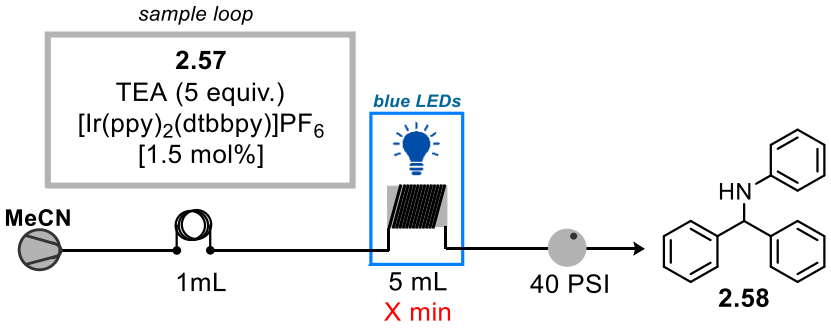

Entry	t(r) (min)	Conversion 2.58 (%)
1	0.5	25
2	2	40
3	4	57
4	6	70
5	8	86
6	10	87
7	12	100
8	15	100
9	20	100

**Conversion determined by ^{1}H NMR, by determining transformation of 2.57 to 2.58*

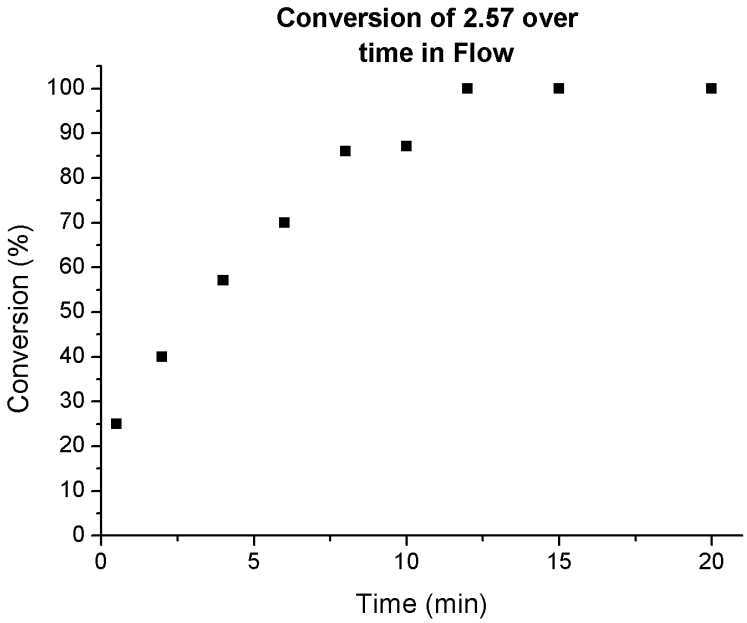

Figure 2.28: Conversion over residence time of the flow hydrogenation of imine **2.57**.

Flow processing allowed for rapid conversion achieving 25% conversion after 30 seconds of irradiation. The efficiency of reaction increased linearly with residence time until full reduction of **2.57** was achieved within a 12 minute residence time (table 2.6 and figure

2.28). With a residence time of 12 minutes, a continuous flow process was applied, achieving gram scale processing, attaining **2.58** in 96% isolated yield (figure 2.29). The flow protocol demonstrates vastly improved throughput compared to batch reactivity allowing 5.40 mmol/hour via flow in contrast to 0.15 mmol/hour by batch, corresponding to a 36-fold increase in throughout.

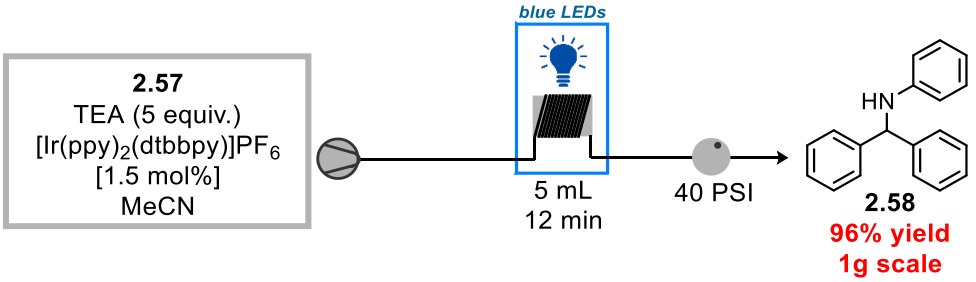

Figure 2.29: Continuous flow protocol for the transfer hydrogenation of imines.

2.6.2 Scope of Reaction in Flow

A representative sample of diaryl-ketimines were nominated for reduction utilising the developed flow conditions. The residence time was increased from 12 to 20 minutes, permitting full conversion of all substrates. All substrates subjected to flow processing gave the corresponding benzhydrylamines in excellent-quantitative yields, proceeding in higher or comparable efficiencies to batch conditions (figure 2.30).

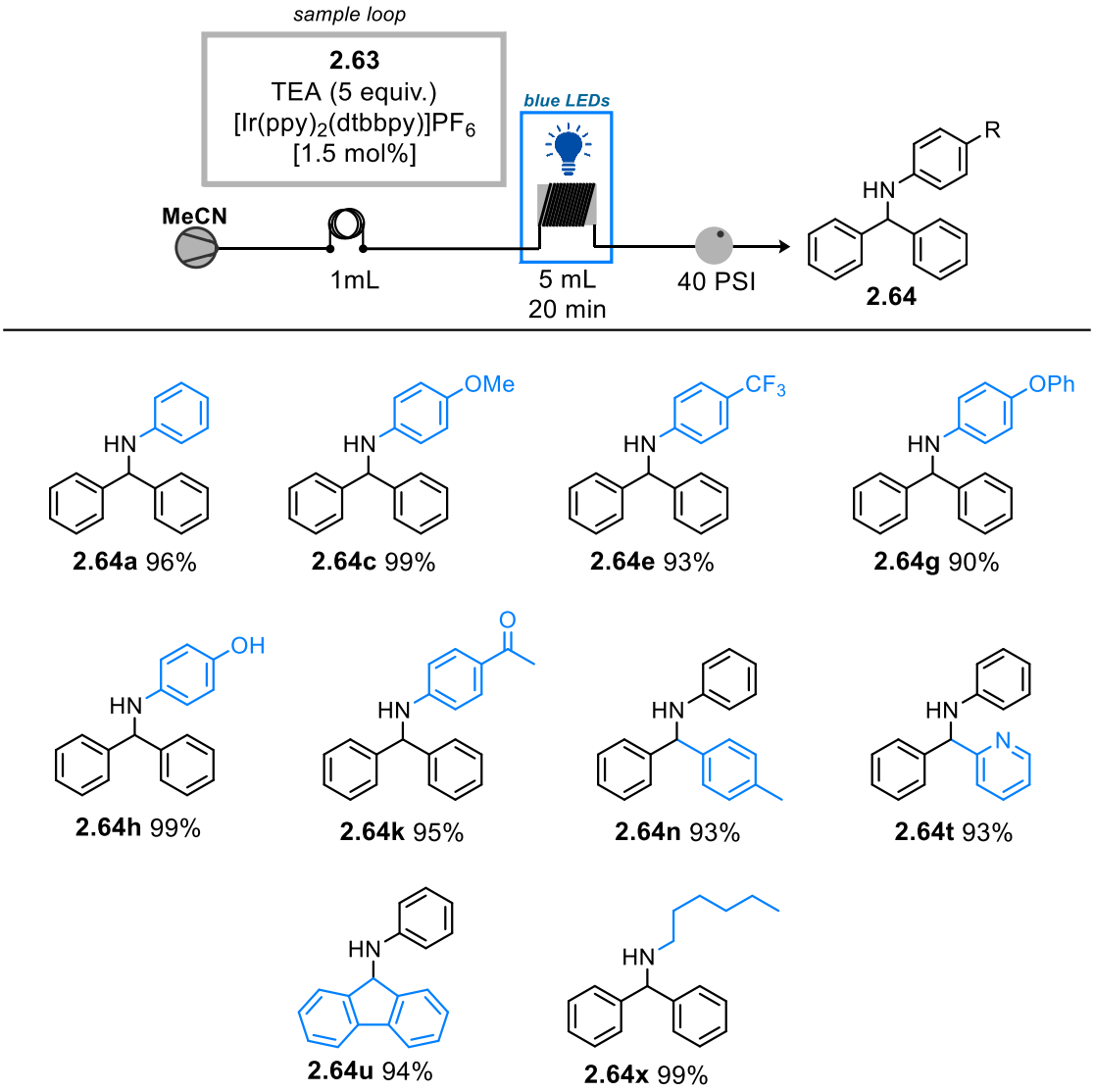

Figure 2.30: Scope of reactions conducted in flow.

Further development of the flow protocol was conducted in collaboration with Mr. Rowan Pilkington and Mr. Nikolai Rossouw.[67] Optimisation and enhanced processing of imines bearing sensitive functional groups were investigated, with imine **2.63i** of particular focus. Under batch conditions, **2.63i** demonstrated the need for strict control of the reaction time to avoid protodehalogenation, rendering this reaction incapable of being efficiently scaled to synthetically useful quantities via batch conditions. A flow protocol was developed allowing strict chemoselective reduction of imine **2.63i** on multi gram scales. This reaction was optimized utilising a Syris Asia series pump fitted with a 1 mL sample loop, 3mL illuminated reactor and a 40 PSI back pressure regulator (Table 2.7).

Table 2.7: Optimization of the reduction of imine 2.63i in flow.

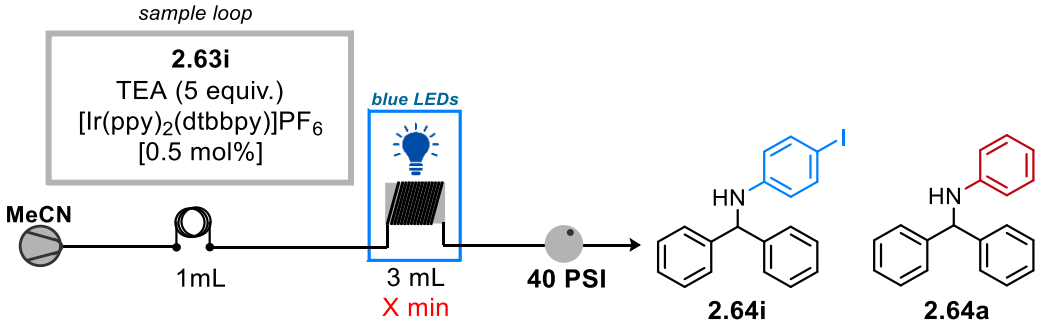

Entry	Residence time (min)	Conversion (%)	Yield 2.64i (%)	Yield 2.64a (%)
1	2.5	48	43	5
2	3.0	45	41	4
3	3.5	49	44	5
4	4.0	76	73	3
5	4.5	82	75	7
6	5.0	82	74	8
7	5.5	85	81	4
8	6.0	92	88	3
9	6.5	97	95	2
10	7.0	98	95	3
11	7.5	98	83	15
12	10	>99	76	23
13	12	>99	72	27

**yield measured via ^{1}H NMR spectroscopy against sulfolene as internal standard*

A residence time of 7 minutes allowed the optimum balance between hydrogenation of **2.63i** and protodehalogenation, achieving 98% conversion of **2.63i** with 95% yield of amine **2.64i** and 3% of **2.64a**. Extended residence times increased the quantity of protodehalogenated product as highlighted in table 2.7. A residence time of 7 minutes allowed isolation of **2.63i** in 87%. Imines furnished with other sensitive functionalities were applicable to chemoselective reduction with increased residence times of 9 minutes allowing isolation of the corresponding amines in excellent yields, similarly to batch conditions, nitro groups gave no reaction (figure 2.31). Pilkington highlighted that the chemoselective reduction of imines functionalised with aryl bromides could be chemoselectively hydrogenated with **2.64y** isolated in 84%.

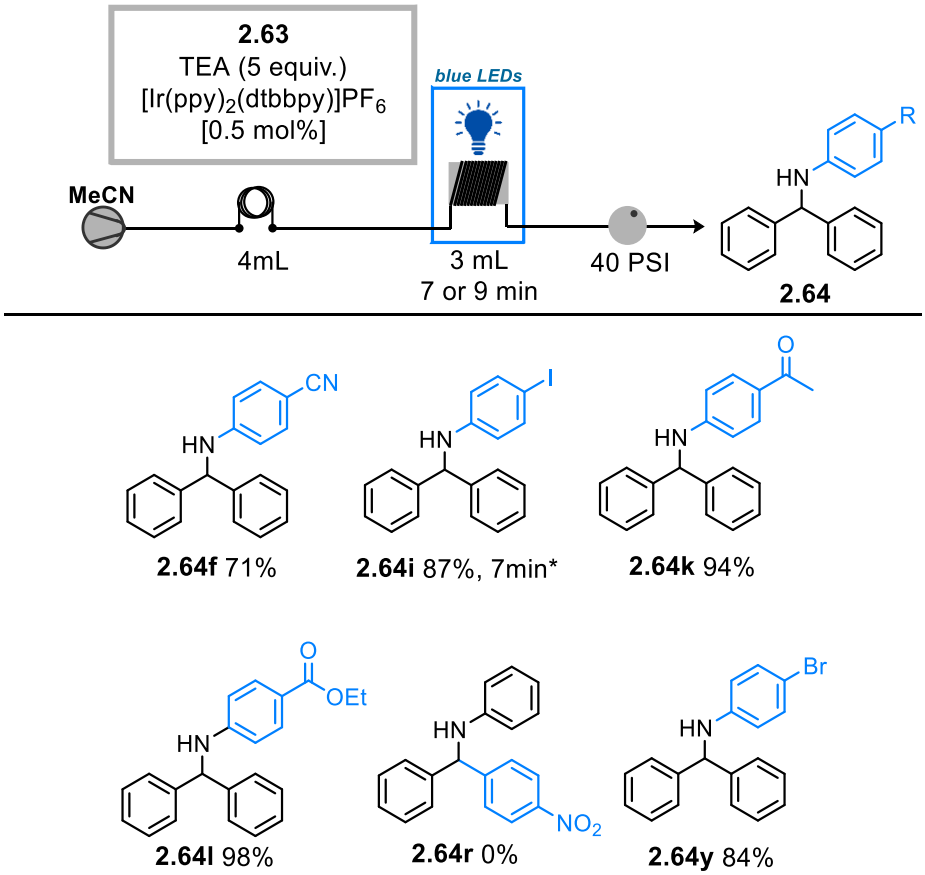

Figure 2.31: Scope for the chemoselective reduction of imines via flow

Reduction of imines **2.63i** and **2.63y** were scaled to demonstrate multigram processability while achieving chemoselective reduction. The transfer hydrogenation of imines **2.63i** and **2.63y** were conducted on 23.89mmol (9.155g) and 27.63mmol (9.289g) scales respectively via continuous flow processing and monitored with FlowIR™, an inline FTIR system allowing observation of steady state formation over time. Imines **2.63i** and **2.63y** were subjected to continuous processing, with the steady state fraction collected, obtaining isolated yields of 77% and 79% respectively.

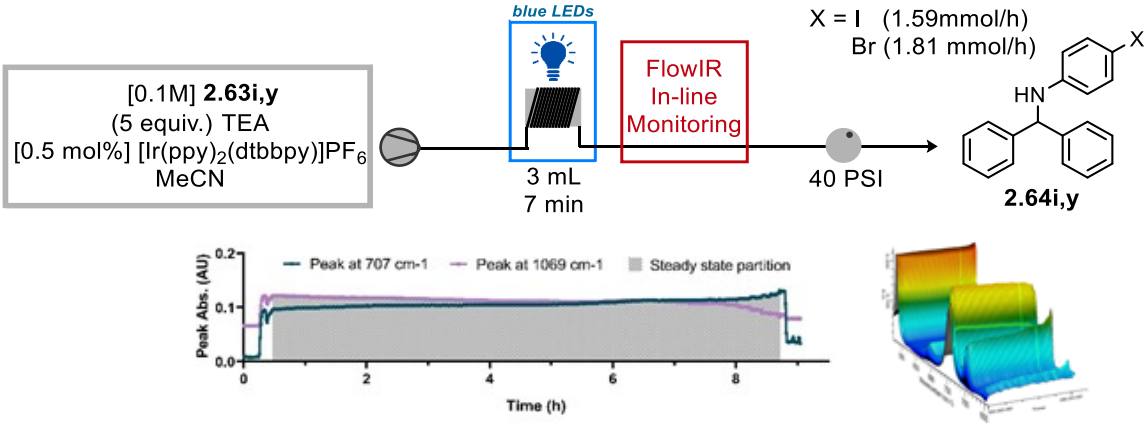

Figure 2.32: Continuous flow chemoselective transfer hydrogenation of imines.

2.7 Conclusions

A method for the transfer hydrogenation of imines via visible light photoredox catalysis was developed. This approach utilises photocatalyst, $[Ir(ppy)_2(dtbbpy)]PF_6$ in the presence of 5 equivalents of triethylamine which undertakes a dual role as single electron donor and hydrogen source. The developed reaction exhibits exceptional chemoselectivity for hydrogenation in the presence of other reducible functionalities. Diaryl-ketimine substrates provided excellent results, however the reaction proved limited being inapplicable to alkylphenone based ketimines. The development of a flow protocol allowed a rapid increase in rate of reaction (3 hours to 20 minutes) while simultaneously allowing gram scale processing. Mechanistic studies highlight the plausibility of the proposed mechanism. Deuterium labelling studies with d_{15}-TEA confirmed the generation of an α-amino radical while elucidating that TEA is the hydrogen source in reaction. Emission quenching studies indicate that triethylamine acts as a reductant, confirming a reductive quenching cycle. Transient absorption spectroscopy simultaneously confirmed a reductive quenching cycle while observing the reduced $[Ir(II)(ppy)_2(dtbbpy)]PF_6$ species in the presence of TEA.

2.8 Bibliography

1. Hu, J.; Wang, J.; Nguyen, T. H.; Zheng, N., *Beilstein J. Org. Chem.* **2013,** *9*, 1977-2001.
2. Kohls, P.; Jadhav, D.; Pandey, G.; Reiser, O., *Org. Lett.* **2012,** *14* (3), 672-675.
3. Ruiz Espelt, L.; Wiensch, E. M.; Yoon, T. P., *J. Org. Chem.* **2013,** *78* (8), 4107-4114.
4. Miyake, Y.; Nakajima, K.; Nishibayashi, Y., *J. Am. Chem. Soc.* **2012,** *134* (7), 3338-3341.
5. Zhu, S.; Das, A.; Bui, L.; Zhou, H.; Curran, D. P.; Rueping, M., *J. Am. Chem. Soc.* **2013,** *135* (5), 1823-1829.
6. Pandey, G.; Tiwari, S. K.; Singh, B., *Tetrahedron Lett.* **2016,** *57* (40), 4480-4483.
7. Xie, J.; Shi, S.; Zhang, T.; Mehrkens, N.; Rudolph, M.; Hashmi, A. S. K., *Angew. Chem. Int. Ed.* **2015,** *54* (20), 6046-6050.
8. Xie, J.; Yu, J.; Rudolph, M.; Rominger, F.; Hashmi, A. S. K., *Angew. Chem. Int. Ed.* **2016,** *55* (32), 9416-9421.
9. McNally, A.; Prier, C. K.; MacMillan, D. W. C., *Science* **2011,** *334* (6059), 1114-1117.
10. Schultz, D. M.; Yoon, T. P., *Science* **2014,** *343* (6174), 1239176.
11. Hager, D.; Macmillan, D. W. C., *J. Am. Chem. Soc.* **2014,** *136* (49), 16986-16989.
12. Nakajima, M.; Fava, E.; Loescher, S.; Jiang, Z.; Rueping, M., *Angew. Chem. Int. Ed.* **2015,** *54* (30), 8828-8832.
13. Uraguchi, D.; Kinoshita, N.; Kizu, T.; Ooi, T., *J. Am. Chem. Soc.* **2015,** *137* (43), 13768-13771.
14. Fava, E.; Millet, A.; Nakajima, M.; Loescher, S.; Rueping, M., *Angew. Chem. Int. Ed.* **2016,** *55* (23), 6776-6779.
15. Hoffmann, S.; Seayad, A. M.; List, B., *Angew. Chem. Int. Ed.* **2005,** *44* (45), 7424-7427.
16. Hoffmann, S.; Nicoletti, M.; List, B., *J. Am. Chem. Soc.* **2006,** *128* (40), 13074-13075.
17. Rueping, M.; Sugiono, E.; Azap, C.; Theissmann, T.; Bolte, M., *Org. Lett.* **2005,** *7* (17), 3781-3783.
18. Rueping, M.; Antonchick, A. P.; Theissmann, T., *Angew. Chem. Int. Ed.* **2006,** *45* (40), 6751-6755.
19. Rueping, M.; Antonchick, A. P.; Theissmann, T., *Angew. Chem. Int. Ed.* **2006,** *45* (22), 3683-3686.
20. Kizu, T.; Uraguchi, D.; Ooi, T., *J. Org. Chem.* **2016,** *81* (16), 6953-6958.
21. Qi, L.; Chen, Y., *Angew. Chem. Int. Ed.* **2016,** *55* (42), 13312-13315.
22. Fuentes De Arriba, A. L.; Urbitsch, F.; Dixon, D. J., *Chem. Commun.* **2016,** *52* (100), 14434-14437.
23. Rossolini, T.; Leitch, J. A.; Grainger, R.; Dixon, D. J., *Org. Lett.* **2018,** *20* (21), 6794-6798.
24. Leitch, J. A.; Fuentes de Arriba, Angel L.; Tan, J.; Hoff, O.; Martínez, C. M.; Dixon, D. J., *Chem. Sci.* **2018,** *9* (32), 6653-6658.
25. Lee, K. N.; Lei, Z.; Ngai, M. Y., *J. Am. Chem. Soc.* **2017,** *139* (14), 5003-5006.
26. Patel, N. R.; Kelly, C. B.; Siegenfeld, A. P.; Molander, G. A., *ACS Catal.* **2017,** *7* (3), 1766-1770.
27. Zhang, H. H.; Yu, S., *J. Org. Chem.* **2017,** *82* (19), 9995-10006.
28. Chen, M.; Zhao, X.; Yang, C.; Xia, W., *Org. Lett.* **2017,** *19* (14), 3807-3810.

29. Seehamongkol, T.; Horngren, T. H.; Alhajji, M. A. M.; Almond-Thynne, J.; Czyz, M. L.; Barrett, A. J.; Polyzos, A., *Aust. J. Chem.* **2019,** *73* (3), 189-194.
30. Alhajji, M. A.; Polyzos, A. The Development of a Visible Light Photoredox Driven Radical Pictet-Spengler Reaction (Master's Thesis). The University of Melbourne, 2017.
31. Brown, D. G.; Boström, J., *J. Med. Chem.* **2016,** *59* (10), 4443-4458.
32. Afanasyev, O. I.; Kuchuk, E.; Usanov, D. L.; Chusov, D., *Chem. Rev.* **2019,** *119* (23), 11857-11911.
33. Clayden, J.; Greeves, N.; Warren, S., *Organic Chemistry*. OUP Oxford: 2012.
34. Uematsu, N.; Fujii, A.; Hashiguchi, S.; Ikariya, T.; Noyori, R., *J. Am. Chem. Soc.* **1996,** *118* (20), 4916-4917.
35. Rueping, M.; Dufour, J.; Schoepke, F. R., *Green Chem.* **2011,** *13* (5), 1084-1105.
36. Zheng, C.; You, S. L., *Chem. Soc. Rev.* **2012,** *41* (6), 2498-518.
37. Zhou, S.; Fleischer, S.; Junge, K.; Das, S.; Addis, D.; Beller, M., *Angew. Chem. Int. Ed.* **2010,** *49* (44), 8121-8125.
38. Wills, M., Imino Transfer Hydrogenation Reductions. In *Top. Curr. Chem.*, Springer: Cham, 2016; pp 69-104.
39. Piotr, R.; Zbigniew, C., *Mini Rev. Org. Chem.* **2007,** *4* (3), 190-200.
40. Wang, C.; Wu, X.; Xiao, J., *Chem.: Asian J.* **2008,** *3* (10), 1750-1770.
41. Foubelo, F.; Yus, M., *Chem. Rec.* **2015,** *15* (5), 907-924.
42. Herrera, R. P., Organocatalytic Transfer Hydrogenation and Hydrosilylation Reactions. In *Hydrogen Transfer Reactions: Reductions and Beyond*, Guillena, G.; Ramón, D. J., Eds. Springer International Publishing: Cham, 2016; pp 105-144.
43. Matsunami, A.; Kayaki, Y., *Tetrahedron Lett.* **2018,** *59* (6), 504-513.
44. Wang, D.; Astruc, D., *Chem. Rev.* **2015,** *115* (13), 6621-6686.
45. Cottney, J.; Rankovic, Z.; Morphy, J. R., *Bioorg. Med. Chem. Lett.* **1999,** *9* (9), 1323-1328.
46. Zhang, Y.; Joseph, D. B.; Bowen, W. D.; Flippen-Anderson, J. L.; Dersch, C. M.; Rothman, R. B.; Jacobson, A. E.; Rice, K. C., *J. Med. Chem.* **2001,** *44* (23), 3937-3945.
47. Bishop, M. J.; McNutt, R. W., *Bioorg. Med. Chem. Lett.* **1995,** *5* (12), 1311-1314.
48. Spencer, C. M.; Faulds, D.; Peters, D. H., *Drugs* **1993,** *46* (6), 1055-1080.
49. McGrath, N. A.; Brichacek, M.; Njardarson, J. T., *J. Chem. Educ.* **2010,** *87* (12), 1348-1349.
50. Litwinienko, G.; Beckwith, A. L. J.; Ingold, K. U., *Chem. Soc. Rev.* **2011,** *40* (5), 2157-2163.
51. Placzek, M.; Dendorfer, M.; Przybilla, B.; Gilbertz, K. P.; Eberlein, B., *Acta Derm. Venereol.* **2013,** *93* (1), 30-32.
52. Sakamoto, M.; Cai, X.; Fujitsuka, M.; Majima, T., *Chem. Eur. J.* **2006,** *12* (6), 1610-1617.
53. Nguyen, J. D.; D'Amato, E. M.; Narayanam, J. M.; Stephenson, C. R., *Nat. Chem.* **2012,** *4* (10), 854-859.
54. Ghosh, I.; Ghosh, T.; Bardagi, J. I.; König, B., *Science* **2014,** *346* (6210), 725-728.
55. Chen, J.-Q.; Wei, Y.-L.; Xu, G.-Q.; Liang, Y.-M.; Xu, P.-F., *Chem. Commun.* **2016,** *52* (38), 6455-6458.
56. Discekici, E. H.; Treat, N. J.; Poelma, S. O.; Mattson, K. M.; Hudson, Z. M.; Luo, Y.; Hawker, C. J.; de Alaniz, J. R., *Chem. Commun.* **2015,** *51* (58), 11705-11708.
57. Cheng, Y.; Gu, X.; Li, P., *Org. Lett.* **2013,** *15* (11), 2664-2667.
58. Chi, Y.; Zhou, Y.-G.; Zhang, X., *J. Org. Chem.* **2003,** *68* (10), 4120-4122.

59. Fustero, S.; Soler, J. G.; Bartolomé, A.; Roselló, M. S., *Org. Lett.* **2003,** *5* (15), 2707-2710.
60. Ibrahem, I.; Casas, J.; Córdova, A., *Angew. Chem. Int. Ed.* **2004,** *43* (47), 6528-6531.
61. Verkade, J. M. M.; van Hemert, L. J. C.; Quaedflieg, P. J. L. M.; Alsters, P. L.; van Delft, F. L.; Rutjes, F. P. J. T., *Tetrahedron Lett.* **2006,** *47* (46), 8109-8113.
62. Buzzetti, L.; Crisenza, G. E. M.; Melchiorre, P., *Angew. Chem. Int. Ed.* **2019,** *58* (12), 3730-3747.
63. Atkins, P.; de Paula, J., *Atkins' Physical Chemistry*. OUP Oxford: 2010.
64. Berera, R.; van Grondelle, R.; Kennis, J. T. M., *Photosynth. Res.* **2009,** *101* (2), 105-118.
65. Orzeł, Ł.; Jańczyk, A.; Brindell, M.; Stopa, G.; Stochel, G., *J. Coord. Chem.* **2010,** *63* (14-16), 2695-2714.
66. Ichimura, K.; Kobayashi, T.; King, K. A.; Watts, R. J., *J. Phys. Chem. A* **1987,** *91* (24), 6104-6106.
67. Pilkington, R. L.; Rossouw, N. P.; van As, D. J.; Polyzos, A., *CHIMA* **2019,** *73* (10), 823-827.

2.9 Experimental Procedures and Characterization

General procedure A –benzophenone condensation

A mixture of the appropriate benzophenone (5.0 mmol, 1.0 equiv), substituted aniline (5.5 mmol, 1.1 equiv), 3 Å molecular sieves (~100mg) and PhMe (10mL) was heated to 90 °C under nitrogen. After 24 hours, the mixture was filtered through Celite® and the filtrate concentrated by rotary evaporation (50 mbar, 40 °C). Unreacted starting materials were removed by Kugelrohr short path distillation to afford the desired imine product in acceptable purity.

General procedure B –benzophenone imine condensation

A mixture of benzophenoneimine (5.0 mmol, 1.0 equiv), substituted aniline (5.5 mmol, 1.1 equiv), 3 Å molecular sieves (~100mg) and PhMe (10 mL) was heated to 90 °C under nitrogen. After 24 hours, the mixture was filtered through Celite® and the filtrate concentrated by rotary evaporation (50 mbar, 40 °C). Unreacted starting materials were removed by Kugelrohr short path distillation to afford the desired imine product in acceptable purity.

General procedure C –$TiCl_4$-mediated benzophenone condensation

A 100mL RBF equipped with a stirrer bar was charged with benzophenone (5.5mmol, 1.0 equiv) and anhydrous dichloromethane (15 mL) under N_2. The solution was cooled in an ice bath and then $TiCl_4$(361.8µL, 3.3 mmol, 0.6 equiv 1M solution in DCM) was added via syringe followed by a solution of substituted aniline (12 mmol, 2.2 equiv.) in anhydrous dichloromethane (15 mL). The mixture was stirred at room temperature overnight then quenched with H_2O (50mL) and extracted with dichloromethane (3 × 20 mL). The combined organic layers were washed with sat. NaCl, dried over $MgSO_4$ and

concentrated by rotary evaporation (50 mbar, 40 °C). Unreacted starting materials were removed by Kugelrohr short path distillation to afford the desired imine product in acceptable purity.

General procedure D–Buchwald-Hartwig amination of aryl iodides

A 50mL Schlenk tube equipped with a stirrer bar was charged with benzophenone imine (2.5 mmol, 1.0equiv), substituted iodobenzene (2.5 mmol, 1.0 equiv), $Pd(OAc)_2$ (25 µmol, 1.0 mol%), (±)-BINAP (75µmol, 3.0 mol%),Cs_2CO_3 (3.5 mmol, 1.4 equiv) and THF (10 mL). The reaction mixture was sparged with N_2 for 10 minutes then heated to 65 °C. After 48h, the mixture was cooled to room temperature, filtered through Celite® and the filtrate concentrated by rotary evaporation (50 mbar, 40 °C). Unreacted starting materials were removed by Kugelrohr short path distillation to afford the desired imine product in acceptable purity.

Characterization of imines

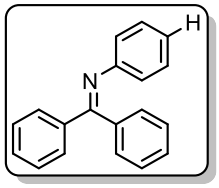

***N*-(diphenylmethylene)aniline 2.57/2.63a**

Method A 49% yield, yellow crystalline material; **MP** 107-112°C; **HRMS** [M+H] calculated for [$C_{19}H_{15}N$ + H] 258.1283 observed 258.1330; **^{1}H NMR** (400 MHz, CDCl3): δ = 7.43-7.36 (m, 8H), 7.31 (t, *J* = 7.3 Hz, 2H), 7.18 (t, *J* = 8.6 Hz, 2H), 6.76 (t, *J* = 7.3 Hz, 1H), 6.60 (d, *J* = 9.6 Hz, 2H), 5.57 (s, *J* = 3.1 Hz, 1H), 4.29 (s, 1H); **^{13}C NMR** (100 MHz, CDCl3): δ = 147.3, 142.9, 129.1, 128.7, 127.4, 127.3, 117.6, 113.4, 63.0; **FTIR** (ν/cm^{-1}, neat): 3385, 3092, 3040, 2960, 1733, 1673, 1598, 1497, 1450, 1426, 1314, 1266, 1184, 1028, 912, 839, 747, 696.

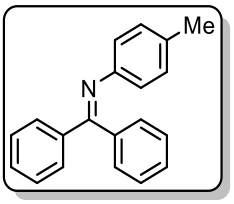

***N*-(diphenylmethylene)-4-methylaniline 2.63b**

Method A Yield 88%, orange solid; **HRMS** [M+H] calculated for [$C_{20}H_{17}N$ + H] 272.1439 observed 272.1435; **^{1}H NMR** (400 MHz, CDCl3): δ = 7.71 (d, *J* = 7.0 Hz, 2H), 7.44 (t, *J* = 7.2 Hz, 1H), 7.37 (t, *J* = 8.6 Hz, 2H), 7.23-7.27 (m, 3H), 7.14-7.06 (m, 2H), 6.92 (d, *J* = 8.0 Hz, 2H), 6.60 (d, *J* = 8.0 Hz, 2H), 2.21 (s, 3H); **^{13}C NMR** (100 MHz, CDCl3): δ = 167.9, 148.6, 139.9, 136.4, 132.6, 130.6, 129.5, 129.2, 129.1, 128.5, 128.1, 127.9, 121.0, 20.8; **FTIR** (ν/cm^{-1}, neat): 3055, 3019, 2915, 1953, 1659, 1610, 1595, 1573, 1499, 1443, 1369, 1315, 1275, 1290, 1275, 1220, 1173, 1141, 1108, 1073, 1027, 1017, 998, 957, 916, 825, 815,784, 772, 755, 724, 691.

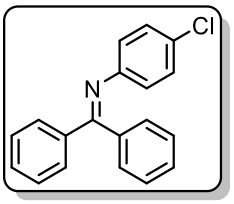

4-chloro-*N*-(diphenylmethylene)aniline 2.63c

Method A Yield 21% Yellow crystalline solid; **MP** 76-79°C; **HRMS** [M+H] calculated for [$C_{19}H_{14}NCl$ + H] 292.0893 observed 292.0889; **^{1}H NMR** (400 MHz, CDCl3): δ = δ = 7.71 (d, *J* = 7.0 Hz, 2H), 7.46 (t, *J* = 7.2 Hz, 1H), 7.39 (t, *J* = 7.2 Hz, 2H), 7.30-7.23 (m, 3H), 7.08 (d, *J* = 8.2Hz, 4H), 6.63 (d, *J* = 8.8 Hz, 2H); **^{13}C NMR** (100 MHz, CDCl3): δ = 168.9, 149.7, 139.3, 135.8, 130.9, 130.1, 129.41, 129.35, 128.8, 128.5, 128.2, 128.1, 122.3; **FTIR** (ν/cm^{-1}, neat): 3046, 1966, 1609, 1594,1586,1571, 1478, 1443, 1317, 1289, 1220, 1142, 1083, 1010, 958, 918, 828, 784, 690.

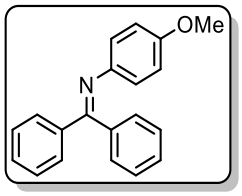

***N*-(diphenylmethylene)-4-methoxyaniline 2.63d**

Method A Yield 46% yellow-orange solid; **HRMS** [M+H] calculated for [$C_{20}H_{18}NO$ + H] 288.1388 observed 288.1501; **^{1}H NMR** (400 MHz, CDCl3): δ = 7.7 (d, *J* = 6.5 Hz, 2H), 7.4 (t, *J* = 7.6 Hz, 1H), 7.37 (t, *J* = 7.6 Hz, 2H), 7.28-7.25 (m, 3H), 7.13-7.07 (m, 2H), 6.66 (s, 4H), 3.71 (s, 3H); **^{13}C NMR** (100 MHz, CDCl3):δ = 167.7, 155.8, 144.3, 140.0, 136.6, 130.5, 129.6, 129.2, 128.5, 128.1, 128.0, 122.6, 113.7, 55.3; **FTIR** (ν/cm^{-1}, KBr): 3058, 3032, 2996, 2946, 2908, 2833, 1607, 1572, 1502, 1464, 1444, 1317, 1288, 1241, 1220, 1178, 1142, 1104, 1073, 1000, 959, 913, 832, 773, 751, 732, 696.

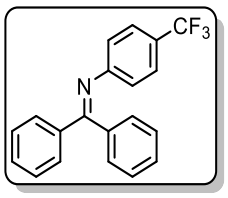

***N*-(diphenylmethylene)-4-(trifluoromethyl)aniline 2.63e**

Method B Yield 69%, thick yellow oil; **HRMS** [M+H] calculated for [$C_{20}H_{14}NF_3$ + H] 326.1157 observed 326.1149; **^{1}H NMR** (400 MHz, CDCl3): δ = 7.76 (d, *J* = 7.4 Hz, 2H), 7.51 (t, *J* = 7.0 Hz, 1H), 7.45-7.40 (m, 4H), 7.34- 7.26 (m, 3H), 7.11 (d, *J* = 6.1 Hz, 2H), 6.80 (d, *J* = 8.8 Hz, 2H); **^{13}C NMR** (100 MHz, CDCl3): δ = 169.2, 154.3, 139.0, 135.5, 131.2, 129.5, 129.4, 129.0, 128.3, 128.12, 128.07, 125.8, 124.8, 120.9; **^{19}F NMR** (376 MHz, CDCl3): δ = –61.8; **FTIR** (ν/cm^{-1}, neat): 3055, 1601, 1576, 1492, 1446, 1410, 1312, 1229, 1159, 1142, 1115, 1062, 1013, 954, 842, 784, 693.

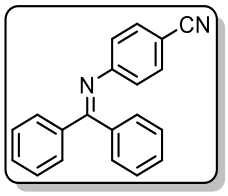

4-((diphenylmethylene)amino)benzonitrile 2.63f

Method A Yield 53% Yellow crystalline solid; **MP** 101-106°C; **HRMS** [M+H] calculated for [$C_{20}H_{14}N_2$ + H] 283.1235 observed 283.1230; **^{1}H NMR** (400 MHz, CDCl3): δ = 7.75 (d, *J* = 7.4 Hz, 2H), 7.49 (t, *J* = 6.5 Hz, 1H), 7.40 (m, 4H), 7.33-7.24 (m, 3H), 7.08 (d, *J* = 6.8 Hz, 2H), 6.76 (d, *J* = 8.8 Hz, 2H); **^{13}C NMR** (100MHz, CDCl3): δ = 169.5, 155.5, 138.6, 135.2, 132.8, 131.5, 130.3, 129.6, 129.2, 128.4, 128.2, 121.4, 119.3, 106.2; **FTIR** (ν/cm^{-1}, neat): 3061, 2221, 1619, 1593, 1491, 1443, 1316, 1296, 1266, 1232, 1169, 1142, 1108, 1073, 958, 918, 843, 783, 772, 734, 693.

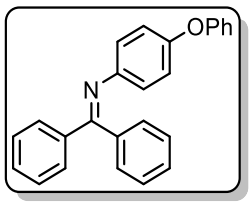

***N*-(diphenylmethylene)-4-phenoxyaniline 2.63g**

Method A Yield 36% fluffy tan solid; **MP** 110-111°C; **HRMS** [M+H] calculated for [$C_{25}H_{19}NO$ + H] 350.1545 observed 350.1540; **^{1}H NMR** (400 MHz, CDCl3): δ = 7.73 (d, *J* = 7.0 Hz, 2H), 7.46 (t, *J* = 6.7 Hz, 1H), 7.39 (t, *J* = 8.0 Hz, 2H), 7.29-7.25 (m, 5H), 7.16-7.09 (m, 2H), 7.02 (t, *J* = 7.8 Hz, 1H), 6.88 (d, *J* = 8.4 Hz, 2H), 6.80 (d, *J* = 8.4 Hz, 2H), 6.68 (d, *J* = 8.6 Hz, 2H); **^{13}C NMR** (100 MHz, CDCl3): δ = 168.5, 157.9, 152.56, 147.0, 139.6, 136.3, 130.7, 129.55, 129.53, 129.3, 128.6, 118.0, 128.2, 128.0, 122.6, 122.5, 119.6; **FTIR** (ν/cm^{-1}, neat): 3040, 1620, 1589, 1572, 1488, 1476, 1444, 1315, 1289, 1234, 1212, 1163, 1141, 1072, 1012, 1000, 959, 870, 848, 760, 751, 688, 648, 603.

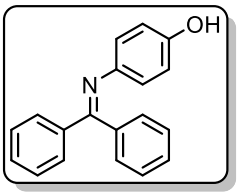

4-((diphenylmethylene)amino)phenol 2.63h

Method B Yield 87%, yellow solid; **MP** 169-173°C; **HRMS** [M+H] calculated for [$C_{19}H_{15}NO$ + H] 274.1232 observed 274.1227; **^{1}H NMR** (400 MHz, CDCl3): δ = 7.71 (d, *J* = 7.8 Hz, 2H), 7.47 (t, *J* = 6.7 Hz, 1H), 7.39 (t, *J* = 8.4 Hz, 2H), 7.25-7.32 (m, 3H), 7.12 (d, *J* = 8.2 Hz, 2H), 6.62 (dd, *J* = 10.8, 8.2Hz, 4H); **^{13}C NMR** (100 MHz, CDCl3): δ = 168.6, 152.2, 143.7, 139.9, 136.5, 130.7, 129.6, 129.3, 128.6, 128.2, 128.0, 122.8, 115.5; **FTIR** (ν/cm^{-1}, neat): 3020, 1600, 1582, 1568, 1499, 1439, 1357, 1320, 1265, 1216, 1098, 1075, 1027, 962, 834, 784, 762, 692.

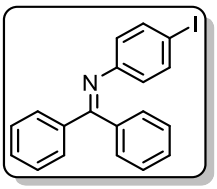

***N*-(diphenylmethylene)-4-iodoaniline 2.63i**

Method B Yield 83%, yellow crystals; **HRMS** [M+H] calculated for [$C_{19}H_{14}NI$ + H] 384.0249 observed 384.0243; **^{1}H NMR** (400 MHz, CDCl3): δ = 7.73 (d, *J* = 7.6 Hz, 2H), 7.48 (t, *J* = 6.8 Hz, 1H), 7.44-.7.38 (m, 4H), 7.33-7.26 (m, 3H), 7.16-7.13 (m, 2H), 6.50 (d, *J* = 8.6 Hz, 2H); **^{13}C NMR** (100 MHz, CDCl3): δ = 169.0, 150.9, 139.3, 137.5, 135.8, 131.0, 129.42, 129.37, 128.8, 128.3, 128.1, 123.3, 87.2; **FTIR** (ν/cm^{-1}, neat): 3051, 3024, 1740, 1617, 1596, 1576, 1475, 1445, 1392, 1316, 1293, 1223, 1141, 1003, 957, 915, 829, 784, 764, 696, 660.

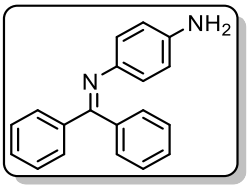

N1-(diphenylmethylene)benzene-1,4-diamine 2.63j

Method B Yield 52%, yellow solid that quickly discoloured to brown; **MP** 131-137°C; **HRMS** [M+H] calculated for [$C_{19}H_{16}N_2$ + H] 273.1392 observed 273.1386; **^{1}H NMR** (400 MHz, cdcl$_3$): δ 6.47 (d, 8.6 Hz,2H), 6.59 (d, 2H,). 7.12 (m, 2H), 7.28 (m, 3H), 7.37 (t, 7.4Hz, 2H) 7.43 (t, 7.4 Hz, 1H), 7.70 (d, 6.7Hz, 2H); **^{13}C NMR** (100 MHz $CDCl_3$) :δ 115.26, 122.91, 128.01, 128.10, 128.32, 129.08 129.59, 130.29, 136.92, 140.26, 142.39, 142.70, 166.93; **FTIR** (ν/cm^{-1}, KBr): 3356, 1733, 1699, 1653, 1605, 1558, 1540, 1506, 1457, 1268, 963, 832, 700.

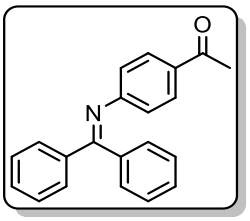

1-(4-((diphenylmethylene)amino)phenyl)ethenone 2.63k

Method D Yield 67%, yellow solid; **MP** 113-116°C; **HRMS** [M+H] calculated for [$C_{21}H_{17}NO$ + H] 300.1388 observed 300.1386; **^{1}H NMR** (400 MHz, CDCl3): δ = 7.80-7.73 (m, 4H), 7.47 (t, *J* = 7.2 Hz, 2H), 7.40 (t, *J* = 7.2 Hz, 2H), 7.28-7.23 (m, 2H), 7.10 (d, *J* = 6.7 Hz, 2H), 6.76 (d, *J* = 8.4 Hz, 2H), 2.49 (s, 3H); **^{13}C NMR** (100 MHz, CDCl3): δ = 197.2, 168.8, 155.9, 132.4, 132.1, 131.2, 130.0, 129.5, 129.3, 129.0, 128.3, 128.2, 128.1, 120.6, 26.4; **FTIR** (ν/cm^{-1}, KBr): 3055, 2961, 2851, 1669, 1631, 1588, 1142, 953, 843, 637.

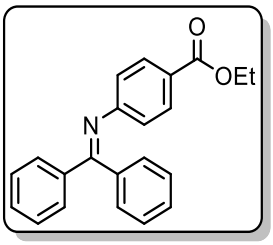

ethyl 4-((diphenylmethylene)amino)benzoate 2.63l

Method C Yield 84%, yellow sandy solid; **MP** 82-86°C; **HRMS** [M+H] calculated for [$C_{22}H_{19}NO_2$ + H] 330.1494 observed 330.1489; **^{1}H NMR** (400 MHz, CDCl3): δ = 7.84 (d, *J* = 9.0 Hz, 2H), 7.77 (d, *J* = 7.2 Hz, 2H), 7.52 (d, *J* = 6.9 Hz, 1H), 7.42 (t, *J* = 6.9 Hz, 2H), 7.33-7.24 (m, 3H), 7.11 (d, *J* = 7.4 Hz, 2H), 6.74 (d, *J* = 7.6 Hz, 2H), 4.29 (q, *J* = 7.0 Hz, 2H), 1.33 (t, *J* = 7.0 Hz, 3H); **^{13}C NMR** (100 MHz, CDCl3): δ = 168.8, 167.0, 166.5, 155.6, 130.3, 130.3, 129.4, 129.3, 128.9, 128.3, 128.0, 125.0, 120.5, 113.7, 60.7, 14.3; **FTIR** (ν/cm^{-1}, neat): 3060, 2982, 2902, 1706,1616, 1592, 1572, 1492, 1475, 1445, 1431, 1391, 1363, 1318, 1264, 1223, 1170, 1142, 1120, 1100, 1015, 958, 915, 855, 781, 698.

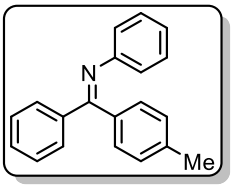

(E/Z)-*N*-(phenyl(p-tolyl)methylene)aniline 2.63m

Method A 61%, yellow oil (1:0.89 mixture of E and Z isomers); **HRMS** [M+H] calculated for [$C_{20}H_{17}N$ + H] 272.1439 observed 272.1434; **^{1}H NMR** (400 MHz, CDCl3): δ = 7.74 and7.65 (d, *J* = 8.0 Hz, 2H), 7.48-7.38 and 7.26-7.10 (m,7H), 7.06-7.00 (,m, 2H), , 6.95-5.89 (m,1H), 6.73 (t, *J* = 7.2 Hz, 2H), 2.41 and 2.31 (s, 3H); **^{13}C NMR** (100 MHz, CDCl3): δ = 168.4, 168.2, 151.4, 151.3, 141.1, 140.0, 138.6, 137.0, 136.4, 133.2, 130.6, 129.6, 129.5, 129.37, 129.31, 128.9, 128.56, 128.49, 128.44, 128.42, 128.1, 127.8, 123.02, 122.99, 121.0, 120.9, 21.5, 21.4; **FTIR** (ν/cm^{-1}, neat): 3095, 3023, 1684, 1606, 1592l 1484, 1445, 1315, 1293, 1220, 1180, 1142, 1072, 1025, 958, 828, 769, 727, 698.

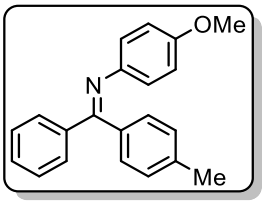

(E/Z)-4-methoxy-*N*-(phenyl(p-tolyl)methylene)aniline 2.63n

Method A Yield 77%, yellow-orange solid (1:0.92mixture of E and Z isomers); **HRMS** [M+H] calculated for [$C_{21}H_{19}NO$ + H] 302.1545 observed 302.1540; **^{1}H NMR** (400 MHz, CDCl3): δ = 7.70 and 7.60 (d, *J* = 8.0 Hz, 2H), 7.4-4 7.35 (t, *J* = 7.4 Hz, 1.5H), 7.28-7.22 (m, 1.5H), 7.18 (d, *J* = 7.0 Hz, 1H), 7.13-7.04 (m,2H), 6.99 (d, 1H), 6.70-6.63 (m,, 4H), 3.72-3.70 (s, 3H), 2.38 and2.31 (s, 3H); **^{13}C NMR** (100 MHz, CDCl3): δ = 192.3, 167.9, 166.6, 155.8, 144.71, 144.59, 141.0, 140.5, 138.5, 137.5, 136.9, 133.7, 130.5, 129.79, 129.69, 129.37, 129.31, 129.0, 128.8, 128.5, 128.24, 128.09, 122.73, 122.67. 113.88, 113.83, 55.44, 55.42, 21.58, 21.52; **FTIR** (ν/cm^{-1}, neat): 3004, 2941, 2834, 1656, 1615. 1599, 1467, 1498, 1465, 1447, 1438, 1315, 1285, 1240, 1218, 1175, 1140, 1106, 1075, 1028, 956, 917, 829, 777, 697.

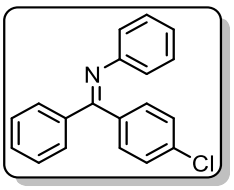

(E/Z)-*N*-((4-chlorophenyl)(phenyl)methylene)aniline 2.63o

Method A Yield 82%, orange solid (mixture of E and Z isomers1:0.6); **MP** 83-85°C; **HRMS** [M+H] calculated for [$C_{19}H_{14}NCl$ + H] 292.0893 observed 292.0889; **^{1}H NMR** (400 MHz, CDCl3): δ = 7.71-7.66 (m, 2H), 7.49-7.34 (m, 2.5H), 7.27-7.21 (m, 2H), 7.17-7.03 (m, 4.5H), 6.92 (q, *J* = 8.6Hz, 1H), 6.69 (d, *J* = 7.0 Hz, 2H); **^{13}C NMR** (100 MHz, CDCl3): 167.19, 167.16, 151.05, 151.03, 139.4, 138.2, 137.0, 135.8, 134.75, 134.63, 131.08, 131.06, 130.7, 129.52, 129.37, 128.90, 128.78, 128.63, 128.55, 128.43, 128.40, 128.2, 123.52, 123.48, 121.00, 120.90; **FTIR** (ν/cm^{-1}, neat): 3036, 1659, 1605, 1596,

`583, 1562, 1484, 1441, 1396, 1305, 1290, 1214, 1174, 1142, 1083, 959, 916, 899, 839. 780, 729, 696.

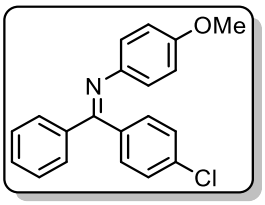

(E/Z)-*N*-((4-chlorophenyl)(phenyl)methylene)-4-methoxyaniline 2.63p

Method A Yield 79%, yellow-brown solid (~1:0.81X mixture of *E* and *Z* isomers); **MP** 83-85°C; **HRMS** [M+H] calculated for [$C_{20}H_{16}NOCl + H$] 322.0999 observed 322.0995; **^{1}H NMR** (400 MHz, CDCl3): δ = 7.39-7.68 (d, *J* = 7.2 Hz, 2H) 7.34-7.65 (d, *J* = 8.8 Hz, 2H), 7.23-7.29 (m, 3H), 7.01-7.09 (m, 2H) 6.63-6.71 (m, 4H), 3.71 and 3.73 (s, 3H); **^{13}C NMR** (100 MHz, CDCl3): δ = 166.6, 156.1, 144.1, 139.8, 138.6, 136.8, 136.3, 135.1, 134.7, 131.6, 131.2, 130.9, 130.6, 130.1, 129.6, 129.3, 128.82, 128.77, 128.53, 128.51, 128.39, 128.32, 122.75, 122.58, 114.03, 113.89, 55.45, 55.43; **FTIR** (ν/cm^{-1}, KBr): 3059, 3043, 3003, 2967, 2946, 2934, 2912, 2837, 1650, 1612, 1584, 1573, 1502, 1485, 1465, 1444, 1414, 1397, 1316, 1301, 1284, 1243, 1215, 1179, 1167, 1141, 1105, 1086, 1032, 1013, 961, 945, 923, 845, 829, 802, 789, 778, 752, 728 694, 664, 640, 619, 606.

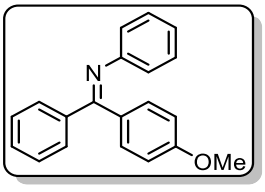

(E/Z)-*N*-((4-methoxyphenyl)(phenyl)methylene)aniline 2.63q

Method B Yield 62%, thick yellow oil (*E* and *Z* isomeric ratio: 1:0.6); **HRMS** [M+H] calculated for [$C_{20}H_{17}NO$ + H] 288.1388 observed 288.1381; **^{1}H NMR** (400 MHz, CDCl3): δ = 7.78-7.75 (d, *J* = 8.6 Hz, 2H), 7.48-7.41 (t, *J* = 6.5 Hz, 1H), 7.26-7.24 (m, 2H), 7.20-7.07 (m, 4H), 6.95-6.89 (m, 2H), 6.79-6.73 (m, 3H), 3.84 and 3.75 (s, 3H);

^{13}CNMR (100 MHz, CDCl3): δ = 167.9, 167.6, 161.8, 159.7, 151.6, 151.4, 140.3, 136.4, 132.6, 132.3, 131.5, 131.0, 130.6, 129.7, 129.5, 128.6, 128.4, 128.1, 127.8, 122.99, 122.86, 121.1, 121.0, 113.5, 113.2, 55.4, 55.2; **FTIR** (ν/cm^{-1}, KBr): 3057, 1013, 2969, 2929, 2843, 1915, 1742, 1649, 1597, 1576, 1505, 1445, 1416, 1319, 1281, 1262, 1199, 1181, 170, 1150, 1112, 1081, 1062, 1023, 1000, 971, 954, 937, 922, 888, 843, 817, 792, 740, 696, 677, 632.

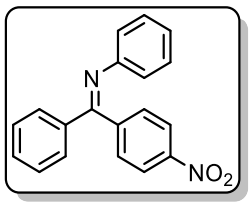

(E/Z)-*N*-((4-nitrophenyl)(phenyl)methylene)aniline 2.63r

Method A Yield 76%, bright orange crystals (*E* and *Z* isomeric ratio: 1:0.92); **MP** 128-132°C; **HRMS** [M+H] calculated for [$C_{19}H_{14}N_2O_2$ + H] 303.1134 observed 303.1129; **^{1}H NMR** (400 MHz, CDCl3): δ 6.66 (d, 2H, 7.0 Hz), 6.70 (d, 2H, 8.1 Hz), 6.95 (q, 2H, 7.04, 7.04Hz), 7.08 (d, 2H, 6.7Hz), 7.15(q, 4H, 7.4), 7.30 (m, 5H), 7.42 (t, 2H, 7.4 Hz), 7.50 (t, 1H, 8.6 Hz), 7.68 (d, 2H, 7.6 Hz), 7.90 (d, 2H, 8.2 Hz), 8.12 (d, 2H, 8.6 Hz), 8.23 (d, 2H, 8.2); **^{13}C NMR** (100 MHz $CDCl_3$) :δ 120.50, 120.69, 123.24, 123.34, 123.82, 123.96, 128.33, 128.50, 128.62, 128.78, 129.03, 129.22, 129.27, 130.14, 130.37, 131.36, 135.05, 138.28, 142.95, 145.27, 147.50, 148.97, 150.38, 150.42, 165.98, 166.13; **FTIR** (ν/cm^{-1}, KBr): 3059, 3031, 1952, 1616, 1596, 1586, 1519, 1485, 1443, 1407, 1345, 1407, 1345, 1407, 1345, 1315, 1302, 1291, 1274, 1219, 1185, 1164, 1141, 1106, 1072, 1026, 1011, 998, 982, 957, 916, 901, 867, 853, 779, 767, 757, 724, 700, 664, 628.

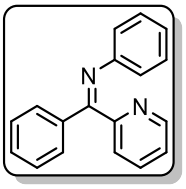

(E/Z)-*N*-(phenyl(pyridin-2-yl)methylene)aniline 2.63s

Method A Yield 74%, yellow solid (~1:1.3 mixture of *E* and *Z* isomers); **MP** 75-79°C; **HRMS** [M+H] calculated for [$C_{18}H_{14}N_2$ + H] 259.1235 observed 259.1230; **^{1}H NMR** (400 MHz, CDCl3): δ = 8.66 (d, *J* = 4.9 Hz, 0.5H), 8.64 (d, *J* = 4.9 Hz, 0.5H), 8.07 (d, *J* = 8.1 Hz, 0.5H), 7.79 (td, *J* = 5.9, 1.6 Hz, 1H), 7.72 (d, *J* = 7.6 Hz, 1H), 7.52-7.32 (m, 3H), 7.27-7.22 (m, 1.5H), 7.18-7.10 (m, 3.5H), 7.00-6.90 (m, 1.5H), 6.73 (d, *J* = 7.4 Hz, 2H); **^{13}C NMR** (100 MHz, CDCl3): δ = 167.6, 166.6, 157.2, 155.2, 153.7, 150.8, 150.7, 149.3, 149.2, 138.2, 136.5, 135.9, 135.1, 130.9, 129.7, 129.1, 128.8, 128.49, 128.47, 128.3, 127.8, 124.7, 124.6, 123.9, 123.56, 123.50, 123.1, 120.9, 120.8; **FTIR** (ν/cm^{-1}, neat): 3060, 1630, 1579, 1478, 1463, 1446, 1317, 1300, 1219, 1157, 1072, 1046, 1029, 993, 959, 928, 894, 789,, 768, 753, 725, 693, 657.

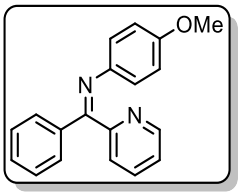

(Z)-4-methoxy-*N*-(phenyl(pyridin-2-yl)methylene)aniline 2.63t

Method A Yield 65%, red viscous oil (~1:1.27 mixture of E and Z isomers); **HRMS** [M+H] calculated for [$C_{19}H_{16}N_2$ + H] 289.1341 observed 289.1337; **^{1}H NMR** (400 MHz, CDCl3): δ =8.65 (d, J = 4.9 Hz, 1H), 8.03 and 7.69(d, J= 8.6 Hz, 1H), 7.75 and 7.53(td, J = 6.3, 2.0 Hz, 1H) 7.69 (d, J = 7.0 Hz, 1H) 7.44-7.35 (m. 2H), 7.31 and 7.18 (dd, J = 4.1, 1.6 Hz, 1H), 7.28-7.24(m, 1.5H), 7.15-7.12 (m, 1H), 6.98 (d, J = 7.0 Hz, 0.5H), 6.72-6.64 (m,4H), 3.70 and 3.69 (s, 3H); **^{13}C NMR** (100 MHz, CDCl3): δ = 167.0, 166.2, 157.5, 156.27, 156.19, 155.8, 149.5, 149.3, 144.0, 143.8, 138.6, 136.5, 136.1, 135.7, 131.0, 130.7, 129.8, 129.0, 128.3, 128.0, 124.8, 124.5, 128.8, 123.1, 122.76, 122.65, 113.80,

113.78, 55.33, 55.32; **FTIR** (ν/cm^{-1}, neat): 2994, 2833, 1739, 1664, 160, 1573, 1500, 1463, 1444, 1430, 1318, 1289, 1234, 1169, 1102, 1032,992, 963, 833, 799, 776 746, 695.

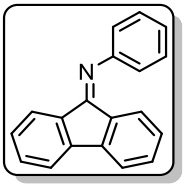

***N*-(9H-fluoren-9-ylidene)aniline 2.63u**

Method A Yield 93%, bright yellow-orange solid; **MP** 69-72°C; **HRMS** [M+H] calculated for [$C_{19}H_{13}N$ + H] 256.1126 observed 256.1122; **^{1}H NMR** (400 MHz, CDCl3): δ = 7.90 (d, *J* = 7.5 Hz, 1H) 7.59 (d, *J* = 7.6 Hz, 2H) 7.46-7.31 (m, 5H), 7.19 (t, *J* = 8.2 Hz, 1H), 6.98 (d, *J* = 8.1 Hz, 2H), 6.90 (t, *J* = 7.6 Hz, 1H), 6.54 (d, *J* = 7.6 Hz, 1H); **^{13}C NMR** (100 MHz, CDCl3): δ 163.2, 151.6, 143.9, 141.9, 137.4, 132.03, 131.94, 131.3, 129.4, 128.6,127.8, 127.2, 124.2, 123.5, 120/3. 119.7, 118.4; **FTIR** (ν/cm^{-1}, KBr): 3056, 2919, 2360, 1644,1591, 1483, 1449, 1384, 1305, 1240, 1209, 1192, 1155, 1141, 1102, 1071, 1024, 946, 832, 794, 780, 754, 733, 715, 697, 652, 618.

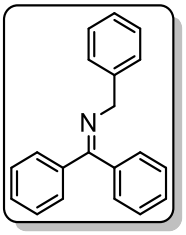

***N*-(diphenylmethylene)-1-phenylmethanamine 2.63v**

Method A Yield 76%, white solid; **MP** 65-66°C; **HRMS** [M+H] calculated for [$C_{20}H_{17}N$ + H] 272.1439 observed 272.1433; **^{1}H NMR** (400 MHz, CDCl3): δ = 7.70 (t, *J* = 6.3 Hz, 2H), 7.47 (m, 3H), 7.34 (m, 7H), 7.23 (m, 3H), 4.67 (s, 2H); **^{13}C NMR** (100 MHz, CDCl3): δ = 168.8, 140.7, 139.8, 136.7, 130.1, 128.58, 128.55, 128.52, 128.3, 128.1, 127.8, 127.6, 126.5, 57.4; **FTIR** (ν/cm^{-1}, KBr): 3059, 3020, 2922, 2857, 1619, 1572,

1488, 1442, 1343, 1343, 1313, 1282, 1176, 1152, 1071, 1026, 998, 959, 930, 910, 845, 782, 766, 747, 717, 697, 642.

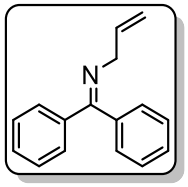

***N*-(diphenylmethylene)prop-2-en-1-amine 2.63w**

Method C Yield 77% at 85% pure as a clear off yellow liquid; **HRMS** [M+H] calculated for [$C_{16}H_{15}N$ + H] 222.1283 observed 222.1275; **^{1}H NMR** (400 MHz, CDCl3): δ = 7.64 (d, J = 7.0/2.0, 2H), 7.42-7.47 (m,3H), 7.30-7.37p (m,3H), 7.17ppm (d, J = 5.9,1.6Hz, 2H), 6.01-6.11 (m, 1H), 5.17 (m, 1H), 5.11 (m, 1H), 4.04 (dt, J = 5.1/1.8Hz, 2H); **^{13}C NMR** (100 MHz, CDCl3): δ = 68.9, 139.8, 137.8, 136.59, 136.56, 132.4, 130.1, 128.4, 128.0, 127.7, 115.1, 56.4; **FTIR** (ν/cm^{-1}, neat): 3043, 1660, 1642, 1620, 1597, 1575, 1490, 1444, 1415, 1313, 1281, 1178, 1154, 1073, 1021, 994, 915, 772, 697, 637.

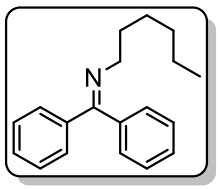

***N*-(diphenylmethylene)hexan-1-amine 2.63x**

Method B Yield 54%, pale yellow-green liquid; **HRMS** [M+H] calculated for [$C_{19}H_{23}N$ + H] 266.1909 observed 266.1906; **^{1}H NMR** (400 MHz, CDCl3): δ = 7.59 (d, *J* = 6.5 Hz, 2H), 7.43 (m, 3H), 7.32 (m, 3H), 7.15 (d, *J* = 6.1 Hz, 2H), 3.36 (t, *J* = 7.0 Hz, 2H), 1.67-1.63(m, 2H), 1.34-1.19(m, 6H), 0.86 (t, *J* = 6.8 Hz, 3H); **^{13}C NMR** (100 MHz, CDCl3): δ = 167.6, 140.1, 137.1, 129.7, 128.4, 128.3, 128.2, 128.0, 127.8, 54.0, 31.7, 31.2, 27.2, 22.6, 14.1; **FTIR** (ν/cm^{-1}, NaCl plate): 3058, 3024, 2928, 2856, 1623, 1577, 1490, 1445, 1314, 1288, 1073, 1028, 778, 695, 642.

Photocatalytic reduction of diarylimines

Imine (0.45mmol), catalyst (0.0068mmol), triethylamine (2.25mmol) were added to a vial with 5mL of acetonitrile. This solution was sparged with nitrogen, then illuminated with 14W Blue LEDs for 3 hours. Acetonitrile and triethylamine were taken off under reduced pressure, the crude mixture was redissolved in ethyl acetate and filtered through a plug of silica. This filtered solution was then dried under reduced vacuum to give product with purity greater than 95%.

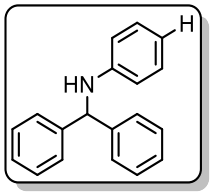

***N*-benzhydrylaniline 2.58/2.64a**

Yield 97%, yellow oil; **HRMS** [M+H] calculated for [$C_{19}H_{17}N$ + H] 260.1439 observed 260.1438; **^{1}H NMR** (400 MHz, CDCl3): δ = 7.43-7.36 (m, 8H), 7.31 (t, *J* = 7.3 Hz, 2H), 7.18 (t, *J* = 8.6 Hz, 2H), 6.76 (t, *J* = 7.3 Hz, 1H), 6.60 (d, *J* = 9.6 Hz, 2H), 5.57 (s, *J* = 3.1 Hz, 1H), 4.29 (s, 1H); **^{13}C NMR** (100 MHz, CDCl3): δ = 147.3, 142.9, 129.1, 128.7, 127.4, 127.3, 117.6, 113.4, 63.0; **FTIR** (ν/cm^{-1}, neat): 3385, 3092, 3040, 2960, 1733, 1673, 1598, 1497, 1450, 1426, 1314, 1266, 1184, 1028, 912, 839, 747, 696.

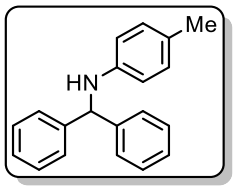

***N*-benzhydryl-4-methylaniline 2.64b**

Yield 100%, yellow oil; **HRMS** [M+H] calculated for [$C_{20}H_{19}N$ + H] 274.1596 observed 274.1591; **^{1}H NMR** (400 MHz, CDCl3): δ = 7.43-7.35 (m, 8H), 7.30 (t, *J* = 6.5 Hz, 2H), 6.98 (d, *J* = 8.4 Hz, 2H), 6.52 (d, *J* = 8.2 Hz, 2H), 5.52 (s, 1H), 4.17 (s, 1H), 2.27 (s, 3H); **^{13}C NMR** (100 MHz, CDCl3): δ = 145.2, 143.2, 129.7, 128.8, 127.5, 127.3, 126.8, 113.6,

63.3, 20.5; **FTIR** (ν/cm^{-1}, neat): 3401, 3024, 2922, 2860, 1733, 1612, 1514, 1490, 1450, 1315, 1300, 1262, 1238, 1125, 1094, 1065, 1027, 916, 806, 773, 741, 697.

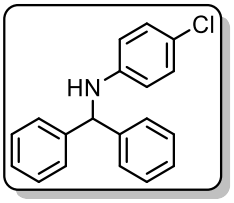

***N*-benzhydryl-4-chloroaniline 2.64c**

Yield 84%, yellow oil; **HRMS** [M+H] calculated for [$C_{19}H_{16}NCl$ + H] 294.1050 observed 294.1043; **^{1}H NMR** (400 MHz, CDCl3): δ = 7.39-7.28 (m, 10H), 7.08 (d, *J* = 9.6 Hz, 2H), 6.48 (d, *J* =9.4 Hz, 2H), 5.50 (d, *J* = 3.1 Hz, 1H), 4.28 (s, 1H); **^{13}C NMR** (100 MHz, CDCl3): δ = 145.8, 142.5, 129.0, 128.9, 127.6, 127.4, 122.3, 114.6, 63.1; **FTIR** (ν/cm^{-1}, neat): 3410. 2989, 1739, 1596, 1492, 1450, 1397, 1311, 1292, 1265, 1089, 813, 743, 698.

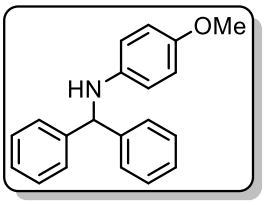

***N*-benzhydryl-4-methoxyaniline 2.64d**

Yield 100%, yellow oil; **HRMS** [M+H] calculated for [$C_{20}H_{19}NO$ + H] 290.1545 observed 290.1555; **^{1}H NMR** (400 MHz, CDCl3): δ = 7.43 (d, *J* = 7.4 Hz, 4H), 7.37 (t, *J* = 7.4 Hz, 4H), 7.30 (t, *J* = 7.4Hz, 2H), 6.77 (d, *J* = 8.6 Hz, 2H), 6.55 (d, *J* = 9.0 Hz, 2H), 5.48 (s, 1H), 4.07 (s, 1H), 3.74 (s, 3H); **^{13}C NMR** (100 MHz, CDCl3): δ = 152.1, 143.2, 141.7, 128.7, 127.4, 127.3, 114.7, 114.6, 63.8, 55.7; **FTIR** (ν/cm^{-1}, neat): 3391, 3027, 2943, 2831, 1739, 1601, 1507, 1450, 1403, 1298, 1234, 1177, 1032, 823, 770, 738, 697.

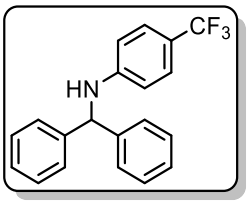

***N*-benzhydryl-4-(trifluoromethyl)aniline 2.64e**

Yield 87%, yellow oil; **HRMS** [M$^-$] calculated for [C20H17F3N]-: m/z =326.1162, found: m/z =326.1154; **^{1}H NMR** (400 MHz, CDCl3): δ = 7.46-7.36 (m, 12H), 6.65 (d, *J* = 8.6 Hz, 2H), 5.66 (d, *J* = 4.3 Hz, 1H), 4.71 (d, J = 4.1 Hz, 1H); **^{13}C NMR** (100 MHz, CDCl3): δ = 149.7, 142.1, 129.0, 127.8, 127.5, 126.6, 123.7, 119.1, 112.8, 62.7; **^{19}F NMR** (376 MHz, CDCl3): δ = –60.91; **FTIR** (ν/cm^{-1}, neat): 3421, 2986, 1738, 1610, 1526 1319, 1268, 1160, 1107, 1061, 825, 736, 698, 656.

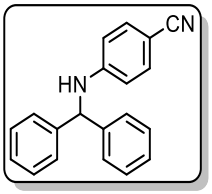

4-(benzhydrylamino)benzonitrile 2.64f

Yield 71%, yellow oil; **HRMS** [M+H] calculated for [$C_{20}H_{16}N_2$ + H] 285.1392 observed 285.1386; **^{1}H NMR** (400 MHz, CDCl3): δ = 7.36-7.27 (m, 12H), 6.52 (d, *J* = 8.8 Hz, 2H), 5.56 (d, *J* = 4.7 Hz, 1H), 4.82 (s, 1H); **^{13}C NMR** (100 MHz, CDCl3): δ = 150.2, 141.4, 133.6, 129.0, 127.9, 127.4, 120.3, 113.2, 99.3, 62.3; **FTIR** (ν/cm^{-1}, neat): 3376, 2987, 2213, 1739, 1601, 1516, 1493, 1451, 1334, 1266, 1173, 823, 733, 697.

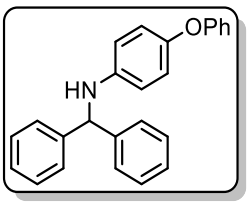

***N*-benzhydryl-4-phenoxyaniline 2.64g**

Yield 90%, orange solid; **MP** 123-125°C; **HRMS** [M+H] calculated for [$C_{25}H_{21}N$ + H] 352.1701 observed 352.1705; **^{1}H NMR** (400 MHz, CDCl3): δ = 7.47 (d, *J* = 7.0 Hz, 4H),

7.41 (t, *J* = 7.0 Hz, 4H), 7.36-7.31 (m, 4H), 7.07 (t, *J* = 7.0 Hz, 1H), 7.02 (d, *J* = 7.8 Hz, 2H), 6.92 (d, *J* = 8.8 Hz, 2H), 6.59 (d, *J* = 9.2 Hz, 2H), 5.46 (s, 1H), 4.26 (s, 1H); **^{13}C NMR** (100 MHz, CDCl3): δ = 158.9, 147.8, 144.0, 142.9, 129.5, 128.8, 127.4, 122.0, 120.9, 117.3, 114.4, 63.5; **FTIR** (ν/cm^{-1}, neat): 3417, 3035, 2924, 2985, 1608, 1584, 1506, 1476, 1452, 1397, 1291, 1230, 866, 824, 835.

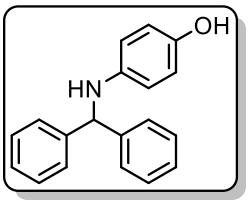

4-(benzhydrylamino)phenol 2.64h

Yield 100%, yellow oil; **HRMS** [M+H] calculated for [$C_{19}H_{17}NO$ + H] 276.1388 observed 276.1382; **^{1}H NMR** (400 MHz, CDCl3): δ = 7.39-7.27 (m, 10H), 6.63 (d, *J* = 9.2 Hz, 2H), 6.45 (d, *J* = 8.6 Hz, 2H), 5.50 (br s, 1H), 5.43 (s, 1H), 4.02 (br s, 1H); **^{13}C NMR** (100 MHz, CDCl3): δ = 147.8, 143.2, 141.6, 128.8, 127.5, 127.3, 116.2, 114.9, 63.9; **FTIR** (ν/cm^{-1}, neat): 3392b, 3093, 3085, 1603, 1520, 1493, 1450, 1228, 1028, 909, 822, 789, 737, 700.

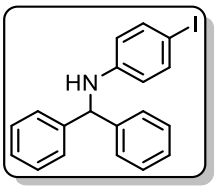

***N*-benzhydryl-4-iodoaniline 2.64i**

Yield 98%, yellow oil; **HRMS** [M+H] calculated for [$C_{19}H_{16}NI$ + H] 386.0406 observed 386.0399; **^{1}H NMR** (400 MHz, CDCl3): δ = 7.36-7.24 (m, 12H), 6.32 (d, *J* = 9.0 Hz, 2H), 5.44 (s, 1H), 4.27 (s, 1H); **^{13}C NMR** (100 MHz, CDCl3): δ =146.8, 142.3, 137.7, 128.8, 127.5, 127.4, 115.7, 78.5, 62.8; **FTIR** (ν/cm^{-1}, neat): 3403, 3093, 3042, 2992, 2929, 1653, 1588, 1489, 1451, 1392, 1313, 1291, 1264, 1238, 1182, 1064, 1028, 997, 912, 809, 743, 699, 659.

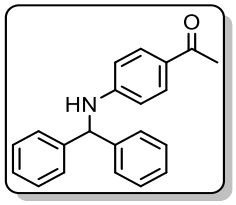

1-(4-(benzhydrylamino)phenyl)ethenone 2.64k

Yield 98%, yellow oil; **HRMS** [M+H] calculated for [$C_{21}H_{19}NO$ + H] 302.1545 observed 302.1539; **^{1}H NMR** (400 MHz, CDCl3): δ = 7.76 (d, *J* = 10.6 Hz, 2H), 7.38-7.25 (m, 10H), 6.53 (d, *J* = 9.8 Hz, 2H), 5.63 (d, *J* = 4.7 Hz, 1H), 4.92 (d, *J* = 4.7 Hz, 1H), 2.44 (s, 3H); **^{13}C NMR** (100 MHz, CDCl3): δ = 196.5, 151.1, 141.8, 130.6, 128.9, 127.7, 127.4, 127.0, 112.4, 62.3, 26.0; **FTIR** (ν/cm^{-1}, neat): 3413, 3349, 3095, 3011, 1737, 1656, 1588, 1522, 1486, 1451, 1421, 1347, 1273, 1178, 1128, 1095, 1071, 1027, 955, 910, 826, 733, 700.

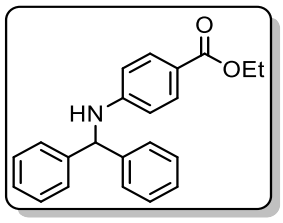

ethyl 4-(benzhydrylamino)benzoate 2.64l

Yield 74%, yellow oil; **HRMS** [M+H] calculated for [$C_{22}H_{21}NO_2$ + H] 332.1651 observed 332.1646; **^{1}H NMR** (400 MHz, CDCl3): δ = 7.82 (d, *J* = 8.8 Hz, 2H), 7.33-7.25 (m, 10H), 6.51 (d, *J* = 8.9 Hz, 2H), 5.59 (d, *J* = 4.7 Hz, 1H), 4.74 (s, 1H), 4.27 (q, *J* = 7.0 Hz, 2H), 1.32 (t, *J* = 7. 1Hz, 3H); **^{13}C NMR** (100 MHz, CDCl3): δ = 166.8, 150.8, 141.9, 131.3, 128.9, 127.6, 127.4, 119.2, 112.4, 62.4, 60.2, 14.4; **FTIR** (ν/cm^{-1}, neat): 3370, 1971, 1694, 1599, 1520, 1488, 1450, 1366, 1335, 1267, 1101, 1021, 839, 770, 737, 697.

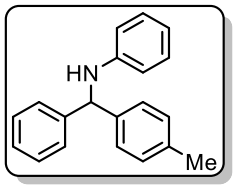

***N*-(phenyl(p-tolyl)methyl)aniline 2.64m**

Yield 98%, yellow oil; **HRMS** [M+H] calculated for [$C_{20}H_{19}N$ + H] 274.1596 observed 274.1592; **^{1}H NMR** (400 MHz, CDCl3): δ = 7.42-7.34 (m, 4H), 7.31-7.27 (m, 2H), 7.19-7.14 (m, 4H), 6.74 (t, *J* = 7.8 Hz, 1H), 6.59 (d, *J* = 8.8 Hz, 2H), 5.52 (s, 1H), 4.26 (s, 1H), 2.38 (s, 3H); **^{13}C NMR** (100 MHz, CDCl3): δ = 147.5, 143.1, 140.1, 137.0, 129.5, 129.1, 128.8, 127.4, 127.3, 117.6, 113.5, 62.8, 21.2; **FTIR** (ν/cm^{-1}, neat): 3407, 3031, 2926, 1738, 1598, 1497, 1450, 1425, 1312, 1264, 1178, 799, 735, 693.

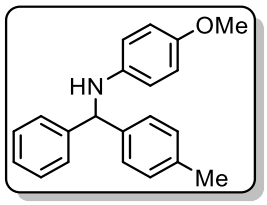

4-methoxy-*N*-(phenyl(p-tolyl)methyl)aniline 2.64n

Yield 90%, orange oil; **HRMS** [M+H] calculated for [$C_{21}H_{21}NO$ + H] 304.1701 observed 304.1693; **^{1}H NMR** (400 MHz, CDCl3): δ = 7.50 (d, *J* = 7.6 Hz, 2H), 7.43 (t, *J* = 7.6 Hz, 2H), 7.37 (t, *J* = 7.6 Hz, 3H), 7.25 (d, *J* = 7.6 Hz, 2H), 6.83 (d, *J* = 8.6 Hz, 2H), 6.62 (d, *J* = 8.6 Hz, 2H), 5.52 (s, 1H), 4.12 (s, 1H), 3.81 (s, 3H), 2.45 (s, 3H); **^{13}C NMR** (100 MHz, CDCl3): δ = 152.2, 143.5, 141.9, 140.5, 137.0, 129.5, 128.8, 127.5, 127.3, 114.8, 114.7, 63.7, 55.8, 21.2; **FTIR** (ν/cm^{-1}, neat): 3408, 2931, 1530, 1451, 1240, 1175, 1111, 1034, 817, 758, 733, 698.

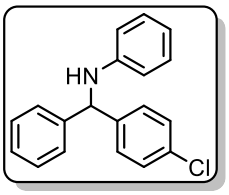

***N*-((4-chlorophenyl)(phenyl)methyl)aniline 2.64o**

Yield 95%, yellow oil; **HRMS** [M+H] calculated for [$C_{19}H_{16}NCl$ + H] 294.1050 observed 294.1045; **^{1}H NMR** (400 MHz, CDCl3): δ = 7.44-7.32 (m, 9H), 7.19 (t, *J* = 7.6 Hz, 2H), 6.76 (t, *J* = 7.3 Hz, 1H), 6.59 (d, *J* = 6.1 Hz, 2H), 5.54 (s, 1H), 4.25 (s, 1H); **^{13}C NMR** (100 MHz, CDCl3): δ = 147.1, 142.6, 141.4, 133.1, 129.1, 128.8, 128.6, 127.6, 127.41, 127.37, 118.0, 113.6, 62.5; **FTIR** (ν/cm^{-1}, neat): 3398, 2981, 1730, 1598, 1500, 1487, 1451, 1426, 1312, 1249, 1155, 1088, 1013, 841, 797, 747, 693.

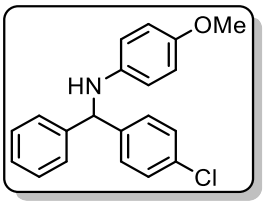

***N*-((4-chlorophenyl)(phenyl)methyl)-4-methoxyaniline 2.64p**

Yield 100%, orange oil; **HRMS** [M+H] calculated for [$C_{20}H_{18}NOCl$ + H] 324.1155 observed 324.1146; **^{1}H NMR** (400 MHz, CDCl3): δ = 7.43-7.35 (m, 9H), 6.82 (d, *J* = 8.2 Hz, 2H), 6.59 (d, *J* = 7.8 Hz, 2H), 5.50 (s, 1H), 4.08 (s, 1H), 3.80 (s, 3H); **^{13}C NMR** (100 MHz, CDCl3): δ = 152.4, 142.9, 141.8, 141.5, 133.0, 129.0, 128.8, 127.7, 127.5, 114.85, 114.81 63.3, 55.8; **FTIR** (ν/cm^{-1}, neat): 3393, 2968, 2832, 1738, 1600, 1509, 1488, 1451, 1404, 1296 1235, 1177, 1089, 1033, 1013, 817, 800, 736, 698.

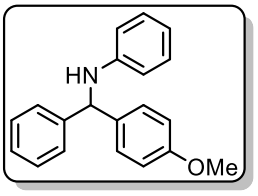

***N*-((4-methoxyphenyl)(phenyl)methyl)aniline 2.64q**

Yield 92%, yellow oil; **HRMS** [M+H] calculated for [$C_{20}H_{19}NO$ + H] 290.1545 observed 290.1536; **^{1}H NMR** (400 MHz, CDCl3): δ = 7.42-7.30 (m, 7H), 7.17 (t, *J* = 7.6 Hz, 2H), 6.91 (d, *J* = 8.4 Hz, 2H), 6.74 (t, *J* = 7.3 Hz, 1H), 6.59 (d, *J* = 8 Hz, 2H), 5.52 (s, 1H), 4.25 (s, 1H), 3.81 (s, 3H); **^{13}C NMR** (100 MHz, CDCl3): δ = 158.9, 147.4, 143.2, 135.2, 129.1, 128.7, 128.7, 127.42, 127.32, 117.6, 114.1, 113.5, 62.4, 55.3; **FTIR** (ν/cm^{-1}, neat): 3408, 2990, 2932, 1733, 1601, 1503, 1453, 1310, 1250, 1180, 1062, 1031, 834, 782, 748, 697.

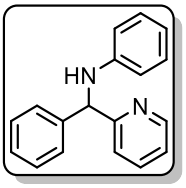

***N*-(phenyl(pyridin-2-yl)methyl)aniline 2.64s**

Yield 97%, orange-red oil; **HRMS** [M+H] calculated for [$C_{18}H_{16}N_2$ + H] 261.1392 observed 261.1387; **^{1}H NMR** (400 MHz, CDCl3): δ = 8.61 (d, *J* = 4.7 Hz, 1H), 7.60 (td, *J* = 6.5, 1.8 Hz, 1H), 7.50 (d, *J* = 7.2 Hz, 2H), 7.40-7.33 (m, 3H), 7.27 (t, *J* = 7.3 Hz, 1H), 7.18-7.13 (m, 3H), 6.74-6.67 (m, 3H), 5.63 (d, *J* = 3.5 Hz, 1H), 5.56 (d, *J* = 4.3 Hz, 1H); **^{13}C NMR** (100 MHz, CDCl3): δ = 160.9, 149.2, 147.1, 142.6, 136.9, 129.2, 128.9, 127.6, 127.4, 122.3, 122.0, 117.5, 113.6, 63.3; **FTIR** (ν/cm^{-1}, neat): 3355,3010, 1597, 1570, 1501, 1453, 1430, 1318, 1262, 1179, 1152, 1049, 1029, 995, 750, 697.

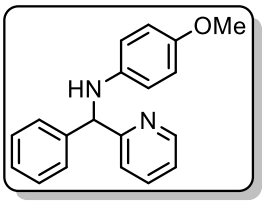

4-methoxy-*N*-(phenyl(pyridin-2-yl)methyl)aniline 2.64t

Yield 90%, orange oil; **HRMS** [M+H] calculated for [$C_{19}H_{18}N_2O$ + H] 291.1497 observed 291.1492; **^{1}H NMR** (400 MHz, CDCl3): δ = 8.58 (d, *J* = 4.9 Hz, 1H), 7.59 (td, *J* = 6.3, 1.8 Hz, 1H), 7.46 (d, *J* = 7.4 Hz, 2H), 7.37-7.30 (m, 3H), 7.23 (t, *J* = 6.9 Hz, 1H), 7.13 (dd, *J* = 5.1, 2.0 Hz, 1H), 6.72 (d, *J* = 8.4, 2.2Hz, 2H), 6.59 (dd, *J* = 9.0, 4.3Hz, 2H), 5.53 (s, 1H), 5.17 (s, 1H), 3.69 (s, 3H); **^{13}C NMR** (100 MHz, CDCl3): δ = 161.2, 152.0, 149.2, 142.6, 141.3, 136.8, 128.8, 127.49, 127.42, 122.2, 121.9, 114.8, 114.7, 64.2, 55.7; **FTIR** (ν/cm^{-1}, neat): 3365. 2966, 1736, 1589, 1570, 1510, 1466, 1433, 1238, 1178, 1035, 825, 756, 700.

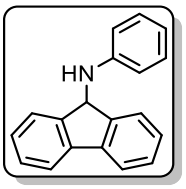

N-phenyl-9H-fluoren-9-amine 2.64u

Yield 95%, yellow solid; **HRMS** [M+H] calculated for [$C_{19}H_{15}N$ + H] 258.1283 observed 258.1278; **^{1}H NMR** (400 MHz, CDCl3): δ = 7.75 (d, *J* = 7.0 Hz, 2H), 7.61 (d, *J* = 7.4 Hz, 2H), 7.42 (t, *J* = 7.4 Hz, 2H), 7.30-7.23 (m, 4H), 6.84-6.79 (m, 3H), 5.70 (s, 1H), 4.04 (s, 1H); **^{13}C NMR** (100 MHz, CDCl3): δ = 147.7, 145.7, 140.2, 129.5, 128.5, 127.6, 124.9, 120.0, 118.0, 113.8, 59.1; **FTIR** (ν/cm^{-1}, neat): 3356, 2988, 1595, 1495, 1442, 1299, 1286, 1243, 1186, 1153, 1107, 1084, 1055, 991, 943, 881, 865, 839, 830, 741, 726, 693.

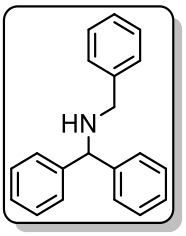

***N*-benzyl-1,1-diphenylmethanamine 2.64v**

Yield 100%, clear-off yellow oil; **HRMS** [M+H] calculated for [$C_{20}H_{19}N$ + H] 274.1596 observed 274.1589; **^{1}H NMR** (400 MHz, CDCl3): δ = 7.51 (d, *J* = 7.8 Hz, 4H), 7.45-7.24 (m, 11H), 5.90 (s, 1H), 4.95 (s, 1H), 3.82 (s, 2H); **^{13}C NMR** (100 MHz, CDCl3): δ = 144.0, 140.5, 128.6, 128.5, 128.2, 127.4, 127.1, 127.0, 66.5, 51.9; **FTIR** (ν/cm^{-1}, neat): 2995, 2958, 1737, 1658, 1598, 1492, 1450, 1364, 1313, 1270, 1090, 1027, 843, 735, 696.

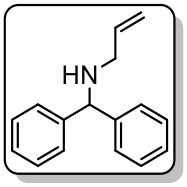

***N*-benzhydrylprop-2-en-1-amine 2.64w**

Yield 81%, clear oil; **HRMS** [M+H] calculated for [$C_{16}H_{17}N$ + H] 224.1439 observed 224.1434; **^{1}H NMR** (400 MHz, CDCl3): δ = 7.46-7.41 (m, 4H), 7.36-7.32 (m, 4H), 7.27-7.22 (m, 2H), 6.00-5.91 (m, 2H), 5.22-5.10 (m, 2H), 4.88 (s, 1H), 3.22 (dt, *J* = 6.0, 1.5 Hz, 2H); **^{13}C NMR** (100 MHz, CDCl3): δ = 144.0, 136.8, 128.5, 127.3, 127.0, 115.9, 66.5, 50.4; **FTIR** (ν/cm^{-1}, neat): 3065, 3026, 2895, 2851, 1689, 1655, 1598, 1588, 1472, 1492, 1449, 1284, 1182, 1086, 1026, 994, 917,744, 696.

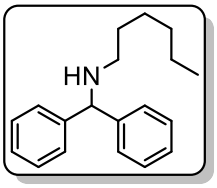

***N*-benzhydrylhexan-1-amine 2.64x**

Yield 98%, clear oil; **HRMS** [M+H] calculated for [$C_{19}H_{25}N$ + H] 258.2065 observed 268.2067; **^{1}H NMR** (400 MHz, CDCl3): δ = 7.42 (d, *J* = 7.4 Hz, 4H), 7.31 (t, *J* = 7.4 Hz,

4H), 7.21 (t, *J* = 7.4 Hz, 2H), 4.83 (s, 1H), 2.59 (t, *J* = 7.1 Hz, 2H), 1.56-1.49 (m, 2H), 1.37-1.24 (m, 7H), 0.90 (t, *J* = 6.6 Hz, 3H); **^{13}C NMR** (100 MHz, CDCl3): δ = 144.4, 128.4, 127.3, 126.9, 67.7, 48.4, 31.8, 30.2, 27.1, 22.7, 14.1; **FTIR** (ν/cm^{-1}, neat): 3026, 2857, 2931, 1738, 1671, 1597, 1492, 1451, 1368, 1276, 1113, 1028, 842, 746, 698, 639.

General procedure for continuous flow transfer hydrogenation

All continuous flow reactions were performed using a Syrris Asia syringe pump module and standard 1/16" Perfluoroalkoxy alkanes (PFA) tubing. A mixture of the imine **2.63(a,c-e,i,j,n,q,s,v)** (0.09mmol, 1.0 equiv), [Ir(ppy)$_2$(dtbbpy)]PF$_6$(1.5 mol%), Et$_3$N (5.0 equiv) and MeCN (2mL) was prepared and then sparged with nitrogen for 10 minutes. An aliquot of the mixture was taken (1 mL) and loaded into a 1 mL sample PTFE loop. The reaction mixture was then pumped with an MeCN flow stream at 0.416 mL min–1through a 5 mL reactor coil that was irradiated with 14W blue LEDs (Figure S3). Once the reaction solution was processed, a further 5mL of MeCN was flushed through the system and collected. The reaction out flow was concentrated by rotary evaporation (50 mbar, 40 °C) and the residue dissolved in EtOAc and filtered through a plug of SiO$_2$ to afford the amine products **2.64(a,c-e,i,j,n,q,s,v)** as a yellow oil.

Stern-Volmer Quenching Experiments

Fluorescence quenching experiments were conducted on a Varian Cary Eclipse fluorescence spectrophotometer. Experiments were conducted with [Ir(ppy)$_2$(dtbbpy)]PF$_6$ (0.1mM) concentrations of 0.1mmol in MeCN with quencher (**2.57** or TEA) varied concentrations. Experiments were carried out with an excitation wavelength of 454nm.

Radical Trapping experiments

Imine **2.57** (0.45mmol), $[Ir(ppy)_2(dtbbpy)]PF_6$ (0.0068mmol), triethylamine (2.25mmol) and Radical trapping agent (0.45 0r 2.25mmol) were added to a vial with 5mL of acetonitrile. This solution was sparged with nitrogen, then illuminated with 14W Blue LEDs for 3 hours. Acetonitrile and triethylamine were taken off under reduced pressure, the crude mixture was then submitted for Mass Spectrommetry and ^1H NMR spectroscopy studies.

Deuterium Labelling Experiments

Imine **2.57** (0.09mmol), $[Ir(ppy)_2(dtbbpy)]PF_6$ (0.0014mmol), d_{15}-triethylamine (0.45mmol) were added to an NMR tube with 1mL of d_3-MeCN. This solution was sparged with nitrogen, then illuminated with 14W Blue LEDs for 3 hours. The crude solution was then analysed via ^1H NMR spectroscopy.

Chapter 3: The Visible Light Mediated Decarboxylative α-Alkylation of Tetrahydroisoquinolines via a Batch and Flow Protocol

3.1 Introduction

3.1.1: α-Amino Radical-Radical Coupling via Photoredox Chemistry

The α-amino radical represents a valuable reactive intermediate that enables the preparation of structurally diverse amine products. Within the context of photoredox catalysis, the generation of α-amino radicals is typically mediated through photooxidative[1-2] or photoreductive[3-4] pathways. Several reaction pathways are available subsequent to radical generation and have been summarised in Chapter 1. A notable pathway is the generation of C-sp^3-C-sp^3 (carbon-carbon) bonds via a radical termination step. In this mode of reactivity, a carbon centred-radical couples with an α-amino radical as shown in Figure 3.1. This reaction generates an α-amino C-sp^3-C-sp^2 or C-sp^3 bond without the limitations imposed by transition metal catalysis. However, despite the obvious advantages and favourable thermodynamics of this transformation, radical-radical cross-coupling of α-amino radicals remains challenging due to:

- the persistent radical effect[5-7]
- matching radical philicity[8]
- rapid reaction kinetics and low radical concentration[9]

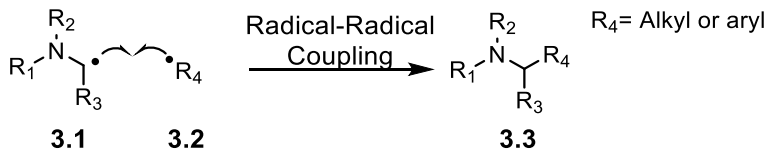

Figure 3.1: Radical coupling of α-amino radicals.

In 2011, MacMillan reported a method for the α-arylation of tertiary amines with electron deficient benzonitriles (figure 3.2).[10] Through the application of high throughput screening, MacMillan *et al.* determined that the triplet excited state of *fac*-[Ir(III)(ppy)$_3$] generates aryl radical **3.5'** via photoinduced single electron reduction of the benzonitrile derivative **3.5**. The photocatalyst is regenerated via subsequent single electron oxidation of a tertiary amine with consequent rearrangement of the amine radical cation to an α-amino radical (**3.5'**). Radical-radical coupling ensues and rearomatisation is achieved via the loss of a cyano group affording the α-arylated product (**3.6**). Macmillan further extended this methodology to generate α-amino radicals via the electrofugal decarboxylative oxidation of amino acid derivatives.[11] Macmillan's procedures represent the first visible light mediated generation of α-amino radicals with synthetic applications resolved by a radical-radical coupling pathway.

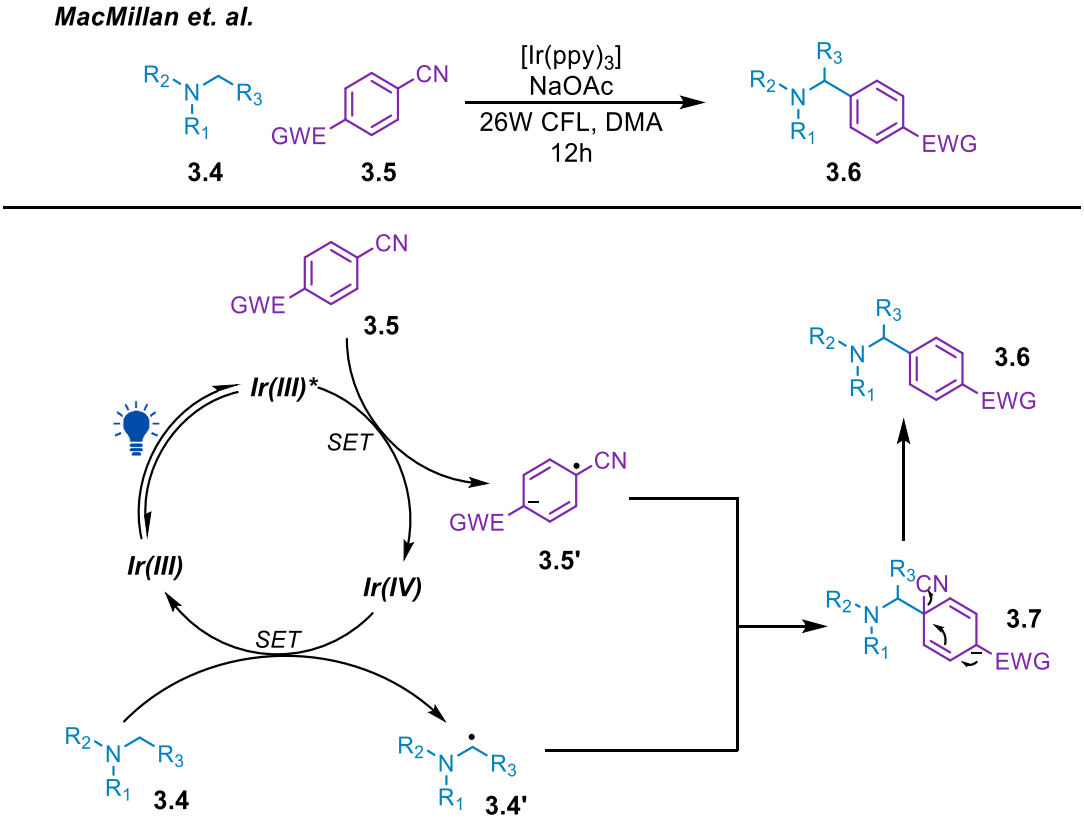

Figure 3.2: α-arylation of amines conducted by MacMillan *et al.*

MacMillan then utilised α-amino radicals derived via a photoreductive pathway to couple α-amino and α-ether radicals to produce 1,2-aminoethers,[12] a further extension of this methodology included the β-Mannich reaction between imines and cyclic ketones.[13] Facilitated by PCET, the Rueping laboratory accessed α-amino radicals via a photoreductive process, enabling the synthesis of 1,2-diamines via aza-pinacol coupling.[14] Extension of this methodology allowed the synthesis of unsymmetrical 1,2-diamines, via coupling two distinct α-amino radicals, generated via both photooxidative and reductive approaches.[15] Ooi developed an analogous enantioselective transformation with the addition of a catalytic quantities of chiral Brønsted acid.[16] Molander, Yu and Lu each reported the reductive alkylation of imines incorporating the photoreductive generation of α-amino radicals and oxidation of a radical precursor with subsequent radical coupling affording the corresponding α-alkylated amine.[17-19]

The photooxidative generation of α-amino radicals and subsequent radical-radical coupling has been applied beyond the α-arylation of amines.[10] This tactic for α-functionalisation competes with iminium generation; necessitating rapid-radical coupling of the α–amino radical to ensure selective formation of the coupled product. Lu *et al.* reported the α-vinylation of tetrahydroisoquinolines (THIQ) via a dual photoredox-palladium catalysed system;[20] while Hashmi disclosed that under irradiation with sunlight, gold complex, $[Au_2(\mu\text{-dppm})_2](OTf)_2$ is an efficient photocatalyst for the α-aza-alkynylation of a variety of tertiary amines via coupling α-amino and *sp* hybridised radicals.[21] Meggers reported the enantioselective coupling of α-amino radicals and trifluoromethyl ketyl radicals utilising a bifunctional Lewis acid/photocatalyst iridium species to attain exceptional selectivity at the cost of reaction scope.[22-23] Xiao *et al.* also reported this transformation incorporating a broader scope of substrates, however did not address selectivity.[24]

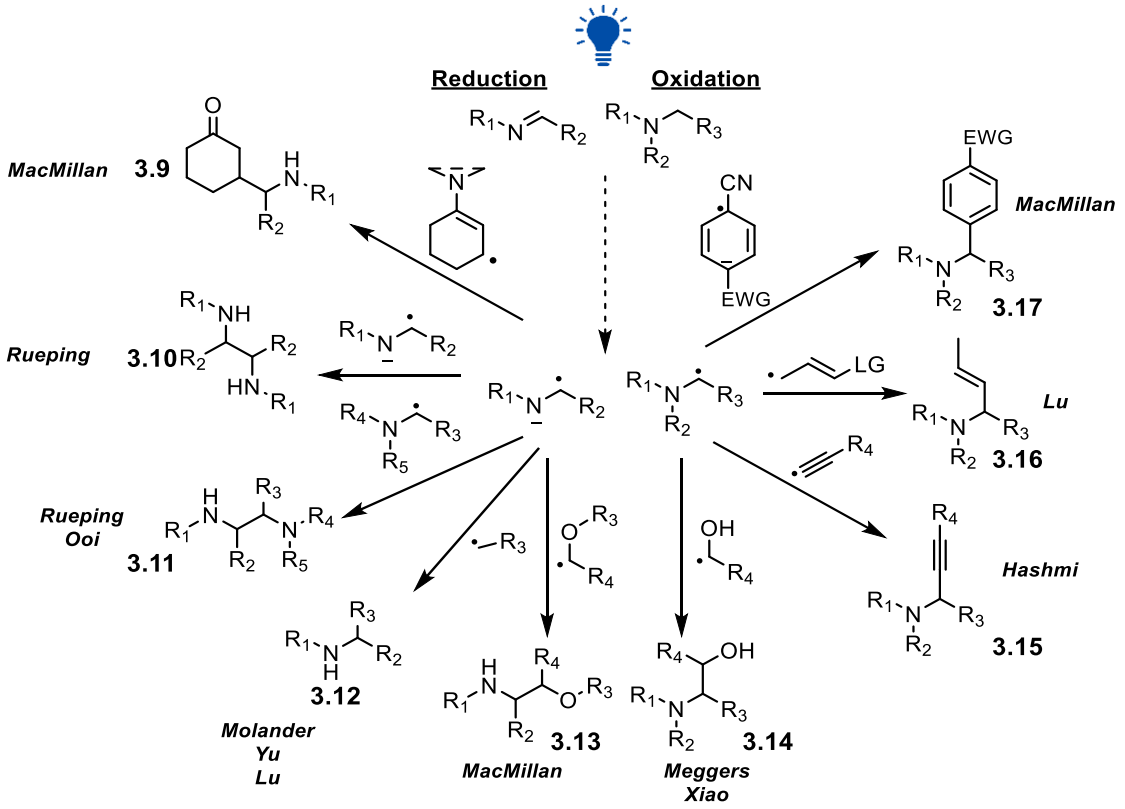

Figure 3.3: Summary of α-amino radical coupling reactions.

The α-alkylation of amines with aliphatic chains can be achieved by radical-radical coupling between α-amino and alkyl radicals. Despite its potential, this transformation remains generally unexplored. In 2017, Yu *et al.* exploited unactivated alkyl bromides as alkyl radical precursors in the presence of catalytic quantities of $[Pd(PPh_3)_4]$, achieving excellent yields of the α-alkylated product.[25] Yu proposes that upon irradiation, the triplet state of $[Pd(PPh_3)_4]$ is reduced by **3.18** with subsequent α-amino radical formation. The photocatalyst is then regenerated via the single electron reduction of an alkyl bromide (**3.19**), ensuing radical-radical coupling furnishes the α-alkylated product (**3.20**). Utilising this system, Yu also achieved the inter and intramolecular sp^2-sp^3 coupling of alkyl bromides and a range of aromatic heterocycles. However, Yu's procedure is restricted by its sensitivity to oxygen necessitating the use of a glovebox, rendering the methodology as operationally onerous. This work, as well as a conceptually similar report by Pandey *et al.*, which utilised exotic substrates, alkyl selenides (**3.21**), as radical precursors[26]

represent the only procedures that involve coupling α-amino and unactivated aliphatic radicals. Therefore, this project sought to further explore this transformation utilising *N*-hydroxyphthalimide ester's (NHP ester) as radical precursors.

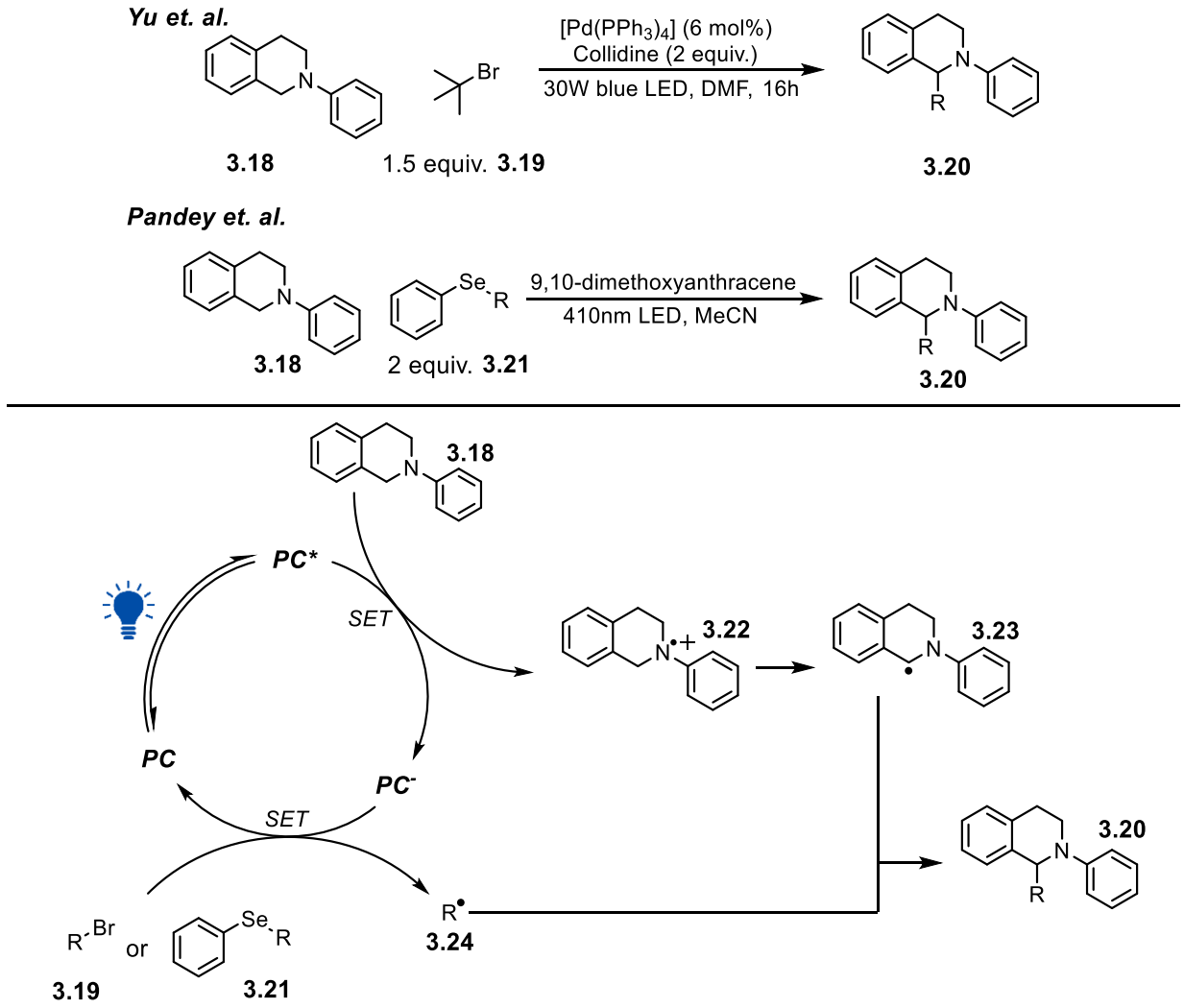

Figure 3.4: Conditions and general mechanism of the α-alkylation of amines by Yu and Pandey.

3.1.2 *N*-Hydroxy Phthalimides Esters - A Convenient Alkyl Radical Source

N-hydroxy phthalimide (NHP) esters are readily synthesised via a one-step procedure from the corresponding carboxylic acid and represent a convenient source for alkyl radical generation.[27-28] Upon single electron reduction, NHP esters readily undergo decarboxylative fragmentation generating a phthalimide anion, carbon dioxide and an alkyl radical (figure 3.5). NHP esters readily generate the corresponding primary, secondary and tertiary carbon radicals owing to their mild reduction potential of approximately -1.2 V vs SCE. NHP esters have been applied as radical precursors in a broad range of methodologies mediated by photoredox catalysis.

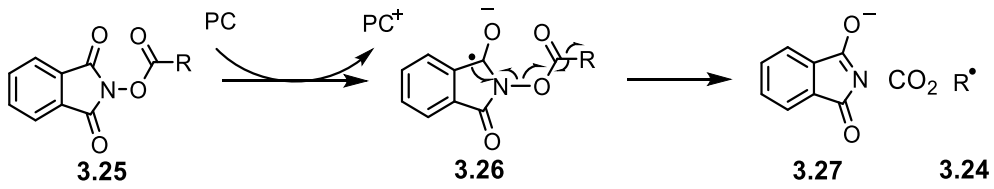

Figure 3.5: Decarboxylative fragmentation of NHP ester

NHP esters were initially reported in photocatalytic transformations in 1991 when Okada[29] disclosed the decarboxylative Michael addition of alkyl radicals to electron deficient alkenes. This process was achieved by utilising photocatalyst $[Ru(bpy)_3]Cl_2$ and 1-benzyl-1,4-dihydronicotinamide (BNAH) as a hydrogen source. The conjugate addition of 1°, 2° and 3° alkyl radicals with a selection of acceptors proceeded smoothly in typically good yields.

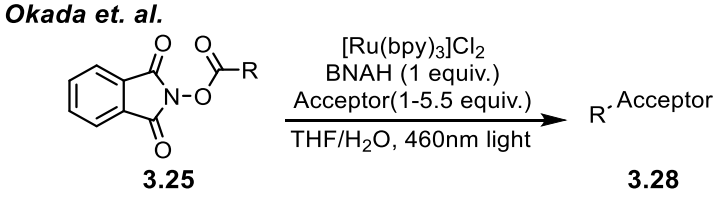

Figure 3.6: Okada's decarboxylative Michael addition of alkyl radicals into electron deficient alkenes.

Since Okada's initial report, the synthetic utility of NHP esters as a radical precursor in photoredox processes was not further elaborated on until 2012 when Overman exploited an NHP ester derivative for the construction of a key intermediate in the total synthesis of (-)-aplyviolene.[30] Overman further examined the use of tertiary NHP esters[31] and their phthalimidoyl oxalate ester counterparts[31] to generate tertiary radicals. Subsequent intermolecular radical addition into electron deficient alkenes, and allylations via addition and consequent halide elimination provided an effective method for generating a range of quaternary carbon centres.

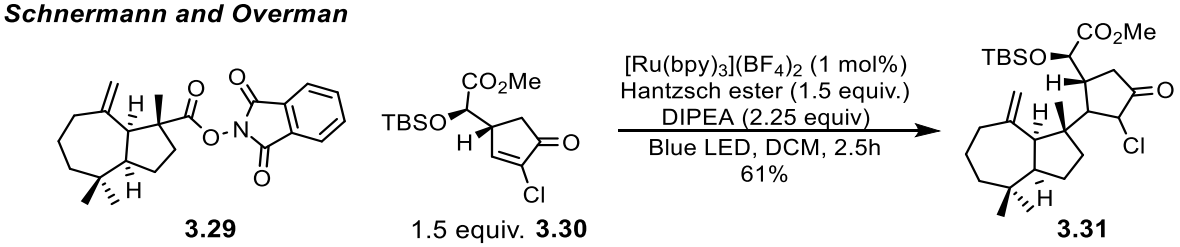

Figure 3.7: The decarboxylative radical addition as a key step in the synthesis of (-)-aplyviolene.

A variety of methodologies have since been published that utilise alkyl radical intermediates derived from the visible-light mediated decarboxylation of NHP esters. These procedures include: further studies into the intermolecular radical additions to electron deficient alkenes,[32-35] radical additions with unsaturated nitrogen systems,[36-40] decarboxylative borylations,[41-43] the formation of thioethers[44] and α-selenoamino acid[45] derivatives.

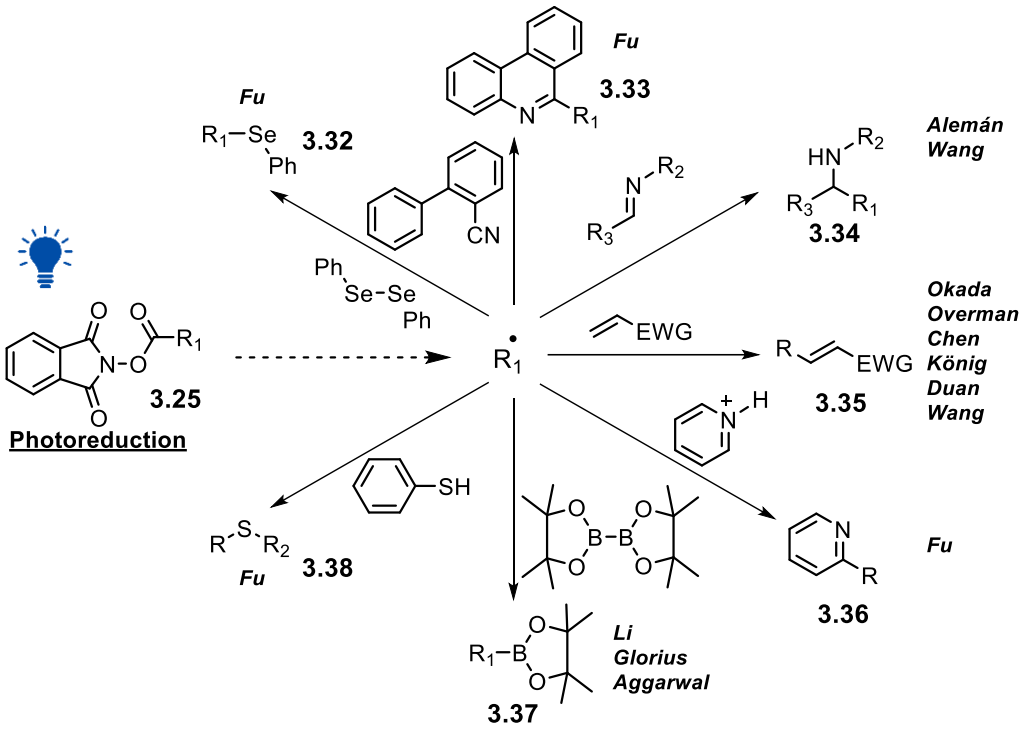

Figure 3.8: Summary of the visible-light mediated methodology surrounding NHP esters.

3.2 Project Proposal

3.2.1 Project Aims

With the ubiquity of heterocyclic amines within pharmaceuticals and natural products, protocols for their efficient synthesis and functionalisation remain an ongoing challenge. Specifically, I was inspired to utilise photoredox catalysis to further develop the aliphatic α-alkylation of heterocyclic amines via a radical-radical coupling pathway; a transformation previously reported only by Pandey[26] and Yu[25]. This project proposes a photooxidative approach for the generation of α-amino radicals while exploiting NHP esters as radical precursors with radical-radical coupling conferring the α-alkylated product. I specifically focused upon coupling alkyl radicals with α-amino radicals derived from THIQ as a model transformation.

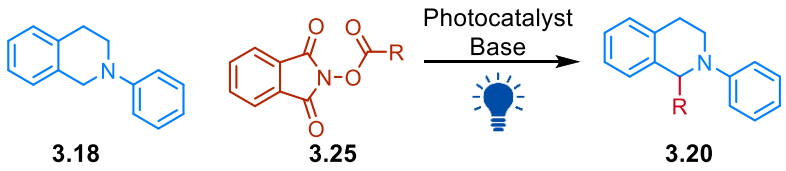

Figure 3.9: Proposed scheme for the decarboxylative α-alkylation of tetrahydroisoquinolines employing a photo-catalytic strategy.

3.2.2 Reaction Design

A reductive quenching cycle is proposed in figure 3.10; upon excitation, the triplet excited state of the photocatalyst is reduced by *N*-phenyl tetrahydrisoquinoline (**3.18**) with radical cation **3.18'** subsequently rearranging to an α-amino radical (**3.23**) facilitated by deprotonation of the α-hydrogen by an alkali additive. Simultaneously, the photocatalyst's ground state is reinstated via single electron reduction of an NHP ester (approx. $E_{1/2}$ = -1.20V vs. SCE). Single electron reduction induces fragmentation of the NHP ester generating an alkyl radical (**3.24'**), carbon dioxide and a phthalimide anion. The alkyl and α-amino radicals generated *in situ* undergo radical-radical coupling affording the desired α-functionalised THIQ product (**3.20**).

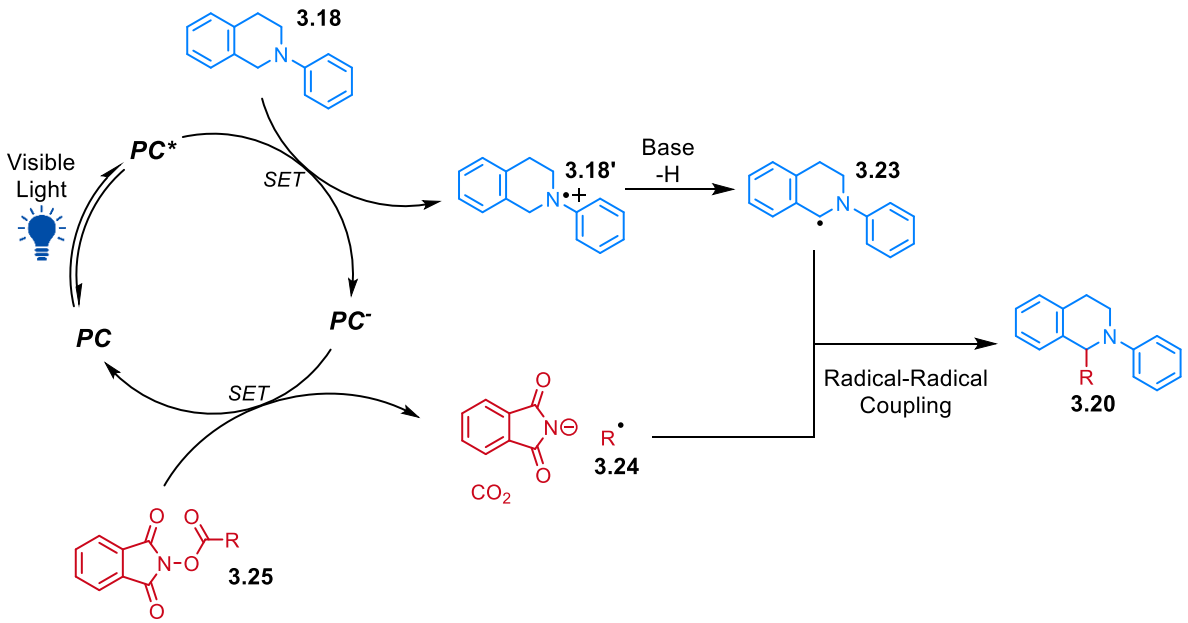

Figure 3.10: Hypothesised mechanism for a photocatalytic decarboxylative α-alkylation of tetrahydroisoquinoline.

3.3 The Decarboxylative Radical-Radical Coupling via Batch Conditions

3.3.1 Optimisation

With a mechanistic proposal for the α-alkylation of amines established, reaction conditions were optimised to couple *N*-phenyltetrahydroisoquinoline (**3.18**) with NHP ester **3.39** derived from cyclohexane carboxylic acid. Preliminary investigations involved screening a selection of photocatalysts capable of promoting single electron oxidation of **3.18** and single electron reduction of **3.39**. A selection of photocatalysts (1 mol%) were screened in the presence of **3.18** and 1.5 equivalents **3.39** in MeCN, while 2 equivalents of Na_2CO_3 were employed to facilitate α-amino radical formation.

Table 3.1: Catalyst screen for the α-alkylation of THIQ.

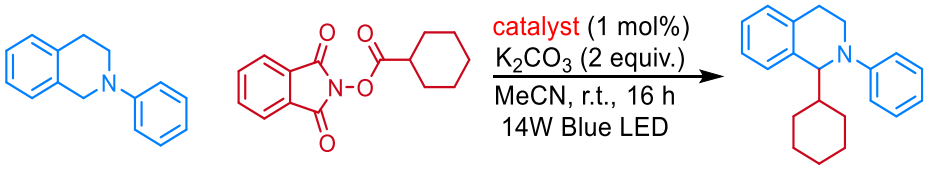

3.18 1.5 equiv. **3.39** **3.40**

Entry	Catalyst	Oxidation Potential (V vs. SCE)	Reduction Potential (V vs. SCE)	Yield 3.40 (%)*
1	$[Ir(ppy)_2(dtbbpy)]PF_6$	0.66	-1.51	6
2	$[Ir(dF\text{-}ppy)_3]$	1.18	-2.00	10
3	*fac*-$[Ir(ppy)_3]$**	0.77	-1.73	15
4	$[Ru(bpy)_3]Cl_2$	0.77	-1.33	14
5	4CzTPN	1.35	-1.21	8

**yield estimated by ^1H NMR against 2,5-dimethylfuran as internal standard.*
redox potentials to the respective proposed reductive quenching cycle.

A summary of the photocatalysts screened, their oxidation and reduction potentials as well as yield obtained is summarised in table 3.1. $[Ir(ppy)_2(dtbbpy)]PF_6$ afforded a low yield of 6%, this was determined by comparing the integration of products in the ^1H NMR spectrum against 2,5-dimethylfuran as an internal standard. Other iridium photocatalysts: $[Ir(dFppy)_3]$ and *fac*-$[Ir(ppy)_3]$ enhanced yields slightly to 10% and 15%, respectively. It

is suspected that reactivity with *fac*-[Ir(ppy)$_3$] proceeds via an oxidative quenching cycle, as the single electron reduction of the **3.39** from the triplet excited state (-1.73V vs. SCE) is more favourable than the single electron oxidation of **3.18** (0.31V vs. SCE). [Ru(bpy)$_3$]Cl$_2$ furnished **3.40** in 14% yield, while utilising 1,2,3,5-tetrakis(carbazol-9-yl)-4,6-dicyanobenzene (4CzIPN) provided an 8% yield. Further optimisation was conducted with [Ru(bpy)$_3$]Cl$_2$ due to its comparatively higher yields, availability, lower cost and cleaner crude ^{1}H NMR.

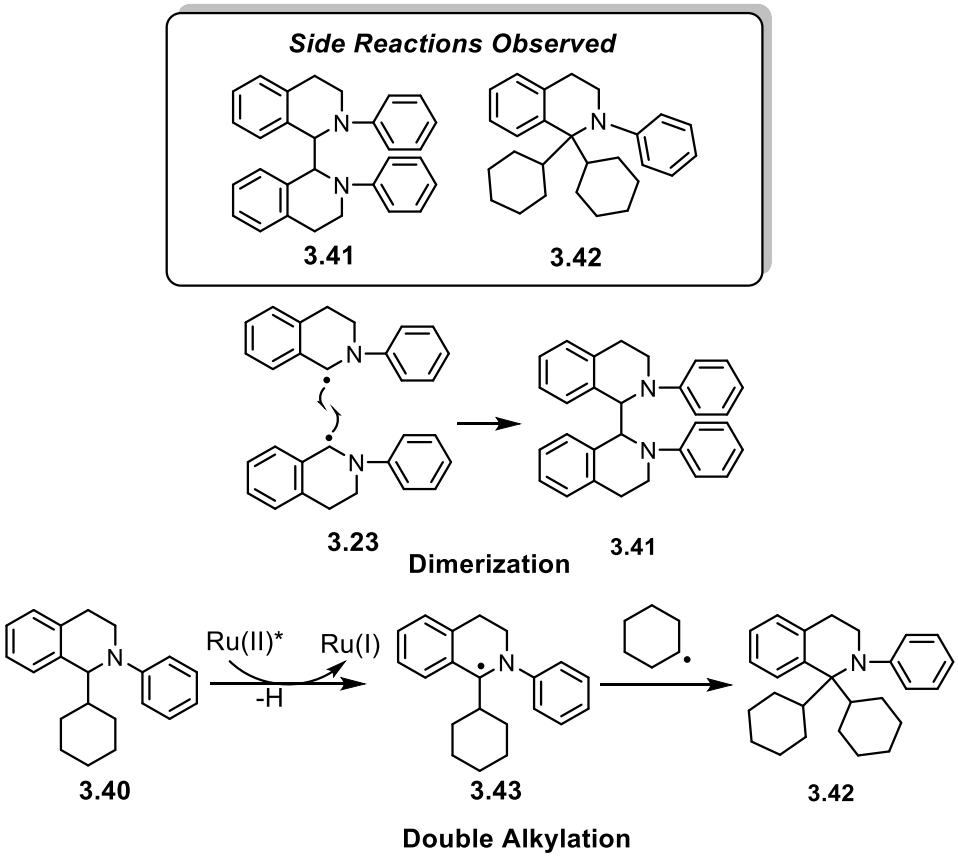

Figure 3.11: Side reactions identified in the decarboxylative α-alkylation of amines.

Initial experiments provided low yields of the desired alkylated amine (**3.40**), with the observation of two undesired by-products in the crude ^{1}H NMR, namely **3.41** and **3.42**. **3.41** has been reported via the homocoupling of two α-amino radicals,[46-47] its detection would imply a disproportionate rate of alkyl and α-amino radical formation. However, this product was typically only observed in small quantities in the crude reaction mixture

(<10%) and in later optimisation, was not detected. The major side product identified was **3.42**; dialkylation is hypothesised to proceed via overoxidation of **3.40** with subsequent formation of a stabilized tertiary α-amino radical (**3.43**), coupling to an additional cyclohexyl radical furnishes the undesired dialkylated product. Another unidentified product was observed in the crude ^{1}H NMR when utilising iridium-centred photocatalysts.

Table 3.2: Solvent screen for the α-alkylation of THIQ.

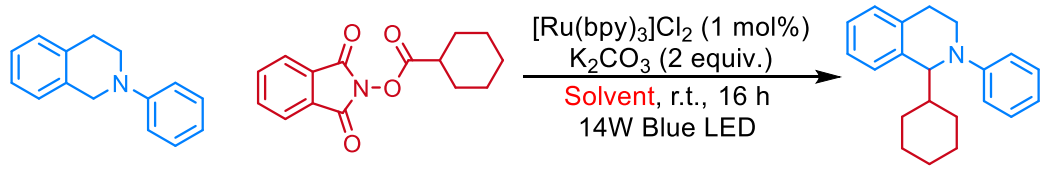

3.18 1.5 eqiv. **3.39** **3.40**

Entry	Solvent	Yield 3.40 (%)*
1	MeCN	23
2	DMSO	13
3	DMF	13
4	DCM	3
5	EtOAc	3

Reactions were sonicated prior to irradiation
**yield estimated by ^{1}H NMR against 2,5-dimethylfuran as internal standard*

Upon determining $[Ru(bpy)_3]Cl_2$ as the optimum photocatalyst, a solvent screen was performed. Reaction mixtures were briefly sonicated prior to irradiation to further disperse particles of K_2CO_3. When repeating the reaction utilising MeCN, sonication was revealed to enhance the yield to 23%. Alternative polar solvents, DMSO and DMF both achieved lower yields of 13% against internal standard, while non-polar solvents, DCM and EtOAc revealed trace quantities of **3.40**. Sonication is hypothesised to enhance yields by increasing the surface area between K_2CO_3 and the reaction mixture, facilitating proton abstraction of the acidic α-proton from **3.18'** consequently expediting α-amino radical formation.

Table 3.3: Base screen for the α-alkylation of THIQ.

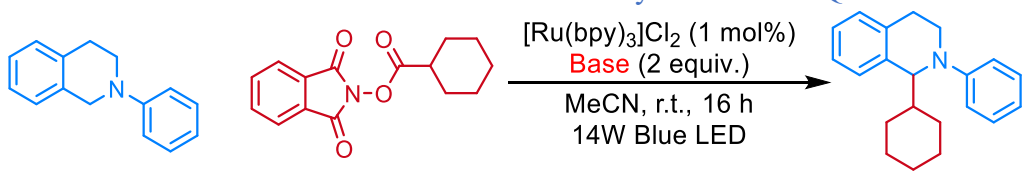

3.18 1.5 equiv. **3.39** **3.40**

Entry	Base	Yield 3.40 (%)*
1	K_2CO_3	23
2	KOAc	27
3	K_3PO_4	21
4	K_2HPO_4	29
5	Pyridine	23
6	Lutidine	19
7	Collidine	18
8	Imidazole	25
9	Quinuclidine	38
10	Diphenylamine	41
11	DABCO	17
12	TEA	12
13	DIPEA	9
14	Trizma Base	19
15	No Base	22

Reactions were sonicated prior to irradiation
**yield estimated by ^1H NMR against 2,5-dimethylfuran as internal standard*

A variety of alkali and organic bases were screened to determine their effect on α-amino radical formation, the results are summarised in table 3.3. Alkali bases provided diverse results with KOAc and K_2HPO_4 slightly enhancing efficiency (27% and 29%, respectively), while K_3PO_4 yielded 21% (table 3.3 entries 2-4). Aromatic nitrogen bases: pyridine, lutidine, collidine and imidazole failed to substantially improve the reaction, acquiring 23%, 19%, 18% and 25% yields, respectively (table 3.3, entries 5-8). The addition of quinuclidine and diphenylamine ($HNPh_2$) both significantly enhanced the reaction efficiency with corresponding yields of 38% and 41%; while other amine bases either hindered or did not affect the reaction, (table 3.3, entries 11-14) it is suspected that

competitive oxidation over **3.18**, inhibits reactivity. The absence of base yielded 22%, this was attributed to the phthalimide anion generated fulfilling the role of a base (pk_b 5.7) and facilitates α-amino radical formation. Establishing that basic additives do not significantly enhance the reaction, the role of $HNPh_2$ was re-evaluated. It is hypothesised that $HNPh_2$ promotes an alternative pathway for α-amino radical formation (Pathway B, figure 3.12). It was posited that the triplet excited state of $[Ru(bpy)_3]Cl_2$ is reduced by $HNPh_2$ producing aminyl radical cation **3.45**; subsequent α-hydrogen abstraction of **3.18** by **3.45** generates α-amino radical **3.23** and ammonium cation **3.46**. The photocatalyst is regenerated via the single electron reduction of **3.25**, with the corresponding alkyl and α-amino radicals coupling to furnish **3.20**. The phthalimide anion deprotonates the ammonium cation, reinstating $HNPh_2$. Analogous mechanisms have been proposed throughout the literature[48-51], with $HNPh_2$ specifically utilised in the optimisation of Yoon's photocatalytic thiol-ene coupling[52]. Pathway B (figure 3.12) is hypothesised to run concurrently to the initially proposed mechanism (figure 3.10) with phthalimide anion assuming the role of base.

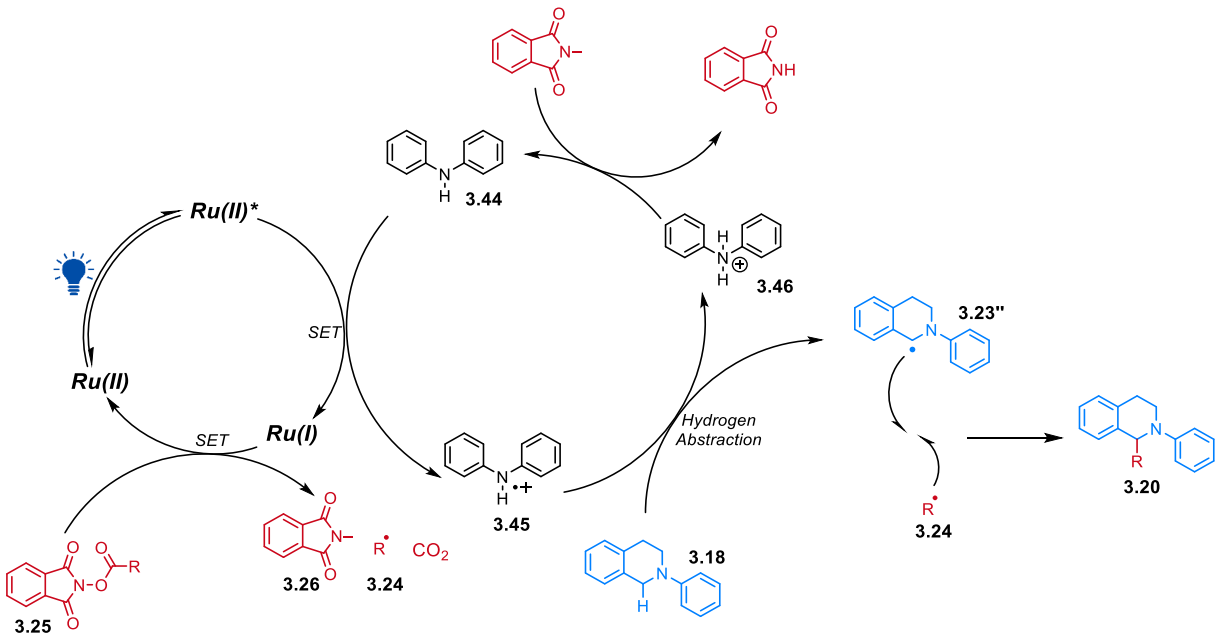

Figure 3.12: Proposed mechanism of pathway B for the α-alkylation of THIQ in the presence of diphenylamine.

Table 3.4: Stoichiometry screen of NHP ester for the α-alkylation of THIQ.

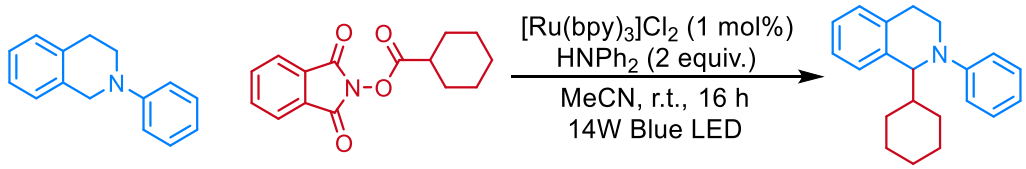

3.18 X equiv. **3.39** **3.40**

Entry	Equiv. of 3.39	Yield 3.40 (%)*
1	1.0	43
2	1.5	41
3	2.0	60
4	2.5	60
5	3.0	41
6	4.0	40

**yield estimated by ^{1}H NMR against 2,5-dimethylfuran as internal standard*

Upon decarboxylation, alkyl radicals are susceptible to hydrogen abstraction, eradicating the pathway for THIQ alkylation. The stoichiometry of **3.39** was screened to determine whether providing additional cyclohexyl radical precursor to the reaction mixture influences the outcome, the results are summarised in table 3.4. 2 equivalents of **3.39** lead to an improved yield of 60%, however additional increases beyond 2.5 equivalents hindered yields (table 3.4, entries 5 and 6).

Table 3.5: Catalyst loading of $Ru(bpy)_3Cl_2$ for the α-alkylation of THIQ.

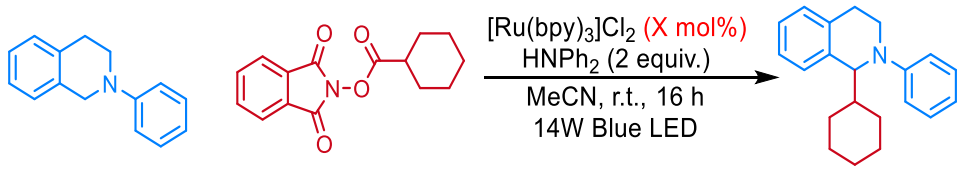

3.18 2.0 equiv. **3.39** **3.40**

Entry	$Ru(bpy)_3Cl_2$ (mol %)	Yield 3.40 (%)*
1	0.5	28
2	1.0	60
3	1.5	57
4	2.0	60
5	2.5	71

**yield estimated by ^{1}H NMR against 2,5-dimethylfuran as internal standard*

A substantial quantity of **3.18** remained in the crude solution; to enable full conversion, the concentration of $[Ru(bpy)_3]Cl_2$ was screened. Increasing the catalyst loading to 2.5 mol % allowed full conversion of **3.18** and an increased yield of 71%, the remainder forming **3.42**. As expected, decreasing the concentration of $[Ru(bpy)_3]Cl_2$ to 0.5 mol% inhibited reaction conversion.

Table 3.6: Co-reductant screen for the α-alkylation of THIQ.

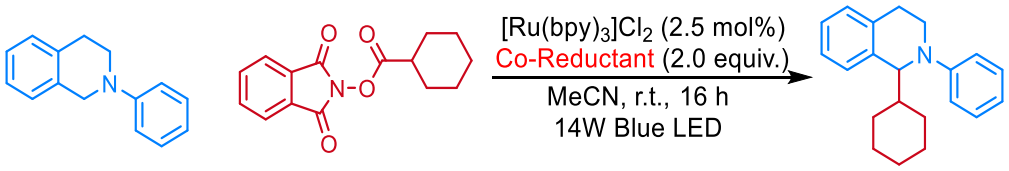

3.18 2.0 equiv. **3.39** **3.40**

Entry	Co-reductant	Yield 3.40 (%)*
1	Diphenylamine	71
2	p-toluidine	63
3	p-anisidine	24
4	Quinuclidin-3-ol	21
5	Triphenylamine	42
6	4,4′-Dimethoxydiphenylamine	29

**yield measured via ^1H NMR against 2,5-dimethylfuran as internal standard*

The efficiency of pathway B was probed via substituting $HNPh_2$ for other possible co-reductants as summarised in table 3.6. Yoon's previous studies successfully exploited *p*-toluidine as a co-reductant.[52] When applied to the decarboxylative α-alkylation of THIQ, *p*-toluidine achieved 63% yield against 2,5-dimethylfuran as an internal standard; achieving lower conversions, however **3.42** was absent in the crude ^1H NMR spectrum. *p*-anisidine and quinuclidin-3-ol obtained poor yields of 24% and 21%, respectively. Triphenylamine and 4,4'-dimethoxyldiphenylamine were explored due to the structural relationships to $HNPh_2$ obtaining 42% and 29% yields, respectively. Due to higher conversions and overall yield, this reaction was continued to be optimised with $HNPh_2$ as co-reductant.

Table 3.7: $HNPh_2$ equivalents screen for the α-alkylation of THIQ.

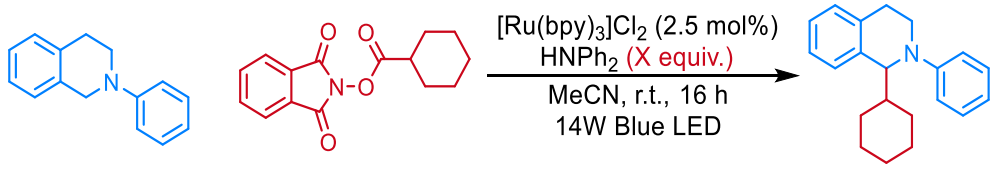

3.18 2.0 equiv. **3.39** **3.40**

Entry	Equiv. $HNPh_2$	Yield 3.40 (%)*
1	0.1	59
2	0.2	55
3	0.5	67
4	1	66
5	1.5	62
6	2.0	71
7	4.0	76

**yield measured by ^1H NMR against 2,5-dimethylfuran as internal standard*

Next, the stoichiometry of $HNPh_2$ was screened with the results summarised in table 3.7. Sub-stoichiometric loadings of $HNPh_2$ proved effective, attaining a 66% yield utilising 0.5 equivalents of $HNPh_2$ suggesting the possibility to instigate pathway B with catalytic quantities of $HNPh_2$ (table 3.7, entry 3). Further reduction to catalytic loadings unfortunately reduced the yield, resulting in yields ranging from 55-59%. (table 3.7, entries 1-2). The addition of 4.0 equivalents of $HNPh_2$ marginally raised the yield to 76% (table 3.7, entry 7) indicating the improvement in efficiency of pathway B could be dependent of $HNPh_2$ concentration. However, 2.0 equivalents were utilised for this reaction, achieving optimum yields while avoiding overly excessive quantities of $HNPh_2$. At this point the reaction was considered optimised for batch processing.

3.3.2 Determination of Substrate Scope

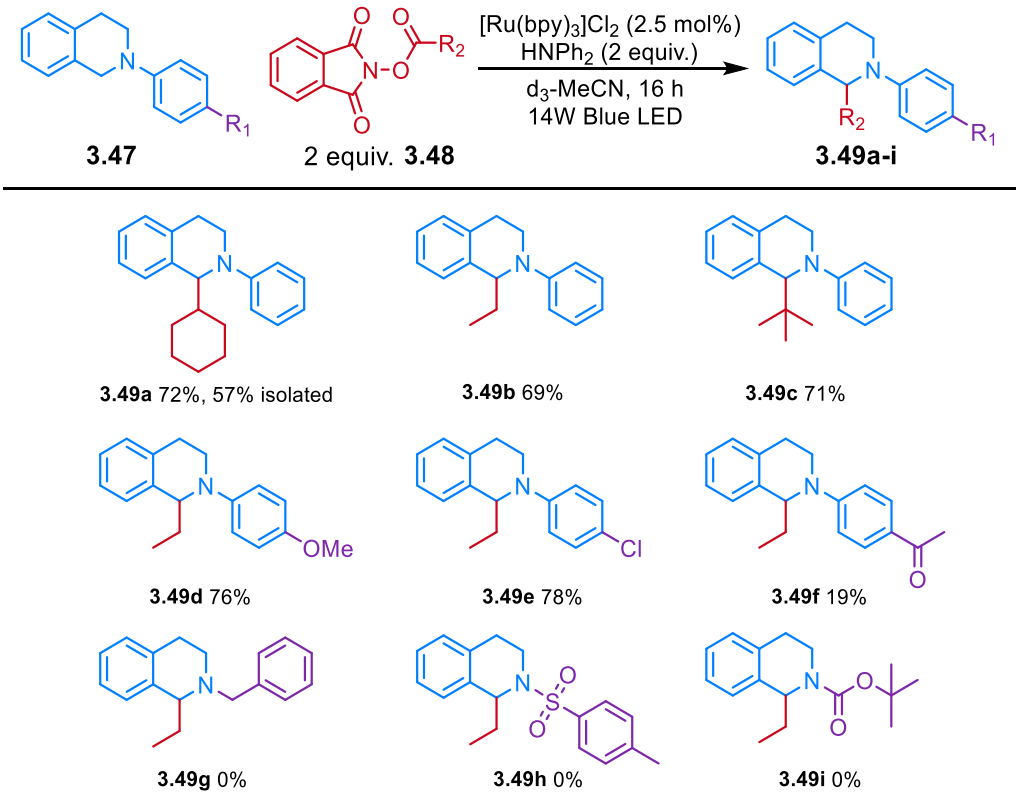

Figure 3.13: NHP ester scope for the α-alkylation of THIQ under batch conditions. Yields obtained via ^{1}H NMR against 2,5-dimethylfuran as an internal standard unless mentioned.

A small scope of substrates were submitted to the optimised conditions. **3.49a** was isolated in 57% yield, while **3.49b** and **3.49c** were obtained in 69% and 71% respectively against internal standard; establishing applicability of this methodology towards primary, secondary and tertiary radicals. Incorporation of methoxy and chloro groups on the *N*-phenyl ring demonstrated good yields, however a methyl-ketone substituent achieved poor yields of **3.49f** (19%). The addition of electron withdrawing substituents increases the oxidation potential of the tertiary amine, hindering single electron oxidation and subsequent formation of the α-amino radical. This was evident with substitution of the *N*-phenyl ring which proved problematic; benzyl, tosyl and Boc protecting groups observed no reactivity, this is attributed to the triplet state of $[Ru(bpy)_3]Cl_2$ being too mild an

oxidant to induce the single electron oxidation of highly electron deficient tertiary amines (approximately 2.0V vs. SCE). Nicewicz *et al*. reported the need for a highly oxidising photocatalyst to access similar electron deficient nitrogen systems.[53]

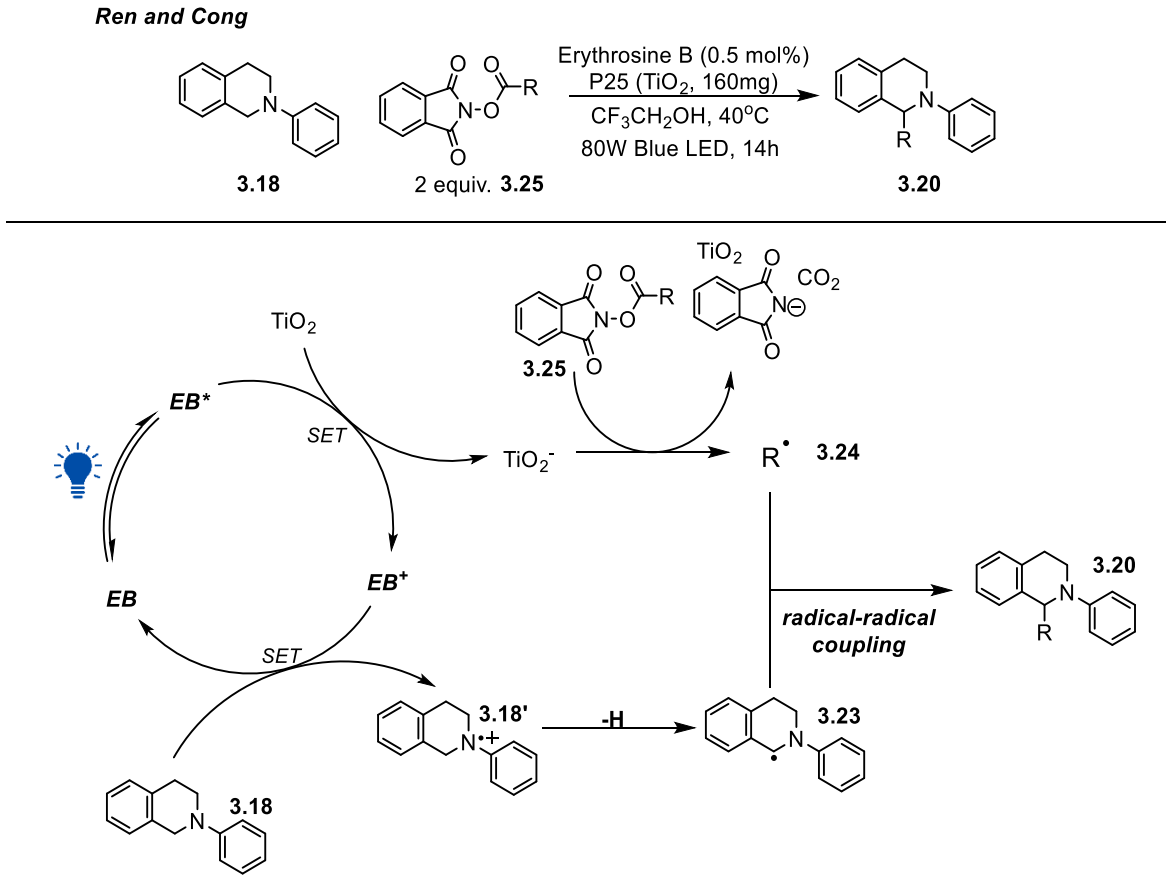

Figure 3.14: Ren and Cong's decarboxylative α-alkylation of tetrahydroisoquinolines.

Ren and Cong subsequently reported a method for the decarboxylative α-functionalisation of THIQ via an oxidative quenching cycle (figure 3.14).[54] They propose that upon irradiation with blue light, the triplet state of erythrosine B (EB) donates an electron into the conduction band of TiO_2, consequent electron donation to NHP ester **3.25** instigates the decarboxylative generation of an alkyl radical. The ground state of erythrosine B is regenerated via the single electron oxidation of **3.18** with ensuing α-amino radical formation. Coupling between the α-amino and alkyl radical furnishes the α-alkylated bicyclic heterocycle. Ren and Cong accessed a range of primary, secondary

and tertiary NHP ester derivatives in typically good to excellent yields. Ren and Cong's methodology suffers from several practical aspects, including the use of a glovebox, elevated reaction temperatures and 80W of irradiation; while the Polyzos methodology is mild employing sparging with N_2, and 14W irradiation at room temperature albeit lower yields.

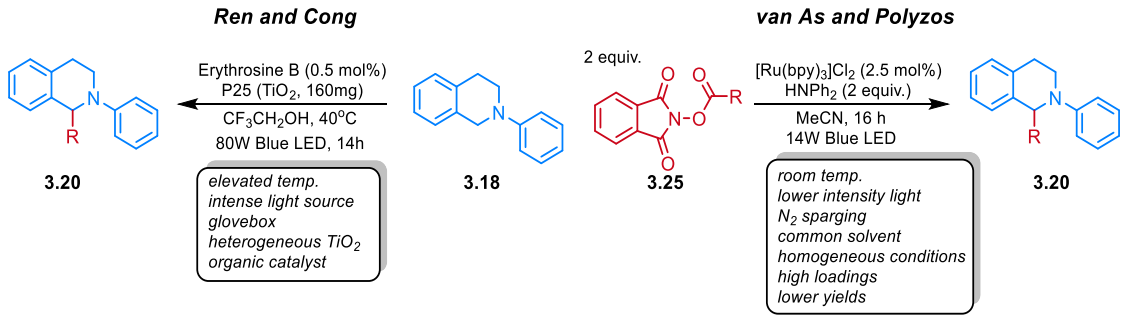

Figure 3.15: Comparison of the methods developed by Cong and Polyzos.

3.4 The Decarboxylative α-Alkylation of THIQ via Flow Processing.

3.4.1 Flow Optimisation.

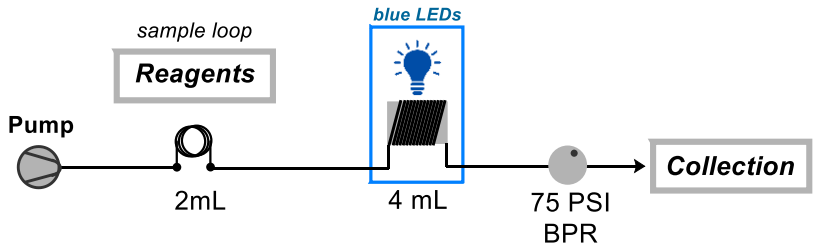

Figure 3.16: Schematic of setup used for the optimisation of the decarboxylative α-alkylation via flow processing.

To further enrich the developed conditions, attention was drawn towards optimisation of this process via a flow protocol. It's hypothesised that transferring to flow would increase the efficiency of this process in many aspects, namely: enhanced yields, lower reaction times while potentially reducing the quantity of reagents added. Optimisation proceeded utilising a commercially available Syyris Asia series pump, fitted with a 2mL sample

loop, 4mL illuminated reactor coil (14W) and a 75 PSI back pressure regulator (Schematic of setup in figure 3.16 and image in figure 3.17).

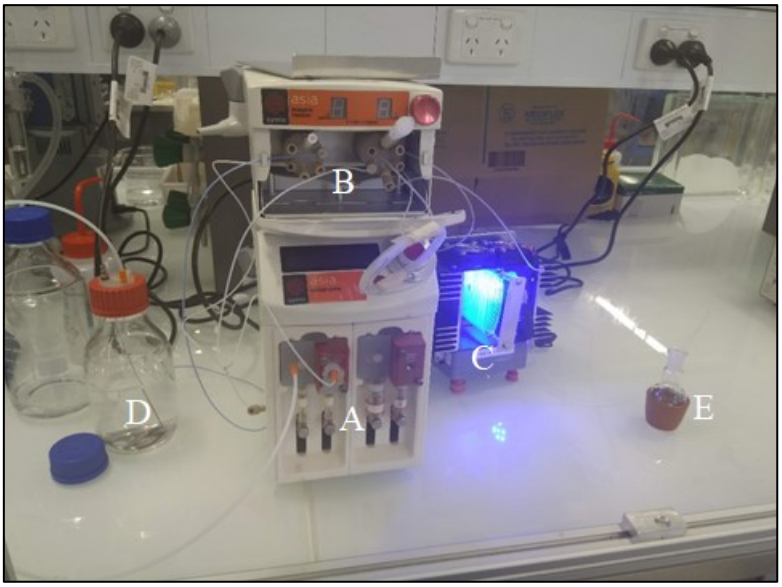

Figure 3.17: Image of setup for flow optimisation. A pump, B sample loop, C illuminated reactor, D Solvent reservoir, E product collection.

Table 3.8: Screening of residence time for the α-alkylation of THIQ in flow.

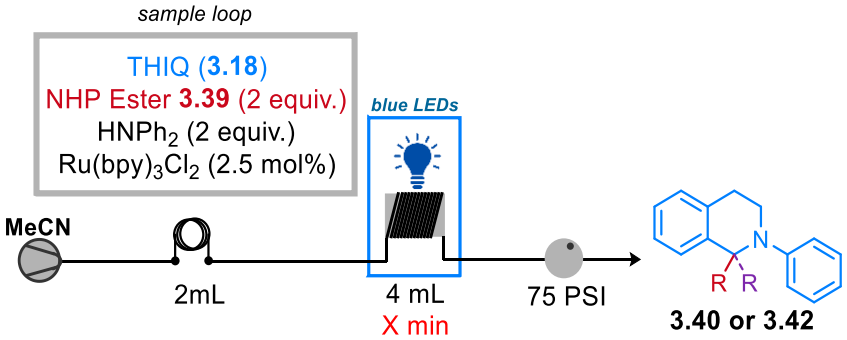

Entry	Residence Time (min)	Ratio 3.40 (%)*	Ratio 3.18 (%)*	Ratio 3.42 (%)*
1	5	59	27	14
2	10	65	17	18
3	15	65	11	25
4	20	69	11	19
5	25	66	8	26
6	30	68	8	24
7	40	63	8	29
8	50	58	7	35

**Conversion measured via ^{1}H NMR by comparing integration against 3.18*

Initially, a series of residence time were screened, comparing the conversion of **3.18** to the generation of **3.40** and **3.42**. Rapid conversion was initially observed with 57% of **3.40** detected in 5 minutes, increasing the residence time to 20 minutes permitted optimum conversions to **3.40** of 69%, with 19% of **3.42** and 11% of **3.18** remaining. Further increasing residence time did not facilitate further conversion of **3.18** and instead lead to conversion of **3.40** to **3.42** as summarised in the reaction profile in figure 3.18.

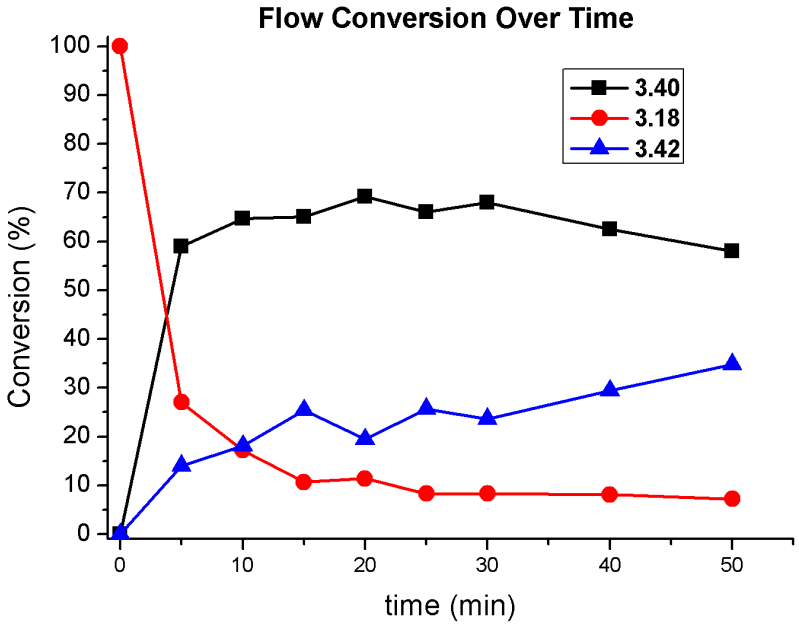

Figure 3.18: Reaction profile with variation in residence time, estimated by monitoring the conversion of **3.18** via ^{1}H NMR.

Table 3.9: Equivalents of NHP ester for the decarboxylative α-alkylation of THIQ in flow.

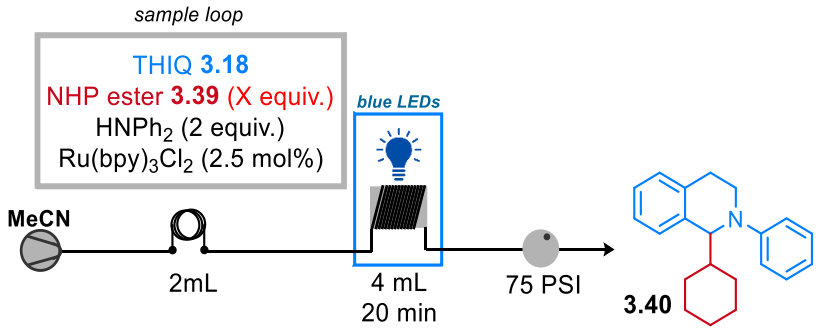

Entry	3.39a (equiv.)	Conversion 3.40 (%)*
1	1.8	63
2	1.6	63
3	1.4	62
4	1.2	63
5	1.05	54

**Conversion measured via ^1H NMR against 3.18*

The stoichiometry of **3.39** was re-screened to determine the optimal quantity of NHP ester via flow processing, this is summarised in table 3.9. Via batch processing, 2.0 equivalents of **3.39** was optimal, however a flow protocol facilitated the reduction in stoichiometry of **3.39**. Reducing to 1.2 equivalents of **3.39** gave identical reaction profiles, however further reduction to 1.05 equivalents saw a marked decrease in reaction conversion obtaining 54% of **3.20**, presumably due to the lower availability of cyclohexyl radical for coupling. Further optimisation for the flow protocol utilised 1.2 equivalents of **3.39** achieving comparable yields with a lower quantity of reactant, enhancing the atom economy of the transformation.

Table 3.10: Concentration screen for the decarboxylative α-alkylation of THIQ in flow.

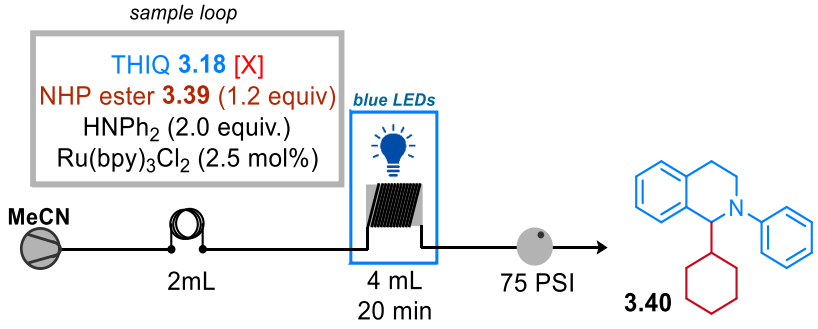

Entry	Residence Time (min)	Concentration (M)	Conversion 3.20 (%)*
1	20	0.0281	74
2	20	0.1125	64
3	20	0.1688	59
4	20	0.2250	48
6	30	0.0281	80

Conversion measured via ^{1}H NMR against 3.18

It was hypothesised that increasing the concentration of the reaction would increase the concentration of radicals in solution, favouring a radical-radical coupling pathway. However, progressively more concentrated solutions inhibited the conversion of reaction (table 3.10, entries 2-4). Counter-intuitively diluting the reaction from [0.0563M] to [0.0281M] improved the yield to 74% (table 3.10, entry 1). Dilution suppressed the formation of **3.42** (decreasing the **3.40:3.42** ratio from approx. 3:1 to 4:1) however it was noted that **3.18** was still present in substantial quantities (approximately 10% yield). Upon dilution, further extension of the residence time to 30 minutes enabled 80% of the desired product, with only **3.40** and **3.42** present in a (4:1 ratio).

Table 3.11: Equivalents of diphenylamine for the decarboxylative α-alkylation of THIQ in flow.

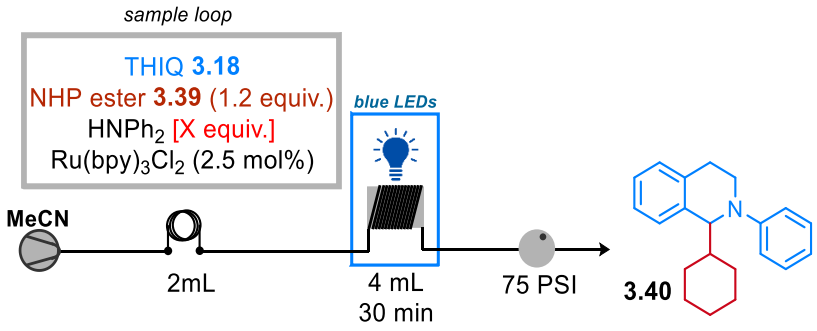

Entry	Equiv. $HNPh_2$	Conversion 3.40 (%)*
1	2.0	80
2	1.5	76
3	1.0	66
4	0.5	78
5	0.25	76
6	0.0	55

Conversion measured via ^1H NMR against 3.18

Having optimized residence time, NHP ester loading and concentration, the stoichiometry of $HNPh_2$ was reoptimized for flow processing (table 3.11). Similarly, to batch conditions, sub-stoichiometric levels of $HNPh_2$ could be applied, with 0.5 equivalents achieving comparable conversions to 2.0 equivalents (78% compared to 80% as in table 3.11, entries 1 and 4) while further reduction to 0.25 gave a slightly lower result of 76%. The absence of $HNPh_2$ obtained 55% conversion to **3.40**; a 25% improvement with the addition of $HNPh_2$ supports my postulate that the redox mediated pathway (pathway B, figure 3.12) proceeds simultaneously to the initially proposed mechanism (pathway A, figure 3.10). 0.5 equivalents of $HNPh_2$ was employed, obtaining comparable conversion to 2.0 equivalents while providing a substantially more atom economical process.

At this point the reaction was considered optimised, achieving the α-alkylation of **3.18** in the presence of 1.2 equivalents of NHP ester **3.39**, 0.5 equivalents $HNPh_2$ and photocatalyst $[Ru(bpy)_3]Cl_2$. Transferring this methodology to a flow protocol greatly benefited the reaction conditions, improving yield and reaction time while substantially decreasing the stoichiometry of both **3.39** and $HNPh_2$.

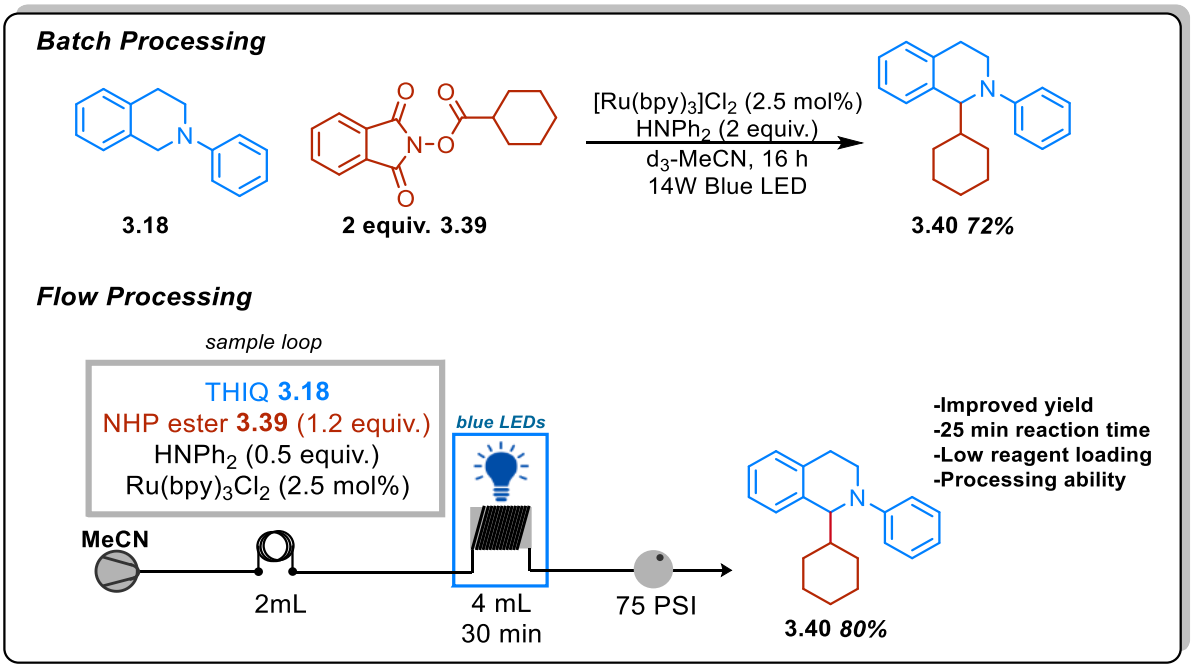

Figure 3.19: Comparison of the batch and flow conditions.

3.4.2 Scope of α-alkylation via flow.

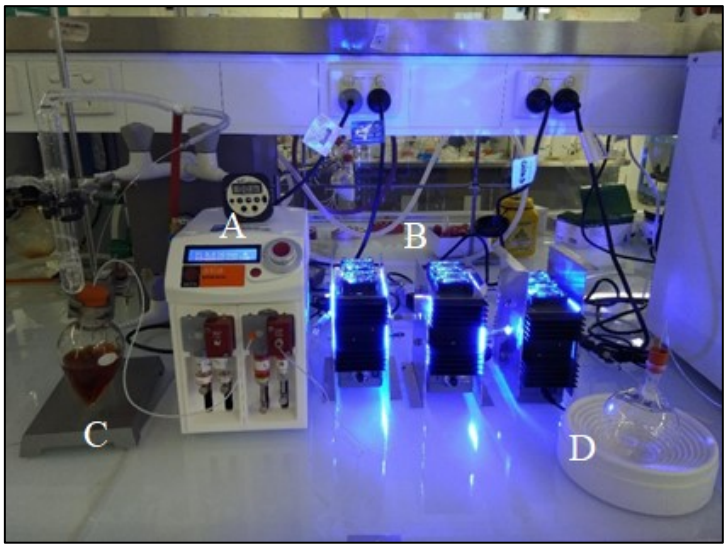

Figure 3.20: Continuous flow setup for scaling up reaction. A- Pump. B- Illuminated reactors in series. C- Reaction Mixture. D- Collection flask.

Having optimised conditions, the reaction was scaled to 2.39 mmol (500 mg with respect to **3.18**) via a continuous flow process, this was achieved through removal of the sample loop and directly pumping the reaction mixture, reaction setup can be observed in figure 3.20. The volume of the illuminated reactor coil was increased from 4mL to either 8mL or 11.7 mL to achieve a higher throughput, accomplished via connecting successive illuminated photoreactors in series. Continuous flow conditions allowed the isolation of **3.51a** in 68% (474mg), while **3.51b** and **3.51c** were isolated in 81% (460mg) and 61% (388mg) respectively, validating the efficient scale up of the α-alkylation with primary, secondary and tertiary radicals.

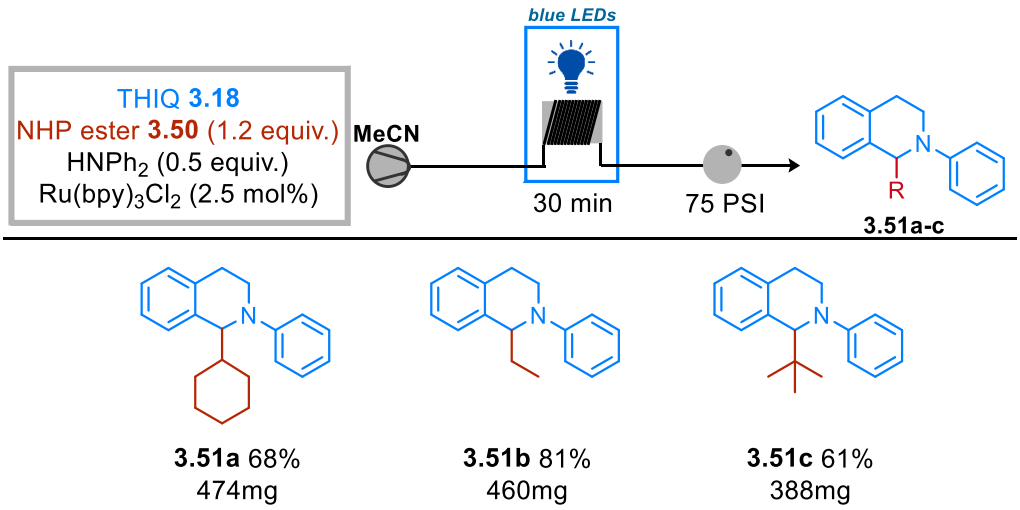

Figure 3.21: Scale up of the decarboxylative α-alkylation of THIQ via a continuous flow process.

The developed flow protocol was then applied to an extensive range of NHP esters on smaller scales; including an array of primary, secondary and tertiary radicals. The scope of reaction was conducted by injecting 5 consecutive solutions through a 2 mL sample loop, combining each solution together for isolation (each reaction was examined at 0.2813mmol scale).

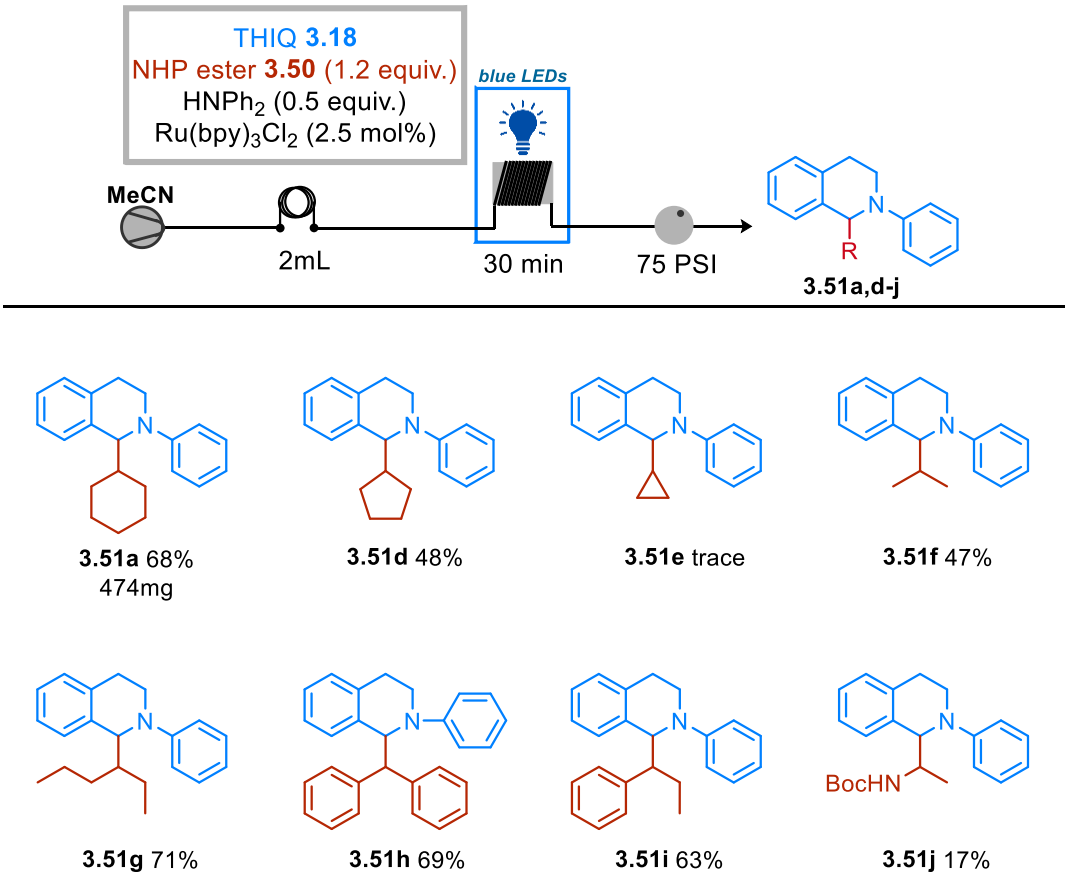

Figure 3.22: Scope of secondary NHP esters.

Secondary NHP esters were typically well tolerated, with cyclopentyl coupled THIQ (**3.51d**) isolated in 48%. Cyclopropyl groups were not tolerated, with consumption of NHP ester **3.50e** and small amounts dimerization of **3.18** observed, this is attributed to the highly reactive nature of cyclopropyl radical decomposing prior to coupling, subsequent homocoupling of **3.18** produces **3.41**. Iso-propyl and 2-ethylpentyl NHP esters afforded the corresponding THIQ adducts in 47% and 71% respectively. Benzylic secondary radicals were well tolerated with **3.51h** and **3.51i** correspondingly isolated in 69% and 63% yields. An NHP ester derived from Boc-protected alanine was coupled to **3.18** with both diastereomers of 1,2-diamine **3.51j** isolated in a combined 17% yield.

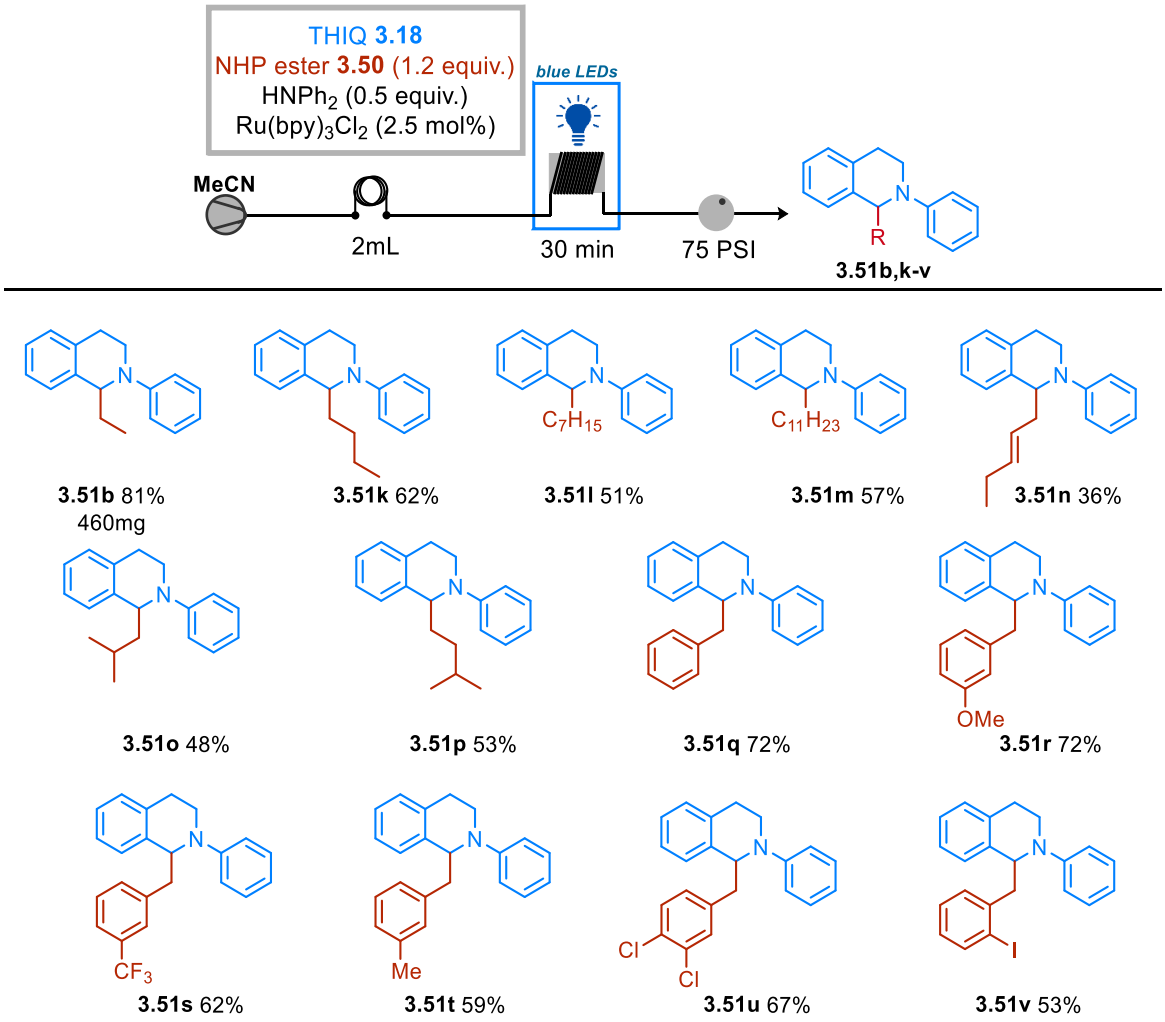

Figure 3.23: Scope of primary NHP esters.

Primary NHP esters were next examined as summarised in figure 3.23. α-alkylation of **3.18** with shorter linear chains achieved good to excellent yields with **3.51b** and **3.51k** isolated in 81% (2.39 mmol scale) and 62% yields respectively, while larger linear chains proceeded in moderate yields of **3.51l** and **3.51m** attained in 51% and 57%, respectively. A 2-penteneyl chain was coupled in 36% with an additional 19% of **3.52** isolated, occurring via coupling of a rearranged stabilized secondary radical as described in figure 3.24.

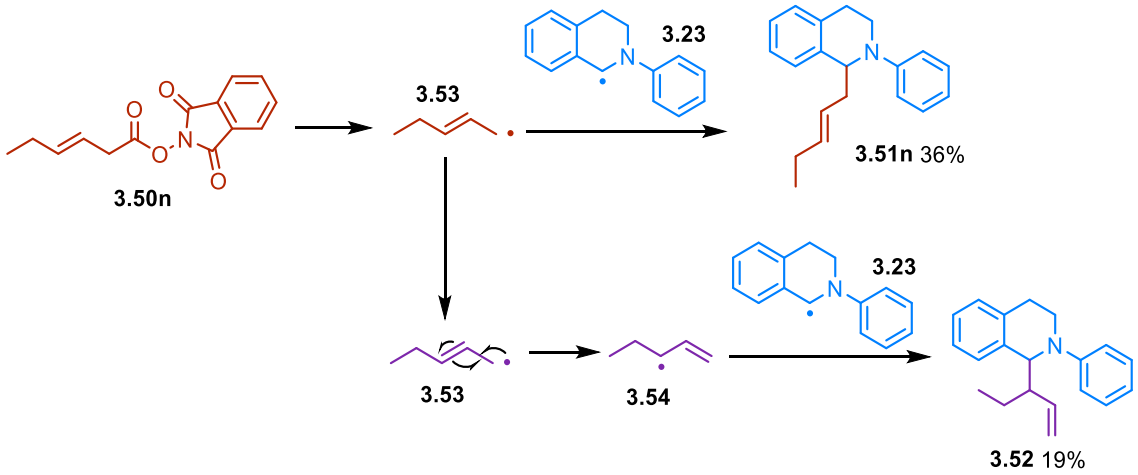

Figure 3.24: Possible rearrangement of the 2-pent-ene-yl radical and coupling to THIQ.

Branched primary alkyl chains proved successful with iso-butyl and 3-methylbutyl chains alkylating **3.18** in 48% and 53% respectively. The α-benzylation of **3.18** from an NHP ester derived from phenylacetic acid generated **3.51q** in 72% yield. Other α-benzylations with a variety of substituents acquired typically good yields. Methoxy, methyl and trifluoromethyl *meta*-functionalised NHP esters were effectively executed with 72%, 59% and 62% isolated respectively, whereas 3,4-dichlorophenyl and 2-iodo phenyl derivatives obtained **3.51u** in 67%, and **3.51v** in a modest yield of 53%. The developed protocol allowed effective α-benzylation of THIQ, a highly privileged motif; with tubocurarine, metocurine, laudanosine and tetrahydropapaveroline among many biologically active compounds bearing this motif.

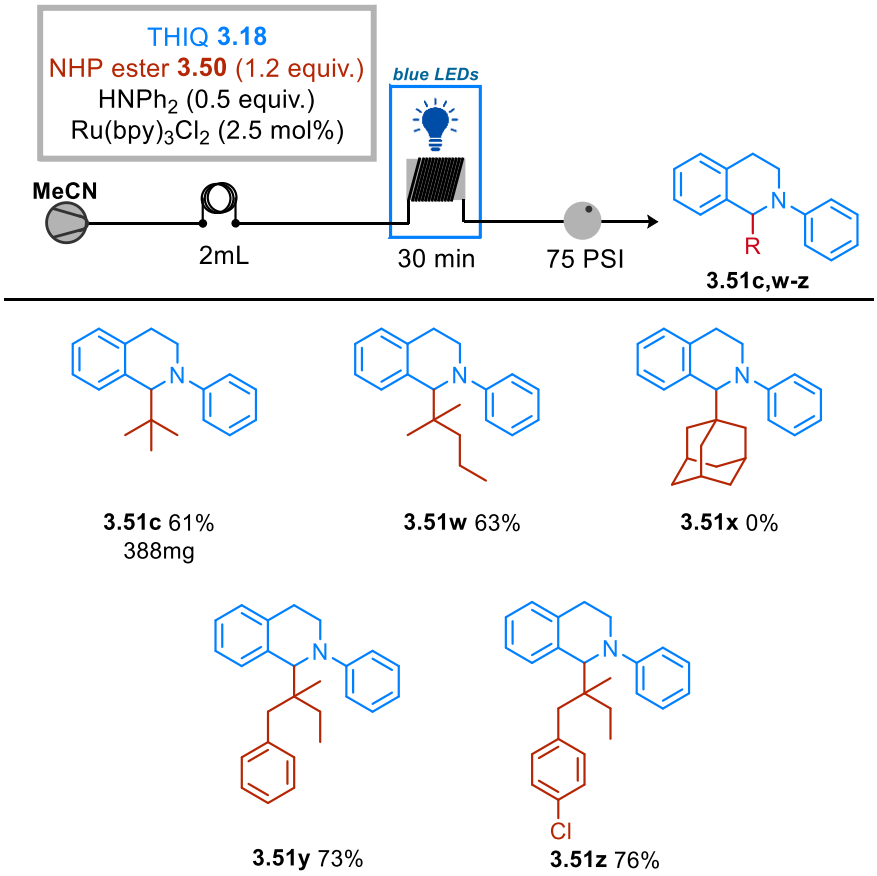

Figure 3.25: Scope of tertiary NHP esters.

This methodology was extended to tertiary radicals in typically good yields, with product **3.51c** isolated in 61% (2.39mmol scale). Extension of the alkyl chain to a 1,1-dimethylbutane group allowed equivalent yields of **3.51w**. Alkylation with a 1-methyl-1-benzyl butane chain was well tolerated with product **3.51y** achieved in 73% yield, while the *para*-chloro derivative **3.51z** was isolated in 76% yield. An adamantane derivative was not compatible under the developed conditions; in this instance the crude ^{1}H NMR revealed no reduction of the NHP ester however some dimerization of THIQ was observed. This was surprising, as consequent research (chapter 4) and literature[25] have synthesised this substrate utilising alkyl halides, highlighting applicability of coupling between adamantyl and α-amino radicals. Also, reduction of **3.50x** should be more favourable than its primary and secondary counterparts as decarboxylation generates a stabilised tertiary radical. It is uncertain as to why this derivative was not compatible.

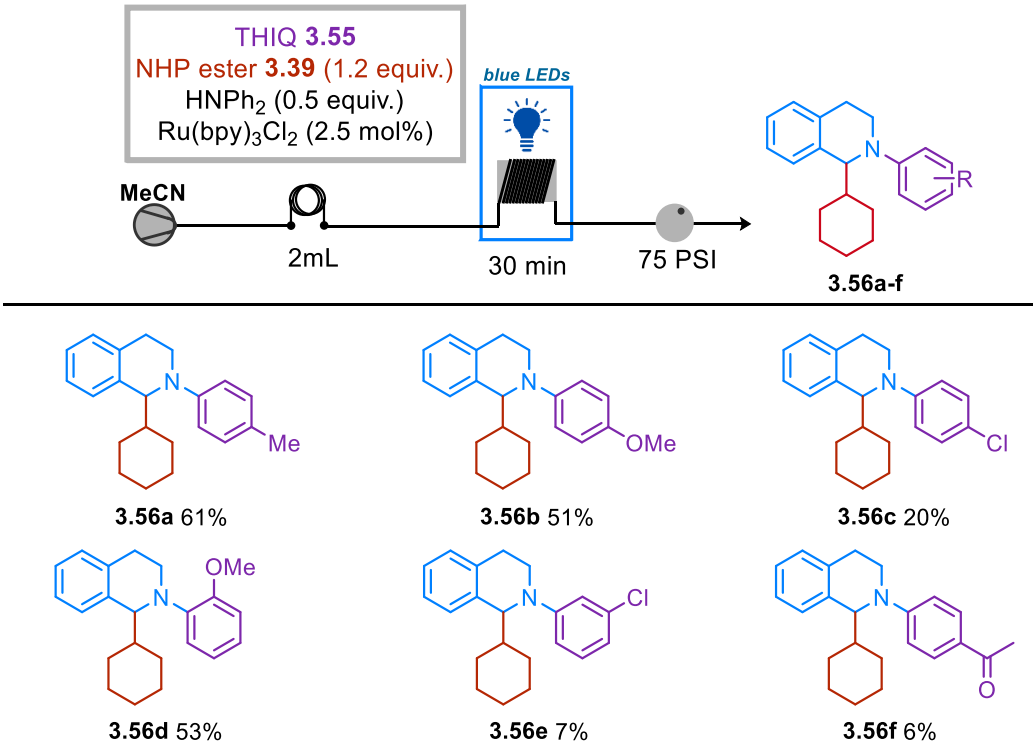

Figure 3.26: variation of the *N*-Phenyl ring.

Substitution on the *N*-phenyl ring of THIQ was examined. Addition of electron donating methyl (**3.56a)** and methoxy (**3.56b**,**d**) substituents were well tolerated. *Para* and *ortho*-chloro substitution (**3.56c,e**) as well as methyl ketone (**3.56f**) substitution achieved low yields, with poor conversions observed with these substrates. Stagnant conversions occur due to the heightened oxidation potential of the THIQ moiety with the addition of an electron withdrawing group, this consequently subdues the rate of reaction. The developed protocol is not inapplicable to these substrates, however with drastically reduced rates, substrates **3.56c,e,f** were not viable for synthetic utility.

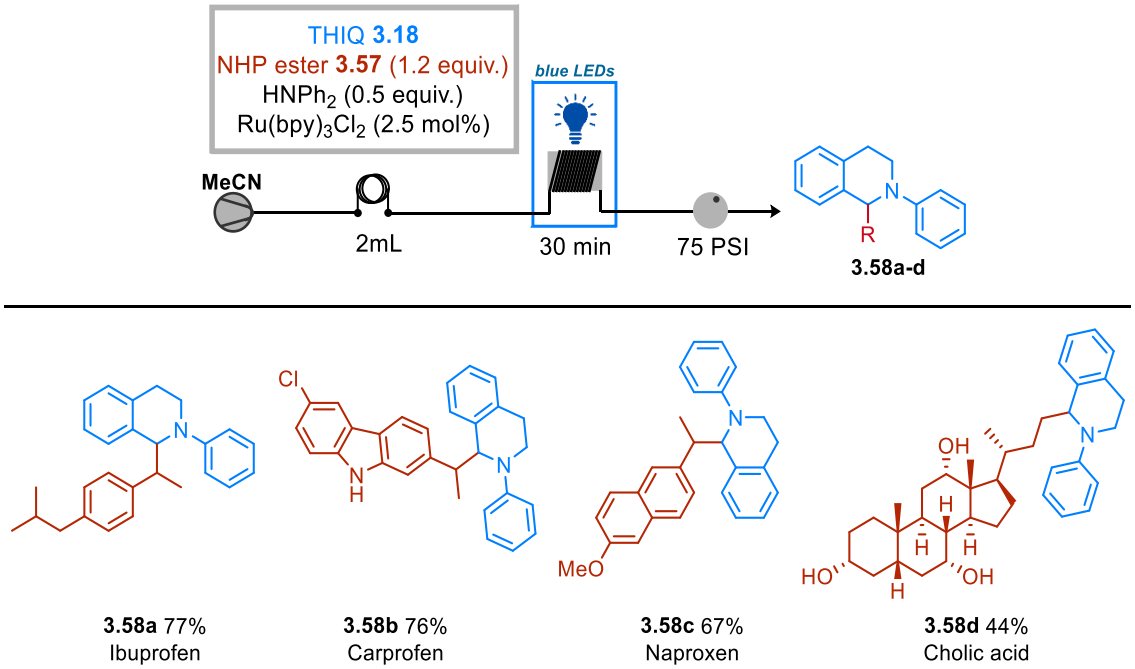

Figure 3.27: Reaction of NHP ester's derived from biologically active substrates

A selection of non-steroidal anti-inflammatory drugs were converted into NHP esters and subjected to the optimised conditions. Derivatives synthesised from ibuprofen, carprofen and naproxen (**3.57a-c**) were all effectively coupled to **3.18** attaining yields of 77%, 76% and 67% respectively. An NHP ester derived from cholic acid was synthesised and submitted to the optimised coupling conditions, yielding **3.58d** in 44%. The α-alkylation of THIQ with structurally complex drug-like and biologically relevant molecules demonstrates applications toward late and mid-stage functionalisation, while concurrently facilitating the synthesis of molecules with potentially bioactive properties.

3.5 Mechanistic studies

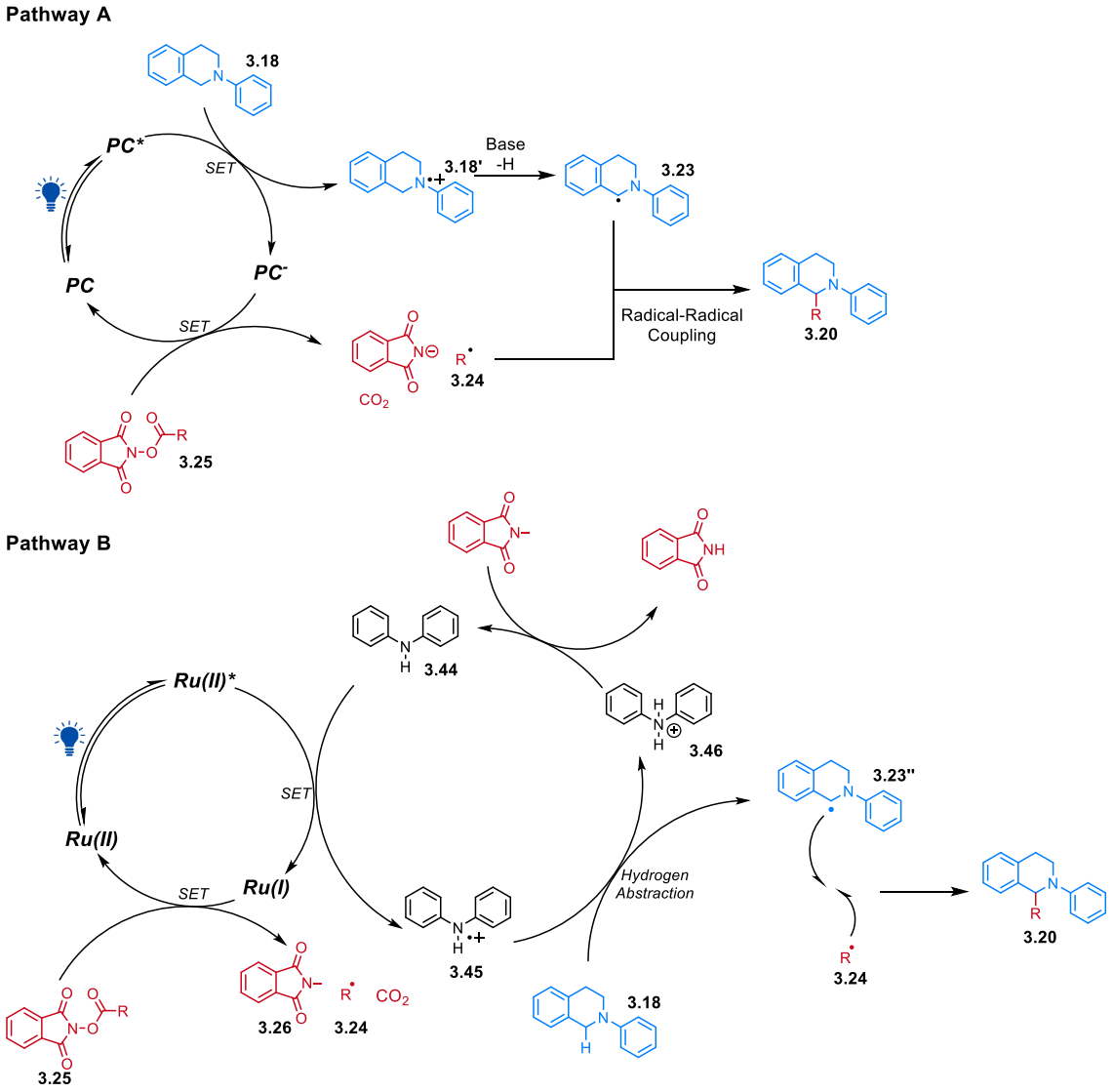

Figure 3.28: Proposed pathways for the decarboxylative α-alkylation of THIQ.

Attention was directed towards exploring the reaction mechanism. I hypothesise that α-amino radicals are generated by two pathways simultaneously; via the direct photooxidation of THIQ (figure 3.28, pathway A), or a redox mediated pathway facilitated by $HNPh_2$ (figure 3.28, pathway B). Both mechanisms proceed simultaneously, as highlighted by the developed reaction achieving 55% yield in the absence of $HNPh_2$;

while the addition of 0.5 equivalents of $HNPh_2$ enhances the yield to 78%, implying the possibility of another mechanism (Table 3.11, entries 4 and 6). Stern-Volmer quenching, cyclic voltammetry and radical trapping experiments were employed to further investigate mechanistic pathways A and B.

3.5.1 Stern-Volmer Quenching.

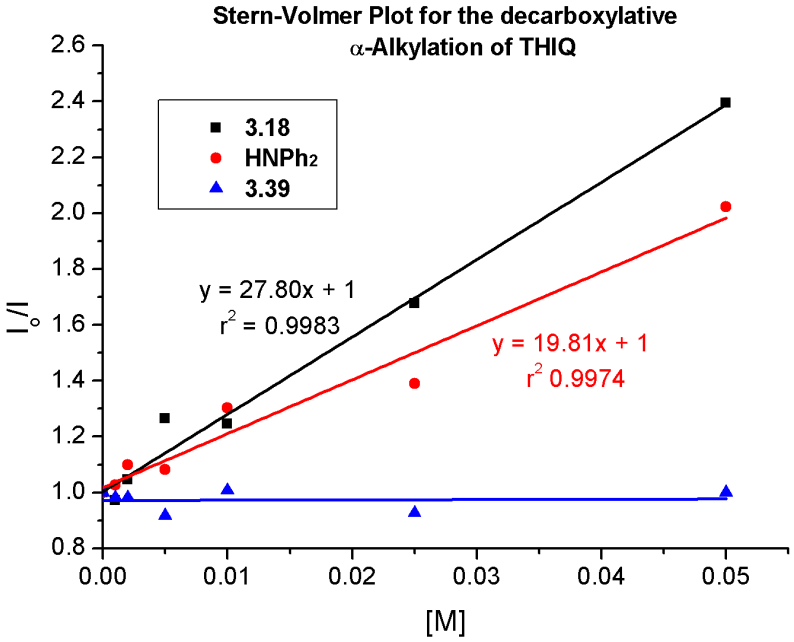

Figure 3.29: Stern-Volmer quenching studies for the α-alkylation of THIQ.

Emission quenching studies were performed to determine which species would interact with triplet photocatalyst, $[Ru(III)(bpy)_2(bpy^{\bullet-})]Cl_2$. The addition of either **3.18** and $HNPh_2$ to a solution of $[Ru(bpy)_3]Cl_2$ (100μM) both resulted in linear quenching relationships, while quenching was absent with the addition of **3.39**; this would signify a reductive quenching cycle. Quenching by both **3.18** and $HNPh_2$ would denote single electron reduction of triplet $[Ru(bpy)_3]Cl_2$ from both substrates, agreeing with both proposed mechanisms. The stronger quenching constant exhibited by **3.18** (3.25×10^7 vs 2.32×10^7 mol^{-1} s^{-1} for $HNPh_2$ when τ of $[Ru(bpy)_3]Cl_2$ is 855ns[55]), indicates that pathway A is the major route.

3.5.2 Cyclic Voltammetry

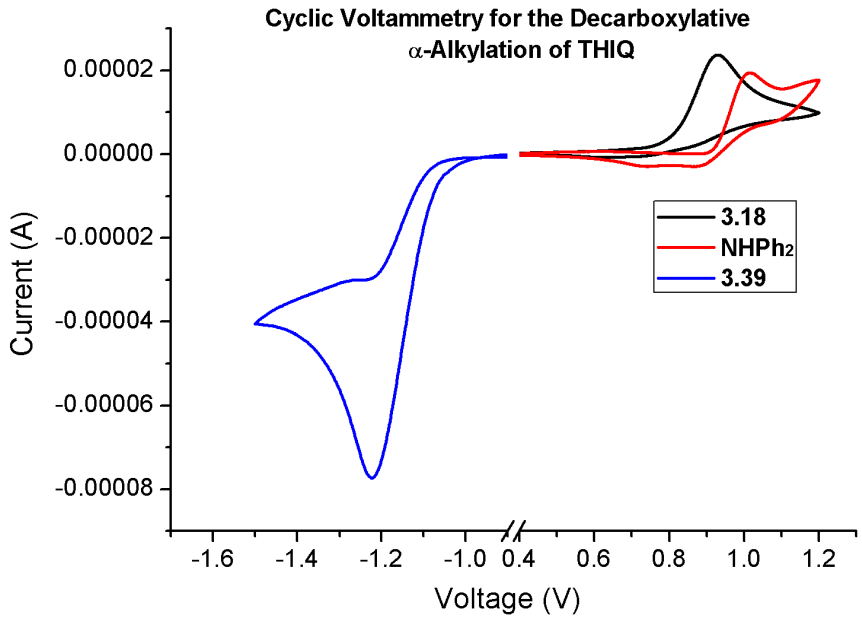

Figure 3.30: Cyclic voltammetry studies for the α-alkylation of THIQ in flow.

The redox potentials of each reaction component were measured via CV and mapped against the potentials of $[Ru(bpy)_3]Cl_2$. The oxidation potential of **3.18** was measured at approximately 0.80 V vs. SCE, while the potential of $HNPh_2$ was assessed to be approximately 0.90 V vs. SCE (comparable to that measured by Yoon of 0.86 V vs. SCE).[56] The milder reduction potential of **3.18** alludes that triplet $[Ru(bpy)_3]Cl_2$ ($Ru^*(II)/Ru(I)$ $E_{1/2}$ = 0.77 V vs. SCE) preferentially oxidises **3.18** over $HNPh_2$ emphasising that pathway A is more favourable than B. This is reinforced by the stronger emission quenching constant observed by **3.18** however this implies each pathway proceeds simultaneously. The onset of reduction of **3.39** was measured to be approximately -1.1 V vs. SCE, this corresponds to the reduction potential of $[Ru(I)(bpy)_3]Cl_2$ ($Ru(II)/Ru(I)$ $E_{1/2}$ = -1.33V). Mapping the redox potentials of $[Ru(bpy)_3]Cl_2$ to the reaction components highlight the plausibility of the hypothesised mechanisms.

3.5.3 Radical Trapping

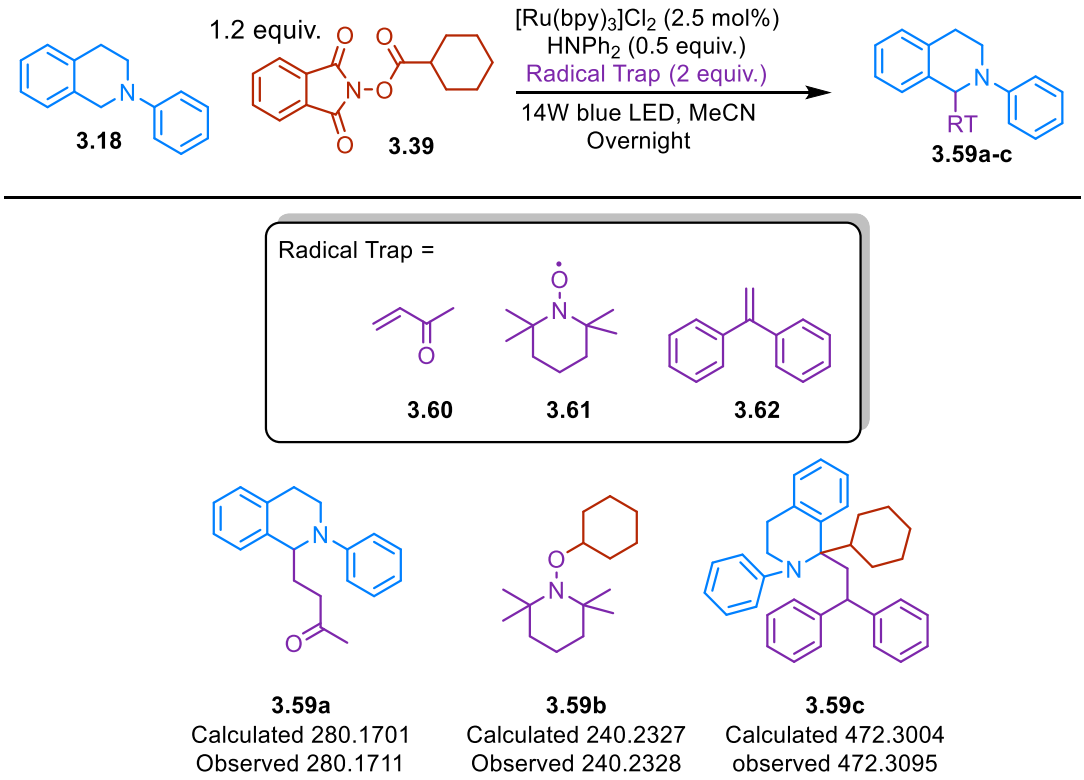

Figure 3.31: Radical trapping experiments.

A series of radical trapping experiments were conducted, with the intention of intercepting and detecting the α-amino and alkyl radicals. 1,1-diphenylethene (DPE), TEMPO and methyl vinyl ketone were utilised as radical traps with the crude solution analysed via HRMS. The addition of methyl vinyl ketone attained the intermolecular radical addition product **3.59a**, achieving reactivity reported by Reiser[47], Yoon[57] and Nishibayashi[58], widely understood to proceed via an α-amino radical. The addition of TEMPO allowed trapping of the cyclohexyl-radical, emphasising the decarboxylation of **3.39**. Surprisingly, addition of 1,1-diphenylethene allowed detection of **3.59c** verifying oxidation of **3.40** and subsequent generation of a second α-amino radical. Radical trapping experiments highlight the generation of α-amino radicals as well as the decarboxylation of the NHP ester, corroborating the anticipated radical-radical coupling mechanism.

3.6 Conclusions

This chapter describes the decarboxylative radical-radical coupling between NHP esters and *N*-phenyltetrahydroisoquinolines. Initially this process was developed via batch processing, revealing that the addition of $HNPh_2$ accesses an alternative, complementary pathway for α-amino radical generation. A flow protocol was then established, greatly improving the reaction conditions with respect to yield, reaction times and atom economy. A wide selection of NHP esters were applicable achieving α-alkylation in typically good yields and allowing incorporation of biologically active motifs. Mechanistic studies revealed that two mechanisms are likely to proceed independently, both achieving the desired α-alkylated product.

3.7 Bibliography

1. Hu, J.; Wang, J.; Nguyen, T. H.; Zheng, N., *Beilstein J. Org. Chem.* **2013,** *9*, 1977-2001.
2. Prier, C. K.; Rankic, D. A.; MacMillan, D. W., *Chem. Rev.* **2013,** *113* (7), 5322-5363.
3. Leitch, J. A.; Rossolini, T.; Rogova, T.; Maitland, J. A. P.; Dixon, D. J., *ACS Catal.* **2020,** *10* (3), 2009-2025.
4. Guo, X.; Okamoto, Y.; Schreier, M. R.; Ward, T. R.; Wenger, O. S., *Eur. J. Org. Chem.* **2020,** *2020* (10), 1288-1293.
5. Xie, J.; Jin, H.; Hashmi, A. S. K., *Chem. Soc. Rev.* **2017,** *46* (17), 5193-5203.
6. Yi, H.; Zhang, G.; Wang, H.; Huang, Z.; Wang, J.; Singh, A. K.; Lei, A., *Chem. Rev.* **2017,** *117* (13), 9016-9085.
7. Leifert, D.; Studer, A., *Angew. Chem. Int. Ed.* **2020,** *59* (1), 74-108.
8. De Vleeschouwer, F.; Van Speybroeck, V.; Waroquier, M.; Geerlings, P.; De Proft, F., *Org. Lett.* **2007,** *9* (14), 2721-2724.
9. Studer, A.; Curran, D. P., *Angew. Chem. Int. Ed.* **2016,** *55* (1), 58-102.
10. McNally, A.; Prier, C. K.; MacMillan, D. W. C., *Science* **2011,** *334* (6059), 1114-1117.
11. Zuo, Z.; MacMillan, D. W. C., *J. Am. Chem. Soc.* **2014,** *136* (14), 5257-5260.
12. Hager, D.; MacMillan, D. W., *J. Am. Chem. Soc.* **2014,** *136* (49), 16986-16989.
13. Jeffrey, J. L.; Petronijević, F. R.; MacMillan, D. W. C., *J. Am. Chem. Soc.* **2015,** *137* (26), 8404-8407.
14. Nakajima, M.; Fava, E.; Loescher, S.; Jiang, Z.; Rueping, M., *Angew. Chem. Int. Ed.* **2015,** *54* (30), 8828-8832.
15. Fava, E.; Millet, A.; Nakajima, M.; Loescher, S.; Rueping, M., *Angew. Chem. Int. Ed.* **2016,** *55* (23), 6776-6779.
16. Uraguchi, D.; Kinoshita, N.; Kizu, T.; Ooi, T., *J. Am. Chem. Soc.* **2015,** *137* (43), 13768-13771.
17. Patel, N. R.; Kelly, C. B.; Siegenfeld, A. P.; Molander, G. A., *ACS Catal.* **2017,** *7* (3), 1766-1770.
18. Zhang, H. H.; Yu, S., *J. Org. Chem.* **2017,** *82* (19), 9995-10006.
19. Guo, J.; Wu, Q. L.; Xie, Y.; Weng, J.; Lu, G., *J. Org. Chem.* **2018,** *83* (20), 12559-12567.
20. Xuan, J.; Zeng, T. T.; Feng, Z. J.; Deng, Q. H.; Chen, J. R.; Lu, L. Q.; Xiao, W. J.; Alper, H., *Angew. Chem. Int. Ed.* **2015,** *54* (5), 1625-1628.
21. Xie, J.; Shi, S.; Zhang, T.; Mehrkens, N.; Rudolph, M.; Hashmi, A. S. K., *Angew. Chem. Int. Ed.* **2015,** *54* (20), 6046-6050.
22. Wang, C.; Qin, J.; Shen, X.; Riedel, R.; Harms, K.; Meggers, E., *Angew. Chem. Int. Ed.* **2016,** *55* (2), 685-688.
23. Ma, J.; Harms, K.; Meggers, E., *Chem. Commun.* **2016,** *52* (66), 10183-10186.
24. Ding, W.; Lu, L. Q.; Liu, J.; Liu, D.; Song, H. T.; Xiao, W. J., *J. Org. Chem.* **2016,** *81* (16), 7237-7243.
25. Zhou, W.-J.; Cao, G.-M.; Shen, G.; Zhu, X.-Y.; Gui, Y.-Y.; Ye, J.-H.; Sun, L.; Liao, L.-L.; Li, J.; Yu, D.-G., *Angew. Chem. Int. Ed.* **2017,** *56* (49), 15683-15687.
26. Pandey, G.; Tiwari, S. K.; Singh, B., *Tetrahedron Lett.* **2016,** *57* (40), 4480-4483.
27. Toriyama, F.; Cornella, J.; Wimmer, L.; Chen, T.-G.; Dixon, D. D.; Creech, G.; Baran, P. S., *J. Am. Chem. Soc.* **2016,** *138* (35), 11132-11135.

28. Huihui, K. M. M.; Caputo, J. A.; Melchor, Z.; Olivares, A. M.; Spiewak, A. M.; Johnson, K. A.; DiBenedetto, T. A.; Kim, S.; Ackerman, L. K. G.; Weix, D. J., *J. Am. Chem. Soc.* **2016,** *138* (15), 5016-5019.
29. Okada, K.; Okamoto, K.; Morita, N.; Okubo, K.; Oda, M., *J. Am. Chem. Soc.* **1991,** *113* (24), 9401-9402.
30. Schnermann, M. J.; Overman, L. E., *Angew. Chem. Int. Ed.* **2012,** *51* (38), 9576-9580.
31. Pratsch, G.; Lackner, G. L.; Overman, L. E., *J. Org. Chem.* **2015,** *80* (12), 6025-6036.
32. Hu, C.; Chen, Y., *Org. Chem. Front.* **2015,** *2* (10), 1352-1355.
33. Schwarz, J.; König, B., *Green Chem.* **2016,** *18* (17), 4743-4749.
34. Zhang, J. J.; Yang, J. C.; Guo, L. N.; Duan, X. H., *Chem. Eur. J.* **2017,** *23* (43), 10259-10263.
35. Xu, K.; Tan, Z.; Zhang, H.; Liu, J.; Zhang, S.; Wang, Z., *Chem. Commun.* **2017,** *53* (77), 10719-10722.
36. Jin, Y.; Jiang, M.; Wang, H.; Fu, H., *Sci. Rep.* **2016,** *6*, 20068.
37. Cheng, W.-M.; Shang, R.; Fu, M.-C.; Fu, Y., *Chem. Eur. J.* **2017,** *23* (11), 2537-2541.
38. Ji, P.; Zhang, Y.; Wei, Y.; Huang, H.; Hu, W.; Mariano, P. A.; Wang, W., *Org. Lett.* **2019,** *21* (9), 3086-3092.
39. Cheng, W. M.; Shang, R.; Fu, Y., *ACS Catal.* **2017,** *7* (1), 907-911.
40. Garrido-Castro, A. F.; Choubane, H.; Daaou, M.; Maestro, M. C.; Alemán, J., *Chem. Commun.* **2017,** *53* (55), 7764-7767.
41. Hu, D.; Wang, L.; Li, P., *Org. Lett.* **2017,** *19* (10), 2770-2773.
42. Candish, L.; Teders, M.; Glorius, F., *J. Am. Chem. Soc.* **2017,** *139* (22), 7440-7443.
43. Fawcett, A.; Pradeilles, J.; Wang, Y.; Mutsuga, T.; Myers, E. L.; Aggarwal, V. K., *Science* **2017,** *357* (6348), 283-286.
44. Jin, Y.; Yang, H.; Fu, H., *Chem. Commun.* **2016,** *52* (87), 12909-12912.
45. Jiang, M.; Yang, H.; Fu, H., *Org. Lett.* **2016,** *18* (9), 1968-1971.
46. Bartling, H.; Eisenhofer, A.; König, B.; Gschwind, R. M., *J. Am. Chem. Soc.* **2016,** *138* (36), 11860-11871.
47. Kohl, P.; Jadhav, D.; Pandey, G.; Reiser, O., *Org. Lett.* **2012,** *14* (3), 672-675.
48. Zhang, X.; MacMillan, D. W. C., *J. Am. Chem. Soc.* **2017,** *139* (33), 11353-11356.
49. Shaw, M. H.; Shurtleff, V. W.; Terrett, J. A.; Cuthbertson, J. D.; MacMillan, D. W. C., *Science* **2016,** *352* (6291), 1304-1308.
50. Czyz, M. L.; Weragoda, G. K.; Monaghan, R.; Connell, T. U.; Brzozowski, M.; Scully, A. D.; Burton, J.; Lupton, D. W.; Polyzos, A., *Org. Biomol. Chem.* **2018,** *16* (9), 1543-1551.
51. Jeffrey, J. L.; Petronijevi, F. R.; Macmillan, D. W. C., *J. Am. Chem. Soc.* **2015,** *137* (26), 8404-8407.
52. Tyson, E. L.; Niemeyer, Z. L.; Yoon, T. P., *J. Org. Chem.* **2014,** *79* (3), 1427-1436.
53. McManus, J. B.; Onuska, N. P. R.; Nicewicz, D. A., *J. Am. Chem. Soc.* **2018,** *140* (29), 9056-9060.
54. Ren, L.; Cong, H., *Org. Lett.* **2018,** *20* (11), 3225-3228.
55. Caspar, J. V.; Meyer, T. J., *J. Am. Chem. Soc.* **1983,** *105* (17), 5583-5590.
56. Tyson, E. L.; Niemeyer, Z. L.; Yoon, T. P., *J. Org. Chem.* **2014,** *79*, 1427-1436.

57. Ruiz Espelt, L.; Wiensch, E. M.; Yoon, T. P., *J. Org. Chem.* **2013,** *78* (8), 4107-4114.
58. Miyake, Y.; Nakajima, K.; Nishibayashi, Y., *J. Am. Chem. Soc.* **2012,** *134* (7), 3338-3341.

3.8 Experimental Procedures and Characterisation

The synthesis of *N*-Hydroxyphthalimide Esters

N-Hydroxyphthalimide (1 equiv.), aliphatic carboxylic acid (1 equiv.) and DMAP (0.2 equivalents) were weighed into a flask charged with a stirrer bar. The mixture was dissolved in DCM (approximately 10mL) and stirred, subsequently N,N'-Diisopropylcarbodiimide (1.1 equiv.) was added to the solution. The solution was stirred overnight, then any precipitate was filtered through a plug of filter aid. The corresponding solution was evaporated until dry then purified via column chromatography.

Dichloromethane was substituted for THF for substrate **3.57d** (an NHP ester derived from Cholic acid).

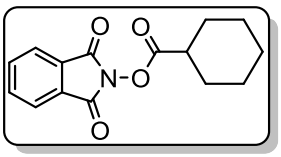

1,3-dioxoisoindolin-2-yl cyclohexanecarboxylate 3.39/3.50a

75% Yield, White Solid; **MP** 66-68°C; **HRMS** predicted for [$C_{15}H_{15}NO_4$+H] 274.1079 Observed 274.1030; **^{1}H NMR** (400 MHz, cdcl$_3$) δ 7.86 (dd, *J* = 5.3, 3.2 Hz, 2H), 7.76 (dd, *J* = 5.6, 3.0 Hz, 2H), 2.76 – 2.66 (m, 1H), 2.14 – 2.04 (m, 2H), 1.86 – 1.78 (m, 2H), 1.70 – 1.58 (m, 3H), 1.43 – 1.27 (m, 3H); **^{13}C NMR** (101 MHz, $CDCl_3$) δ 171.79, 162.05, 134.65, 128.95, 123.86, 40.42, 28.76, 25.43, 24.99; **FTIR** (ν/cm^{-1}, neat)2936.8, 28855.0, 1810.2, 1785.0, 1740.8, 1450.8, 1467.0, 1357.7, 1184.7, 1139.7, 1-72.0, 995.9, 967.7, 877.3, 835.9, 795.5, 694.0.

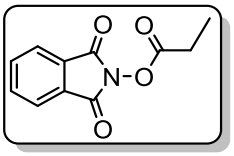

1,3-dioxoisoindolin-2-yl propionate 3.50b

75% Yield, White solid; **MP** 88-89°C; **HRMS** predicted [$C_{11}H_9NO_4$+H] 220.0610 Observed 220.0623; **^{1}H NMR** (400 MHz, $CDCl_3$) δ 7.90 – 7.83 (m, 2H), 7.81 – 7.74 (m, 2H), 2.69 (q, *J* = 7.5 Hz, 2H), 1.29 (t, *J* = 7.5 Hz, 3H); **^{13}C NMR** (101 MHz, $CDCl_3$) δ 170.32, 161.96, 134.72, 128.88, 123.93, 24.50, 8.70; **FTIR** (ν/cm^{-1}, neat) 2975.8, 2948.1, 2815.8, 2888.3, 1818.7, 1806.2, 17854, 11733.5, 1467.5, 1360.5, 1185.6, 1102.8, 1057.2, 1000.0, 875.9, 790.4, 696.0.

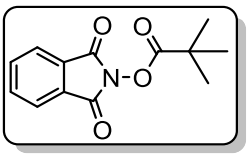

1,3-dioxoisoindolin-2-yl pivalate 3.50c

Synthesised and purified by *Caroline Virbel*, characterised by *Dean van As* 75% yield, white solid; **MP** 62°C; **HRMS** predicted [$C_{13}H_{13}NO_4$+H] 248.0923 Observed 248.0894; **^{1}H NMR** (400 MHz, $CDCl_3$) δ 7.86 (dt, *J* = 7.2, 3.6 Hz, 1H), 7.80 – 7.72 (m, 1H), 1.41 (s, 5H); **^{13}C NMR** (101 MHz, $CDCl_3$) δ 174.35, 162.08, 134.63, 129.00, 123.84, 38.39, 27.01; **FTIR** (ν/cm^{-1}, neat) 2973.5, 1933.8, 2875.0, 1803.3, 1779.6, 1743.0, 1469.2, 1365.3, 1186.7, 1130.1, 1059.4, 1020.6, 963.1, 875.6, 855.4, 788.5, 693.8.

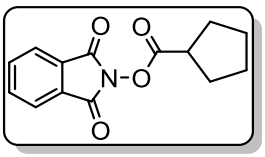

1,3-dioxoisoindolin-2-yl cyclopentanecarboxylate 3.50d

67% Yield, white solid; **MP** 62-63°C; **HRMS** predicted [$C_{14}H_{13}NO_4$ +H] 260.0923 Observed 260.0963; **^{1}H NMR** (400 MHz, $CDCl_3$) δ 7.86 (dd, *J* = 5.5, 3.1 Hz, 2H), 7.79 – 7.74 (m, 2H), 3.09 (td, *J* = 8.5, 4.2 Hz, 1H), 2.14 – 1.95 (m, 4H), 1.81 – 1.71 (m, 2H),

1.70 – 1.60 (m, 2H); **^{13}C NMR** (101 MHz, $CDCl_3$) δ 173.02, 162.27, 134.83, 129.11, 124.05, 40.77, 30.36, 26.08; **FTIR** (ν/cm^{-1}, neat) 2967.8, 2874.8, 1817.9, 1784.9, 1742.9, 1466.1, 1361.6, 1138.1, 1080.1, 1055.0, 975.6, 879.1, 694.1.

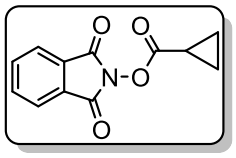

1,3-dioxoisoindolin-2-yl cyclopropanecarboxylate 3.50e

Synthesised and purified by *Nikolai Rossouw*, characterised by *Dean van As* white solid; **MP** 128-130°C; **HRMS** predicted [$C_{12}H_9NO_4$+H] 232.0610 Observed 232.0590; **^{1}H NMR** (400 MHz, $CDCl_3$) δ 7.87 (dd, *J* = 5.5, 3.1 Hz, 2H), 7.77 (dd, *J* = 5.5, 3.1 Hz, 2H), 1.95 (tt, *J* = 8.0, 4.7 Hz, 1H), 1.28 – 1.21 (m, 2H), 1.23 – 1.13 (m, 2H); **^{13}C NMR** (101 MHz, $CDCl_3$) δ 171.15, 162.01, 134.70, 128.88, 123.92, 10.62, 10.28; **FTIR** (ν/cm^{-1}, neat) 3101.2, 3029.8, 1775.9, 1744.9, 1464.7, 1372.4, 1182.3, 1113.4, 1063.1, 875.0, 787.9, 692.4.

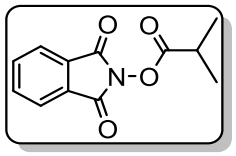

1,3-dioxoisoindolin-2-yl isobutyrate 3.50f

56% Yield, White solid; **MP** 62-65°C; **HRMS** predicted [$C_{12}H_{11}NO_4$+H] 234.0766 Observed 234.0752; **^{1}H NMR** (400 MHz, $CDCl_3$) δ 7.85 (dd, *J* = 5.5, 3.1 Hz, 2H), 7.76 (dd, *J* = 5.5, 3.1 Hz, 2H), 2.93 (dt, *J* = 14.0, 7.0 Hz, 1H), 1.35 (d, *J* = 7.0 Hz, 6H); **^{13}C NMR** (101 MHz, $CDCl_3$) δ 173.03, 162.01, 134.69, 128.91, 123.88, 31.71, 18.81; **FTIR** (ν/cm^{-1}, neat) 2981.5, 2940.9, 1809.8, 1786.4, 1733.5, 1708,1, 1464.7, 1363.2, 1185.9, 1137.2, 1045.8, 967.9, 877.4, 695.6.

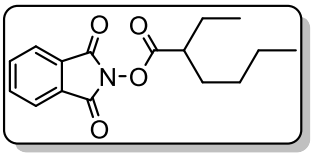

1,3-dioxoisoindolin-2-yl 2-ethylhexanoate 3.50g

85% Yield, clear liquid; **HRMS** predicted [$C_{16}H_{20}NO_4$+H] 290.1392 Observed 290.1373; **^{1}H NMR** (400 MHz, $CDCl_3$) δ 7.85 (dd, *J* = 5.5, 3.1 Hz, 2H), 7.75 (dd, *J* = 5.5, 3.1 Hz, 2H), 2.63 (ddd, *J* = 10.6, 7.1, 4.5 Hz, 1H), 1.71 (dddd, *J* = 34.1, 20.6, 9.9, 4.2 Hz, 4H), 1.48 – 1.31 (m, 4H), 1.05 (t, *J* = 7.4 Hz, 3H), 0.91 (t, *J* = 7.1 Hz, 3H); **^{13}C NMR** (101 MHz, $CDCl_3$) δ 172.55, 162.18, 134.80, 129.11, 123.99, 44.96, 31.85, 29.33, 25.76, 22.64, 14.00, 11.71; **FTIR** (ν/cm^{-1}, neat) 2964.8, 2936.4, 2864.7, 1811.7, 1784.5, 1740.5, 1467.1, 1365.4, 1185.7, 1051.9, 877.3, 694.7.

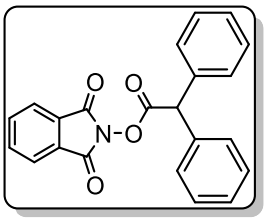

1,3-dioxoisoindolin-2-yl 2,2-diphenylacetate 3.50h

40% Yield, White solid; **MP** 129-130°C; **HRMS** predicted [$C_{22}H_{15}NO_4$+H] 358.1079 Observed 358.1051; **^{1}H NMR** (400 MHz, $cdcl_3$) δ 7.86 (dd, *J* = 5.4, 3.1 Hz, 2H), 7.76 (dd, *J* = 5.5, 3.1 Hz, 2H), 7.44 – 7.28 (m, 10H), 5.41 (s, 1H); **^{13}C NMR** (101 MHz, $cdcl_3$) δ 169.03, 161.81, 136.73, 134.78, 128.85, 128.67, 127.88, 123.96, 53.99; **FTIR** (ν/cm^{-1}, neat) 3088.6, 1810.1, 1779.3, 1741.5, 1492.0, 1454.8, 1356.8, 1186.4, 1132.0, 1063.1, 964.6, 902.2, 875.1, 794.6, 747.2, 696.6.

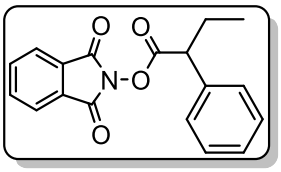

1,3-dioxoisoindolin-2-yl 2-phenylbutanoate 3.50i

Synthesised and purified by *Rowan Pilkington*, characterised by *Dean van As* white solid; **MP** 55-57°C; **HRMS** predicted [$C_{18}H_{15}NO_4$+H] 310.1079 Observed 310.1029; **^{1}H NMR** (400 MHz, $CDCl_3$) δ 7.83 (d, *J* = 2.7 Hz, 2H), 7.78 – 7.70 (m, 2H), 7.41 – 7.27 (m, 5H), 3.84 (t, *J* = 7.6 Hz, 1H), 2.23 (dt, *J* = 14.7, 7.4 Hz, 1H), 1.95 (dt, *J* = 14.4, 7.4 Hz, 1H), 1.02 (t, *J* = 7.4 Hz, 3H); **^{13}C NMR** (101 MHz, $CDCl_3$) δ 170.43, 161.99, 136.92, 134.84, 129.01, 128.95, 128.74, 128.16, 127.96, 124.02, 50.54, 27.35, 12.01; **FTIR** (ν/cm^{-1}, neat) 3094.1, 2968.9, 2937.1, 2878.4, 1807.6, 1784.3, 1736.9, 1707.7, 1464.2, 1454.2, 1184.2, 1133.9, 1050.5, 874.3, 693.8.

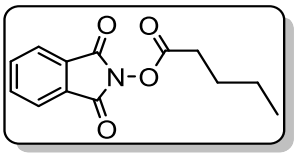

1,3-dioxoisoindolin-2-yl pentanoate 3.50k

88% Yield, yellow oil; **HRMS** predicted [$C_{13}H_{13}NO_4$+H] 248.0923 Observed 248.0947; **^{1}H NMR** (400 MHz, $CDCl_3$) δ 7.87 (dd, *J* = 5.5, 3.1 Hz, 2H), 7.77 (dd, *J* = 5.5, 3.1 Hz, 2H), 2.65 (t, *J* = 7.5 Hz, 2H), 1.80 – 1.71 (m, 2H), 1.52 – 1.40 (m, 2H), 0.95 (t, *J* = 7.4 Hz, 3H); **^{13}C NMR** (101 MHz, $CDCl_3$) δ 169.62, 161.98, 134.70, 128.90, 123.92, 30.68, 26.65, 21.98, 13.58; **FTIR** (ν/cm^{-1}, neat) 2961.6, 2935.8, 2875.3, 1815.5, 1787.2, 1738.4, 1609.4, 1467.4, 1361.1, 1185.7, 1126.1, 1061.9, 965.5, 877.0, 694.2.

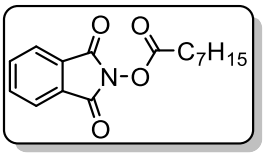

1,3-dioxoisoindolin-2-yl octanoate 3.50l

45% Yield, White sticky solid; **HRMS** predicted [$C_{16}H_{19}NO_4$+H] 290.1392 Observed 290.1371; **^{1}H NMR** (400 MHz, cdcl$_3$) δ 7.87 (dd, *J* = 5.4, 3.1 Hz, 1H), 7.77 (dd, *J* = 5.3, 3.2 Hz, 1H), 2.64 (t, *J* = 7.5 Hz, 1H), 1.82 – 1.71 (m, 1H), 1.48 – 1.21 (m, 5H), 0.87 (t, *J* = 6.7 Hz, 2H); **^{13}C NMR** (101 MHz, $CDCl_3$) δ 169.77, 162.12, 134.84, 129.04, 124.05, 31.68, 31.10, 28.89, 24.79, 22.69, 14.18; **FTIR** (ν/cm^{-1}, neat) 2925.1, 2857.2, 1814.2, 1787.4, 1739.9, 1610.2, 14665, 1361.0, 1185.0, 136.1, 1070.5, 877.3, 789.0, 754.6, 695.0.

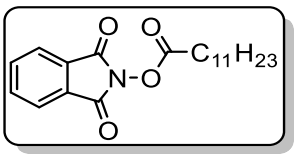

1,3-dioxoisoindolin-2-yl dodecanoate 3.50m

44% Yield, white solid; **MP** 53-55°C; **HRMS** predicted [$C_{20}H_{27}NO_4$+H] 346.2018 Observed 346.2003; **^{1}H NMR** (400 MHz, cdcl$_3$) δ 7.86 (dd, *J* = 5.5, 3.1 Hz, 2H), 7.77 (dd, *J* = 5.5, 3.1 Hz, 2H), 2.64 (t, *J* = 7.5 Hz, 2H), 1.83 – 1.72 (m, 2H), 1.41 (dd, *J* = 9.5, 5.4 Hz, 2H), 1.37 – 1.21 (m, 14H), 0.86 (t, *J* = 6.8 Hz, 3H); **^{13}C NMR** (101 MHz, cdcl$_3$) δ 169.80, 162.14, 134.85, 129.07, 124.07, 32.04, 31.13, 29.71, 29.51, 29.47, 29.26, 28.97, 24.81, 22.83, 14.27; **FTIR** (ν/cm^{-1}, neat) 2954.3 2919.2, 2851.3, 1827.0, 1789.1, 1740.0, 1612.6, 1466.8, 1375.0, 1185.7, 1141.7, 1067.1, 1057.5, 962.1, 878.8, 854.7, 791.6, 694.7.

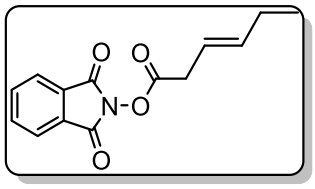

(E)-1,3-dioxoisoindolin-2-yl hex-3-enoate 3.50n

41% Yield, Sticky pale yellow solid (small amounts of Z isomer); **HRMS** predicted [$C_{14}H_{13}NO_4$+H] 260.0923 Observed 260.0924; **^{1}H NMR** (400 MHz, cdcl$_3$) δ 7.86 (dd, *J* = 5.4, 3.2 Hz, 2H), 7.76 (dd, *J* = 5.5, 3.1 Hz, 2H), 5.82 – 5.71 (m, 1H), 5.58 – 5.46 (m, 1H), 3.36 (dd, *J* = 6.7, 1.2 Hz, 2H), 2.13 – 1.98 (m, 2H), 0.99 (t, *J* = 7.5 Hz, 3H); **^{13}C NMR** (101 MHz, cdcl$_3$) δ 168.07, 161.88, 138.43, 134.73, 128.86, 123.94, 117.85, 34.52, 25.51, 13.25; **FTIR** (ν/cm^{-1}, neat) 2964.7, 2933.5, 1812.5, 1787.7, 1744.5, 1465.1, 1358.3, 1137.0, 1079.8, 1058.8, 967.1, 873.9, 789.7, 692.5.

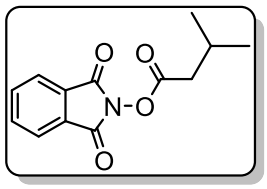

1,3-dioxoisoindolin-2-yl 3-methylbutanoate 3.50o

51% Yield, White crystalline solid; **MP** 32-33°C; **HRMS** predicted [$C_{13}H_{13}NO_4$+H] 248.0923 Observed 248.0882; **^{1}H NMR** (400 MHz, cdcl$_3$) δ 7.89 – 7.83 (m, 2H), 7.80 – 7.73 (m, 2H), 2.52 (d, *J* = 7.1 Hz, 2H), 2.23 (dp, *J* = 13.6, 6.8 Hz, 1H), 1.07 (d, *J* = 6.7 Hz, 6H); **^{13}C NMR** (101 MHz, cdcl$_3$) δ 168.80, 161.98, 134.70, 128.90, 123.90, 39.81, 26.02, 22.21; **FTIR** (ν/cm^{-1}, neat) 3103.9, 2965.2, 2932.9, 2876.2, 1810.7, 1785.2, 1743.0, 1466.1, 1356.7, 1184.6, 1135.7, 1058.1, 971.7, 877.1, 789.4, 683.4.

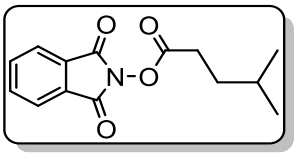

1,3-dioxoisoindolin-2-yl 4-methylpentanoate 3.50p

57% Yield, Pale yellow solid; **MP** 37-39°C; **HRMS** predicted[$C_{14}H_{15}NO_4$+H] 262.1079 Observed 262.1085; **^{1}H NMR** (400 MHz, $CDCl_3$) δ 7.86 (dd, *J* = 5.4, 3.1 Hz, 2H), 7.76 (dd, *J* = 5.5, 3.1 Hz, 2H), 2.64 (dd, *J* = 9.6, 5.6 Hz, 2H), 1.72 – 1.59 (m, 3H), 0.97 – 0.91 (m, 6H); **^{13}C NMR** (101 MHz, $CDCl_3$) δ 169.96, 162.13, 134.86, 129.03, 124.06, 33.41, 29.20, 27.65, 22.23; **FTIR** (ν/cm^{-1}, neat) 2954.8, 2927.6, 2871.1, 1820.2, 1789.2, 1737.9, 1611.7, 1466.5, 1367.4, 1185.9, 1136.0, 1064.6, 1044.7, 965.9, 870.8, 817.4, 791.0, 694.0.

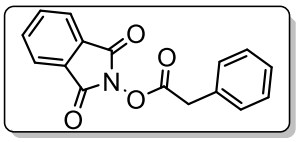

1,3-dioxoisoindolin-2-yl 2-phenylacetate 3.50q

70% Yield, white solid; **MP** 63-65°C; **HRMS** predicted[$C_{16}H_{11}NO_4$+H] 282.0766 Observed 282.0724; **^{1}H NMR** (400 MHz, $CDCl_3$) δ 7.86 (dt, *J* = 7.2, 3.6 Hz, 1H), 7.79 – 7.74 (m, 1H), 7.41 – 7.25 (m, 2H), 3.98 (s, 1H); **^{13}C NMR** (101 MHz, $CDCl_3$) δ 167.65, 161.80, 134.77, 131.48, 129.26, 128.84, 127.78, 123.96, 123.79, 37.67; **FTIR** (ν/cm^{-1}, neat) 3031.1, 1811.4, 1785.3, 1736.3, 1607.7, 1463.7, 1363.8, 1184.7, 1132.6, 1077.2, 1060.4, 969.6, 877.5, 790.3, 722.7, 697.1.

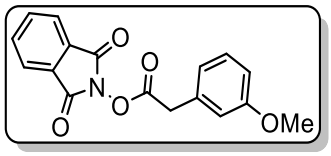

1,3-dioxoisoindolin-2-yl 2-(3-methoxyphenyl)acetate

3.50r

Synthesised and purified by *Nikolai Rossouw*, characterised by *Dean van As* 22% Yield, white solid; **MP** 69-70°C; **HRMS** predicted[$C_{17}H_{13}NO_5$+H] 312.0872 Observed 312.0896; **^{1}H NMR** (400 MHz, $CDCl_3$) δ 7.86 (dt, *J* = 7.3, 3.7 Hz, 2H), 7.81 – 7.71 (m, 2H), 7.27 (t, *J* = 8.0 Hz, 1H), 6.94 (d, *J* = 6.9 Hz, 2H), 6.88 – 6.82 (m, 1H), 3.96 (s, 2H), 3.82 (s, 3H); **^{13}C NMR** (101 MHz, $CDCl_3$) δ 167.51, 161.79, 159.86, 134.77, 132.84, 129.81, 128.84, 123.98, 121.51, 114.51, 113.64, 55.27, 37.73; **FTIR** (ν/cm^{-1}, neat) 2965.5, 2936.8, 2835.4, 1822.4, 1788.8, 1736.4, 1601.0, 1467.8, 1268.7, 1136.7, 1059.3, 1034.2, 873.0, 797.1, 762.8, 690.1.

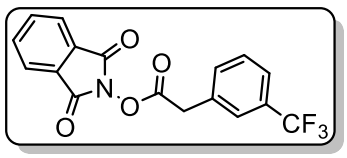

1,3-dioxoisoindolin-2-yl 2-(3-(trifluoromethyl)phenyl)acetate 3.50s

59% Yield, yellow solid; **MP** 96-97°C; **HRMS** predicted [$C_{17}H_{11}F_3NO_4$+H] 350.0640 Observed 350.0627; **^{1}H NMR** (400 MHz, $cdcl_3$) δ 7.86 (dt, *J* = 7.0, 3.6 Hz, 2H), 7.78 (td, *J* = 5.2, 2.0 Hz, 2H), 7.64 (s, 1H), 7.58 (d, *J* = 8.0 Hz, 2H), 7.52 – 7.47 (m, 1H), 4.05 (s, 2H); **^{13}C NMR** (101 MHz, $cdcl_3$) δ 167.24, 161.85, 135.02, 132.83, 132.53, 129.51, 128.92, 126.37, 126.34, 124.93, 124.90, 124.20, 37.50; **^{19}F NMR** (376 MHz, $cdcl_3$) δ -62.71; **FTIR** (ν/cm^{-1}, neat) 3521.0, 2931.5, 1849.4, 1809.6, 1784.9, 1741.8, 1467.0, 1346.9, 1322.7, 1170.9, 1108.1, 1066.9, 968.0, 874.9, 812.3, 786.0, 694.5, 662.6.

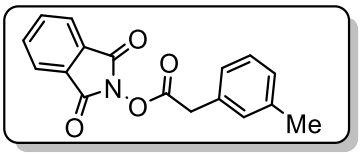

1,3-dioxoisoindolin-2-yl 2-(m-tolyl)acetate 3.50t

68% Yield, White solid; **MP** 93-95°C; **HRMS** predicted [$C_{17}H_{13}NO_4$+H] 296.0892 Observed 296.0881; **^{1}H NMR** (400 MHz, cdcl$_3$) δ 7.85 (dd, *J* = 5.5, 3.1 Hz, 2H), 7.76 (dd, *J* = 5.5, 3.1 Hz, 2H), 7.25 (dd, *J* = 9.6, 5.4 Hz, 1H), 7.20 – 7.14 (m, 2H), 7.12 (d, *J* = 7.5 Hz, 1H), 3.94 (s, 2H), 2.35 (s, 3H); **^{13}C NMR** (101 MHz, cdcl$_3$) δ 167.88, 161.93, 138.67, 134.88, 131.48, 130.13, 128.96, 128.83, 128.63, 126.38, 124.06, 37.70, 21.46; **FTIR** (ν/cm^{-1}, neat) 2972.8, 2931.5, 1805.9, 1779.8, 1734.2, 1608.5, 1466.7, 1372.5, 1187.8, 1136.6, 1068.5, 969.8, 877.9, 863.9, 689.1.

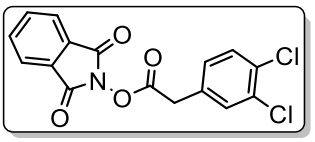

1,3-dioxoisoindolin-2-yl 2-(3,4-dichlorophenyl)acetate 3.50u

9% Yield, white solid; **MP** 134-136°C; **HRMS** predicted [$C_{16}H_9Cl_2NO_4$+H] 349.9987 Observed 349.9952; **^{1}H NMR** (400 MHz, cdcl$_3$) δ 7.88 (dd, *J* = 5.5, 3.1 Hz, 2H), 7.78 (dd, *J* = 5.5, 3.1 Hz, 2H), 7.49 (d, *J* = 2.1 Hz, 1H), 7.44 (d, *J* = 8.3 Hz, 1H), 7.22 (dd, *J* = 8.3, 2.1 Hz, 1H), 3.94 (s, 2H); **^{13}C NMR** (101 MHz, cdcl$_3$) δ 166.86, 161.67, 134.89, 134.32, 132.22, 131.43, 131.32, 130.77, 128.74, 128.65, 124.06, 36.70; **FTIR** (ν/cm^{-1}, neat) 3202.3, 1824.4, 1782.3, 1731.6, 1468.6, 1362.9, 1185.6, 1140.4, 1062.7, 1029.9, 975.1, 872.6, 695.7.

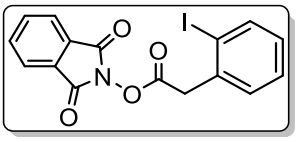

1,3-dioxoisoindolin-2-yl 2-(2-iodophenyl)acetate 3.50v

80% Yield, White Solid; **MP** 137-139°C; **HRMS** predicted [$C_{16}H_{10}NO_4$+H] 407.9733 Observed 407.9742; **^{1}H NMR** (400 MHz, cdcl$_3$) δ 7.90 – 7.84 (m, 3H), 7.77 (dd, *J* = 5.4, 3.1 Hz, 2H), 7.43 (dd, *J* = 7.7, 1.6 Hz, 1H), 7.36 (td, *J* = 7.5, 1.2 Hz, 1H), 7.00 (td, *J* = 7.7, 1.7 Hz, 1H), 4.16 (s, 2H); **^{13}C NMR** (101 MHz, cdcl$_3$) δ 166.97, 161.84, 139.78, 135.46, 134.91, 130.63, 129.66, 128.88, 128.79, 124.07, 100.86, 43.16; **FTIR** (ν/cm^{-1}, neat) 3046.3, 1813.3, 1788.1, 1732.5, 1467.0, 1397.8, 1363.5, 1186.9, 1016.1, 1070.6, 971.0, 877.9, 772.8, 743.7, 694.0.

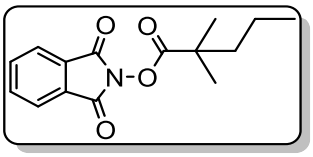

1,3-dioxoisoindolin-2-yl 2,2-dimethylpentanoate 3.50w

83% Yield, white solid; **MP** 53-55°C; **HRMS** predicted [$C_{15}H_{17}NO_4$+H] 276.1236 Observed 276.1229; **^{1}H NMR** (400 MHz, $CDCl_3$) δ 7.85 (td, *J* = 5.2, 2.0 Hz, 2H), 7.77 (td, *J* = 5.2, 2.0 Hz, 2H), 1.72 – 1.65 (m, 2H), 1.50 – 1.41 (m, 2H), 1.37 (s, 6H), 0.96 (t, *J* = 7.3 Hz, 3H); **^{13}C NMR** (101 MHz, $CDCl_3$) δ 173.93, 162.11, 134.61, 129.02, 123.80, 42.93, 42.16, 25.08, 18.03, 14.47; **FTIR** (ν/cm^{-1}, neat) 2959.3, 2872.4, 1803.4, 1776.2, 1736.7, 1466.5, 1363.8, 1187.0, 1080.0, 1058.4, 1033.9, 875.8, 790.4, 695.1.

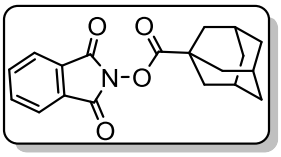

(3r,5r,7r)-1,3-dioxoisoindolin-2-yl adamantane-1-carboxylate 3.50x

56% Yield, white solid; **MP** 134-135°C; **HRMS** predicted [$C_{19}H_{19}NO_4$+H] 326.1392 Observed 326.1366; **^{1}H NMR** (400 MHz, $CDCl_3$) δ 7.85 (dd, *J* = 5.5, 3.1 Hz, 2H), 7.75 (dd, *J* = 5.5, 3.1 Hz, 2H), 2.10 (t, *J* = 7.8 Hz, 9H), 1.76 (d, *J* = 2.6 Hz, 6H); **^{13}C NMR** (101 MHz, $CDCl_3$) δ 173.22, 162.12, 134.59, 129.03, 123.81, 123.64, 40.48, 38.41, 36.16, 27.60; **FTIR** (ν/cm^{-1}, neat) 2927.4, 2911.4, 1899.9, 2851.6, 1804.7, 1773.4, 1746.0, 1348.2, 1169.8, 1008.2, 974.1, 878.7, 864.3, 780.9, 691.5.

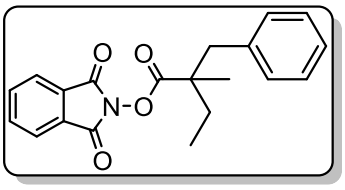

1,3-dioxoisoindolin-2-yl 2-benzyl-2-methylbutanoate 3.50y

55% Yield, yellow oil; **HRMS** predicted [$C_{20}H_{19}NO_4$+H] 338.1392 Observed 338.1345; **^{1}H NMR** (400 MHz, $CDCl_3$) δ 7.87 (dd, *J* = 5.5, 3.1 Hz, 2H), 7.77 (dd, *J* = 5.5, 3.1 Hz, 2H), 7.33 – 7.23 (m, 5H), 3.24 (d, *J* = 13.7 Hz, 1H), 2.91 (d, *J* = 13.7 Hz, 1H), 2.00 (dd, *J* = 13.9, 7.4 Hz, 1H), 1.63 (dd, *J* = 13.9, 7.5 Hz, 1H), 1.23 (s, 3H), 1.10 (t, *J* = 7.5 Hz, 3H); **^{13}C NMR** (101 MHz, $CDCl_3$) δ 172.99, 162.06, 136.35, 134.66, 130.53, 128.99, 128.16, 126.77, 123.84, 47.50, 44.65, 32.29, 20.41, 8.94; **FTIR** (ν/cm^{-1}, neat) 3031.3, 2974.1, 2940.4, 1807.0, 1781.6, 1739.1, 1606.5, 1496.9, 1466.8, 1455.3, 1368.7, 1185.6, 1131.4, 1051.0, 964.2, 877.2, 693.6.

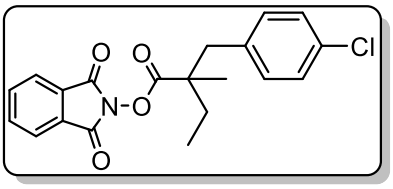

1,3-dioxoisoindolin-2-yl 2-(4-chlorobenzyl)-2-methylbutanoate 3.51z

69% Yield, pale yellow solid; **MP**. 102-104°C; **HRMS** predicted [$C_{20}H_{18}NClO_4$+H] 372.1003 Observed 372.1050; **^{1}H NMR** (400 MHz, $CDCl_3$) δ 7.88 (dd, *J* = 5.5, 3.1 Hz, 2H), 7.78 (dd, *J* = 5.5, 3.1 Hz, 2H), 7.30 – 7.22 (m, 4H), 3.22 (d, *J* = 13.7 Hz, 1H), 2.84 (d, *J* = 13.7 Hz, 1H), 1.99 (dd, *J* = 13.9, 7.4 Hz, 1H), 1.61 (dd, *J* = 13.9, 7.5 Hz, 1H), 1.21 (s, 3H), 1.09 (t, *J* = 7.5 Hz, 3H); **^{13}C NMR** (101 MHz, $CDCl_3$) δ 172.71, 134.81, 134.71, 132.74, 131.79, 128.93, 128.34, 123.88, 47.47, 44.10, 32.45, 20.31, 8.87; **FTIR** (ν/cm^{-1}, neat) 2971.2, 2943.6, 2869.0, 1804.0, 1783.5, 1735.3, 1492.0, 1466.1, 1374.8, 1184.6, 1142.3, 1025.2, 1017.2, 971.8, 877.9, 821.4, 776.3, 690.9.

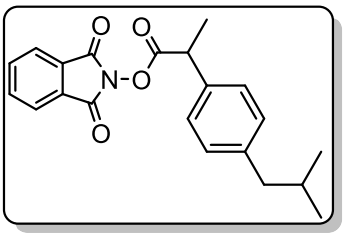

1,3-dioxoisoindolin-2-yl 2-(4-isobutylphenyl)propanoate 3.57a

Synthesised and purified by *Nikolai Rossouw*, characterised by *Dean van As* white solid; **MP** 80-81°C; **HRMS** predicted [$C_{21}H_{21}NO_4$+H] 352.1549 Observed 352.1509; **^{1}H NMR** (400 MHz, $CDCl_3$) δ 7.84 (dd, *J* = 5.4, 3.1 Hz, 2H), 7.78 – 7.72 (m, 2H), 7.29 (d, *J* = 8.1 Hz, 2H), 7.15 (d, *J* = 8.1 Hz, 2H), 4.08 (q, *J* = 7.2 Hz, 1H), 2.46 (d, *J* = 7.2 Hz, 2H), 1.85 (dt, *J* = 13.6, 6.8 Hz, 1H), 1.65 (d, *J* = 7.2 Hz, 3H), 0.89 (d, *J* = 6.6 Hz, 6H); **^{13}C NMR** (101 MHz, $CDCl_3$) δ 170.93, 161.85, 141.24, 135.52, 134.69, 129.58, 128.90, 127.22, 123.88, 45.04, 42.55, 30.14, 22.39, 19.02; **FTIR** (ν/cm^{-1}, neat) 3040.51, 2967.8,

2954.9, 2915.5, 2867.6, 2845.1, 1804.9, 1779.5, 1740.1, 1514.7, 1462.4, 1366.8, 1346.4, 1185.6, 1104.2, 1049.3, 987.5, 954.0, 876..7, 856.6, 789.9, 755.5, 708.6, 696.5.

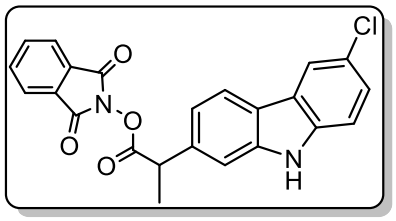

1,3-dioxoisoindolin-2-yl 2-(6-chloro-9H-carbazol-2-yl)propanoate 3.57b

96% yield, Yellow solid; **MP** 184-185°C; **HRMS** predicted [$C_{23}H_{15}ClN_2O_4$+H] 419.0799 Observed 419.0827; **^{1}H NMR** (400 MHz, cdcl$_3$) δ 8.17 (s, 1H), 7.89 (dd, *J* = 8.3, 4.7 Hz, 2H), 7.82 (s, 2H), 7.74 (dd, *J* = 5.4, 3.1 Hz, 2H), 7.39 (s, 1H), 7.31 (dd, *J* = 8.6, 1.8 Hz, 1H), 7.25 (d, *J* = 8.7 Hz, 1H), 7.21 (d, *J* = 8.1 Hz, 1H), 4.25 (q, *J* = 7.1 Hz, 1H), 1.71 (d, *J* = 7.2 Hz, 3H); **^{1}H NMR** (400 MHz, *d*$_6$-DMSO) δ 11.49 (s, 1H), 8.18 (t, *J* = 4.1 Hz, 1H), 8.15 (d, *J* = 8.1 Hz, 1H), 7.87 (dd, *J* = 7.5, 4.6 Hz, 4H), 7.54 (s, 1H), 7.49 (d, *J* = 8.6 Hz, 1H), 7.37 (dt, *J* = 8.6, 4.1 Hz, 1H), 7.20 (dd, *J* = 8.2, 1.3 Hz, 1H), 4.50 (q, *J* = 7.0 Hz, 1H), 1.61 (d, *J* = 7.1 Hz, 3H); **^{13}C NMR** (101 MHz, *d*$_6$-DMSO) δ 171.70, 162.18, 140.93, 138.93, 137.20, 135.88, 128.58, 125.85, 124.33, 123.89, 123.47, 121.51, 120.28, 120.24, 119.00, 112.91, 110.67, 110.58, 42.69, 19.65; **FTIR** (ν/cm^{-1}, neat) 3429.3, 2939.0, 1803.1, 1782.3, 1735.7, 1607.9, 1464.8, 1450.2, 1343.7, 1273.5, 1182.5, 1051.9, 874.6, 820.8, 694.5.

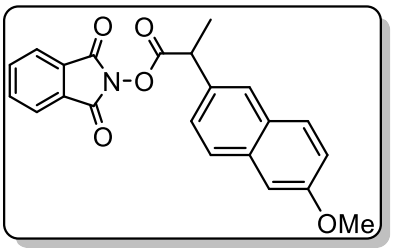

1,3-dioxoisoindolin-2-yl 2-(6-methoxynaphthalen-2-yl)propanoate 3.57c

66% Yield, white solid; **MP** 111-113°C; **HRMS** predicted [$C_{22}H_{18}NO_5$+H] 376.1185 Observed 376.1160; **^{1}H NMR** (400 MHz, $CDCl_3$) δ 7.83 (dd, *J* = 5.2, 3.0 Hz, 2H), 7.79 – 7.72 (m, 5H), 7.47 (dd, *J* = 8.5, 1.8 Hz, 1H), 7.18 – 7.10 (m, 2H), 4.24 (q, *J* = 7.1 Hz, 1H), 3.90 (s, 3H), 1.73 (d, *J* = 7.2 Hz, 3H); **^{13}C NMR** (101 MHz, $CDCl_3$) δ 170.90, 157.83, 134.70, 133.95, 133.41, 129.41, 128.90, 128.88, 127.52, 126.34, 125.87, 123.89, 119.17, 105.60, 55.31, 42.91, 19.01; **FTIR** (ν/cm^{-1}, neat) 2972.4, 2941.0, 1807.2, 1783.4, 1736.1, 1606.7, 1462.8, 1372.4, 1137.5, 1037.7, 1001.2, 849.6, 782.7, 692.0.

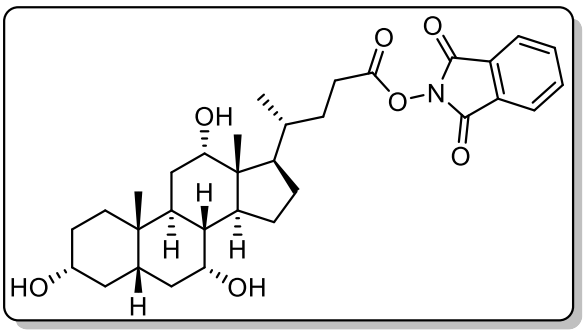

(R)-1,3-dioxoisoindolin-2-yl 4-((3R,5S,7R,8R,9S,10S,12S,13R,14S,17R)-3,7,12-trihydroxy-10,13-dimethylhexadecahydro-1H-cyclopenta[a]phenanthren-17-yl)pentanoate 3.57d

Yield 35%, white solid; **MP** 92°C; **HRMS** predicted[$C_{32}H_{43}NO_7$+H] 554.3118 Observed 554.3084; **^{1}H NMR** (400 MHz, cdcl$_3$) δ 7.86 (dd, *J* = 5.5, 3.1 Hz, 2H), 7.77 (dd, *J* = 5.5, 3.1 Hz, 2H), 3.97 (s, 1H), 3.83 (d, *J* = 2.3 Hz, 1H), 3.43 (dd, *J* = 9.9, 5.5 Hz, 1H), 2.76 – 2.67 (m, 1H), 2.61 (dd, *J* = 15.8, 8.1 Hz, 1H), 2.55 – 2.15 (m, 5H), 2.00 – 1.64 (m, 10H), 1.58 – 1.46 (m, 6H), 1.36 (dd, *J* = 8.2, 4.8 Hz, 3H), 1.16 (t, *J* = 4.6 Hz, 2H), 1.03 (d, *J* =

5.9 Hz, 3H), 0.96 (d, *J* = 2.7 Hz, 1H), 0.87 (s, 3H), 0.70 (s, 3H); **^{13}C NMR** (101 MHz, cdcl$_3$) δ 170.25, 162.14, 134.86, 129.02, 124.07, 73.15, 72.05, 68.59, 46.97, 46.64, 41.81, 41.58, 39.62, 35.38, 35.20, 34.89, 34.79, 30.74, 30.57, 28.35, 28.18, 27.59, 26.50, 23.47, 23.36, 22.59, 17.41, 12.61; **FTIR** (ν/cm^{-1}, neat) 3395.1, 2932.0, 2867.1, 1815.34, 1787.0, 1739.6, 1656.4, 1549.0, 1467.0, 1367.4, 1186.3, 1074.6, 878.0, 752.2, 696.7.

Synthesis of tetrahydroisoquinoline derivatives

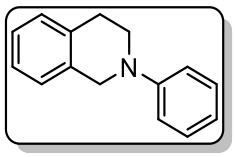

2-phenyl-1,2,3,4-tetrahydroisoquinoline 3.18

A round bottom flask was charged with a stirrer bar, then CuI (200mg, 1mmol), K_3PO_4 (4.25g, 20mmol), THIQ (2mL, 15mmol), iodobenzene(1.12mL, 10 mmol), ethylene glycol (1.11mL, 20mmol). The resultant mixture was dissolved in isopropanol (10mL) and the solution was thoroughly degassed with N_2 and kept under inert atmosphere.The reaction was heated at 85°C for 24 hours, the reaction was then allowed to cool to room temperature and filtered through a pad of celite. The reaction mixture was evaporated then purified via column chromatography (5% EtOAc/hexane).

Off white solid; **HRMS** predicted [$C_{15}H_{15}N$+H] 210.1283 found 210.1266; **^{1}H NMR** (400 MHz, $CDCl_3$) δ 7.28 (dd, *J* = 8.4, 7.5 Hz, 2H), 7.22 – 7.12 (m, 4H), 6.98 (d, *J* = 8.1 Hz, 2H), 6.82 (t, *J* = 7.2 Hz, 1H), 4.40 (s, 2H), 3.55 (t, *J* = 5.9 Hz, 2H), 2.98 (t, *J* = 5.8 Hz, 2H); **^{13}C NMR** (101 MHz, cdcl$_3$) δ 150.50, 134.85, 134.43, 129.20, 128.51, 126.53, 126.32, 126.02, 118.68, 115.14, 50.73, 46.53, 29.10.

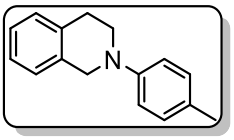

2-(p-tolyl)-1,2,3,4-tetrahydroisoquinoline 3.55b

A 25mL Schlenk flask was charged THIQ (400mg, 3mmol) 4-iodotoluene (698mg, 3.2mmol), Na-tOBu (308mg, 3.2 mmol), $Pd(OAc)_2$ (2 mol%) and BINAP (5 mol%) as well as a stirrer bar. The reagents were then dissolved in toluene (10mL) and the mixture was then sparged with N_2 to degass, the resultant solution was kept at under an inert N_2 atmosphere and heated at 90°C until completion. The reaction was allowed to cool to room temperature and then washed with water and brine. The organic layer was taken, evaporated then purified via column chromatography.

HRMS predicted [$C_{16}H_{17}N$+H] 224.1439 found 224.1476; **^{1}H NMR** (400 MHz, cdcl$_3$) δ 7.23 – 7.12 (m, 6H), 7.09 (t, *J* = 7.1 Hz, 3H), 6.92 (d, *J* = 8.5 Hz, 3H), 4.35 (s, 3H), 3.51 (t, *J* = 5.9 Hz, 3H), 2.98 (t, *J* = 5.8 Hz, 3H), 2.28 (s, 5H); **^{13}C NMR** (101 MHz, cdcl$_3$) δ 148.62, 134.74, 134.56, 129.72, 128.61, 128.39, 126.54, 126.26, 125.94, 115.86, 51.49, 47.29, 29.09, 20.44.

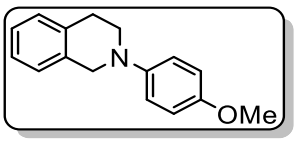

2-(4-methoxyphenyl)-1,2,3,4-tetrahydroisoquinoline 3.55c

A round bottom flask was charged with a stirrer bar, then CuI (200mg, 1mmol), K_3PO_4 (4.25g, 20mmol), THIQ (2mL, 15mmol), 4-iodoanisole(2.34g, 10 mmol), ethylene glycol (1.11mL, 20mmol). The resultant mixture was dissolved in isopropanol (10mL) and the solution was thoroughly degassed with N_2 and kept under inert atmosphere.The reaction was heated at 85°C for 24 hours, the reaction was then allowed to cool to room temperature and filtered through a pad of celite. The reaction mixture was evaporated then purified via column chromatography (5% EtOAc/hexane).

^{1}H NMR (400 MHz, cdcl$_3$) δ 7.20 – 7.10 (m, 4H), 7.01 – 6.95 (m, 2H), 6.89 – 6.83 (m, 2H), 4.29 (s, 2H), 3.77 (d, *J* = 4.0 Hz, 3H), 3.44 (t, *J* = 5.9 Hz, 2H), 2.98 (t, *J* = 5.8 Hz, 2H); **^{13}C NMR** (101 MHz, cdcl$_3$) δ 153.50, 145.22, 134.48, 128.65, 126.47, 126.23, 125.88, 118.03, 114.53, 55.64, 52.66, 48.46, 29.05.

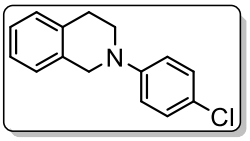

2-(4-chlorophenyl)-1,2,3,4-tetrahydroisoquinoline 3.55d

A 25mL Schlenk flask was charged THIQ (400mg, 3mmol) 1-cloro-4-iodobenzene (763mg, 3.2mmol), Na-tOBu (308mg, 3.2 mmol), Pd(OAc)$_2$ (2 mol%) and BINAP (5 mol%) as well as a stirrer bar. The reagents were then dissolved in toluene (10mL) and the mixture was then sparged with N_2 to degass, the resultant solution was kept at under an inert N_2 atmosphere and heated at 90°C until completion. The reaction was allowed to cool to room temperature and then washed with water and brine. The organic layer was taken, evaporated then purified via column chromatography.

HRMS predicted [$C_{15}H_{14}NCl$+H] 244.0893 found 244.0890; **^{1}H NMR** (400 MHz, cdcl$_3$) δ 7.28 – 7.16 (m, 5H), 6.93 – 6.87 (m, 2H), 4.39 (s, 2H), 3.54 (t, *J* = 5.9 Hz, 2H), 2.99 (t, *J* = 5.8 Hz, 2H); **^{13}C NMR** (101 MHz, cdcl$_3$) δ 149.06, 134.70, 134.08, 129.02, 128.54, 126.55, 126.51, 126.16, 123.27, 116.12, 50.61, 46.50, 28.99.

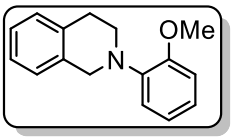

2-(2-methoxyphenyl)-1,2,3,4-tetrahydroisoquinoline 3.55e

A round bottom flask was charged with a stirrer bar, then CuI (200mg, 1mmol), K_3PO_4 (4.25g, 20mmol), THIQ (2mL, 15mmol), 2-iodoanisole(2.34g, 10 mmol), ethylene glycol (1.11mL, 20mmol). The resultant mixture was dissolved in isopropanol (10mL) and the

solution was thoroughly degassed with N_2 and kept under inert atmosphere. The reaction was heated at 85°C for 24 hours, the reaction was then allowed to cool to room temperature and filtered through a pad of celite. The reaction mixture was evaporated then purified via column chromatography (5% EtOAc/hexane).

HRMS predicted [$C_{16}H_{17}NO$+H] 240.1388 found 240.1379; **^{1}H NMR** (400 MHz, cdcl$_3$) δ 7.18 – 7.12 (m, 3H), 7.09 (dt, *J* = 7.2, 3.6 Hz, 1H), 7.05 – 6.98 (m, 2H), 6.94 – 6.88 (m, 2H), 4.29 (s, 2H), 3.88 (d, *J* = 2.3 Hz, 3H), 3.41 (t, *J* = 5.8 Hz, 2H), 2.98 (t, *J* = 5.7 Hz, 2H); **^{13}C NMR** (101 MHz, cdcl$_3$) δ 152.54, 141.06, 135.08, 134.50, 128.86, 126.34, 126.10, 125.70, 122.98, 120.87, 118.97, 111.20, 55.45, 53.07, 48.98, 28.81.

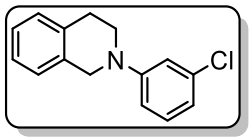

2-(3-chlorophenyl)-1,2,3,4-tetrahydroisoquinoline 3.55f

A round bottom flask was charged with a stirrer bar, then CuI (200mg, 1mmol), K_3PO_4 (4.25g, 20mmol), THIQ (2mL, 15mmol), 1-cloro-4-iodobenzene (2.38g, 10 mmol), ethylene glycol (1.11mL, 20mmol). The resultant mixture was dissolved in isopropanol (10mL) and the solution was thoroughly degassed with N_2 and kept under inert atmosphere.The reaction was heated at 85°C for 24 hours, the reaction was then allowed to cool to room temperature and filtered through a pad of celite. The reaction mixture was evaporated then purified via column chromatography (5% EtOAc/hexane).

HRMS predicted [$C_{15}H_{14}NCl$+H] 244.0893 found 244.0873; **^{1}H NMR** (400 MHz, cdcl$_3$) δ 7.22 – 7.12 (m, 5H), 6.90 (t, *J* = 2.1 Hz, 1H), 6.81 (dd, *J* = 8.4, 2.3 Hz, 1H), 6.76 (dd, *J* = 7.8, 1.6 Hz, 1H), 4.39 (s, 2H), 3.54 (t, *J* = 5.9 Hz, 2H), 2.97 (t, *J* = 5.8 Hz, 2H); **^{13}C NMR** (101 MHz, cdcl$_3$) δ 151.29, 135.03, 134.75, 133.92, 130.07, 128.40, 126.51, 126.49, 126.18, 117.97, 114.34, 112.57, 50.05, 45.89, 28.99.

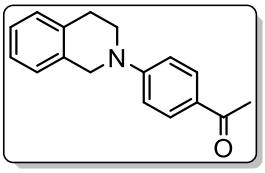

1-(4-(3,4-dihydroisoquinolin-2(1H)-yl)phenyl)ethenone 3.55g

A round bottom flask was charged with a stirrer bar, then CuI (200mg, 1mmol), K_3PO_4 (4.25g, 20mmol), THIQ (2mL, 15mmol), 4-iodoacetophenone (2.46g, 10 mmol), ethylene glycol (1.11mL, 20mmol). The resultant mixture was dissolved in isopropanol (10mL) and the solution was thoroughly degassed with N_2 and kept under inert atmosphere.The reaction was heated at 85°C for 24 hours, the reaction was then allowed to cool to room temperature and filtered through a pad of celite. The reaction mixture was evaporated then purified via column chromatography (5% EtOAc/hexane).

^{1}H NMR (400 MHz, $CDCl_3$) δ 7.95 – 7.86 (m, 2H), 7.23 – 7.13 (m, 4H), 6.87 (t, *J* = 5.9 Hz, 2H), 4.53 (s, 2H), 3.66 (t, *J* = 5.9 Hz, 2H), 2.99 (t, *J* = 5.9 Hz, 2H), 2.51 (s, 3H).

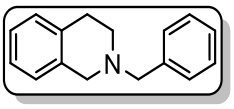

2-benzyl-1,2,3,4-tetrahydroisoquinoline 3.47g

THIQ (10mmol) and TEA (5mmol) were dissolved in DCM and cooled to 0°C. Benzyl Bromide was added dropwise and allowed to stir overnight. The reaction was filtered, washed with brine and dried with $MgSO_4$. The resulting filtrate was evaporated under vacuum The crude material was then purified by column chromatography (20:80 EtOAc:Hexane)

HRMS predicted [$C_{16}H_{17}N$+H] 224.1439 found 224.1435; **^{1}H NMR** (400 MHz, $CDCl_3$) δ 7.39 (d, *J* = 7.4 Hz, 2H), 7.33 (t, *J* = 7.4 Hz, 2H), 7.27 (d, *J* = 7.2 Hz, 1H), 7.14 – 7.05 (m, 3H), 6.97 (d, *J* = 7.4 Hz, 1H), 3.69 (s, 2H), 3.64 (s, 2H), 2.90 (t, *J* = 5.9 Hz, 2H), 2.75 (t, *J* = 5.9 Hz, 2H); **^{13}C NMR** (101 MHz, $cdcl_3$) δ 138.22, 134.76, 134.31, 129.12, 128.69, 128.30, 127.14, 126.60, 126.11, 125.57, 62.71, 56.04, 50.58, 29.07.

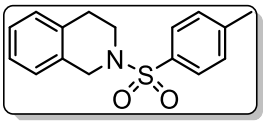

2-tosyl-1,2,3,4-tetrahydroisoquinoline 3.47h

THIQ (533 mg 2 mmol) and pyridine (1mL) and a stirrer bar were added to a vial and dissolved in 5mL of DCM. Tosyl chloride was dissolved in DCM in a separate vial. The Tosyl chloride solution was slowly added to the THIQ solution and allowed to stir at room temperature for 1.5 hours. The reaction was then quenched with 1M HCl and extracted into diethyl ether. The organic layer was washed with water and brine solutions, collected, dried with $MgSO_4$, filtered and subsequently evaporated. The crude product was then purified via column chromatography (5:95 EtOAc:hex), achieving a white solid at 88% yield.

88% yield, white solid; **HRMS** predicted [$C_{16}H_{17}NSO_2$ +H] 288.1058 found 288.1129; **^{1}H NMR** (400 MHz, $CDCl_3$) δ 7.71 (d, *J* = 8.2 Hz, 2H), 7.30 (d, *J* = 8.0 Hz, 2H), 7.12 (dd, *J* = 8.8, 4.7 Hz, 2H), 7.10 – 7.04 (m, 1H), 7.04 – 6.97 (m, 1H), 4.23 (s, 2H), 3.34 (t, *J* = 5.9 Hz, 2H), 2.91 (t, *J* = 5.9 Hz, 2H), 2.40 (s, 3H); **^{13}C NMR** (101 MHz, $cdcl_3$) δ 143.64, 133.15, 133.03, 131.59, 129.67, 128.77, 127.72, 126.68, 126.33, 126.29, 47.51, 43.70, 28.84, 21.50.

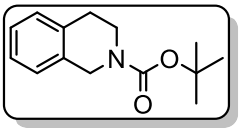

tert-butyl 3,4-dihydroisoquinoline-2(1H)-carboxylate 3.47i

THIQ (2 mmol) and di-tert-butyl decarbonate (2.2mmol) was dissolved in THF (15mL). The reaction solution was stirred at room temperature overnight. The reaction was washed with H_2O and brine, dried with $MgSO_4$. The dried solution was filtered and evaporated achieving a clean product in 80% yield

80% yield, white solid; **^{1}H NMR** (400 MHz, $CDCl_3$) δ 7.20 – 7.05 (m, 2H), 4.56 (s, 1H), 3.63 (t, *J* = 5.6 Hz, 1H), 2.82 (t, *J* = 5.8 Hz, 1H), 1.48 (s, 4H); **^{13}C NMR** (101 MHz, $cdcl_3$) δ 154.92, 134.73, 133.67, 129.44, 128.66, 126.30, 126.17, 79.78, 45.63, 41.06, 28.97, 28.48, 28.34.

Procedure for the α-alkylation of THIQ under batch conditions

THIQ (0.1125mmol), NHP ester (0.225mmol), diphenylamine (0.225mmol) and $[Ru(bpy)_3]Cl_2$ (2.5 mol%) were weighed and placed in a 4mL reaction vial, a stirrer bar was placed in the vial then dissolved in MeCN (2mL). The solution was briefly sonicated to ensure all materials were dissolved, then sparged with nitrogen gas for 10 minutes to degas the mixture. Upon degassing, the reaction vial was sealed with parafilm then illuminated under a 14W blue light source for 16 hours.

Method for conducting the α-alkylation of THIQ under Flow conditions

THIQ 0.3516mmol NHP ester (0.4219mml), diphenylamine (0.1759mmol) and $[Ru(bpy)_3]Cl_2$ (2.5 mol%) were weighed and placed in a 20mL reaction vial then dissolved in MeCN (12.5mL). The solution was briefly sonicated to ensure all materials were dissolved, then sparged with nitrogen gas for 10 minutes to degas the mixture. 2.5mL of the solution were then taken and loaded into a 2mL sample loop (0.05625mmol in sample loop). The solution was then pumped through the sample loop into either an 8mL or 11.7mL reactor coil which is under constant 14W illumination7mL (either 2 or 3 4mL reactors in series, each with a 14W illuminated light source). Once the solution had left the 2mL sample loop, another 2.5mL solution was injected into the loop and pumped through the reactor coil. This process was repeated 5 consecutive times and collected

(total collection is 0.28125 mmol of product). Upon completion of reaction, the crude reaction mixture was evaporated, dissolved in a small amount of non-polar solvent (eg. EtOAc, $CHCl_3$) and filtered through a small plug of tissue to remove excess solids from reaction. The filtrate was then evaporated again, and the crude material was purified via preparatory TLC (solvent system EtOAc:Hexane 0-10% EtOAc) affording pure product.

Characterisation of alkylated tetrathydroisoquinolines

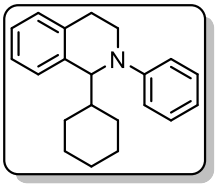

1-cyclohexyl-2-phenyl-1,2,3,4-tetrahydroisoquinoline 3.40/3.51a

Yield 68%, Yellow oil; **HRMS** predicted [$C_{21}H_{25}N$+H] 292.2065 Observed 292.2054; **^{1}H NMR** (400 MHz, cdcl$_3$) δ 7.24 – 7.18 (m, 2H), 7.18 – 7.05 (m, 4H), 6.86 (d, *J* = 8.0 Hz, 2H), 6.68 (t, *J* = 7.2 Hz, 1H), 4.42 (d, *J* = 8.1 Hz, 1H), 3.72 (dd, *J* = 11.9, 5.9 Hz, 1H), 3.51 – 3.42 (m, 1H), 3.07 – 2.94 (m, 2H), 1.98 (d, *J* = 10.7 Hz, 1H), 1.71 (dd, *J* = 30.9, 20.7 Hz, 6H), 1.23 – 0.99 (m, 6H); **^{13}C NMR** (101 MHz, cdcl$_3$) δ 149.91, 137.79, 135.26, 129.09, 128.32, 128.14, 126.55, 125.15, 116.23, 112.88, 63.71, 44.07, 42.96, 30.90, 30.64, 27.36, 26.64, 26.40, 26.38; **FTIR** (ν/cm^{-1}, neat) 3020.6, 2928.1,2848.2, 1591.7, 1502.3, 1318.0, 749.3, 738.8, 684.9.

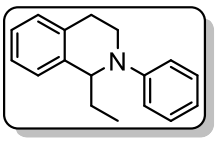

1-ethyl-2-phenyl-1,2,3,4-tetrahydroisoquinoline 3.51b

Yield 81%, Yellow oil; **HRMS** predicted [$C_{17}H_{19}N$+H] 238.1596 Observed 238.158; **^{1}H NMR** (400 MHz, cdcl$_3$) δ 7.24 (dd, *J* = 9.1, 6.9 Hz, 2H), 7.19 – 7.05 (m, 4H), 6.89 (t, *J* = 8.7 Hz, 2H), 6.72 (t, *J* = 7.0 Hz, 1H), 4.55 (t, *J* = 7.0 Hz, 1H), 3.67 – 3.51 (m, 2H), 3.02

(ddd, J = 15.6, 7.4, 5.6 Hz, 1H), 2.87 (dt, J = 15.5, 5.4 Hz, 1H), 1.98 (td, J = 14.2, 7.1 Hz, 1H), 1.75 (dp, J = 14.4, 7.3 Hz, 1H), 1.00 (t, J = 7.4 Hz, 3H); **^{13}C NMR** (101 MHz, cdcl$_3$) δ 149.62, 138.84, 135.01, 129.21, 128.40, 127.37, 126.40, 125.69, 116.81, 113.55, 60.64, 41.95, 29.53, 27.22, 11.38; **FTIR** (ν/cm^{-1}, neat) 3022.7, 2960.2, 2929.3, 2870.9, 1918.8, 1596.3, 1501.8, 1390.2, 1330.9, 1221.1, 1034.6, 936.9, 743,6, 689.4.

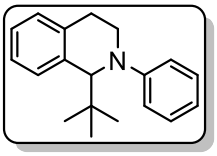

1-(tert-butyl)-2-phenyl-1,2,3,4-tetrahydroisoquinoline 3.51c

Yield 61%, Yellow oil; **HRMS** predicted [$C_{19}H_{23}N$ +H] 266.1909 Observed 266.1874; **^{1}H NMR** (400 MHz, cdcl$_3$) δ 7.24 – 7.06 (m, 6H), 6.93 (d, J = 7.9 Hz, 2H), 6.68 (t, J = 7.1 Hz, 1H), 4.67 (d, J = 5.7 Hz, 1H), 3.88 (dt, J = 12.5, 6.3 Hz, 1H), 3.60 – 3.48 (m, 1H), 3.14 – 2.92 (m, 2H), 1.03 (s, 9H); **^{13}C NMR** (101 MHz, cdcl$_3$) δ 151.13, 137.00, 135.42, 128.96, 128.74, 128.32, 126.56, 125.04, 116.60, 114.13, 65.99, 44.00, 39.16, 29.20, 27.30; **FTIR** (ν/cm^{-1}, neat) 3064.02, 3028.5, 2950.7, 2865.1, 1923.8, 1745.6, 1592.7, 1501.9, 1473.4, 1291.3, 1231.5, 926.0, 743.2, 689.7.

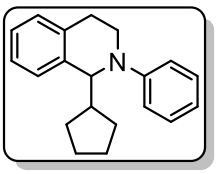

1-cyclopentyl-2-phenyl-1,2,3,4-tetrahydroisoquinoline 3.51d

Yield 48%, Yellow oil; **HRMS** predicted [$C_{20}H_{23}N$ +H] 278.1909 Observed 278.1890; **^{1}H NMR** (400 MHz, cdcl$_3$) δ 7.21 (dd, J = 8.7, 7.3 Hz, 2H), 7.18 – 7.07 (m, 4H), 6.90 (d, J = 8.0 Hz, 2H), 6.69 (t, J = 7.1 Hz, 1H), 4.54 (d, J = 8.8 Hz, 1H), 3.80 – 3.69 (m, 1H), 3.69 – 3.59 (m, 1H), 3.02 (td, J = 15.9, 7.8 Hz, 1H), 2.89 (dt, J = 16.3, 5.4 Hz, 1H), 2.40 – 2.26 (m, 1H), 1.89 – 1.80 (m, 1H), 1.73 – 1.61 (m, 3H), 1.57 – 1.41 (m, 4H); **^{13}C NMR** (101 MHz, cdcl$_3$) δ 149.96, 138.82, 134.83, 129.12, 128.57, 127.61, 127.49, 126.46,

125.33, 116.76, 113.79, 62.74, 47.14, 41.94, 31.07, 30.60, 26.71, 25.14, 24.41; **FTIR** (ν/cm^{-1}, neat) 3022.0, 2950.9, 2866.1, 1595.8, 1501.4, 1450.6, 1205.6, 1153.1, 931.0, 743.4, 688.7.

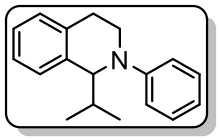

1-isopropyl-2-phenyl-1,2,3,4-tetrahydroisoquinoline 3.51f

Yield 47%, Yellow oil; **HRMS** predicted[$C_{18}H_{21}N$+H] 252.1752 Observed 252.1743; **^{1}H NMR** (400 MHz, cdcl$_3$) δ 7.25 – 7.20 (m, 2H), 7.20 – 7.08 (m, 4H), 6.87 (d, *J* = 8.3 Hz, 2H), 6.69 (t, *J* = 7.2 Hz, 1H), 4.39 (d, *J* = 8.2 Hz, 1H), 3.74 (dt, *J* = 12.1, 6.1 Hz, 1H), 3.47 (dt, *J* = 12.1, 7.0 Hz, 1H), 3.00 (td, *J* = 6.7, 3.5 Hz, 2H), 2.13 (dd, *J* = 14.6, 6.9 Hz, 1H), 1.07 (d, *J* = 6.9 Hz, 3H), 0.95 (d, *J* = 6.7 Hz, 3H); **^{13}C NMR** (101 MHz, cdcl$_3$) δ 149.98, 137.73, 135.32, 129.08, 128.25, 128.17, 126.56, 125.24, 116.41, 113.12, 64.58, 42.98, 34.38, 27.36, 20.63, 20.08; **FTIR** (ν/cm^{-1}, neat) 3059.8, 3023.0, 2956.8, 2868.8, 1595.6, 1501.9, 1322.5, 1219.9, 743.3, 688.8.

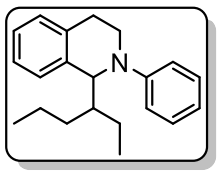

1-(hexan-3-yl)-2-phenyl-1,2,3,4-tetrahydroisoquinoline 3.51g

Yield 71%, Yellow oil; **HRMS** predicted [$C_{22}H_{29}N$ +H] 308.2378 Observed 308.2383; **^{1}H NMR** (400 MHz, cdcl$_3$) δ 7.21 (dd, *J* = 8.9, 7.2 Hz, 2H), 7.17 – 7.09 (m, 4H), 6.87 (d, *J* = 8.5 Hz, 2H), 6.68 (td, *J* = 7.2, 0.8 Hz, 1H), 4.62 (dd, *J* = 8.8, 2.6 Hz, 1H), 3.71 (dt, *J* = 12.6, 6.4 Hz, 1H), 3.57 – 3.47 (m, 1H), 2.98 (t, *J* = 6.5 Hz, 2H), 1.79 (ddd, *J* = 8.7, 6.2, 3.2 Hz, 1H), 1.54 – 1.22 (m, 7H), 0.93 – 0.82 (m, 6H); **^{13}C NMR** (101 MHz, cdcl$_3$) δ 150.26, 138.54, 135.28, 129.06, 129.04, 128.34, 128.32, 127.93, 126.44, 125.24, 116.63, 116.59, 113.66, 113.55, 60.63, 60.58, 45.15, 44.64, 43.08, 29.26, 28.95, 28.50, 26.96,

23.17, 23.02, 22.69, 22.39, 14.12, 11.51, 10.55; **FTIR** (ν/cm^{-1}, neat) 3022.4, 2956.3, 2928.2, 2871.1, 1596.1, 1502.1, 1321.5, 1296.9, 929.9, 743.7, 688.6.

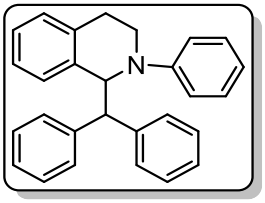

1-benzhydryl-2-phenyl-1,2,3,4-tetrahydroisoquinoline 3.51h

Yield 69%, Yellow oil; **HRMS** predicted [$C_{28}H_{25}N$+H] 376.2065 Observed 376.2191; **^{1}H NMR** (400 MHz, cdcl$_3$) δ 7.40 – 7.33 (m, 2H), 7.27 – 7.05 (m, 12H), 6.92 (d, *J* = 8.0 Hz, 2H), 6.86 – 6.73 (m, 2H), 6.29 (d, *J* = 7.7 Hz, 1H), 5.43 (d, *J* = 9.2 Hz, 1H), 4.49 (d, *J* = 9.3 Hz, 1H), 3.65 – 3.52 (m, 2H), 3.04 – 2.89 (m, 1H), 2.64 (dt, *J* = 16.7, 4.3 Hz, 1H); **^{13}C NMR** (101 MHz, cdcl$_3$) δ 149.96, 142.32, 142.16, 136.65, 134.86, 129.64, 129.15, 128.90, 128.56, 128.31, 128.16, 128.11, 126.67, 126.62, 126.16, 124.60, 118.07, 115.77, 61.81, 58.54, 41.64, 25.73; **FTIR** (ν/cm^{-1}, neat) 3059.2, 3025.8, 2919.0, 1745.5, 1594.6, 1492.7, 1450.1, 1208.9, 1031.4, 942.0, 741.6, 694.0.

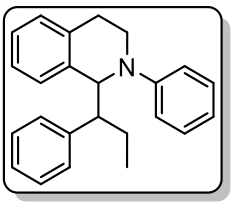

2-phenyl-1-(1-phenylpropyl)-1,2,3,4-tetrahydroisoquinoline 3.51

Yield 63%, Yellow oil; **HRMS** predicted [$C_{24}H_{25}N$ +H] 328.2065 Observed 328.2054; **^{1}H NMR** (400 MHz, cdcl$_3$) δ 7.30 (dd, *J* = 8.9, 7.2 Hz, 3H), 7.24 – 7.07 (m, 14H), 6.97 (ddd, *J* = 20.4, 13.6, 7.5 Hz, 6H), 6.81 (dd, *J* = 7.8, 1.5 Hz, 2H), 6.78 – 6.72 (m, 3H), 6.66 – 6.60 (m, 2H), 4.88 (t, *J* = 6.9 Hz, 2H), 3.59 (dt, *J* = 11.2, 5.5 Hz, 1H), 3.50 (ddd, *J* = 13.6, 7.7, 6.1 Hz, 1H), 3.41 (dd, *J* = 12.7, 6.3 Hz, 1H), 3.29 (ddd, *J* = 11.4, 9.5, 5.4 Hz, 1H), 3.10 (ddd, *J* = 14.9, 7.2, 3.8 Hz, 2H), 3.01 – 2.91 (m, 1H), 2.85 (dd, *J* = 14.2, 8.1

Hz, 1H), 2.65 (dt, *J* = 15.8, 5.2 Hz, 1H), 2.13 – 1.94 (m, 3H), 1.80 (dtdd, *J* = 18.2, 13.4, 9.3, 5.8 Hz, 3H), 0.80 (t, *J* = 7.3 Hz, 3H), 0.71 (t, *J* = 7.3 Hz, 3H); **^{13}C NMR** (101 MHz, $cdcl_3$) δ 149.99, 149.38, 141.89, 141.73, 129.38, 129.26, 128.88, 128.72, 128.55, 128.06, 127.90, 127.82, 127.57, 126.62, 126.46, 126.17, 125.07, 124.95, 116.97, 116.39, 114.16, 112.41, 64.32, 63.94, 53.79, 53.43, 43.21, 42.42, 27.14, 26.63, 25.33, 25.24, 12.54, 12.47; **FTIR** (ν/cm^{-1}, neat) 3060.3, 3025.9, 2959.8, 2929.2, 2872.3, 1595.8, 1501.7, 1452.3, 1321.1, 1155.2, 1036.8, 907.7, 744.0, 698.1.

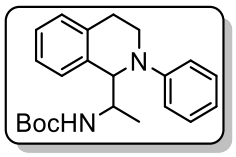

tert-butyl (1-(2-phenyl-1,2,3,4-tetrahydroisoquinolin-1-yl)ethyl)carbamate 3.51j

Yield 17% total, Yellow oil; **HRMS** predicted [$C_{22}H_{28}N_2O_2$+H] 353.2229 Observed 353.2232; **isomer 1 ^{1}H NMR** (400 MHz, $cdcl_3$) δ 7.22 (t, *J* = 4.6 Hz, 2H), 7.20 – 7.07 (m, 4H), 6.95 (d, *J* = 8.3 Hz, 2H), 6.71 (t, *J* = 7.2 Hz, 1H), 4.65 (d, *J* = 7.6 Hz, 1H), 4.48 (d, *J* = 37.0 Hz, 1H), 4.04 (s, 1H), 3.72 (dd, *J* = 9.4, 5.0 Hz, 1H), 3.22 (dd, *J* = 11.8, 8.1 Hz, 2H), 2.92 (dt, *J* = 19.7, 6.6 Hz, 1H), 1.41 – 1.25 (m, 9H), 1.11 (d, *J* = 6.6 Hz, 3H); **Isomer 2 ^{1}H NMR** (400 MHz, $cdcl_3$) δ 7.21 (t, *J* = 7.9 Hz, 3H), 7.15 (dd, *J* = 8.8, 4.6 Hz, 3H), 6.92 (t, *J* = 10.4 Hz, 2H), 6.74 (t, *J* = 7.2 Hz, 1H), 4.79 (s, 1H), 4.61 (d, *J* = 8.5 Hz, 1H), 4.25 (s, 1H), 3.65 (s, 2H), 2.99 (dt, *J* = 14.0, 7.1 Hz, 1H), 2.84 (t, *J* = 17.1 Hz, 1H), 1.46 – 1.28 (m, 8H), 1.19 (d, *J* = 7.0 Hz, 3H).

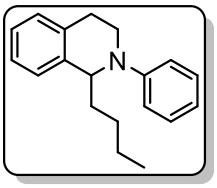

1-butyl-2-phenyl-1,2,3,4-tetrahydroisoquinoline 3.51k

Yield 62%, Yellow oil; **HRMS** predicted [$C_{19}H_{23}N$ +H] 266.1909 Observed 266.1914; **^{1}H NMR** (400 MHz, cdcl$_3$) δ 7.30 – 7.22 (m, 5H), 7.21 – 7.07 (m, 8H), 6.90 (d, *J* = 8.2 Hz, 4H), 6.74 (t, *J* = 7.2 Hz, 2H), 4.67 (t, *J* = 7.1 Hz, 2H), 3.71 – 3.57 (m, 4H), 3.03 (tt, *J* = 16.1, 7.0 Hz, 2H), 2.92 – 2.82 (m, 2H), 2.05 – 1.92 (m, 2H), 1.79 – 1.67 (m, 2H), 1.55 – 1.31 (m, 9H), 0.92 (dd, *J* = 9.1, 5.2 Hz, 6H); **^{13}C NMR** (101 MHz, cdcl$_3$) δ 149.67, 139.21, 134.98, 129.34, 129.24, 128.49, 128.41, 127.33, 126.37, 125.71, 117.79, 116.87, 113.63, 59.22, 41.81, 36.57, 29.10, 27.07, 22.83, 14.14; **FTIR** (ν/cm^{-1}, neat) 3022.6, 2954.4, 29286, 2857.2, 1596.7, 1502.0, 1390.5, 1218.5, 933.7, 743.2, 689.4.

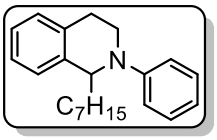

1-heptyl-2-phenyl-1,2,3,4-tetrahydroisoquinoline 3.51l

Yield 51%, Yellow oil; **HRMS** predicted [$C_{22}H_{29}N$+H] 308.2378 Observed 308.2390; **^{1}H NMR** (400 MHz, cdcl$_3$) δ 7.25 (dd, *J* = 8.7, 7.2 Hz, 2H), 7.20 – 7.08 (m, 4H), 6.88 (d, *J* = 8.2 Hz, 2H), 6.72 (t, *J* = 7.1 Hz, 1H), 4.65 (t, *J* = 7.0 Hz, 1H), 3.68 – 3.56 (m, 2H), 3.08 – 2.97 (m, 1H), 2.86 (dt, *J* = 15.8, 5.3 Hz, 1H), 1.96 (dd, *J* = 9.8, 4.2 Hz, 1H), 1.76 – 1.65 (m, 1H), 1.62 – 1.20 (m, 10H), 0.88 (t, *J* = 6.8 Hz, 3H); **^{13}C NMR** (101 MHz, cdcl$_3$) δ 149.66, 139.20, 134.96, 129.22, 128.46, 127.31, 126.34, 125.69, 116.83, 113.59, 59.23, 41.77, 36.81, 31.86, 29.68, 29.30, 27.05, 26.91, 22.67, 14.12; **FTIR** (ν/cm^{-1}, neat) 3023.3, 2924.3, 2853.5, 1596.9, 1502.4, 1390.6, 1219.3, 744.0, 689.9.

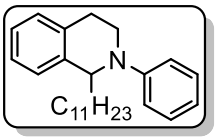

2-phenyl-1-undecyl-1,2,3,4-tetrahydroisoquinoline 3.51m

Yield 57%, Yellow oil; **HRMS** predicted [$C_{26}H_{37}N$+H] 364.3004 Observed 364.3052; **^{1}H NMR** (400 MHz, cdcl$_3$) δ 7.24 (t, *J* = 8.0 Hz, 2H), 7.21 – 7.08 (m, 4H), 6.87 (d, *J* = 8.2 Hz, 2H), 6.72 (t, *J* = 7.2 Hz, 1H), 4.64 (t, *J* = 7.0 Hz, 1H), 3.61 (dt, *J* = 11.1, 5.4 Hz, 2H), 3.07 – 2.98 (m, 1H), 2.85 (dt, *J* = 15.9, 5.4 Hz, 1H), 2.01 – 1.90 (m, 1H), 1.76 – 1.65 (m, 1H), 1.51 – 1.24 (m, 18H), 0.89 (t, *J* = 6.8 Hz, 3H); **^{13}C NMR** (101 MHz, cdcl$_3$) δ 149.66, 139.20, 134.95, 129.21, 128.46, 127.31, 126.33, 125.68, 116.84, 113.60, 59.22, 41.77, 36.80, 31.93, 29.72, 29.63, 29.36, 27.05, 26.90, 22.71, 14.15; **FTIR** (ν/cm^{-1}, neat) 3022.0, 2922.2, 2852.3, 1597.4, 1502.5, 1390.7, 1218.1, 744.1, 689.8.

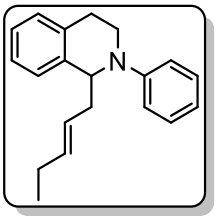

(E)-1-(pent-2-en-1-yl)-2-phenyl-1,2,3,4-tetrahydroisoquinoline 3.51n

Yield 36%, Yellow oil; **HRMS** predicted [$C_{20}H_{23}N$+H] 278.1909 Observed 278.1883; **^{1}H NMR** (400 MHz, cdcl$_3$) δ 7.29 – 7.22 (m, 2H), 7.20 – 7.07 (m, 4H), 6.90 (d, *J* = 8.2 Hz, 2H), 6.74 (t, *J* = 7.2 Hz, 1H), 5.54 – 5.39 (m, 2H), 4.70 (t, *J* = 6.8 Hz, 1H), 3.71 – 3.53 (m, 2H), 3.03 (ddd, *J* = 15.6, 7.7, 5.4 Hz, 1H), 2.90 (dt, *J* = 15.8, 5.5 Hz, 1H), 2.74 – 2.62 (m, 1H), 2.47 – 2.33 (m, 1H), 2.06 – 1.95 (m, 2H), 0.95 (t, *J* = 7.5 Hz, 3H); **^{13}C NMR** (101 MHz, cdcl$_3$) δ 149.47, 138.34, 134.98, 134.76, 129.19, 128.36, 127.46, 126.44, 125.80, 125.59, 116.92, 113.62, 59.88, 41.94, 39.61, 27.60, 25.65, 13.73; **FTIR** (ν/cm^{-1}, neat) 3062.8, 3024.0, 2960.0, 2925.0, 2846.0, 1596.9, 1502.5, 1390.8, 1328.7, 1220.4, 968.9, 744.0, 690.0.

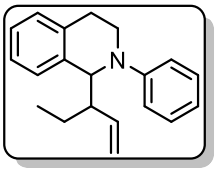

1-(pent-1-en-3-yl)-2-phenyl-1,2,3,4-tetrahydroisoquinoline 3.52

Yield 19%, Yellow oil; **HRMS** predicted [$C_{20}H_{23}N$+H] 278.1909 Observed 278.1864; **^{1}H NMR** (400 MHz, cdcl$_3$) δ (E/Z isomer 1:1 ratio)7.16 (dddd, *J* = 18.9, 12.0, 7.5, 3.1 Hz, 6H), 6.85 (d, *J* = 8.0 Hz, 2H), 6.70 (dd, *J* = 16.5, 7.3 Hz, 1H), 5.73 – 5.60 (m, 0.5H), 5.47 – 5.40 (m, 0.5H), 5.06 – 4.96 (m, 1.5H), 4.85 (dd, *J* = 17.1, 1.7 Hz, 0.5H), 4.61 (dd, *J* = 18.6, 6.8 Hz, 1H), 3.78 – 3.67 (m, 1H), 3.50 – 3.38 (m, 2H), 3.08 – 2.92 (m, 2H), 2.47 – 2.34 (m, 1H), 1.81 (ddd, *J* = 13.4, 7.5, 3.2 Hz, 0.5H), 1.67 (ddd, *J* = 13.2, 7.4, 3.6 Hz, 0.5H), 1.40 – 1.27 (m, 1H), 0.84 (dt, *J* = 20.5, 7.4 Hz, 3H).

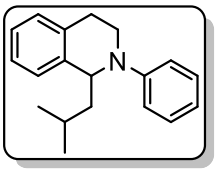

1-isobutyl-2-phenyl-1,2,3,4-tetrahydroisoquinoline 3.51o

Yield 48%, Yellow oil; **HRMS** predicted [$C_{19}H_{23}N$ +H] 266.1909 Observed 266.1865; **^{1}H NMR** (400 MHz, cdcl$_3$) δ 7.22 (dd, *J* = 8.4, 7.2 Hz, 2H), 7.19 – 7.05 (m, 4H), 6.90 (d, *J* = 8.3 Hz, 2H), 6.72 (t, *J* = 7.2 Hz, 1H), 4.76 (t, *J* = 7.3 Hz, 1H), 3.69 – 3.57 (m, 2H), 3.06 – 2.95 (m, 1H), 2.78 (dt, *J* = 16.1, 4.9 Hz, 1H), 1.97 – 1.86 (m, 1H), 1.73 (td, *J* = 13.3, 6.6 Hz, 1H), 1.52 (dt, *J* = 13.8, 6.8 Hz, 1H), 1.05 (d, *J* = 6.6 Hz, 3H), 0.95 (d, *J* = 6.5 Hz, 3H); **^{13}C NMR** (101 MHz, cdcl$_3$) δ 149.77, 139.39, 134.86, 129.22, 128.66, 127.19, 126.28, 125.67, 117.15, 114.13, 56.77, 45.85, 41.54, 26.45, 25.08, 22.93, 22.82; **FTIR** (ν/cm^{-1}, neat) 3063.4, 3022.3, 2953.0, 2924.9, 2866.9, 1596.0, 1502.0, 1390.5, 1215.7, 1030.3, 937.5, 743.5, 689.2.

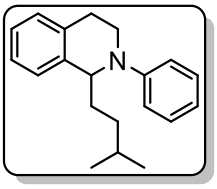

1-isopentyl-2-phenyl-1,2,3,4-tetrahydroisoquinoline 3.51p

Yield 53%, Yellow oil; **HRMS** predicted [$C_{20}H_{25}N$ +H] 280.2065 Observed 280.2075; **^{1}H NMR** (400 MHz, cdcl$_3$) δ 7.28 – 7.20 (m, 3H), 7.19 – 7.09 (m, 4H), 6.88 (d, *J* = 8.1 Hz, 2H), 6.72 (t, *J* = 7.2 Hz, 1H), 4.62 (t, *J* = 7.1 Hz, 1H), 3.67 – 3.57 (m, 2H), 3.08 – 2.98 (m, 1H), 2.84 (dt, *J* = 16.0, 5.3 Hz, 1H), 2.04 – 1.90 (m, 1H), 1.77 – 1.65 (m, 1H), 1.55 (dt, *J* = 13.2, 6.6 Hz, 1H), 1.46 – 1.23 (m, 2H), 0.88 (dd, *J* = 8.8, 6.6 Hz, 6H); **^{13}C NMR** (101 MHz, cdcl$_3$) δ 149.69, 139.27, 134.93, 129.23, 128.51, 127.31, 126.34, 125.70, 120.96, 117.78, 116.87, 113.66, 59.48, 41.66, 36.00, 34.69, 28.17, 26.93, 22.75, 22.58; **FTIR** (ν/cm^{-1}, neat) 3022.3, 2952.4, 2868.3, 1596.2, 1502.1, 1390.6, 1329.7, 1218.4, 1152.8, 743.94, 689.6.

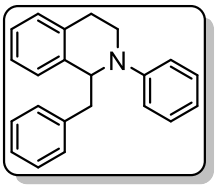

1-benzyl-2-phenyl-1,2,3,4-tetrahydroisoquinoline 3.51q

Yield 72%, Yellow oil; **HRMS** predicted [$C_{22}H_{21}N$+H] 300.1708 Observed 300.1708; **^{1}H NMR** (400 MHz, cdcl$_3$) δ 7.29 – 7.21 (m, 6H), 7.17 (t, *J* = 4.6 Hz, 2H), 7.09 – 7.01 (m, 3H), 6.87 (d, *J* = 8.2 Hz, 2H), 6.77 (d, *J* = 7.5 Hz, 2H), 4.93 (t, *J* = 6.6 Hz, 1H), 3.67 (ddd, *J* = 12.5, 7.6, 5.0 Hz, 1H), 3.61 – 3.53 (m, 1H), 3.28 (dd, *J* = 13.3, 5.8 Hz, 1H), 3.01 (ddd, *J* = 10.7, 9.6, 6.4 Hz, 2H), 2.84 – 2.71 (m, 1H); **^{13}C NMR** (101 MHz, cdcl$_3$) δ 149.42, 138.96, 137.72, 135.19, 129.90, 129.34, 128.35, 128.26, 127.76, 126.71, 126.37, 125.62, 117.28, 113.71, 61.61, 42.53, 42.22, 27.59; **FTIR** (ν/cm^{-1}, neat) 3060.2, 3025.1, 2919.8, 1835.5, 1596.2, 1501.7, 1494.1, 1390.5, 1327.7, 1219.8, 987.1, 745.3, 690.0.

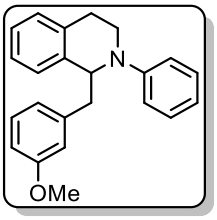

1-(3-methoxybenzyl)-2-phenyl-1,2,3,4-tetrahydroisoquinoline 3.51r

Yield 72%, Yellow oil; **HRMS** predicted [$C_{23}H_{23}NO+H$] 330.1858 Observed 330.1866; **^{1}H NMR** (400 MHz, cdcl$_3$) δ 7.28 – 7.24 (m, 2H), 7.17 – 7.13 (m, 3H), 7.09 – 7.04 (m, 1H), 6.88 (d, *J* = 8.1 Hz, 2H), 6.80 – 6.73 (m, 3H), 6.66 (d, *J* = 7.4 Hz, 1H), 6.55 – 6.52 (m, 1H), 4.92 (dd, *J* = 15.5, 8.9 Hz, 1H), 3.69 (d, *J* = 3.8 Hz, 3H), 3.63 (ddd, *J* = 7.6, 3.2, 2.1 Hz, 1H), 3.60 – 3.51 (m, 1H), 3.25 (dd, *J* = 13.3, 5.7 Hz, 1H), 3.00 (dt, *J* = 13.4, 6.0 Hz, 2H), 2.83 – 2.73 (m, 1H); **^{13}C NMR** (101 MHz, cdcl$_3$) δ 159.34, 149.28, 140.38, 137.59, 135.08, 129.24, 129.07, 128.23, 127.69, 126.61, 125.51, 122.21, 117.23, 115.29, 113.71, 111.90, 61.26, 55.10, 42.43, 42.16, 27.56; **FTIR** (ν/cm^{-1}, neat) 3059.8, 3023.7, 2919.3, 2833.6, 1595.8, 1502.4, 1489.5, 1260.0, 1151.0, 1039.1, 744.6, 690.7.

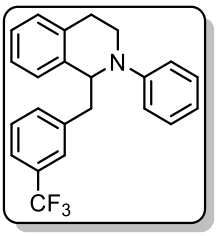

2-phenyl-1-(3-(trifluoromethyl)benzyl)-1,2,3,4-tetrahydroisoquinoline 3.51s

Yield 62%, Yellow oil; **HRMS** predicted [$C_{23}H_{20}F_3NO+H$] 368.1626 Observed 368.1665; **^{1}H NMR** (400 MHz, cdcl$_3$) δ 7.47 (d, *J* = 7.7 Hz, 1H), 7.36 – 7.13 (m, 8H), 7.10 (t, *J* = 7.3 Hz, 1H), 6.87 (d, *J* = 8.2 Hz, 2H), 6.79 (d, *J* = 7.3 Hz, 2H), 4.94 (s, 1H), 3.65 (td, *J* = 7.4, 3.8 Hz, 1H), 3.55 (dt, *J* = 12.1, 5.9 Hz, 1H), 3.30 (dd, *J* = 13.4, 6.1 Hz, 1H), 3.11 (dd, *J* = 13.4, 6.9 Hz, 1H), 3.05 – 2.94 (m, 1H), 2.70 (dt, *J* = 15.9, 5.7 Hz, 1H);

^{13}C NMR (101 MHz, cdcl$_3$) δ 149.24, 139.68, 136.96, 135.12, 133.19, (130.76, 130.44, 130.12, 129.80 CF_3 group), 129.30, 128.48, 128.43, 127.48, 126.87, 126.62, 126.58, 125.72, 123.12, 123.09, 117.67, 113.99, 61.09, 42.31, 42.18, 27.42; **^{19}F NMR** (376 MHz, cdcl$_3$) δ -62.55; **FTIR** (ν/cm^{-1}, neat) 3065.0, 3024.1, 2927.2, 2856.7, 1738.0, 1597.5, 1503.1, 1449.7, 1391.5, 1326.4 1159.9, 1120.5, 1072.9, 747.5, 701.8, 691.6.

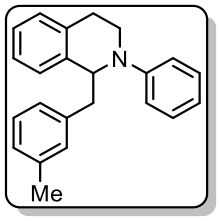

1-(3-methylbenzyl)-2-phenyl-1,2,3,4-tetrahydroisoquinoline 3.51t

Yield 59%, Yellow oil; **HRMS** predicted [$C_{23}H_{23}N$+H] 314.1909 Observed 314.1938; **^{1}H NMR** (400 MHz, cdcl$_3$) δ 7.27 (d, *J* = 7.5 Hz, 2H), 7.17 (d, *J* = 14.2 Hz, 3H), 7.04 (d, *J* = 23.0 Hz, 2H), 6.88 (d, *J* = 8.2 Hz, 2H), 6.84 (s, 2H), 6.75 (s, 2H), 4.91 (s, 1H), 3.67 (t, *J* = 12.4 Hz, 1H), 3.56 (t, *J* = 12.1 Hz, 1H), 3.24 (dd, *J* = 13.3, 5.7 Hz, 1H), 2.99 (t, *J* = 22.4 Hz, 2H), 2.79 (dd, *J* = 21.7, 5.8 Hz, 1H), 2.29 (s, 3H); **^{13}C NMR** (101 MHz, cdcl$_3$) δ 149.34, 138.73, 137.67, 137.60, 135.05, 130.59, 129.21, 128.18, 128.01, 127.74, 126.94, 126.79, 126.57, 125.41, 117.13, 113.63, 61.48, 42.37, 42.14, 27.52, 21.40; **FTIR** (ν/cm^{-1}, neat) 3060.1, 3022.9, 2917.2, 2852.4, 17380, 1596.8, 1502.0, 1390.2, 1328.8, 1221.8, 908.5, 744.2, 690.3.

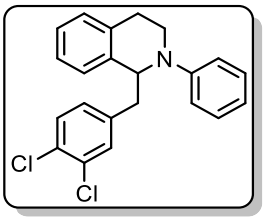

1-(3,4-dichlorobenzyl)-2-phenyl-1,2,3,4-tetrahydroisoquinoline 3.51u

Yield 67%, Yellow oil; **HRMS** predicted [$C_{22}H_{19}NCl_2$+H] 368.0973 Observed 369.0957; **^{1}H NMR** (400 MHz, cdcl$_3$) δ 7.25 (dd, *J* = 3.9, 2.6 Hz, 2H), 7.21 – 7.06 (m, 5H), 6.88 – 6.73 (m, 5H), 4.88 (t, *J* = 6.5 Hz, 1H), 3.69 – 3.48 (m, 2H), 3.18 (dd, *J* = 13.5, 6.1 Hz, 1H), 2.97 (ddd, *J* = 9.8, 6.3, 2.2 Hz, 2H), 2.71 (dt, *J* = 16.0, 5.7 Hz, 1H); **^{13}C NMR** (101 MHz, cdcl$_3$) δ 149.20, 139.07, 136.87, 135.06, 131.60, 129.96, 129.33, 129.21, 128.47, 127.46, 126.90, 125.75, 117.77, 114.07, 60.98, 42.24, 41.48, 27.37; **FTIR** (ν/cm^{-1}, neat) 3023.0, 2924.2, 2835.2, 1919.0, 1595.5, 1501.7, 1470.7, 1393.5, 1322.2, 1210.0, 1130.0, 1029.3, 744.1, 689.4.

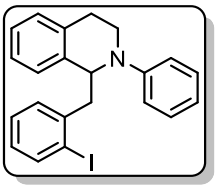

1-(2-iodobenzyl)-2-phenyl-1,2,3,4-tetrahydroisoquinoline 3.51v

Yield 53%, Yellow oil; **HRMS** predicted [$C_{22}H_{20}NI$+H] 426.0719 Observed 426.0802; **^{1}H NMR** (400 MHz, cdcl$_3$) δ 7.83 (dd, *J* = 7.9, 1.0 Hz, 1H), 7.20 – 7.06 (m, 8H), 6.87 (td, *J* = 7.7, 1.7 Hz, 1H), 6.75 – 6.63 (m, 3H), 5.07 (dd, *J* = 8.7, 5.8 Hz, 1H), 3.85 – 3.71 (m, 2H), 3.38 (dd, *J* = 13.6, 8.9 Hz, 1H), 3.26 (dd, *J* = 13.7, 5.7 Hz, 1H), 3.13 (ddd, *J* = 15.5, 9.0, 6.1 Hz, 1H), 2.86 (dt, *J* = 16.1, 4.4 Hz, 1H); **^{13}C NMR** (101 MHz, cdcl$_3$) δ 149.53, 141.64, 139.22, 137.65, 135.07, 131.49, 129.06, 128.65, 128.19, 128.14, 127.42, 126.67, 125.74, 117.32, 113.95, 101.27, 59.86, 46.24, 41.19, 26.72; **FTIR** (ν/cm^{-1}, neat)

3057.7, 3020.1, 2917.1, 2849.5, 1918.7, 1728.7, 1595.9, 1500.8, 1464.9, 1391.6, 1323.2, 1220.6, 1145.2, 1009.5, 740.4, 689.2.

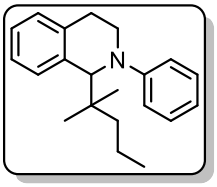

1-(2-methylpentan-2-yl)-2-phenyl-1,2,3,4-tetrahydroisoquinoline 3.51w

Yield 63%, Yellow oil; **HRMS** predicted [$C_{21}H_{27}N$+H] 294.2222 Observed 294.2198; **^{1}H NMR** (400 MHz, cdcl$_3$) δ 7.22 – 7.01 (m, 6H), 6.90 (d, *J* = 8.2 Hz, 2H), 6.66 (t, *J* = 7.3 Hz, 1H), 4.69 (s, 1H), 3.86 (dt, *J* = 13.5, 6.9 Hz, 1H), 3.59 (dt, *J* = 13.1, 6.7 Hz, 1H), 2.98 (t, *J* = 7.0 Hz, 2H), 1.44 – 1.27 (m, 4H), 0.95 (s, 3H), 0.92 (s, 3H), 0.86 (t, *J* = 6.8 Hz, 3H); **^{13}C NMR** (101 MHz, cdcl$_3$) δ 151.42, 137.00, 135.50, 128.90, 128.59, 128.48, 126.42, 124.95, 116.83, 114.66, 114.30, 69.75, 65.00, 47.12, 43.96, 43.61, 41.57, 28.86, 27.27, 26.90, 26.62, 25.43, 17.52, 15.05; **FTIR** (ν/cm^{-1}, neat) 3022.7, 2957.1, 2931.2, 2870.5, 1595.5, 1502.1, 1316.1, 1291.3, 1206.6, 1152.9, 943.1, 743.6, 689.2.

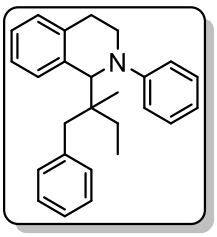

1-(2-methyl-1-phenylbutan-2-yl)-2-phenyl-1,2,3,4-tetrahydroisoquinoline 3.51y

Yield 73%, Yellow oil; **HRMS** predicted [$C_{26}H_{29}N$+H] 356.2378 observed 356.2383; **^{1}H NMR** (400 MHz, cdcl$_3$) δ 7.32 – 7.10 (m, 22H), 6.85 (dd, *J* = 8.5, 2.1 Hz, 4H), 6.73 – 6.66 (m, 2H), 4.97 (s, 1H), 4.92 (s, 1H), 3.93 (ddd, *J* = 15.8, 12.1, 7.4 Hz, 2H), 3.83 – 3.70 (m, 2H), 3.13 – 2.86 (m, 7H), 2.77 (dd, *J* = 13.2, 6.4 Hz, 1H), 2.56 (d, *J* = 13.1 Hz,

1H), 1.53 (qt, *J* = 13.1, 6.7 Hz, 2H), 1.45 – 1.36 (m, 2H), 1.33 (t, *J* = 7.3 Hz, 1H), 1.11 (t, *J* = 7.4 Hz, 3H), 1.01 (q, *J* = 7.8 Hz, 3H), 0.93 (s, 3H), 0.85 (s, 3H); **^{13}C NMR** (101 MHz, cdcl$_3$) δ 151.65, 151.61, 139.38, 138.84, 136.99, 136.92, 135.70, 135.66, 131.15, 131.03, 129.12, 129.06, 128.98, 128.91, 128.27, 128.02, 127.74, 127.72, 126.52, 126.45, 125.90, 125.84, 125.22, 125.19, 117.37, 117.34, 115.23, 115.17, 61.93, 61.59, 45.63, 44.87, 44.49, 44.27, 44.12, 43.60, 42.16, 30.18, 29.11, 26.60, 26.37, 23.86, 22.72, 9.09, 9.07; **FTIR** (ν/cm^{-1}, neat) 3060.5, 3025.8, 2965.0, 2978.8, 1741.4, 1595.8 1502.0, 1493.2, 1217.2, 745.8, 700.1, 691.1.

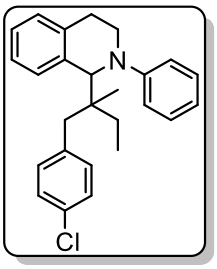

1-(1-(4-chlorophenyl)-2-methylbutan-2-yl)-2-phenyl-1,2,3,4-tetrahydroisoquinoline 3.51

Yield 76%, Yellow oil; **HRMS** predicted [$C_{26}H_{28}NCl$+H] 390.1989 observed 390.1993; **^{1}H NMR** (400 MHz, cdcl$_3$) δ 7.23 – 7.11 (m, 15H), 7.08 (d, *J* = 8.3 Hz, 2H), 7.01 (d, *J* = 8.3 Hz, 2H), 6.87 (dd, *J* = 8.2, 3.6 Hz, 4H), 6.76 – 6.67 (m, 2H), 4.92 (s, 1H), 4.85 (s, 1H), 3.99 – 3.84 (m, 2H), 3.80 – 3.70 (m, 2H), 3.10 – 2.98 (m, 2H), 2.96 – 2.84 (m, 4H), 2.71 (d, *J* = 13.5 Hz, 1H), 2.49 (d, *J* = 13.1 Hz, 1H), 1.54 – 1.34 (m, 4H), 1.20 (t, *J* = 7.1 Hz, 1H), 1.09 (t, *J* = 7.4 Hz, 3H), 0.97 (t, *J* = 7.4 Hz, 3H), 0.91 (s, 3H), 0.80 (s, 3H); **^{13}C NMR** (101 MHz, cdcl$_3$) δ 151.84, 151.74, 137.98, 137.42, 136.77, 136.74, 135.83, 135.78, 132.48, 132.33, 131.87, 131.79, 129.26, 129.19, 129.10, 129.07, 128.40, 128.13, 127.91, 127.87, 126.71, 126.66, 125.35, 117.81, 117.77, 115.76, 115.52, 62.13, 61.73, 46.08, 44.98, 44.60, 44.49, 43.98, 43.66, 41.44, 30.10, 29.37, 26.62, 26.45, 23.99, 22.77,

9.16, 9.14; **FTIR** (ν/cm^{-1}, neat) 3061.5, 3027.4, 2965.3, 2984.3, 2879.5. 1595.4, 1490.2, 1216.5, 1092.4, 1015.1, 944/5, 746.6, 690.8, 665.9.

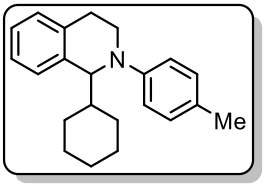

1-cyclohexyl-2-(p-tolyl)-1,2,3,4-tetrahydroisoquinoline 3.56a

Yield 61%, Yellow oil; **HRMS** predicted [$C_{22}H_{27}N$+H] 306.2222 Observed 306.2237; **^{1}H NMR** (400 MHz, cdcl$_3$) δ 7.21 – 7.07 (m, 8H), 7.04 (d, *J* = 8.4 Hz, 4H), 6.80 (d, *J* = 8.6 Hz, 4H), 4.38 (d, *J* = 8.1 Hz, 2H), 3.73 (dt, *J* = 12.3, 6.2 Hz, 2H), 3.53 – 3.42 (m, 2H), 2.99 (t, *J* = 6.5 Hz, 4H), 2.25 (s, 6H), 2.01 (d, *J* = 12.0 Hz, 2H), 1.81 – 1.63 (m, 11H), 1.23 – 1.02 (m, 11H); **^{13}C NMR** (101 MHz, cdcl$_3$) δ 148.08, 137.96, 135.45, 129.73, 128.51, 128.34, 126.56, 125.61, 125.17, 113.41, 64.01, 44.19, 43.14, 34.63, 31.04, 30.80, 27.31, 26.79, 26.56, 20.31; **FTIR** (ν/cm^{-1}, neat) 3021, 2922.7, 2848.7, 1617.5, 1515.9, 1445.4, 1387.5, 1315.4, 1199.7, 1149.5, 789.7, 750.5.

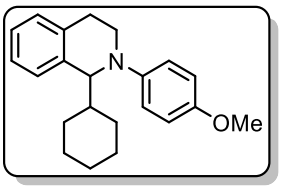

1-cyclohexyl-2-(4-methoxyphenyl)-1,2,3,4-tetrahydroisoquinoline 3.56b

Yield 51%, Yellow-orange oil; **HRMS** predicted [$C_{22}H_{27}NO$+H] 322.2171 Observed 322.2179; **^{1}H NMR** (400 MHz, cdcl$_3$) δ 7.19 – 7.05 (m, 4H), 6.86 – 6.75 (m, 4H), 4.25 (d, *J* = 8.0 Hz, 1H), 3.73 (s, 3H), 3.69 (dd, *J* = 12.6, 6.5 Hz, 1H), 3.44 (dt, *J* = 12.6, 6.4 Hz, 1H), 3.03 – 2.83 (m, 2H), 2.01 (d, *J* = 12.2 Hz, 1H), 1.77 – 1.60 (m, 5H), 1.20 – 1.01 (m, 5H); **^{13}C NMR** (101 MHz, cdcl$_3$) δ 151.60, 145.10, 137.88, 135.42, 128.60, 128.50, 126.49, 125.13, 115.45, 114.72, 64.63, 55.87, 44.10, 43.56, 34.62, 31.09, 30.85, 26.98,

26.81, 26.58; **FTIR** (ν/cm^{-1}, neat) 2922.2, 2849.1, 1610.7, 1507.4, 1448.8, 1241.7, 1038.3, 811.1, 750.63.

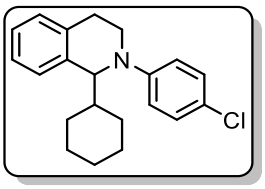

2-(4-chlorophenyl)-1-cyclohexyl-1,2,3,4-tetrahydroisoquinoline

3.56c

Yield 20%, Yellow-orange oil; **HRMS** predicted [$C_{21}H_{24}NCl$+H] 326.1676 observed 326.1675; **^{1}H NMR** (400 MHz, cdcl$_3$) δ 7.13 (ddt, *J* = 8.7, 5.9, 4.2 Hz, 5H), 7.07 – 7.03 (m, 1H), 6.77 – 6.71 (m, 2H), 4.33 (d, *J* = 8.3 Hz, 1H), 3.68 (dt, *J* = 11.9, 6.0 Hz, 1H), 3.39 (ddd, *J* = 11.9, 8.0, 6.4 Hz, 1H), 3.09 – 2.91 (m, 2H), 1.91 (d, *J* = 11.8 Hz, 1H), 1.76 – 1.59 (m, 5H), 1.17 – 0.98 (m, 5H); **^{13}C NMR** (101 MHz, cdcl$_3$) δ 148.49, 137.51, 134.96, 128.77, 128.25, 128.16, 126.71, 125.27, 120.84, 113.95, 63.85, 44.03, 43.15, 30.89, 30.63, 27.22, 26.56, 26.32, 26.30; **FTIR** (ν/cm^{-1}, neat) 2923.0, 2850.6, 1594.6, 1493.6, 1325.7, 1214.9, 908.1, 803.9, 750.3, 699.1.

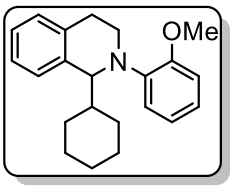

1-cyclohexyl-2-(2-methoxyphenyl)-1,2,3,4-tetrahydroisoquinoline

3.56d

Yield 53%, Yellow oil; **HRMS** predicted [$C_{22}H_{27}NO$+H] 322.2171 Observed 322.2217; **^{1}H NMR** (400 MHz, cdcl$_3$) δ 7.16 – 7.00 (m, 4H), 6.90 – 6.80 (m, 2H), 6.79 – 6.69 (m, 2H), 4.07 (d, *J* = 8.1 Hz, 1H), 3.84 (s, 3H), 3.63 (dd, *J* = 8.7, 4.4 Hz, 2H), 2.82 (dt, *J* = 17.0, 8.6 Hz, 1H), 2.68 (dt, *J* = 16.8, 4.3 Hz, 1H), 2.11 (d, *J* = 13.0 Hz, 1H), 1.90 – 1.62 (m, 5H), 1.19 – 0.97 (m, 5H); **^{13}C NMR** (101 MHz, cdcl$_3$) δ 152.68, 141.78, 138.29,

135.19, 128.93, 128.50, 125.99, 124.70, 121.66, 121.23, 120.95, 112.21, 64.98, 55.72, 43.16, 42.77, 31.22, 31.05, 26.69, 26.57, 26.43; **FTIR** (ν/cm^{-1}, neat) 3058.1, 2996.1, 2918.8, 2848.5, 1682.5, 1590.0, 1498.1, 1449.2, 1239.1, 1026.8, 742.2, 664.0.

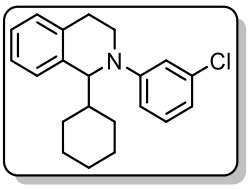

2-(3-chlorophenyl)-1-cyclohexyl-1,2,3,4-tetrahydroisoquinoline 3.56e

Yield 7%, Yellow oil; **HRMS** predicted [$C_{21}H_{24}NCl$+H] 326.1676 observed 326.1705; **^{1}H NMR** (400 MHz, cdcl$_3$) δ 7.20 – 7.03 (m, 5H), 6.77 (t, *J* = 2.2 Hz, 1H), 6.69 (dd, *J* = 8.5, 2.5 Hz, 1H), 6.61 (dd, *J* = 7.7, 1.3 Hz, 1H), 4.36 (d, *J* = 8.4 Hz, 1H), 3.68 (dt, *J* = 11.8, 5.9 Hz, 1H), 3.40 (ddd, *J* = 11.9, 8.4, 6.3 Hz, 1H), 3.10 – 2.94 (m, 2H), 1.90 (d, *J* = 11.4 Hz, 1H), 1.69 (dd, *J* = 30.4, 18.3 Hz, 5H), 1.08 (dt, *J* = 10.6, 5.8 Hz, 5H); **^{13}C NMR** (101 MHz, cdcl$_3$) δ 150.89, 137.46, 134.96, 134.90, 129.89, 128.23, 128.13, 126.77, 125.32, 115.90, 112.50, 110.78, 63.70, 44.00, 43.09, 30.85, 30.64, 27.29, 26.55, 26.31, 26.26.

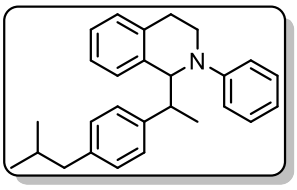

1-(1-(4-isobutylphenyl)ethyl)-2-phenyl-1,2,3,4-tetrahydroisoquinoline 3.58a

Yield 77%, Yellow oil; **HRMS** predicted [$C_{27}H_{31}N$+H] 370.2535 Observed 370.2508; **^{1}H NMR** (400 MHz, cdcl$_3$) δ 7.30 (dd, *J* = 8.8, 7.2 Hz, 2H), 7.18 – 7.11 (m, 5H), 7.10 – 7.04 (m, 4H), 7.00 (dd, *J* = 8.3, 2.3 Hz, 3H), 6.97 – 6.85 (m, 6H), 6.83 – 6.71 (m, 5H), 6.68 – 6.59 (m, 2H), 4.85 (d, *J* = 6.8 Hz, 1H), 4.77 (d, *J* = 6.7 Hz, 1H), 3.61 (dq, *J* = 12.0,

5.9 Hz, 2H), 3.48 – 3.32 (m, 4H), 2.98 (t, *J* = 6.4 Hz, 2H), 2.64 (dd, *J* = 13.4, 7.9 Hz, 1H), 2.44 (dd, *J* = 10.1, 7.2 Hz, 4H), 2.08 – 1.96 (m, 1H), 1.82 (dt, *J* = 20.2, 6.7 Hz, 2H), 1.45 (d, *J* = 7.3 Hz, 3H), 1.30 (t, *J* = 6.7 Hz, 3H), 0.91 (d, *J* = 6.6 Hz, 6H), 0.87 (d, *J* = 6.6 Hz, 6H); **^{13}C NMR** (101 MHz, cdcl$_3$) δ 149.96, 149.59, 141.32, 140.82, 140.03, 139.66, 136.86, 136.11, 135.98, 135.64, 129.38, 129.00, 128.82, 128.79, 128.69, 128.62, 128.51, 128.32, 127.80, 127.77, 126.76, 126.72, 125.22, 124.91, 116.93, 116.60, 113.80, 112.77, 65.23, 65.18, 45.14, 44.44, 43.13, 30.39, 30.35, 27.42, 27.13, 22.58, 22.50, 22.42, 18.60, 18.22; **FTIR** (ν/cm^{-1}, neat) 3060.4, 3022.5, 2954.5, 2923.7, 2867.8, 1596.4, 1502.4, 1322.5, 1217.3, 908.6, 744.3, 689.1.

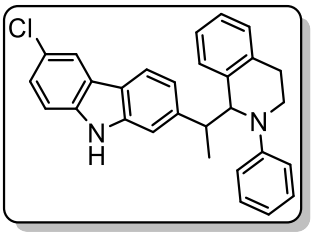

6-chloro-2-(1-(2-phenyl-1,2,3,4-tetrahydroisoquinolin-1-yl)ethyl)-9H-carbazole 3.58b

Yield 76%, Orange-red oil; **HRMS** predicted [$C_{29}H_{25}N_2Cl$+H] 437.1785 Observed 437.1775; **^{1}H NMR** (400 MHz, cdcl$_3$) δ 7.88 (ddd, *J* = 16.7, 14.0, 3.7 Hz, 5H), 7.37 – 7.06 (m, 16H), 7.01 – 6.88 (m, 7H), 6.79 (d, *J* = 11.4 Hz, 2H), 6.68 (t, *J* = 7.3 Hz, 2H), 4.99 (d, *J* = 6.5 Hz, 1H), 4.88 (t, *J* = 12.8 Hz, 1H), 3.72 – 3.48 (m, 4H), 3.42 (dt, *J* = 12.4, 6.0 Hz, 1H), 3.36 – 3.26 (m, 1H), 3.01 – 2.82 (m, 2H), 2.58 (dt, *J* = 15.7, 5.2 Hz, 1H), 1.96 – 1.80 (m, 1H), 1.52 (d, *J* = 7.2 Hz, 3H), 1.41 (d, *J* = 7.0 Hz, 3H); **^{13}C NMR** (101 MHz, cdcl$_3$) δ 150.02, 149.42, 143.20, 142.49, 140.20, 139.99, 137.87, 137.85, 136.59, 136.07, 135.75, 135.51, 129.39, 129.08, 128.76, 128.53, 128.38, 127.71, 126.75, 126.73, 125.45, 125.29, 125.15, 124.97, 124.69, 124.59, 124.43, 121.04, 120.85, 120.09, 119.96,

119.85, 119.73, 117.31, 116.63, 114.27, 112.66, 111.51, 111.44, 111.01, 110.02, 65.12, 64.96, 45.84, 45.73, 43.13, 42.72, 27.17, 26.86, 19.07, 19.00; **FTIR** (ν/cm^{-1}, neat) 3402.7, 3022.2, 2963.9. 1711.2, 1595.0, 1501.9, 1470.7, 1451.0, 1270.7, 1215.7, 1065.9, 930.2, 745.2, 690.6.

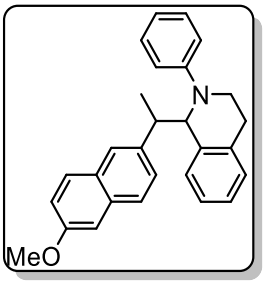

1-(1-(6-methoxynaphthalen-2-yl)ethyl)-2-phenyl-1,2,3,4-tetrahydroisoquinoline 3.58c

Yield 67%, Yellow oil; **HRMS** predicted [$C_{28}H_{27}NO$+H] 394.2171 Observed 394.2215; **^{1}H NMR** (400 MHz, cdcl$_3$) δ 7.65 – 7.49 (m, 5H), 7.31 (ddd, *J* = 10.0, 8.6, 4.4 Hz, 3H), 7.23 – 7.05 (m, 11H), 6.95 (dd, *J* = 16.7, 8.1 Hz, 6H), 6.87 (d, *J* = 8.2 Hz, 2H), 6.78 (t, *J* = 7.2 Hz, 1H), 6.66 (dd, *J* = 14.3, 7.2 Hz, 2H), 4.97 (d, *J* = 6.6 Hz, 1H), 4.88 (d, *J* = 6.6 Hz, 1H), 3.91 (d, *J* = 3.9 Hz, 6H), 3.66 – 3.48 (m, 4H), 3.45 – 3.29 (m, 2H), 3.03 – 2.82 (m, 2H), 2.60 (dt, *J* = 15.8, 5.4 Hz, 1H), 1.96 (ddd, *J* = 15.4, 8.9, 5.9 Hz, 1H), 1.53 (d, *J* = 7.3 Hz, 3H), 1.42 (d, *J* = 7.1 Hz, 3H); **^{13}C NMR** (101 MHz, cdcl$_3$) δ 157.39, 157.31, 150.13, 149.61, 139.55, 138.85, 136.73, 136.01, 135.94, 135.63, 133.51, 133.35, 129.42, 129.30, 129.26, 129.09, 128.94, 128.82, 128.59, 128.45, 127.84, 127.76, 127.37, 127.21, 126.79, 126.77, 126.44, 126.28, 126.21, 125.22, 125.06, 118.68, 118.61, 117.28, 116.70, 114.35, 112.82, 105.62, 105.55, 65.06, 64.85, 55.37, 45.60, 44.99, 43.12, 42.82, 27.31, 27.02, 18.97, 18.79; **FTIR** (ν/cm^{-1}, neat) 3057.8, 3029.8, 2959.8, 2933.1, 2837.8, 1632.5, 1596.28, 1502.2, 1391.2, 1263.8, 1213.8, 1159.4, 1031.1, 851.0, 744.8, 689.9.

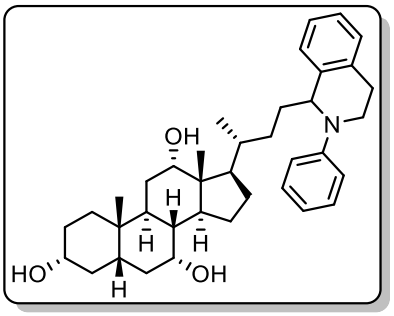

(3R,5S,7R,8R,9S,10S,12S,13R,14S,17R)-10,13-dimethyl-17-((2R)-4-(2-phenyl-1,2,3,4-tetrahydroisoquinolin-1-yl)butan-2-yl)hexadecahydro-1H-cyclopenta[a]phenanthrene-3,7,12-triol 3.58d

Yield 44%, Foaming tan solid; **HRMS** predicted [$C_{38}H_{53}NO_3$+H] 572.4104 Observed 572.4076; **^{1}H NMR** (400 MHz, cdcl$_3$) δ 7.23 – 7.16 (m, 2H), 7.14 – 7.06 (m, 4H), 6.84 (d, *J* = 7.3 Hz, 2H), 6.68 (td, *J* = 7.2, 3.5 Hz, 1H), 4.56 (dd, *J* = 14.7, 7.5 Hz, 1H), 3.90 (s, 1H), 3.78 (s, 1H), 3.64 – 3.52 (m, 2H), 3.39 (dd, *J* = 12.5, 8.6 Hz, 1H), 3.05 – 2.95 (m, 1H), 2.82 – 2.31 (m, 5H), 2.18 (d, *J* = 12.3 Hz, 2H), 1.92 – 1.82 (m, 3H), 1.73 – 1.66 (m, 4H), 1.63 – 1.57 (m, 3H), 1.53 – 1.47 (m, 3H), 1.41 – 1.31 (m, 4H), 1.18 (d, *J* = 7.4 Hz, 3H), 0.93 (d, *J* = 6.9 Hz, 3H), 0.85 (d, *J* = 6.0 Hz, 3H), 0.61 (d, *J* = 10.3 Hz, 3H); **^{13}C NMR** (101 MHz, cdcl$_3$) δ 149.75, 149.67, 139.38, 139.21, 134.83, 129.18, 128.57, 128.46, 127.26, 127.20, 126.34, 126.26, 125.67, 116.89, 116.80, 113.86, 113.60, 73.10, 71.85, 68.46, 59.81, 59.26, 47.04, 47.00, 46.94, 46.34, 45.94, 41.68, 41.58, 41.44, 39.47, 36.92, 35.54, 35.25, 35.18, 34.73, 34.65, 33.14, 33.02, 32.83, 30.42, 28.24, 28.07, 27.49, 27.04, 26.79, 26.32, 23.50, 23.19, 22.43, 17.88, 17.80, 17.13, 12.49, 12.44, 10.54, 10.19; **FTIR** (ν/cm^{-1}, neat) 3378.14, 2932.5, 2865.8, 1597.3, 1503.2, 1375.4, 1097.0, 1039.2, 980.5, 913.0, 745.9, 690.8.

Radical Trapping Experiments

THIQ **3.18** (0.1125mmol), NHP ester **3.39** (0.225mmol), diphenylamine (0.225mmol), Radical trap (0.45mmol) and $[Ru(bpy)_3]Cl_2$ (2.5 mol%) were weighed and placed in a 4mL reaction vial, a stirrer bar was placed in the vial then dissolved in MeCN (2mL). The solution was briefly sonicated to ensure all materials were dissolved, then sparged with nitrogen gas for 10 minutes to degas the mixture. Upon degassing, the reaction vial was sealed with parafilm then illuminated under a 14W blue light source for 16 hours. The reaction was taken, evaporated and a sample was submitted for HRMS.

Stern-Volmer Quenching Experiments

Fluorescence quenching experiments were conducted on a Varian Cary Eclipse fluorescence spectrophotometer. Experiments were conducted with $[Ru(bpy)_3]Cl_2$ (0.1mM) concentrations of 0.1mmol in MeCN with quencher (**3.18**, **3.39** or $HNPh_2$) varied concentrations. Experiments were carried out with an excitation wavelength of 454nm

Cyclic Voltammetry

Cyclic Voltammetry experiments were conducted on a Potentiostat 466 using Ag/AgCl, Carbon and platinum electrodes as the reference, working and auxiliary electrodes respectively. Tetrabutylammoniumhexafluorophosphate was used as an electrolyte being dissolved in acetonitrile as solvent as a with a 0.1mol concentration. Analyte was added to the electrolyte solution to make a 5mmol.

Chapter 4: Direct C-H Functionalization of Tetrahydroisoquinolines via Radical-Radical Coupling Enabled by Redox Neutral Tandem Photoredox Catalysis.

4.1 Tandem Photoredox Catalysis

Chapter 2 describes the visible light mediated transfer hydrogenation of diarylimines utilizing photocatalyst $[Ir(ppy)_2(dtbbpy)]PF_6$ and TEA as both a sacrificial reductant and hydrogen source[1]. As a tentative mechanism it's proposed that the triplet state of $[Ir(ppy)_2(dtbbpy)]PF_6$ is reduced by TEA. Facilitated by PCET, the corresponding Ir(II) species undergoes single electron reduction of imine **4.1**, engendering an α-amino radical. The reductively generated α-amino radical abstracts a hydrogen from oxidised TEA, furnishing the hydrogenated product (figure 4.1). The Polyzos laboratory further studied this mechanistic proposal, revealing heretofore unprecedented reactivity between $[Ir(ppy)_2(dtbbpy)]PF_6$, a tertiary amine under visible light.[2]

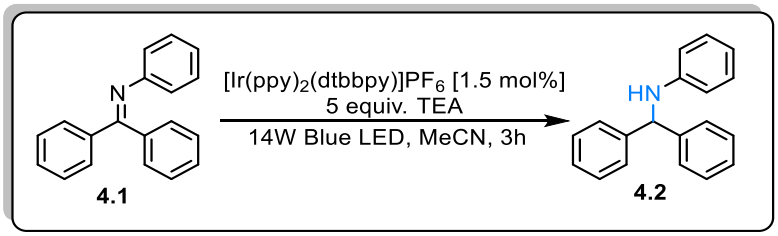

Figure 4.1: Photocatalytic transfer hydrogenation of imines

Transient absorption studies revealed a continuously absorbing species in the decay profile of a $[Ir(ppy)_2(dtbbpt)]PF_6$ and triethylamine solution (Chapter 2.5.2). This long lived species was attributed to the reduced Ir(II) species, which facilitated by PCET, undergoes the single electron reduction of **4.1**. Recent studies by the Polyzos group further elaborate on this mechanism. Upon irradiation of a deoxygenated solution of $[Ir(ppy)_2(dtbbpy)]PF_6$ (0.1mM) and triethylamine (50mM), a hypsochromic shift in emission was observed from 576nm (yellow emission) to an emission profile containing two maxima measured at 489nm and 510nm (green emission) as observed in figure 4.2.

The absorption spectra of the green emitting [Ir(II)(ppy)$_2$(dtbbpy)]PF$_6$-TEA solution revealed little change to the absorption profile compared to a solution of [Ir(ppy)$_2$(dtbbpy)]PF$_6$ in the absence of TEA. The spectrum retained a broad absorption profile into the visible region with a slight reduction of the absorption shoulder at 300nm. However, the emission lifetimes of the yellow and green emitting species were measured to be vastly different at 0.57µs and 2.22µs, respectively. The complete disappearance of the yellow emitting species indicates a transformation from [Ir(ppy)$_2$(dtbbpy)]PF$_6$ to a new chemically distinct long-lived iridium species (figure 4.2). To discount whether the green emitting species is the result of further absorption[3-5] of the reduced [Ir(II)(ppy)$_2$(dtbbpy)]PF$_6$ photocatalyst; a solution of [Ir(ppy)$_2$(dtbbpy)]PF$_6$ - TEA was electrochemically reduced with subsequent measurement of the photophysical properties, revealing an intense orange solution with major absorption bands at 500 and 530nm and a weaker broad absorption band beyond 800nm. Importantly the electrochemically reduced species did not emit upon irradiation, which is indicative that green emission occurs due to a chemically distinct species.

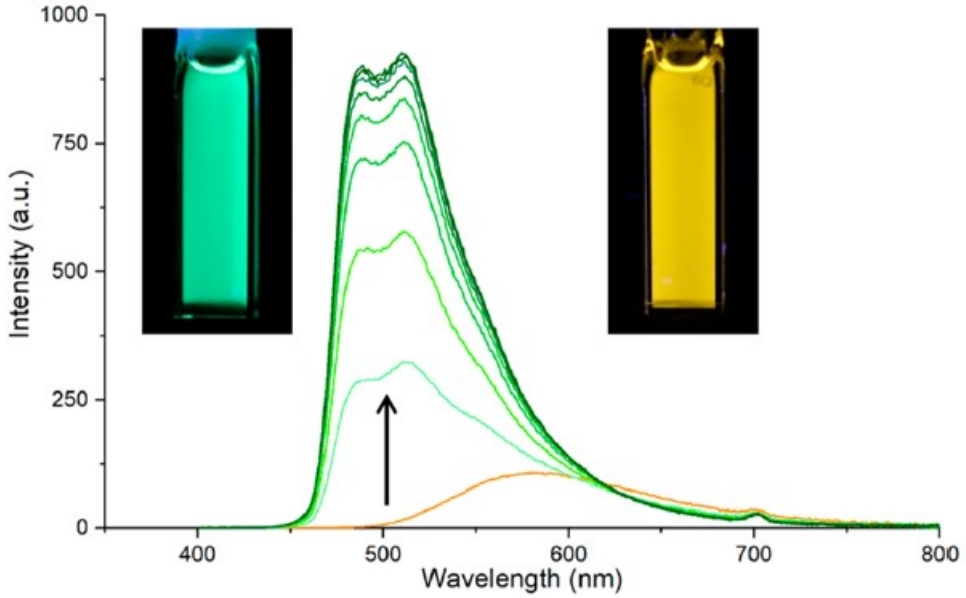

Figure 4.2: Emission spectra before and after illumination of [Ir(ppy)$_2$(dtbbpy)]PF$_6$ in the presence of triethylamine. Taken from reference 2.

The structure of the new chemically distinct species designated as **Ir-2** (**4.5**), was determined via rigorous NMR and MS analysis unveiling that $[Ir(ppy)_2(dtbbpy)]PF_6$ had acquired 4 protons, bearing semi-saturation of the ancillary di-*t*-butyl-bipyridine ligand,[6-8] generating a novel complex without its initial C_{2v} symmetry; as depicted in figure 4.3. When substituting triethylamine for d_{15}-triethylamine, the mass spectra revealed the addition of 8 mass units while the ^1H NMR depicted the absence of the saturated ancillary signals of **Ir-2**, revealing that the origin of the 4 protons to be from triethylamine.

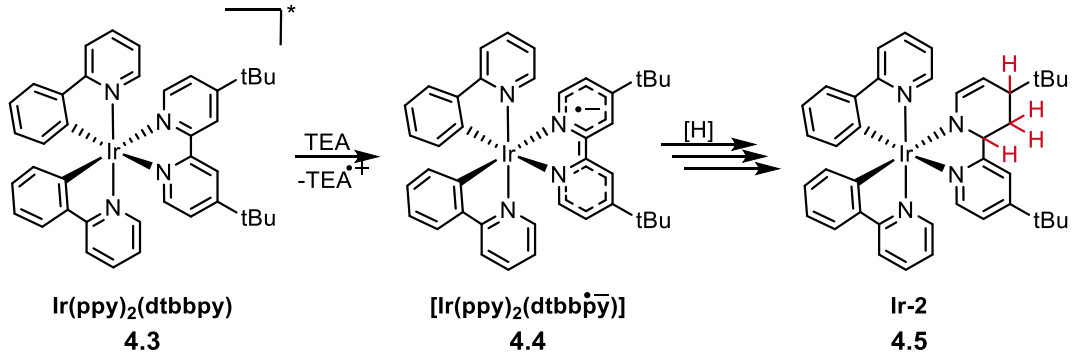

Figure 4.3: Formation and elucidated structure of the Ir-2 photocatalyst.

Cyclic voltammetry and electrochemiluminescence were employed to measure the redox properties of **Ir-2**. Polyzos *et al.* conservatively estimated the reduction potential of the triplet state of **Ir-2** to be -1.70 V vs. SCE, with an oxidation potential of 0.6 V vs. SCE. Upon *in situ* generation of **Ir-2,** the direct reduction of diarylmethimine **4.1** was examined via Stern-Volmer quenching experiments. The addition of **4.1** to a solution of **Ir-2** revealed linear concentration dependant quenching with quenching constants of 1.2×10^6 $M^{-1}s^{-1}$ and 1.6×10^6 $M^{-1}s^{-1}$ measured via steady state and time resolved quenching, respectively. A linear quenching relationship between **4.1** and **Ir-2** alludes to the direct single electron reduction of imine **4.1** by **Ir-2**.

Understanding that $[Ir(ppy)_2(dtbbpy)]PF_6$ accesses the highly reducing species, **Ir-2**, Polyzos *et al.* proposed an updated mechanism of the photocatalytic transfer

hydrogenation of diarylmethimines developed in chapter 2 (figure 4.4). Upon excitation, $[Ir(ppy)_2(dtbbpy)]PF_6$ is reduced by triethylamine, with consequent hydrogen abstractions from triethylamine instilling semi-saturation of the dtbbpy ligand engendering the **Ir-2** photocatalyst. Further irradiation of **Ir-2** promotes the formation of the green emitting triplet excited state **Ir-2***, with subsequent single electron reduction of **4.1** generating an α-amino radical, ensuing hydrogen abstraction affords the hydrogenated product. The oxidized **Ir-2** species is regenerated via single electron reduction by $[Ir(II)(ppy)_2(dtbbpy)]PF_6$. It is hypothesised that the two catalytic species work in tandem as highlighted in figure 4.4.

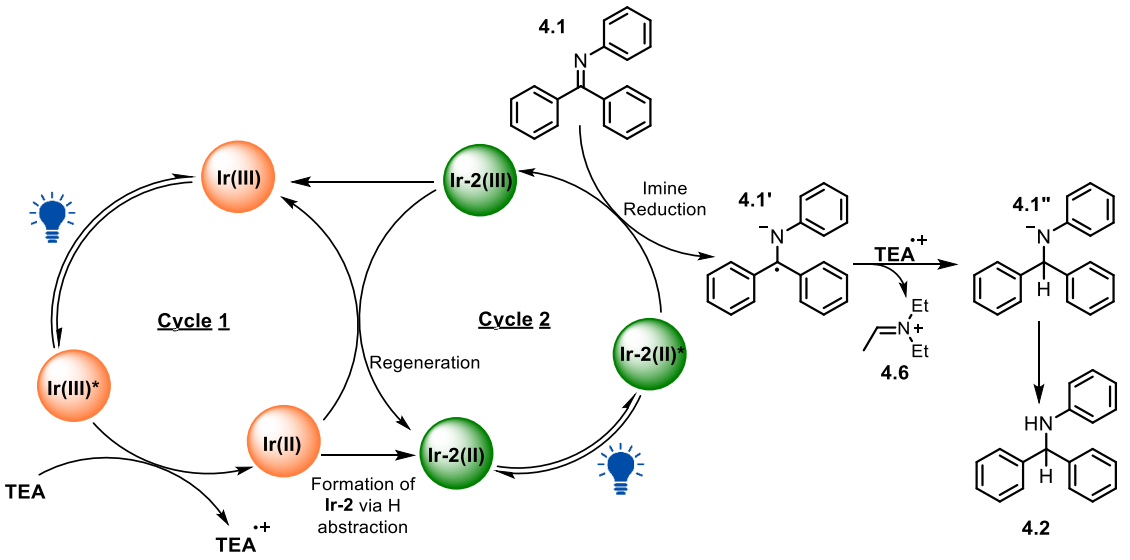

Figure 4.4: Updated mechanism for the photocatalytic transfer hydrogenation of diarylimines.

The Polyzos group applied this tandem catalytic system towards the protodehalogenation of aryl halides; a benchmark reaction for highly reducing systems[9-17] (figure 4.5). The protodehalogenation reaction obtained outstanding results with excellent-quantitative yields acquired for aryl iodides, bromides and chlorides bearing both electron donating and withdrawing functionalities while displaying promise toward alkyl halide derivatives.

Highly energy demanding substrates with reduction potentials (down to -2.8 V vs SCE) well beyond the theoretical reduction potential of $[Ir(ppy)_2(dtbbpy)]PF_6$ were accessed by the dual catalytic **Ir-2** system. The proposed tandem catalytic system is the first report with two distinct photoredox cycles proceeding in tandem. The transformation of $[Ir(ppy)_2(dtbbpy)]PF_6$ to **Ir-2** provides a novel mechanistic pathway involving an *in situ* chemical transformation of the photocatalyst allowing access to previously unattainable substrates.

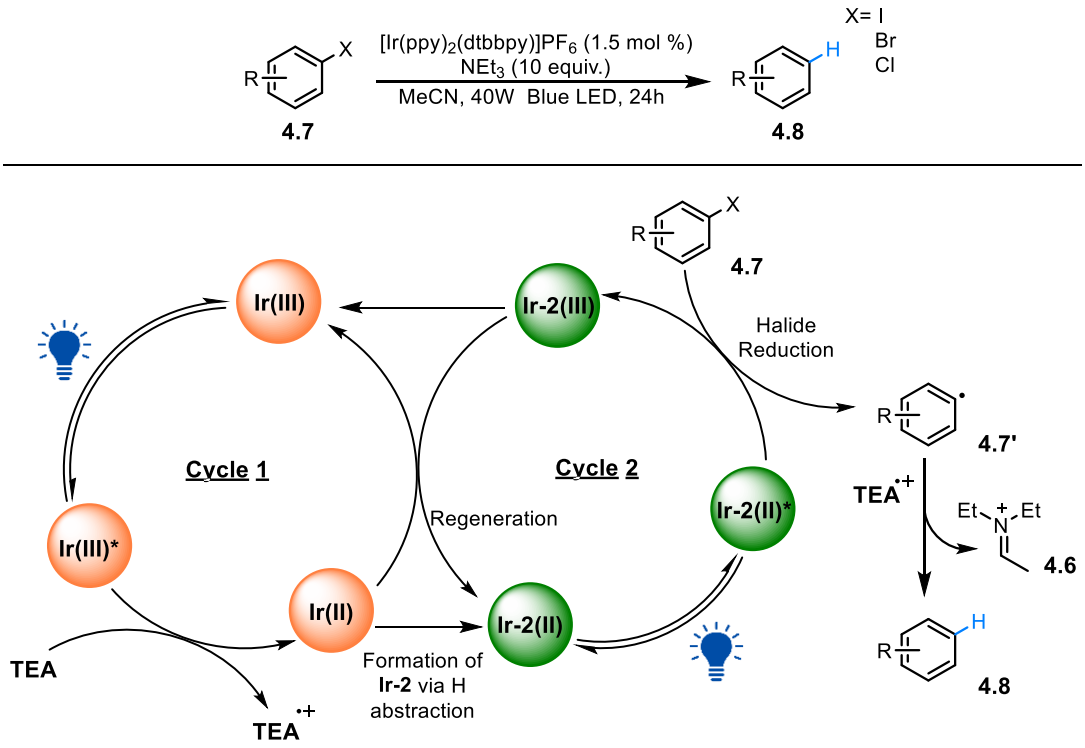

Figure 4.5: Protodehalogenation of aryl halides utilising the tandem photocatalytic pathway.

4.2 Project Proposal

Given my interest in the development of radical methods for the α-functionalisation of amines, I sought to address the limitations of the decarboxylative coupling of α-amino and aliphatic alkyl radicals developed in Chapter 3. Before implementation of a flow process, the decarboxylative approach for α-alkylation was constrained via the addition of high loadings of both the NHP ester alkyl radical precursor and co-reductant, diphenylamine. While flow conditions addressed these concerns, utilising NHP esters as radical precursors are not ideal, representing high value reagents which require additional synthetic steps prior to use. It's envisioned that the **Ir-2** species could access alkyl radicals from cheap and commercially available alkyl halides (specifically iodides and bromides, Figure 4.6). Unactivated aliphatic halides are typically difficult to access due to their demanding reduction potentials (typically -2.1 to -2.6 V vs. SCE for iodides and bromides respectively).

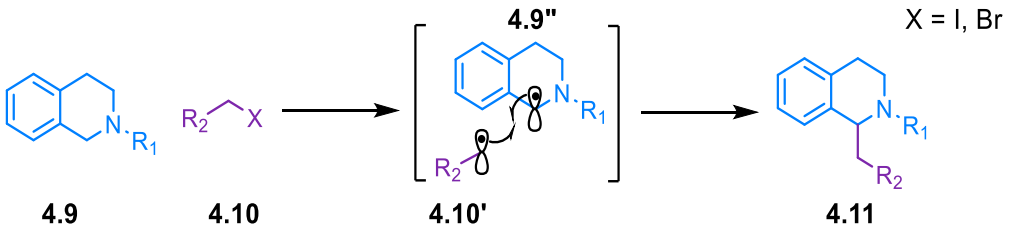

Figure 4.6: Radical coupling between THIQ and alkyl halides.

The proposed reaction will expand the synthetic utility surrounding the tandem catalytic system, constructing carbon-carbon bonds while incorporating the tertiary amine used to generate **Ir-2** into the product to synthesise potentially biologically relevant molecules from unactivated radical precursors.

4.3 Reaction design

In figure 4.7 a mechanism is proposed in which upon irradiation with blue light the triplet state of $[Ir(ppy)_2(dtbbpy)]PF_6$ oxidises **4.9**, which facilitated by a basic additive,[18-23] subsequently rearranges to an α-amino radical. Simultaneously to α-amino radical formation, the reduced Ir(II) species undergoes transformation to the **Ir-2** photocatalyst via 4 subsequent hydrogen abstractions from **4.9**, subsequent irradiation generates the highly reducing triplet state, **Ir-2***. Single electron reduction of an alkyl halide by **Ir-2*** engenders alkyl radical **4.10'** which consequently couplings with the persistent α-amino radical (**4.9'**) furnishing the α-alkylated product, **4.11**. **Ir-2** is regenerated via single electron reduction by Ir(II) returning both photocatalysts to their respective ground states permitting further reactivity to proceed.

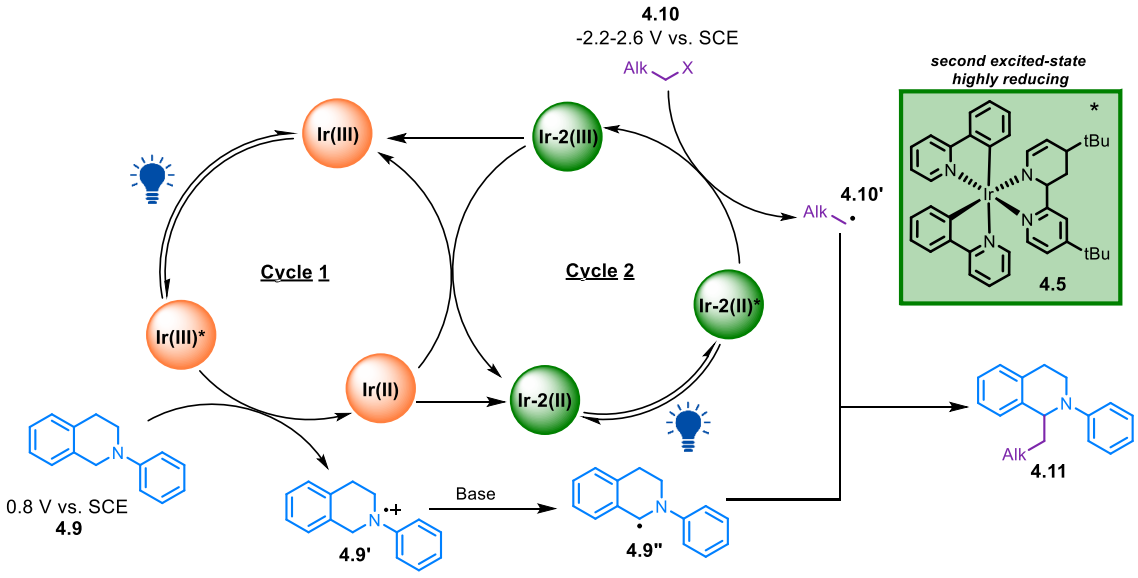

Figure 4.7: Proposed reaction mechanism for the α-alkylation of amines via tandem photocatalytic pathway.

4.4 Optimisation

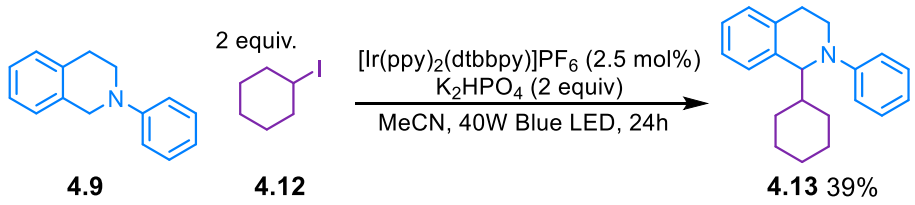

Figure 4.8: Initial reaction conditions for the α-alkylation of THIQ with alkyl iodides.

Utilising photocatalyst $[Ir(ppy)_2(dtbbpy)]PF_6$, initial optimisation involved screening solvents with 1 equivalent of **4.9**, 2 equivalents of cyclohexyl iodide (**4.12**) as a model secondary radical surrogate and 2 equivalents of K_2HPO_4 to facilitate α-amino radical formation. Utilising MeCN as solvent allowed 39% conversion to the desired α-alkylated amine (figure 4.8); a distribution of products were detected in the crude ^1H NMR spectrum by comparing the relative intensities of peaks to each other (their formation and distinguishing peaks are summarised in figure 4.9). Analysis of the crude ^1H NMR revealed the following products: the desired α-alkylated **4.13**, starting material **4.9**, the alkylated dihydroisoquinoline **4.14**, dimerised THIQ **4.15** and amide **4.16**.

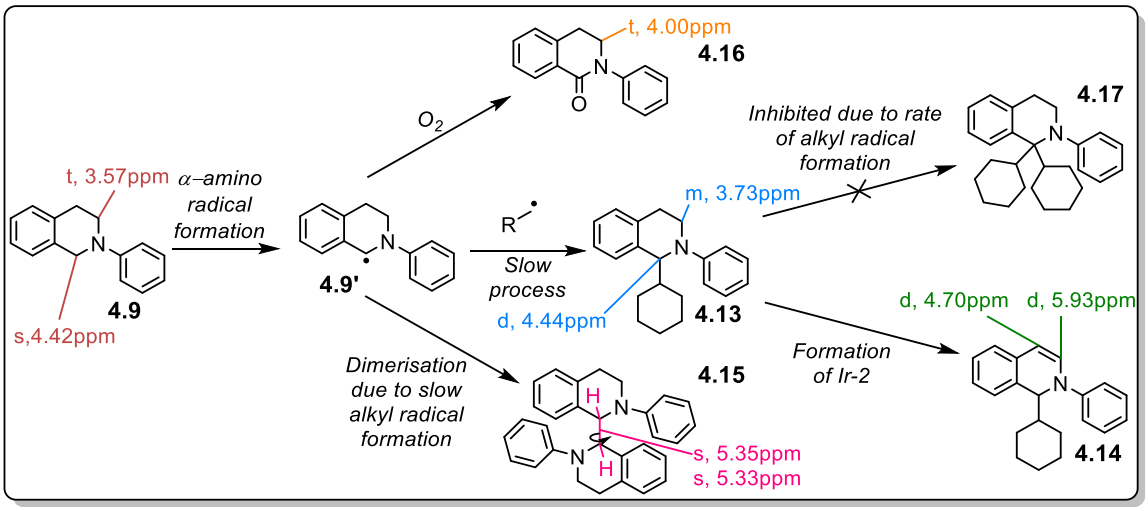

Figure 4.9: Pathways for reactivity for the α-alkylation of THIQ with alkyl iodides

Homocoupling of **4.9** transpires in an absence of other coupling partners leading to **4.15**,[24] this is indicative that alkyl radical formation is the rate limiting step in this reaction. The presence of **4.16** is observed via reactivity of an α-amino radical in the presence of triplet

oxygen, signifying that despite degassing the solution thoroughly by sparging with N_2 that trace oxygen is present, highlighting the sensitivity of this process.[18] It is hypothesised that **4.14** is generated via abstraction of hydrogen from the 3-position of **4.13** when generating **Ir-2** with consequent enamine formation to **4.14** facilitated by K_2HPO_4. Interestingly, **4.17**, observed during the decarboxylative α-alkylation of **4.9** in chapter 3 was not detected, the absence of further reactivity of the **4.13** implies a slower reaction rate in which a second alkylation does not proceed. The absence of **4.17** complements the presence of **4.15**, emphasizing that alkyl radical formation is the rate determining step. It is hypothesised that due to the limited rate of alkyl radical formation, additional reactivity of **4.13** to **4.17** is not observed.

Table 4.1: Solvent screen for the α-alkylation of THIQ.

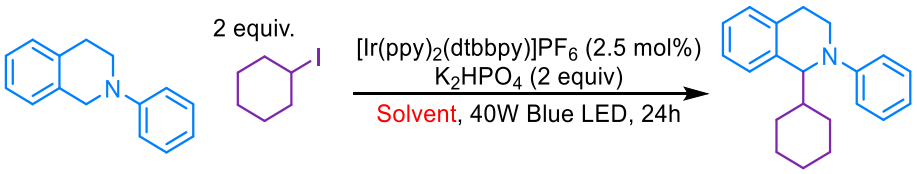

4.9 **4.12** **4.13**

Products

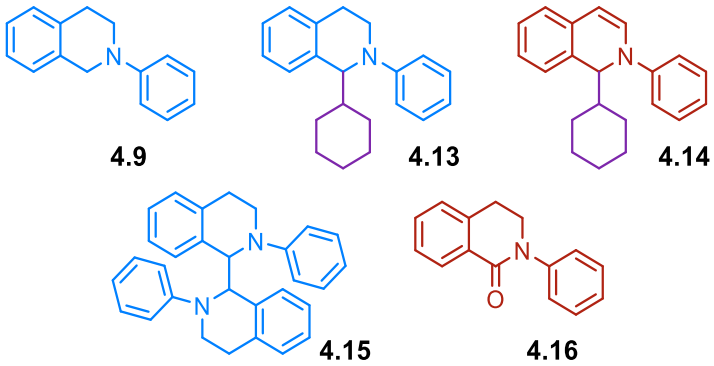

4.9 **4.13** **4.14** **4.15** **4.16**

Entry	Solvent	4.9(%)*	4.13(%)*	4.14(%)*	4.15(%)*	4.16(%)*
1	MeCN	48	39	7	3	2
2	DMF	41	29	2	24	3
3	DMSO	11	47	4	34	4
4	DCE	15	18	2	61	4
5	PhMe	9	26	5	55	4
6	Dioxane	48	15	3	29	3
7	i-prOH	0	81	19	0	0
8	MeOH	0	84	16	0	0
9	t-BuOH	33	21	4	41	1
10	TFE	11	80	9	0	0
11	HFIP	53	47	0	0	0

**Conversions measured by monitoring the distribution of products in the crude ^{1}H NMR.*

A wide selection of solvents beyond MeCN were screened. Polar solvents, DMF and DMSO resulted in 29% and 47% conversion to **4.13** respectively, with significant side product formation (table 4.1 entries 2 and 3). A reduction in solvent polarity (table 4.1, entries 4-6) resulted in reduced conversions with 18%, 26% and 15% of **4.13** obtained, respectively. Less polar solvents also observed appreciable quantities of **4.15** (61%, 55% and 29% respectively), signifying that solvent choice is an integral parameter in the rate of alkyl radical formation. Isopropanol attained full conversion of the starting material, producing **4.13** in 81% and 19% of **4.14** exclusively (Table 4.1, entry 7).

Having established *i*-PrOH as an effective solvent, other alcoholic solvents were screened to suppress the formation of **4.14**. Methanol proved effective obtaining full conversion of **4.9** generating 84% of **4.13** and 16% of **4.14** exclusively. *t*-BuOH hindered alkylation, with 21% of **4.13** observed; analogous to other less polar solvents, *t*-BuOH obtained substantial quantities of **4.15**. Fluorinated alcohols, trifluoroethanol (TFE) and hexafluoroisopropanol (HFIP) obtained **4.13** in 80% and 47% respectively (table 4.1, entries 10 and 11). Due to achieving high conversions of **4.13** and side product formation, methanol was the optimum solvent for this transformation.

Table 4.2: Control reactions for the α-alkylation of THIQ.

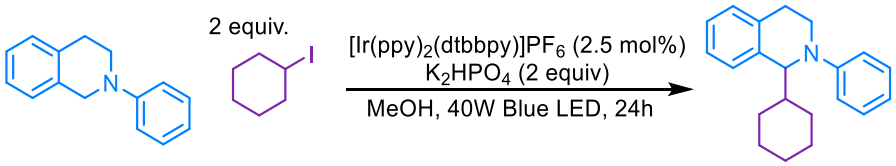

4.9 **4.12** **4.13**

Entry	Deviation	4.9(%)*	4.13(%)*	4.14(%)*	4.15(%)*	4.16(%)*
1	None	0	84	16	0	0
2	no photocatalyst	0	0	0	0	0
3	no light	0	0	0	0	0
4	no base	61	26	13	0	0

**Conversions measured by monitoring the distribution of products in the crude ^1H NMR*

A selection of control reactions were performed to probe the reaction mechanism (table 4.2). No reaction was observed in the absence of either $[Ir(ppy)_2(dtbbpy)]PF_6$ or illumination, confirming a photocatalytic process. The absence of K_2HPO_4 provided 26% of **4.13** emphasising the significance of base-mediated α-amino radical formation in this process.

Table 4.3: Variation of the equivalents of alkyl iodide.

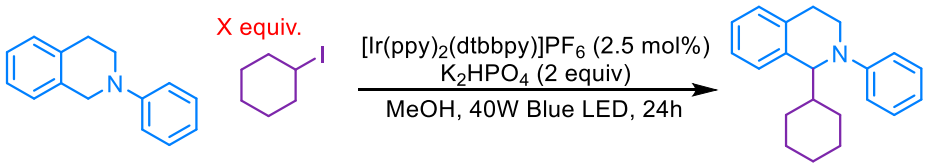

4.9 **4.12** **4.13**

Entry	equiv. 4.12	4.9(%)*	4.13(%)*	4.14(%)*	4.15(%)*	4.16(%)*
1	1.0	51	26	3	20	0
2	1.3	20	62	7	12	0
3	1.5	0	85	15	0	0
4	1.7	0	80	20	0	0
5	2.0	0	84	16	0	0
6	4.0	0	77	23	0	0

**Conversions measured by monitoring the distribution of products in the crude ^{1}H NMR.*

Cyclohexane was observed in the crude ^{1}H NMR spectrum, indicative of hydrogen abstraction by the cyclohexyl radical prior to coupling with **4.13**. Hydrogen abstraction by the cyclohexyl radical inhibits the possibility of alkylation, effectively removing the molecule from reaction. To determine whether this reaction is limited by the quantity of cyclohexyl radical, the stoichiometry of **4.12** was screened. Increasing the equivalents of iodocyclohexane saw a slight decrease in conversion of **4.9** to **4.13** (table 4.3, entry 6) while 1.5 equivalents (table 4.3, entry 3) achieved comparable conversions of **4.13** (85%). Further decreases to 1.3 and 1.0 equivalents however, hindered the reaction, presumably due to a reduced availability of the cyclohexane radical (table 4.3, entries 1 and 2).

Table 4.4: Bases screened for the α-alkylation of THIQ.

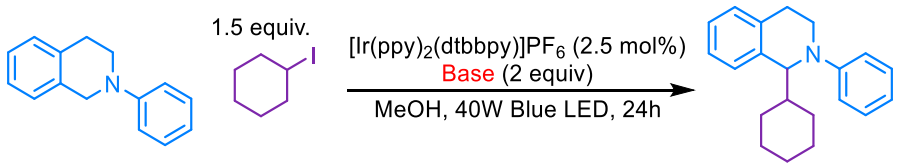

4.9 **4.12** **4.13**

Entry	Base	4.9(%)*	4.13(%)*	4.14(%)*	4.15(%)*	4.16(%)*
1	K_2HPO_4	0	85	15	0	0
2	K_2CO_3	44	33	16	5	3
3	KOAc	9	58	18	15	0
4	K_3PO_4	15	35	7	44	0
5	Pyridine	51	24	5	20	0
6	K_2HPO_4 + H_2O (9:1)	4	76	18	0	1
7	K_2HPO4 + H_2O (1:1)	14	47	18	14	7

**Conversions measured by monitoring the distribution of products in the crude ^1H NMR.*

A variety of bases were then screened to determine their effect on α-amino radical formation; bases of differing strength abstract the α-proton of **4.9'** at a different rate and modulate the rate of α-amino radical formation, the results are summarised in table 4.4. K_2HPO_4 remained the most efficient base with full conversion of starting material and 85% to **4.13**, while K_2CO_3 demonstrated poor reactivity with 56% conversion of **4.9** achieving 33% of **4.13**, 16% of **4.14** and small quantities of **4.15** and **4.16**. Utilising KOAc enabled 91% conversion of **4.9** with 58% **4.13**; side products, **4.14** and **4.15** were detected in 18% and 15% respectively. Substitution of K_2HPO_4 with K_3PO_4 yielded only 35% conversion to the desired product, while 44% of **4.15** was observed. Increased dimerization was rationalised by the elevated basicity of K_3PO_4 (pK_b 1.6) compared to K_2HPO_4 (pK_b 6.8) consequently enhancing the rate of α-amino radical formation without influencing the rate of alkyl radical formation therefore promoting dimerization. Substitution with pyridine observed a reduced conversion of 49% with 24% of **4.13** and comparable conversions to **4.15**. To improve the solubility of K_2HPO_4, MeOH was substituted for a MeOH:H2O mixture (table 4.4, entries 6 and 7). The MeOH:H_2O

solutions provided improved solubility of K_2HPO_4 however the addition of H_2O had a negative effect on the reaction, with a slight reduction in conversion observed with 10% H_2O, while 50% H_2O similarly lead to lower conversions and an increase of undesired products.

During reaction optimisation, employing a 40W light source resulted in elevated reaction temperatures, with refluxing occasionally observed with lower boiling solvents, despite the use of cooling fans. To overcome this issue, the 40W Kessel lamp light source was replaced with a 14W in-house built light source, allowing reactions to proceed at near room temperature with consistent volumes. Reducing the light intensity decreased the rate of reaction (approximately 75-80% total conversion over 24h), however increasing the reaction time to 44 hours allowed conversions between 85-93% of **4.13** to be obtained, with up to 91% yield isolated. At this point the reaction was considered optimised with conditions summarised in figure 4.10.

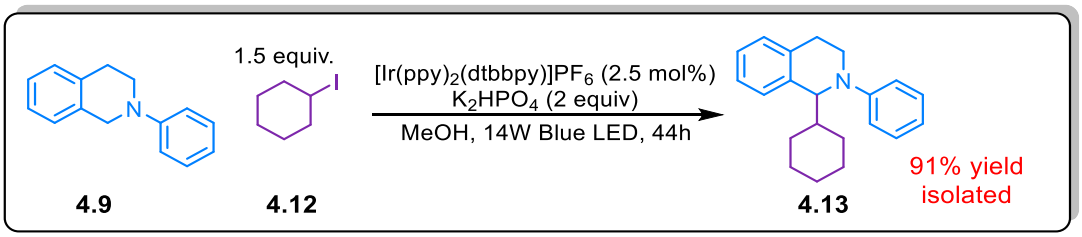

Figure 4.10: Optimised conditions for the α-alkylation of THIQ with alkyl iodides.

4.5 Substrate Scope

A selection of secondary alkyl iodides were submitted to the optimized conditions with the results summarised in Figure 4.11. Secondary radicals were generally well received with iodocyclopentane affording **4.19b** in a 76% isolated yield, while isopropyl chains proved compatible, achieving 81% yield of **4.19c**, 2-iodobutane allowed the isolation of **4.19d** in 59% yield. Heterocyclic rings were tolerated under the optimized conditions

with both 4-iodopyran and 4-iodo-*N*-bocpiperidine affording products **4.19e** and **4.19f** in moderate yields of 54% and 59%, respectively.

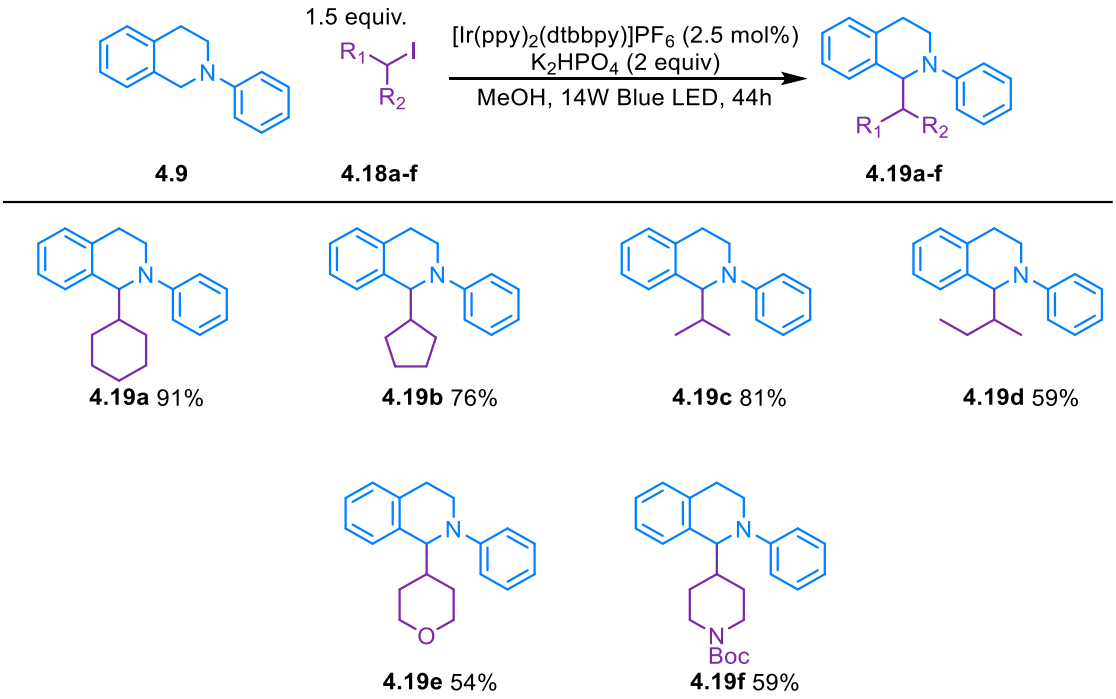

Figure 4.11: Coupling of THIQ with secondary alkyl iodides.

Diverse results were attained when screening primary iodides. Coupling with iodopropane exhibited excellent results with product **4.19g** isolated in 81%, while ethyl and octyl chains were coupled in moderate yields with **4.19h** and **4.19i** synthesised in 52% and 50%, respectively. Branched primary alkyl iodides allowed moderate yields of **4.19j** and **4.19k** isolated accordingly in yields of 56% and 63%. The developed conditions proved to be an efficient method for vinylation with **4.19l** synthesised in 78%, while sterically hindered tetramethylsilane **4.19m** was obtained in 48%. Unfortunately, 1-iodo-2-phenylethane resulted in poor results with product **4.19n** isolated in 10% yield.

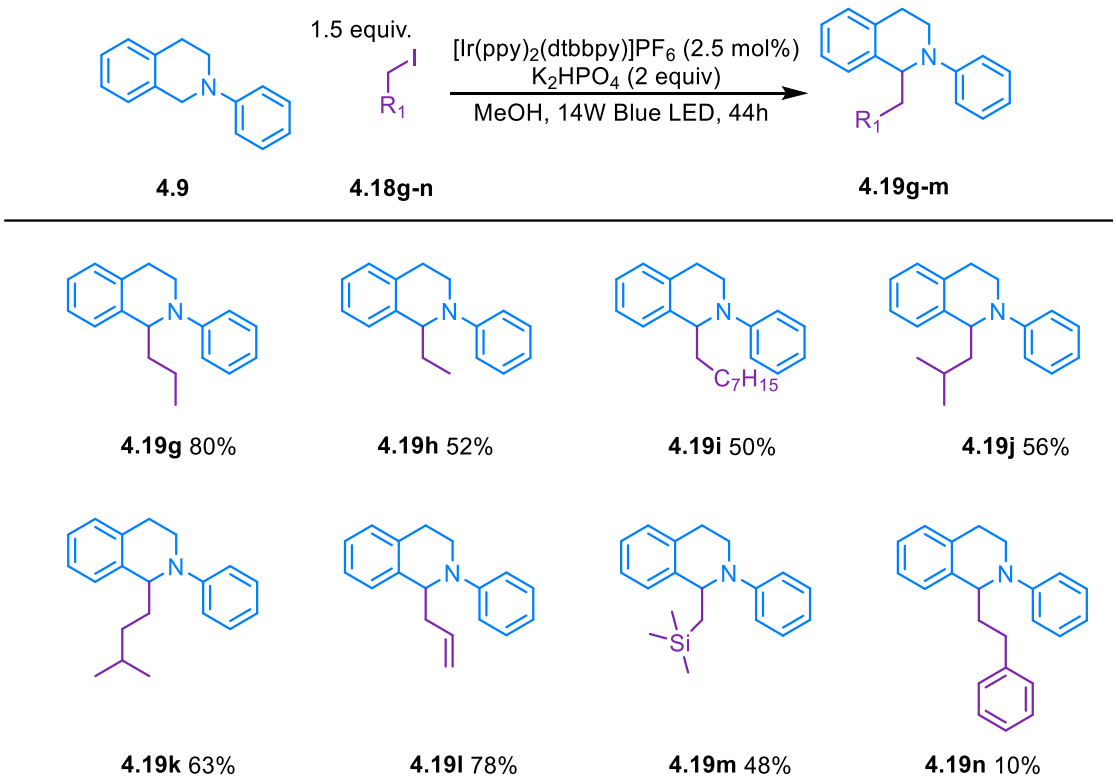

Figure 4.12: Coupling of THIQ to primary alkyl iodides.

Tertiary radicals proved inefficient in comparison to their primary and secondary counterparts with **4.19o** isolated in 28% yield. Coupling with an adamantyl radical allowed a 45% yield of **4.19p**, a substrate not accessible via the decarboxylative method developed in chapter 2. The inefficiency of tertiary radicals is contrary to that observed in the decarboxylative α-alkylation protocol developed in chapter 2, where typically good yields were obtained. Tertiary radicals are not as effective due to their stabilised nature in contrast to primary and secondary radicals. The reaction mixture of **4.19o** contained isoquinoline; it hypothesised that secondary oxidation of **4.19o** occurs, with the radical cation undergoing β-scission ejecting the stabilised tertiary radical and consequent formation of isoquinoline. This process also accounts for the higher yields of **4.19p** as β-scission of adamantyl groups is less likely as pyramidyl radicals are less stable. Substitution on the *N*-phenyl ring was tolerated with *para*- methoxy, methyl and chloro

substituents affording products **4.20a** **4.20b** and **4.20c** in 62%, 63% and 52% yield, respectively. *Ortho*-substitution with a methoxy group achieved identical yields to the *para*-substituted **4.20a** with 62% of **4.20d** isolated.

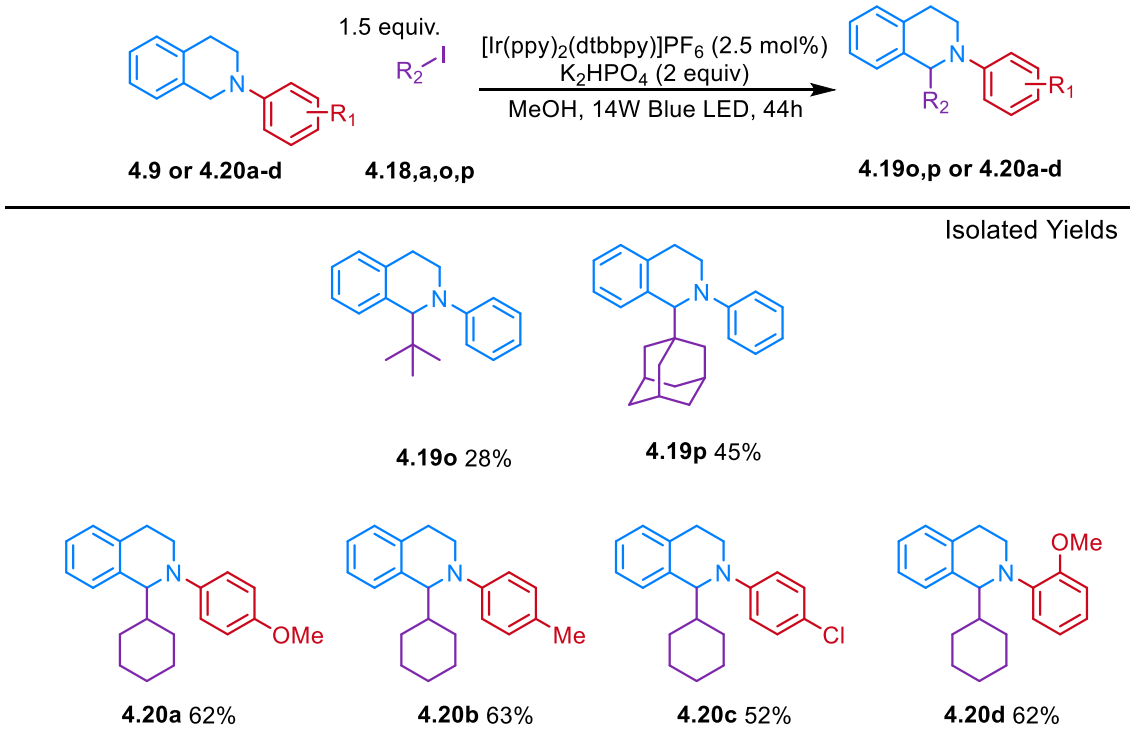

Figure 4.13: coupling of tertiary iodides and THIQ derivatives.

Iodo-substituted cholesterol derivative **4.21** was subjected to the optimised reaction conditions, proving successful albeit a lower yield of 33%. The synthesis of **4.22** however, demonstrates the potential of the developed methodology to be applied towards the late stage functionalisation of complex molecular targets with potentially bioactive properties.

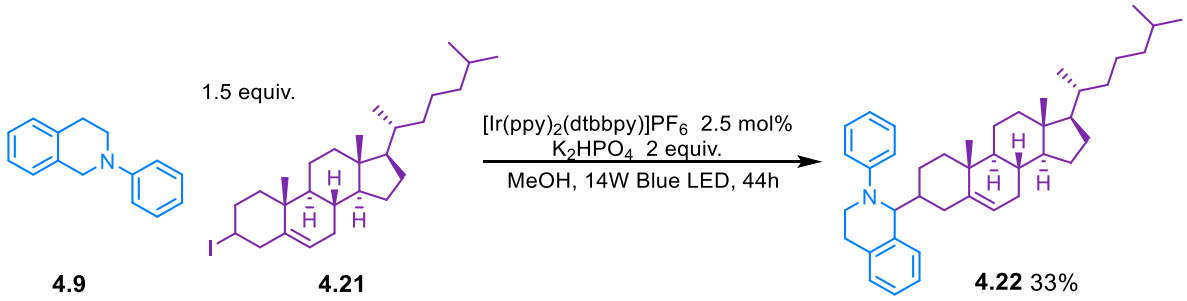

Figure 4.14: coupling of THIQ to a cholesterol derivative.

Substitution of the *N*-phenyl group of **4.9** with benzyl, Boc and tosyl protecting groups (**4.23a-c**) proved incompatible with the developed conditions, displaying no reactivity (figure 4.15). This was attributed to the increase in oxidation potential of THIQ with the addition of electron withdrawing functionalities. The increased oxidation potential of the electron poor nitrogen results in inhibition of the initial oxidation of THIQ by $[Ir(ppy)_2(dtbbpy)]PF_6$, consequently inhibiting formation of **Ir-2**. The increased oxidation potential of the electron poor derivatives inhibits the formation of both α-amino and alkyl radicals, shutting down the reaction.

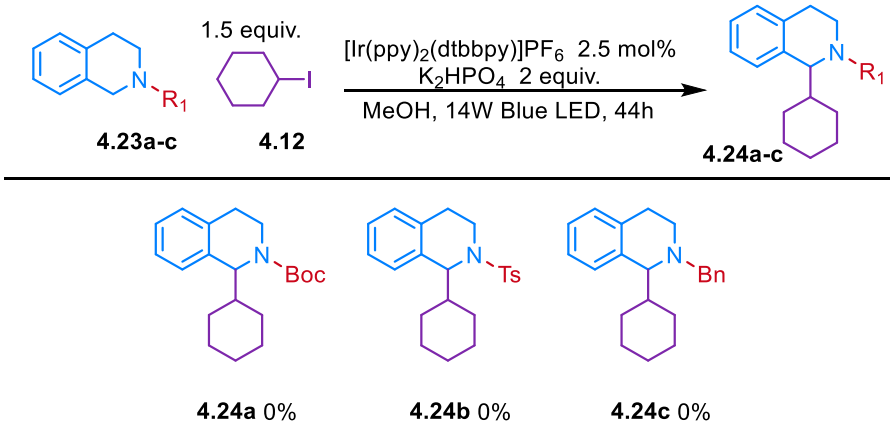

Figure 4.15: Influence of *N*-functionalisation on the THIQ moiety.

Attention was then applied towards extending the reaction's synthetic utility towards α-arylation. A selection of three aryl iodides bearing electron donating and withdrawing functionalities were subjected to the developed conditions (figure 4.16). Unfortunately, α-arylation was not achievable under these conditions; the crude ^{1}H NMR revealed small quantities of hydrodehalogenation products (13-31%) (**4.27a-c**) as well as the **4.15** (16-25%). It is hypothesised that upon formation of the highly reactive[25] and fairly ambiphilic aryl radical[26] that rapid hydrogen abstraction is achieved generating the protodehalogenated product prior to coupling with the α-amino radical. In the absence of a coupling partner, **4.9'** undergoes dimerization leading to **4.15**. The rate of reduction of

the aryl species was stunted in comparison to protodehalogenation in the presence of TEA (figure 4.5), understanding that halide reduction is the rate limiting step, comparison could imply the rate of **Ir-2** formation may be reduced in the presence of **4.9**.

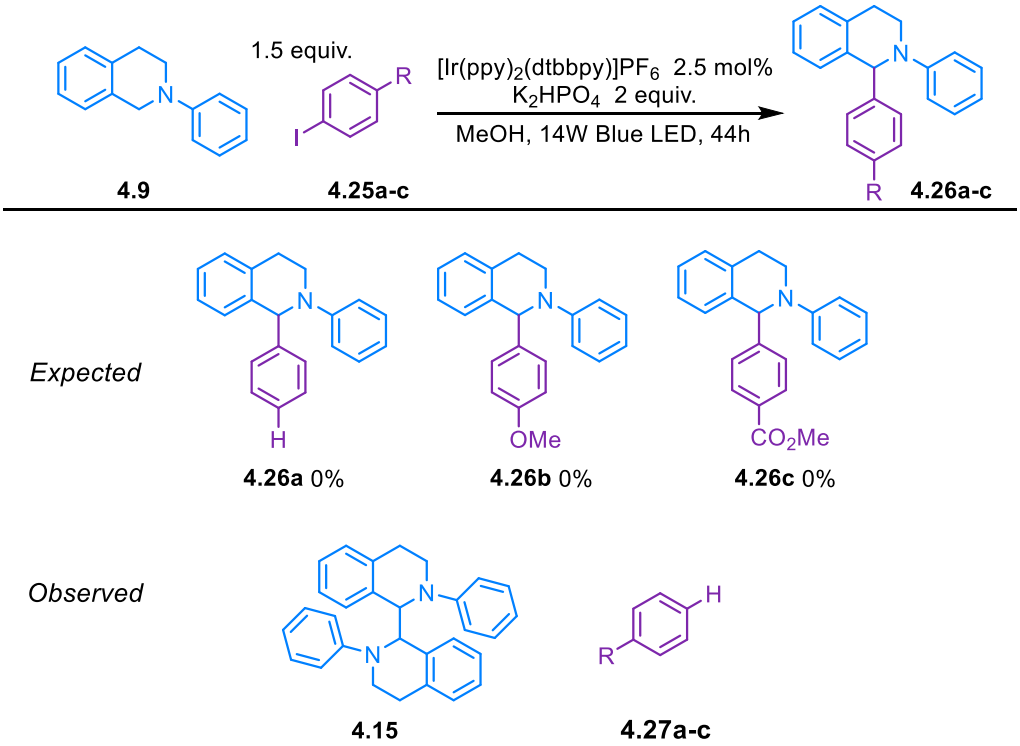

Figure 4.16: α-arylation of THIQ derivatives

Having established the reduction and subsequent coupling of alkyl iodides, attention was turned towards alkyl bromides. Despite lower reduction potentials (approx. -2.6 V vs SCE), reactivity was observed albeit at a reduced reaction rate. After 44 hours of illumination **4.29a** had achieved approximately 37% conversion, while **4.29b-d** were detected in 17-19% conversion (figure 4.17). Reactivity with alkyl bromides further emphasises that the tandem catalytic cycle can access energy demanding substrates well beyond the theoretical potential of $[Ir(ppy)_2(dtbbpy)]PF_6$ and that initially estimated for **Ir-2**. Unfortunately, due to low conversions over long reaction times, the synthetic utility of alkyl bromides towards the α-alkylation of **4.9** is limited.

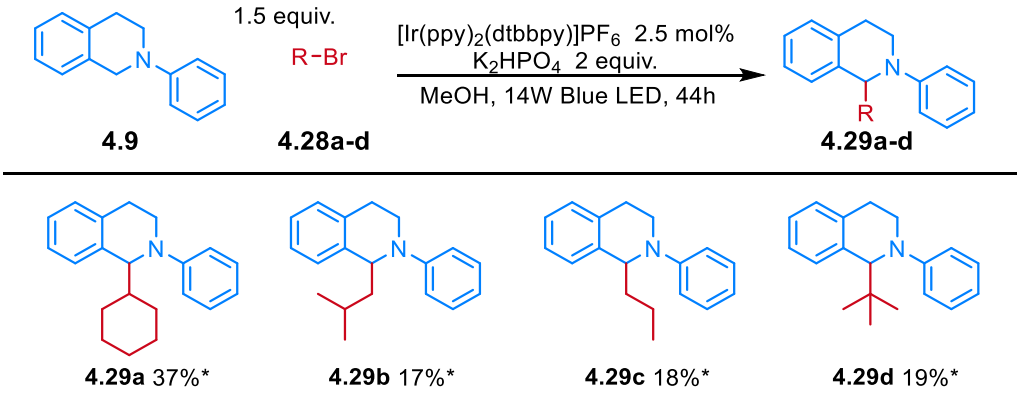

Figure 4.17: α-alkylation of THIQ with alkyl bromides. *Measured by conversion

With a plethora of alkyl radicals applicable towards the α-alkylation of THIQ, it was evident that this transformation is limited, notably due to: extensive reaction times, poor reactivity with tertiary substrates and the small reaction scale (0.225mmol). The increased surface area to volume ratio obtained by transferring from batch to flow processing would facilitate enhanced photon attenuation throughout the reaction vessel. This should lead to reduced reaction times, while a flow protocol would facilitate the efficient scaling of this process.

4.6 Flow Optimization

A flow protocol was implemented to address the tempered reaction rate and to scale this process to synthetically useful quantities. Optimisation proceeded utilising a commercially available Syris Asia series pump fitted with a 2mL sample loop, 4mL illuminated reactor and 75 PSI back pressure regulator. Optimisation of the developed flow procedure is summarised in table 4.5

Table 4.5: Optimization of the tandem photocatalytic α-alkylation of THIQ in flow

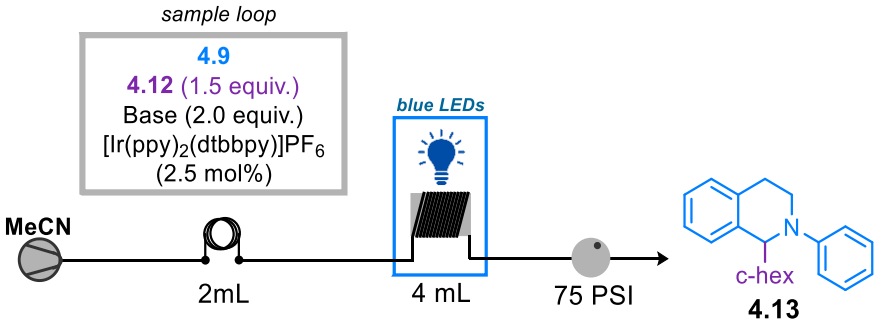

Entry	Residence Time (min)	Flow rate (μL/min)	Base	Light Intensity (W)	Conversion to 4.13a (%)
1	20	200	$KOAcF_3$	14	21
2	20	200	C_5H_5N	14	17
3	20	200	KOAc	14	32
4	40	100	KOAc	14	52
5	60	66.7	KOAc	14	57
6	80	50	KOAc	14	65
7	80	50	KOAc	94	80
8	90	44.4	KOAc	94	81
9	100	40	KOAc	94	86
10	110	36.4	KOAc	94	91

K_2HPO_4 is insoluble in MeOH rendering it incapable of processing via flow, therefore initial optimisation involved screening a variety of soluble bases at a residence time of 20 minutes under 14W irradiation. Potassium acetate displayed modest conversions of **4.13** in 32% while pyridine and potassium trifluoroacetate afforded 17% and 21% respectively. Steadily increasing the residence time to 80 minutes allowed a 65% conversion to **4.13**. To determine whether the reaction mixture was optically saturated, the intensity of light was increased to 94W with the addition of two commercially available Kessel lamps (table 4.5, entry 7). Increasing the optical intensity allowed an improvement in conversion to **4.13** of 80%, further increasing the residence time allowed full conversion of **4.9** and 91% of **4.13** after 110 minutes. These conditions were repeated several times incurring isolation issues and an average isolated yield of 64%.

Processing this reaction via flow substantially decreased the reaction time achieving analogous conversions at a residence time of 110 minutes compared to 44 hours via batch processing and a theoretical throughput of 0.25 mmol h^{-1} compared to 0.0051 mmol h^{-1} respectively. However, this process profoundly suffered from dispersion due to a low flow rate of 36.4 µL/min contributing to extensive total reaction times (approximately 6 hours). The provisional flow optimisation was successful, observing substantially enhanced reaction rates, highlighting the potential for scaling up this process towards synthetically useful quantities.

4.7 Mechanistic Studies

Attention then turned to probing the reaction mechanism via: radical trapping experiments, emission quenching as well as cyclic voltammetry measurements.

4.7.1 Radical Trapping Experiments

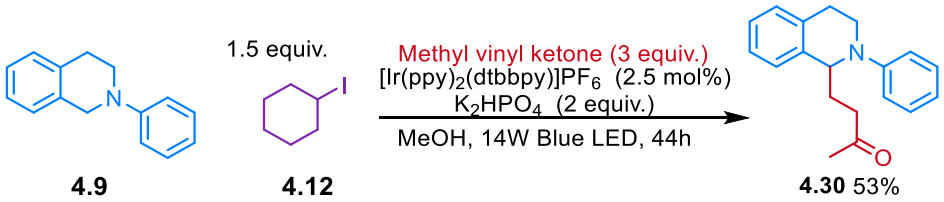

Figure 4.18: Radical trapping of the α-amino radical with methyl vinyl ketone.

To confirm the generation of an α-amino radical, methyl vinyl ketone was utilised as a radical trapping agent. Reiser *et. al*. previously exploited methyl vinyl ketone as a Michael acceptor, reporting intermolecular 1,2-radical addition with an α-amino radical under photoredox conditions[18]. If an α-amino radical is generated by a photooxidative approach as hypothesised, the conjugate addition into methyl vinyl ketone will be favourable, preferentially occurring over alkylation due to its sluggish reaction rate. The

addition of 3 equivalents of methyl vinyl ketone enabled isolation of **4.30** in 53% yield, confirming that an α-amino radical is formed in this reaction.

4.7.2 Emission Quenching Studies

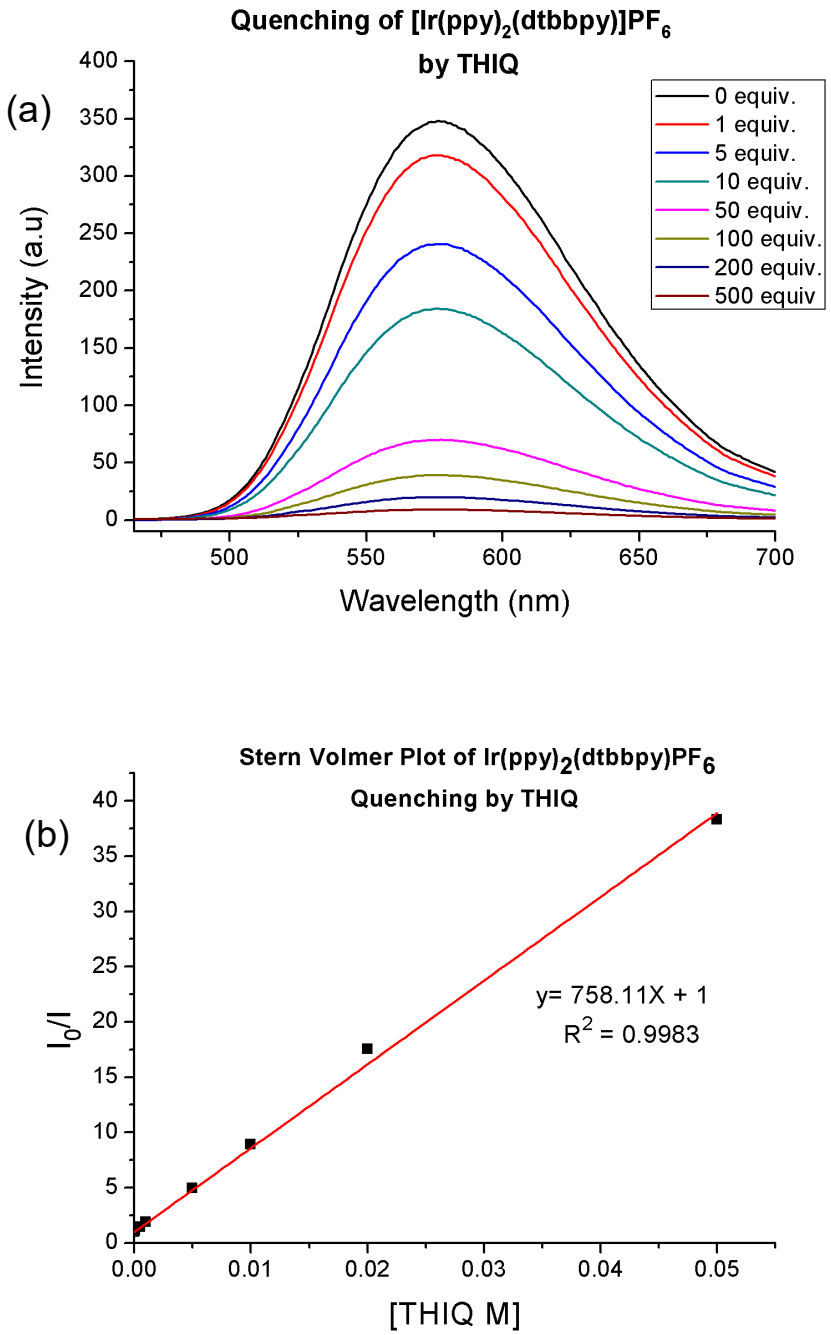

Figure 4.19: Emission quenching between $[Ir(ppy)_2(dtbbpy)]PF_6$ and THIQ (a) quenching profile between $[Ir(ppy)_2(dtbbpy)]PF_6$ and THIQ (b) Stern-Volmer plot

Stern-Volmer quenching experiments were conducted to determine which species the triplet excited state of $[Ir(ppy)_2(dtbbpy)]PF_6$ interacts with. $[Ir(ppy)_2(dtbbpy)]PF_6$ exhibited a concentration dependent linear relationship of quenching with the addition of **4.9** (figure 4.19) with a rapid quenching constant calculated of 1.33×10^9 $mol^{-1}s^{-1}$ (assuming τ of $[Ir(ppy)_2(dtbbpy)]PF_6$ is 570ns[2]). No quenching was achieved in the presence of iodocyclohexane. The linear gradient of the Stern-Volmer plot in conjunction with the knowledge of α-amino radical formation further emboldens the proposed mechanism in which upon excitation, triplet $[Ir(ppy)_2(dtbbpy)]PF_6$ is reduced by THIQ.

4.7.3 Generation and Quenching of the Ir-2 Species

The formation of the **Ir-2** species is signified by a hypsochromic shift in emission which demonstrates two emission maxima at 489nm and 510nm respectively.[2] Polyzos *et al.* observed the complete formation of the highly reducing species via irradiating a degassed solution of $[Ir(ppy)_2(dtbbpy)]PF_6$ (0.1mM) in the presence of triethylamine (50mM) for 46 seconds. To determine whether **Ir-2** is generated in the presence of **4.9**, this experiment was replicated substituting TEA for **4.9**. A degassed solution of $[Ir(ppy)_2(dtbbpy)]PF_6$ (0.1mM) and **4.9** (50mM) was irradiated under a 14W blue light source for 30 minutes, the emission spectra observed an absence of emission at 576nm with the emergence of two blue shifted maxima at 491nm and 514nm (figure 4.20). The appearance of the peaks at 491nm and 514nm demonstrates the generation of **Ir-2** from **4.9**. The delayed generation of **Ir-2** in the presence of **4.9** (30 minutes compared to 46 seconds with TEA) correlates to the extended reaction times for the α-alkylation of **4.9** (44 hours) in contrast to the transfer hydrogenation of diarylmethimines developed in chapter 1 (3 hours).

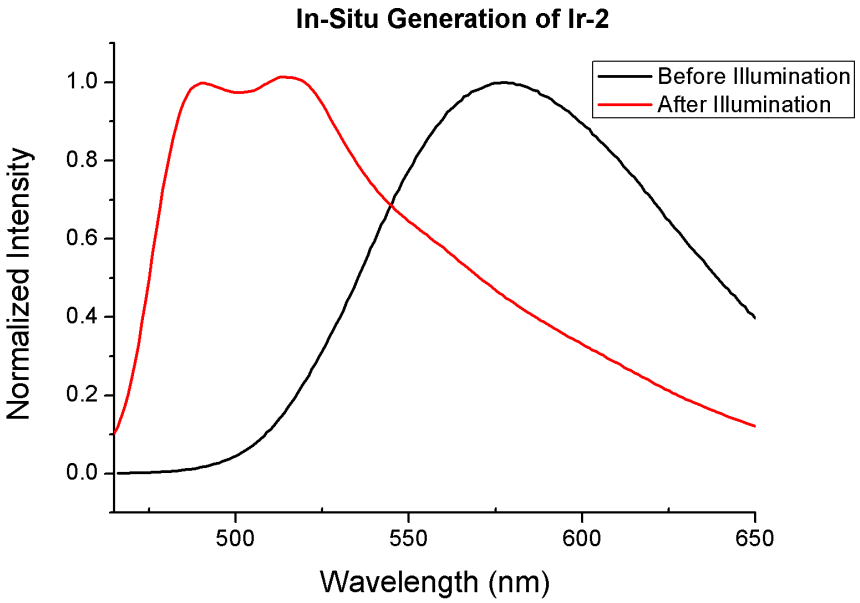

Figure 4.20: Formation of Ir-2 in the presence of THIQ

Upon generation of **Ir-2**, single electron reduction was be observed with the addition of diarylmethimine **4.1**, this process was monitored via Stern-Volmer quenching. An **Ir-2** (0.1mM) solution generated with **4.9** (50mM) was quenched with iodopropane to demonstrate single electron reduction and subsequent generation of the alkyl radical. Addition of iodopropane demonstrated unreliable quenching with the **Ir-2-THIQ** solution, achieving inconsistent results with differing concentrations of iodopropane quencher. The incoherent quenching was attributed to the reduced kinetic propensity for generation and reactivity of **Ir-2** generated with **4.9** causing an unreliable quenching rate, this also accounts for the extensive reaction times of this transformation. With confirmation that **Ir-2** is prepared in the presence of **4.9**, quenching studies were repeated with a solution of **Ir-2** generated from $[Ir(ppy)_2(dtbbpy)]PF_6$ (0.1mM) and DIPEA (50mM), which Polyzos *et al.* have observed to rapidly generate **Ir-2**. Iodopropane was added incrementally (multiples of 5µL) to a solution of **Ir-2-DIPEA** with the emission profile measured after each addition (figure 4.21a). Quenching of triplet **Ir-2** expressed a

linear relationship with increasing concentration of iodopropane with a quenching constant of 1.96×10^6 $mol^{-1}s^{-1}$ (assuming τ of **Ir-2:DIPEA** if the same as **Ir-2:TEA** at 2200ns)[2] indicating the possibility of single electron reduction (figure 4.21b).

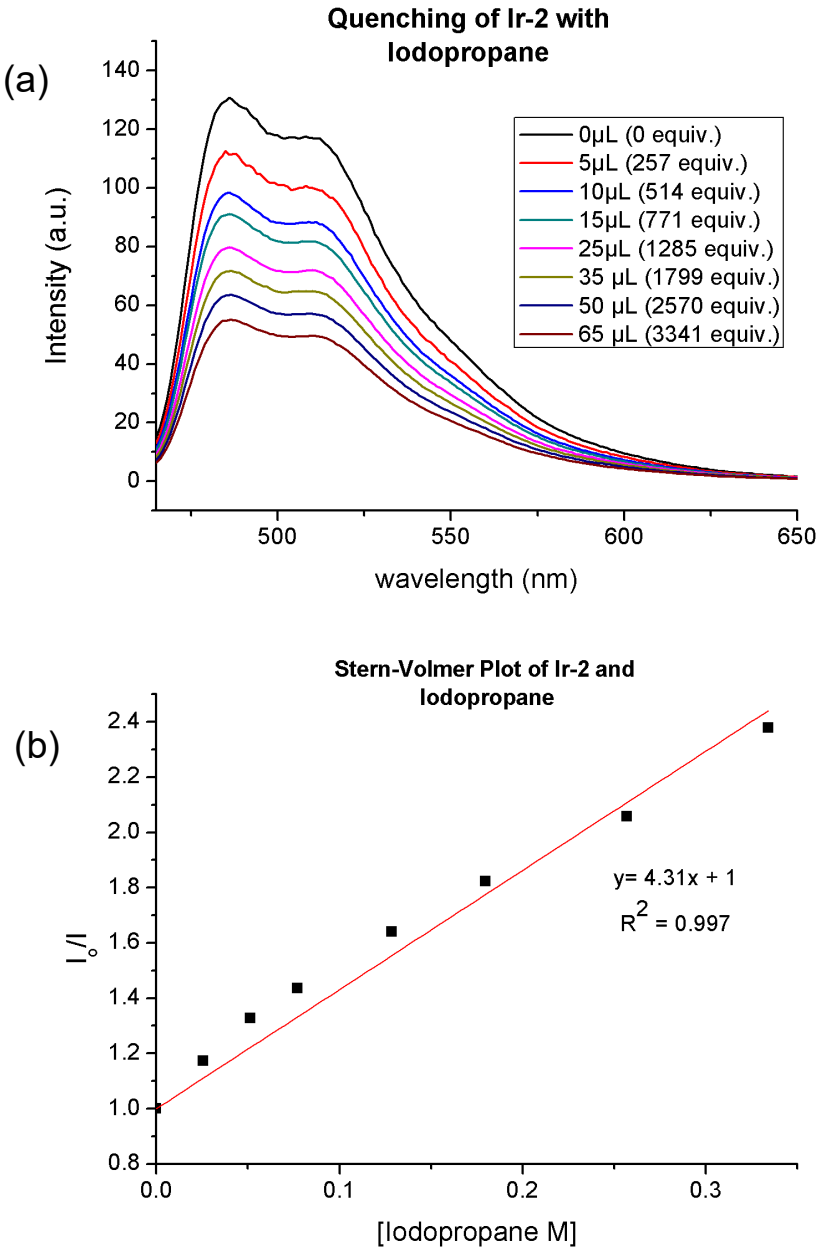

Figure 4.21: Quenching of Ir-2 with the sequential addition of iodopropane (a) emission profile with the addition of iodopropane (in μL and equiv.) to an *in situ* formed solution of Ir-2 (b) Stern-Volmer quenching of Ir-2 with the sequential addition of iodopropane.

The difference in quenching constants between the **[Ir(ppy)$_2$(dtbbpy)]PF$_6$:THIQ** (1.33×10^9 mol^{-1}s^{-1}) and **Ir-2:C$_3$H$_5$I** (1.96×10^6 mol^{-1}s^{-1}) solutions must be highlighted as they represent the respective rates of SET in the reaction. The quenching constants reveal that the oxidation of THIQ by [Ir(ppy)$_2$(dtbbpy)]PF$_6$ occurs at an approximate rate of 680 times greater than the single electron reduction of iodopropane by **Ir-2** (estimated when **Ir-2** is generated with DIPEA, the inconsistent quenching of **Ir-2** generated with **4.9** indicates an even slower process). The accelerated rate of **4.9** oxidation over alkyl radical formation over the two cycles allows accumulation of α-amino radical in solution, enacting a persistent radical effect that facilitates the radical-radical coupling process in this reaction.[27-30]

The quenching of **Ir-2*** by iodopropane agrees with the proposed mechanism, that alkyl radicals are produced via the single electron reduction by the triplet excited state of **Ir-2***. Being able to measure the quenching constants of the two single electron transfers and estimate the rate of formation of two radicals subsequently validates that a radical-radical coupling process furnishes the α-alkylated product while providing indirect evidence of the persistent radical effect.

4.7.4 Cyclic Voltammetry

The cyclic voltammograms of **4.9** and a range of alkyl iodides were measured to determine the feasibility of the reaction (Figure 4.22); the oxidation potential of **4.9** is estimated to be approximately 0.8 V vs. SCE while cyclohexyl, propyl and tertiary butyl iodides displayed onsets of reductions at approximately -2.25 V vs. SCE. Polyzos *et al.* despite conservatively estimating the reduction potential of **Ir-2*** being -1.70 V vs SCE, have accessed the reduction of substrates far more energy demanding (up to -2.8 V vs SCE), hence it was proposed that triplet **Ir-2** is capable of accessing the single electron

reduction of alkyl iodides. The matching redox potentials of the reactants and the estimated potentials of $[Ir(ppy)_2(dtbbpy)]PF_6$ and **Ir-2** indicate that the proposed hypothesis is plausible.

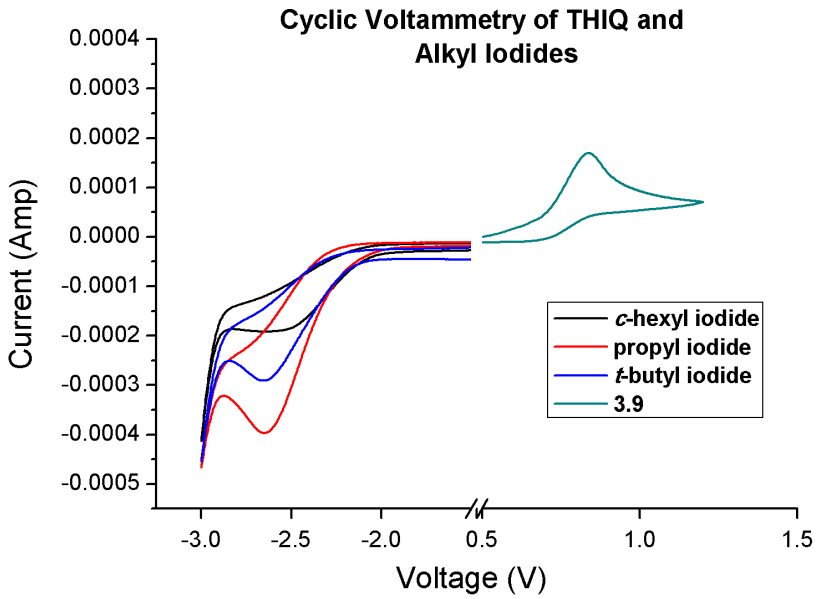

Figure 4.22: Cyclic Voltammograms of THIQ as well as a selection of alkyl iodides.

4.8 Conclusion

A process for the α-alkylation of THIQ derivatives was developed utilising the tandem photocatalytic cycle of $[Ir(ppy)_2(dtbbpy)]PF_6$. This protocol accessed alkyl radicals via the single electron reduction of alkyl iodides to afford the radical coupled α-alkylated product in typically good yields. The hypothesised mechanism was examined through a series of experiments, comprising of extensive quenching studies, radical trapping and cyclic voltammetry. This project extends the knowledge and scope of the tandem mechanism, demonstrating that the amine needed for **Ir-2** formation is not sacrificial and can be incorporated into the product. This project also demonstrates carbon-carbon bond formation utilizing the tandem photocatalytic pathway, highlighting its synthetic potential. Improvement upon the previously developed decarboxylative approach is

observed by utilising commercially available alkyl halide precursors, reducing the number of synthetic steps for α-alkylation. Utilising the dual catalytic system enables access to the single electron reduction of alkyl halides, substrates which until the advent of the dual catalytic mechanism, were previously difficult to access.

4.9 Bibliography

1. Van As, D. J.; Connell, T. U.; Brzozowski, M.; Scully, A. D.; Polyzos, A., *Org. Lett.* **2018,** *20* (4), 905-908.
2. Connell, T. U.; Fraser, C. L.; Czyz, M. L.; Smith, Z. M.; Hayne, D. J.; Doeven, E. H.; Agugiaro, J.; Wilson, D. J. D.; Adcock, J. L.; Scully, A. D.; Gómez, D. E.; Barnett, N. W.; Polyzos, A.; Francis, P. S., *J. Am. Chem. Soc.* **2019,** *141* (44), 17646-17658.
3. Indrajit Ghosh, T. G., Javier I. Bardagi, Burkhard König, *Science* **2014,** *346* (6210), 725-728.
4. Ghosh, I.; König, B., *Angew. Chem. Int. Ed.* **2016,** *55* (27), 7676-7679.
5. Shaikh, R. S.; Düsel, S. J. S.; König, B., *ACS Catal.* **2016,** *6* (12), 8410-8414.
6. Miller, K. L.; Williams, B. N.; Benitez, D.; Carver, C. T.; Ogilby, K. R.; Tkatchouk, E.; Goddard, W. A.; Diaconescu, P. L., *J. Am. Chem. Soc.* **2010,** *132* (1), 342-355.
7. Balaraman, E.; Gunanathan, C.; Zhang, J.; Shimon, L. J. W.; Milstein, D., *Nat. Chem.* **2011,** *3* (8), 609-614.
8. Zell, T.; Milstein, D., *Acc. Chem. Res.* **2015,** *48* (7), 1979-1994.
9. Narayanam, J. M. R.; Tucker, J. W.; Stephenson, C. R. J., *J. Am. Chem. Soc.* **2009,** *131* (25), 8756-8757.
10. Nguyen, J. D.; D'Amato, E. M.; Narayanam, J. M. R.; Stephenson, C. R. J., *Nat. Chem.* **2012,** *4* (10), 854-859.
11. Maji, T.; Karmakar, A.; Reiser, O., *J. Org. Chem.* **2011,** *76* (2), 736-739.
12. McTiernan, C. D.; Pitre, S. P.; Scaiano, J. C., *ACS Catal.* **2014,** *4* (11), 4034-4039.
13. Sakamoto, H.; Imai, J.; Shiraishi, Y.; Tanaka, S.; Ichikawa, S.; Hirai, T., *ACS Catal.* **2017,** *7* (8), 5194-5201.
14. Martinez-Haya, R.; Miranda, M. A.; Marin, M. L., *Eur. J. Org. Chem.* **2017,** *2017* (15), 2164-2169.
15. Ghosh, I.; Ghosh, T.; Bardagi, J. I.; König, B., *Science* **2014,** *346* (6210), 725-728.
16. Discekici, E. H.; Treat, N. J.; Poelma, S. O.; Mattson, K. M.; Hudson, Z. M.; Luo, Y.; Hawker, C. J.; de Alaniz, J. R., *Chem. Commun.* **2015,** *51* (58), 11705-11708.
17. Cheng, Y.; Gu, X.; Li, P., *Org. Lett.* **2013,** *15* (11), 2664-2667.
18. Kohls, P.; Jadhav, D.; Pandey, G.; Reiser, O., *Org. Lett.* **2012,** *14* (3), 672-675.
19. Ide, T.; Shimizu, K.; Egami, H.; Hamashima, Y., *Tetrahedron Lett.* **2018,** *59* (34), 3258-3261.
20. Feng, Z.-J.; Xuan, J.; Xia, X.-D.; Ding, W.; Guo, W.; Chen, J.-R.; Zou, Y.-Q.; Lu, L.-Q.; Xiao, W.-J., *Org. Biomol. Chem.* **2014,** *12* (13), 2037-2040.
21. Feng, Z.; Zeng, T.; Xuan, J.; Liu, Y.; Lu, L.; Xiao, W.-J., *Sci. China Chem.* **2016,** *59* (2), 171-174.
22. Condie, A. G.; González-Gómez, J. C.; Stephenson, C. R. J., *J. Am. Chem. Soc.* **2010,** *132* (6), 1464-1465.
23. Rueping, M.; Zhu, S.; Koenigs, R. M., *Chem. Commun.* **2011,** *47* (30), 8679-8681.
24. Kohls, P.; Jadhav, D.; Pandey, G.; Reiser, O., *Org. Lett.* **2012,** *14* (3), 672-675.
25. Clayden, J.; Greeves, N.; Warren, S. U., *Organic Chemistry*. 2nd ed.; OUP Oxford: 2012; p 1260.
26. De Vleeschouwer, F.; Van Speybroeck, V.; Waroquier, M.; Geerlings, P.; De Proft, F., *Org. Lett.* **2007,** *9* (14), 2721-2724.

27. Fischer, H., *Chem. Rev.* **2001,** *101* (12), 3581-3610.
28. Daikh, B. E.; Finke, R. G., *J. Am. Chem. Soc.* **1992,** *114* (8), 2938-2943.
29. Studer, A., *Chem. Eur. J.* **2001,** *7* (6), 1159-1164.
30. Leifert, D.; Studer, A., *Angew. Chem. Int. Ed.* **2020,** *59* (1), 74-108.

4.9 Experimental Procedures and Characterisation

General procedure for the alpha alkylation of tetrahydroisoquinolines

To a 4mL vial **4.9** (0.225 mmol, 47mg), K_2HPO_4 (0.450mmol, 87mg) and $[Ir(ppy)_2(dtbbpy)]PF_6$ (0.00563mmol, 5.14mg) were added. 2mL of methanol and a stirrer bar was added to the vial along with 0.338mmol of alkyl iodide if non-volatile. The following solution was then sparged with nitrogen to degas. If the alkyl iodide is volatile, it was then injected to the solution. The vials lid was then wrapped with Teflon tape and parafilm then irradiated while stirring for 44 hours. The reaction was then taken and solids were filtered and remaining solution evaporated. Crude solution was then purified via preparatory thin layered chromatography (0-10% ethyl acetate in hexane) to give pure product.

General procedure for the α-alkylation reaction in flow

To a 4mL via fitted with a rubber septum, **4.9** (0.281mmol 58.8mg), KOAc (0.563mmol, 55.2mg) and $Ir(ppy)_2(dtbbpy)PF_6$ (0.007mmol, 6.4mg) were added. 2.5mL of methanol, iodocyclohexane (0.420mmol 54.3µL) and stirrer bar were added to the vial. The solution was lightly sparged with nitrogen gas, then taken and injected into a 2 mL sample loop. The reaction was then pumped at the specified flow rate (Table 4.5) through the irradiated 4mL reactor coil and collected in a round bottom flask. Upon collection the crude reaction mixture was evaporated and redissolved in EtOAc then filtered and reevaporated. The crude sample was analysed via ^1H NMR spectroscopy or purified via preparatory thin layered chromatography.

Characterisation

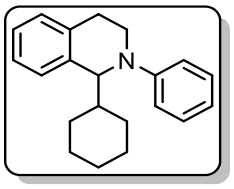

1-cyclohexyl-2-phenyl-1,2,3,4-tetrahydroisoquinoline 4.13/4.19a

Yield 91%-yellow oil; **HRMS** [M+H] calculated for [$C_{21}H_{25}N$+H] 292.20652 observed 292.20595; **^{1}H NMR** (400 MHz, CDCl3): δ 7.23 (t, J= 7.3 Hz, 2H), 706-7.18 (m, 4H), 4.43 (d, J=8.1 Hz,1H), 3.71-3.77 (m, 1H), 3.44-3.51 (m, 1H), 2.97-3.08(m, 2H) 1.99 (d, 10.5 Hz, 1H) 1.63-1.77 (m, 5H), 1.02-1.20 (m, 5H); **^{13}C NMR** (100 MHz $CDCl_3$) :δ 26.52, 26.54, 26.88, 27.50, 30.77, 31.03, 43.08, 44.21, 63.84, 113.01, 116.11, 125.28, 126.68, 128.28, 128.46, 129.21, 135.40, 137.95, 150.06; **FTIR** (ν/cm^{-1}, neat): 3095, 3061, 3024, 2921, 2849, 1596, 1502, 1449, 1392, 1321, 1281, 1212, 1156, 1035, 987, 934, 745, 689.

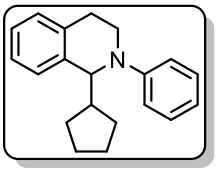

1-cyclopentyl-2-phenyl-1,2,3,4-tetrahydroisoquinoline 4.19b

Yield 76% yellow oil; **HRMS** [M+H] calculated for [$C_{20}H_{23}N$ + H] 278.19087 observed 278.19405; **^{1}H NMR** (400 MHz, CDCl3):δ 7.20 (t, *J* = 7.9 Hz, 2H), 7.17 – 7.06 (m, 4H), 6.89 (d, *J* = 8.2 Hz, 2H), 6.68 (t, *J* = 7.2 Hz, 1H), 4.53 (d, *J* = 8.8 Hz, 1H), 3.69 (ddd, *J* = 38.7, 18.9, 5.9 Hz, 2H), 3.08 – 2.96 (m, 1H), 2.88 (dt, *J* = 16.2, 5.4 Hz, 1H), 2.40 – 2.24 (m, 1H), 1.88 – 1.78 (m, 1H), 1.73 – 1.61 (m, 3H), 1.56 – 1.38 (m, 4H); **^{13}C NMR** (100 MHz $CDCl_3$) :δ 149.97, 138.83, 134.83, 129.11, 128.57, 127.61, 127.48, 127.24, 126.45, 125.32, 116.75, 113.79, 62.72, 47.15, 41.94, 31.07, 30.60, 26.71, 25.14, 24.41; **FTIR** (ν/cm^{-1}, neat): 3061, 3022, 2956, 2867, 1597, 1502, 1451, 1392, 1323, 1219, 932, 746, 691.

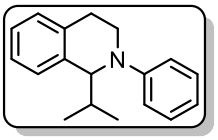

1-isopropyl-2-phenyl-1,2,3,4-tetrahydroisoquinoline 4.19c

Yield 81% yellow oil; **HRMS** [M+H] calculated for [$C_{18}H_{21}N$ + H] 252.17522 observed 252.17978; **^{1}H NMR** (400 MHz, $CDCl_3$) δ 7.23 (d, J = 8.0 Hz 2H), 7.20 – 7.07 (m, 4H), 6.87 (d, *J* = 8.2 Hz, 2H), 6.69 (t, J = 7.2 Hz 1H), 4.39 (d, *J* = 8.1 Hz, 1H), 3.74 (dt, *J* = 12.1, 6.0 Hz, 1H),), 3.47 (dt, *J* = 12.1, 6.0 Hz, 1H),), 3.00 (m, 2H), 2.14 (dd, *J* =14.1, 7.0 Hz, 1H), 1.07 (d, *J* = 6.9 Hz, 3H), 0.95 (d, *J* = 6.7 Hz, 3H); **^{13}C NMR** (100 MHz, $CDCl_3$) δ 149.98, 137.66, 135.27, 129.08, 128.25, 128.09, 126.56, 125.24, 116.42, 113.13, 64.58, 42.98, 34.38, 27.35, 20.62, 20.08; **FTIR** (ν/cm^{-1}, neat):3098, 3092, 3034, 3023, 2597, 2928, 2870, 1662, 1595, 1502, 1472, 1392, 1323, 1296, 122, 1156, 1036, 987, 935, 745, 691.

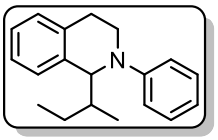

1-(sec-butyl)-2-phenyl-1,2,3,4-tetrahydroisoquinoline 4.19d

Yield 59% yellow oil; **HRMS** [M+H] calculated for [$C_{19}H_{23}N$ + H] 266.19087 observed 266.19608; **^{1}H NMR** (400 MHz, $CDCl_3$) δ 7.22 (dd, *J* = 13.2, 5.4 Hz, 2H), 7.13 (qd, *J* = 8.4, 4.1 Hz, 4H), 6.85 (d, *J* = 8.2 Hz, 2H), 6.68 (t, *J* = 7.1 Hz, 1H), 4.46 (t, *J* = 8.8 Hz, 1H), 3.72 (ddd, *J* = 11.9, 5.9, 2.3 Hz, 1H), 3.50 – 3.39 (m, 1H), 3.09 – 2.88 (m, 2H), 1.71 (dddd, *J* = 13.2, 11.2, 7.6, 4.1 Hz, 2H), 1.26 – 1.14 (m, 1H), 1.04 – 0.86 (m, 6H); **^{13}C NMR** (100 MHz $CDCl_3$) :δ 150.07, 149.95, 138.17, 137.92, 135.36, 129.08, 128.23, 128.16, 126.53, 125.27, 116.38, 113.10, 63.70, 63.25, 43.22, 43.15, 41.22, 41.15, 27.39, 26.61, 26.20, 16.39, 12.19, 11.76; **FTIR** (ν/cm^{-1}, neat): 3061, 3022, 2950, 2930, 2874, 1596, 1502, 1474, 1392, 1322, 1298, 1217, 1155, 1038, 987, 935,745, 690.

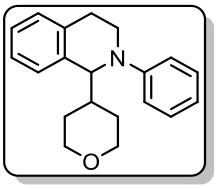

2-phenyl-1-(tetrahydro-2H-pyran-4-yl)-1,2,3,4-tetrahydroisoquinoline 4.19e

Yield 54% yellow oil; **HRMS** [M+H] calculated for [$C_{20}H_{23}NO$ + H] 294.18579 observed 294.1905; **^{1}H NMR** (400 MHz, CDCl3):δ 7.24 – 7.10 (m, 5H), 7.06 (d, *J* = 7.1 Hz, 1H), 6.87 (d, *J* = 8.3 Hz, 2H), 6.70 (t, *J* = 7.2 Hz, 1H), 4.43 (d, *J* = 8.7 Hz, 1H), 3.97 (td, *J* = 11.7, 3.5 Hz, 2H), 3.72 (dt, *J* = 12.5, 6.3 Hz, 1H), 3.51(dt, *J* = 12.5, 6.3 Hz, 1H), 3.31 (td, *J* = 12.0, 1.9 Hz, 1H), 3.23 (td, *J* = 11.6, 2.6 Hz, 1H), 3.07 – 2.92 (m, 2H), 2.03 – 1.91 (m, 1H), 1.85 (d, *J* = 13.5 Hz, 1H), 1.60 – 1.45 (m, 3H); **^{13}C NMR** (100 MHz $CDCl_3$) :δ 27.03, 30.83, 30.89, 41.49, 42.75, 63.19, 67.89, 68.32, 113.35, 116.87, 125.32, 126.86, 128.31, 128.57, 129.17, 135.12, 136.77, 149.83; **FTIR** (ν/cm^{-1}, neat): 3060, 3022, 2947, 2916, 2842, 2759, 1736, 1597, 1503, 1388, 1322, 1272, 1237, 1134,1091, 983, 936, 879, 748, 692.

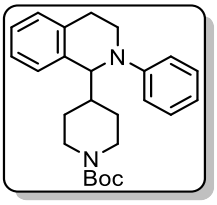

tert-butyl 4-(2-phenyl-1,2,3,4-tetrahydroisoquinolin-1-yl)piperidine-1-carboxylate 4.19f

Yield 59%, yellow oil; **HRMS** calculated for [$C_{25}H_{32}N_2O_2$ + H] 393.25420 observed 393.2618; **^{1}H NMR** (400 MHz, CDCl3):δ 7.03-7.23(m 5H), 6.85 (d, *J* = 7.7 Hz, 2H), 6.70 (t, *J* = 7.0 Hz, 1H), 4.43 (d, *J* = 8.4 Hz, 1H), 4.11 (s-Br, 2H), 3.73 (dt, *J* = 11.9, 5.9 Hz, 1H), 3.54 – 3.44 (m, 1H), 3.00 (t, *J* = 6.3 Hz, 2H), 2.57 (m, 2H), 1.90 (t, *J* = 13.5 Hz, 2H), 1.62 (d, *J* = 12.8 Hz, 1H), 1.44 (s, 9H), 1.38 – 1.19 (m, 3H); **^{13}C NMR** (100 MHz

$CDCl_3$) :δ 27.26, 28.58, 29.83, 29.93, 30.17, 42.70, 44.17, 63.20, 77.36, 79.45, 113.46, 117.05, 125.54, 127.05, 128.38, 128.57, 129.33, 135.29, 136.94, 149.86, 154.85; **FTIR** (ν/cm^{-1}, neat): 3062, 3007, 2974, 2919, 2852, 1684, 1596, 1503, 1475, 1423, 1391, 1365, 1322, 1277, 1248, 1127, 1160, 965, 923, 869, 748, 691.

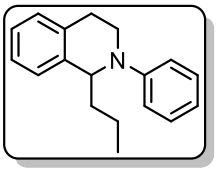

2-phenyl-1-propyl-1,2,3,4-tetrahydroisoquinoline 4.19g

Yield 80% yellow oil; **HRMS** [M+H] calculated for [$C_{18}H_{21}N$ + H] 252.17522 observed 252.17845; **^{1}H NMR** (400 MHz, $CDCl_3$) δ 7.24 – 7.19 (t, J = 7.4 Hz 2H), 7.18 – 7.07 (m, 4H), 6.86 (d, *J* = 8.0 Hz, 2H), 6.70 (t, *J* = 7.1 Hz, 1H), 4.65 (t, *J* = 7.0 Hz, 1H), 3.67 – 3.51 (m, 2H), 3.07 – 2.94 (m, 1H), 2.85 (dt, *J* = 22.2, 8.6 Hz, 1H), 1.99 – 1.88 (m, 1H), 1.68 (d, *J* = 36.5 Hz, 1H), 1.45 (dt, *J* = 26.2, 12.0 Hz, 2H), 0.93 (t, *J* = 7.3 Hz, 3H); **^{13}C NMR** (100 MHz $CDCl_3$) :δ 149.63, 139.13, 134.96, 129.21, 128.45, 127.28, 126.34, 125.68, 116.84, 113.58, 58.94, 41.81, 38.98, 27.08, 20.08, 14.15; **FTIR** (ν/cm^{-1}, neat):3062, 3023, 2956, 2931, 2871, 1735, 1596, 1502, 1390, 1322, 1219, 1153, 1036, 929, 743, 689.

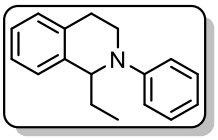

1-ethyl-2-phenyl-1,2,3,4-tetrahydroisoquinoline 4.19h

Yield 52%, orange-brown oil; **HRMS** [M+H] Calculated for [$C_{17}H_{19}N$ + H] 238.1551 observed 238.1577; **^{1}H NMR** (400 MHz, $cdcl_3$) δ 7.24 (t, *J* = 7.9 Hz, 2H), 7.19 – 7.09 (m, 4H), 6.88 (d, *J* = 8.4 Hz, 2H), 6.72 (t, *J* = 7.2 Hz, 1H), 4.56 (t, *J* = 7.0 Hz, 1H), 3.66 – 3.52 (m, 2H), 3.07 – 2.97 (m, 1H), 2.87 (dt, *J* = 15.9, 5.6 Hz, 1H), 1.98 (dt, *J* = 14.3,

7.2 Hz, 1H), 1.75 (dt, *J* = 14.1, 7.2 Hz, 1H), 1.00 (t, *J* = 7.4 Hz, 3H); **^{13}C NMR** (101 MHz, cdcl$_3$) δ 149.64, 138.80, 135.00, 129.19, 128.40, 127.37, 126.39, 125.67, 116.94, 113.65, 60.68, 42.01, 29.50, 27.22, 11.36; **FTIR** (ν/cm^{-1}, neat): 3094, 3061, 3029, 2958, 2929, 2871, 1597, 1501, 1478, 1390, 1331, 1295, 1222, 1155, 1035, 988, 938, 744, 690.

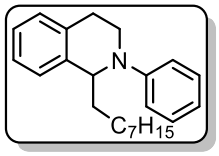

1-octyl-2-phenyl-1,2,3,4-tetrahydroisoquinoline 4.19i

Yield 50% orange-brown oil; **HRMS** [M+H] Calculated for [$C_{17}H_{19}N$ + H] 322.2490 observed 322.2524; **^{1}H NMR** (400 MHz, cdcl$_3$) δ 7.21 (t, *J* = 7.4 Hz, 2H), 7.17 – 7.07 (m, 4H), 6.86 (d, *J* = 8.3 Hz, 2H), 6.71 (t, *J* = 7.2 Hz, 1H), 4.63 (t, *J* = 7.0 Hz, 1H), 3.65 – 3.53 (m, 2H), 3.06 – 2.96 (m, 1H), 2.84 (dt, *J* = 15.9, 5.4 Hz, 1H), 2.00 – 1.89 (m, 1H), 1.75 – 1.62 (m, 1H), 1.51 – 1.19 (m, 13H), 0.86 (t, *J* = 6.8 Hz, 3H); **^{13}C NMR** (101 MHz, cdcl$_3$) δ 149.60, 139.15, 134.91, 129.19, 128.44, 127.28, 126.32, 125.67, 116.93, 113.69, 59.24, 41.83, 36.75, 31.84, 29.68, 29.54, 29.27, 27.02, 26.86, 22.63, 14.08; **FTIR** (ν/cm^{-1}, neat): 3062, 3024, 2954, 2923, 2853, 1598, 1503, 1391, 1331, 1221, 1034m 745, 691.

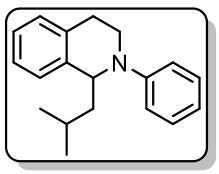

1-isobutyl-2-phenyl-1,2,3,4-tetrahydroisoquinoline 4.19j

Yield 56%, yellow oil; **HRMS** [M+H] calculated for [$C_{19}H_{23}N$ + H] 266.19087 observed 266.19624; **^{1}H NMR** (400 MHz, CDCl3):δ 7.21 (t, *J* = 8.0 Hz, 2H), 7.17 – 7.06 (m, 4H), 6.89 (d, *J* = 8.1 Hz, 2H), 6.71 (t, *J* = 7.1 Hz, 1H), 4.75 (t, *J* = 7.3 Hz, 1H), 3.62 (d, *J* = 39.9 Hz, 2H), 3.06 – 2.94 (m, 1H), 2.78 (dt, *J* = 16.0, 4.6 Hz, 1H), 1.95 – 1.84 (m, 1H), 1.79 – 1.67 (m, 1H), 1.51 (dt, *J* = 13.9, 6.9 Hz, 1H), 1.04 (d, *J* = 6.6 Hz, 3H), 0.94 (d, *J* =

6.5 Hz, 3H); **^{13}C NMR** (100 MHz $CDCl_3$) :δ 22.97, 23.07, 25.24, 26.60, 41.71, 46.03. 56.94, 114.34, 117.34, 125.82, 126.43, 127.33, 128.81, 129.36, 135.01, 139.56, 149.95; **FTIR** (ν/cm^{-1}, neat):3062, 3022, 2956, 2927, 2869, 1597, 1503, 1493, 1467, 1391, 1366, 1216, 1158,1031, 939, 748, 692.

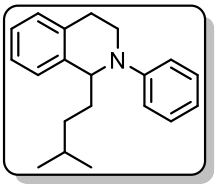

1-isopentyl-2-phenyl-1,2,3,4-tetrahydroisoquinoline 4.19k

Yield 63% pale yellow oil; **HRMS** [M+H] calculated for [$C_{20}H_{25}N$ + H] 280.20652 observed 280.21028; **^{1}H NMR** (400 MHz, CDCl3):δ 7.23 (t, *J* = 8.0 Hz, 2H), 7.20 – 7.06 (m, 4H), 6.87 (d, *J* = 8.4 Hz, 2H), 6.71 (t, *J* = 7.2 Hz, 1H), 4.62 (t, *J* = 7.1 Hz, 1H), 3.65 – 3.58 (m, 2H), 3.08 – 2.98 (m, 1H), 2.84 (dt, *J* = 16.0, 5.3 Hz, 1H), 2.02 – 1.90 (m, 1H), 1.77 – 1.65 (m, 1H), 1.54 (dt, *J* = 20.0, 6.7 Hz, 1H), 1.44 – 1.27 (m, 2H), 0.88 (dd, *J* = 8.6, 6.7 Hz, 6H); **^{13}C NMR** (100 MHz $CDCl_3$) :δ 22.72, 22.88, 27.09, 28.31, 34.83, 36.15, 41.82, 59.62, 113.85, 117.04, 125.84, 126.48, 127.45, 128.66, 129.37, 135.08, 139.42, 149.86; **FTIR** (ν/cm^{-1}, neat): 3064, 3023, 2954, 2931, 2869, 1596, 1502, 1467, 1389, 1365, 1205, 745, 691.

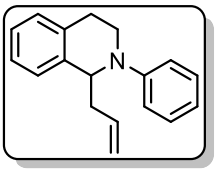

1-allyl-2-phenyl-1,2,3,4-tetrahydroisoquinoline 4.19l

Yield 78%, yellow-orange oil; **HRMS** [M+H] calculated for [$C_{18}H_{19}N$ + H] 250.15957 observed 250.1593; **^{1}H NMR** (400 MHz, CDCl3):δ 7.26 (t, 2H), 7.11-7.19 (m, 3H), 6.91 (d, *J* = 8.3 Hz, 2H), 6.75 (t, *J* = 7.2 Hz, 1H), 5.87 (ddt, *J* = 17.2, 10.1, 7.2 Hz, 1H), 5.09 (d, *J* = 11.0 Hz, 1H), 5.05 (d, *J* = 3.6 Hz, 1H), 4.76 (t, *J* = 6.8 Hz, 1H), 3.64 (m, 2H), 3.10

– 3.00 (m, 1H), 2.89 (dt, *J* = 15.9, 5.4 Hz, 1H), 2.74 (m, 1H), 2.50 (m, 1H); **^{13}C NMR** (100 MHz $CDCl_3$) :δ 27.53, 41.06, 42.03, 59.49, 113.98, 117.15, 117.33, 125.85, 126.68, 127.48, 128.63, 129.37, 135.09, 135.78, 138.26, 149.54; **FTIR** (ν/cm^{-1}, neat): 3063, 3023, 2976, 2914, 2837, 1597, 1502, 1391, 1330, 1222, 1155, 989, 94, 745, 691.

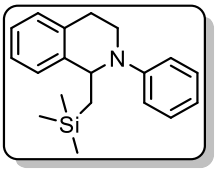

2-phenyl-1-((trimethylsilyl)methyl)-1,2,3,4-tetrahydroisoquinoline 4.19m

Yield 48%, yellow oil; **HRMS** [M+H] calculated for [$C_{19}H_{25}NSi$ + H] 296.18345 observed 296.18497; **^{1}H NMR** (400 MHz, CDCl3):δ 7.18 (t, *J* = 7.9 Hz, 7H), 7.14 – 6.99 (m, 12H), 6.86 (d, *J* = 8.1 Hz, 6H), 6.72 (t, *J* = 7.2 Hz, 3H), 4.81 (dd, *J* = 9.7, 6.0 Hz, 3H), 3.71 – 3.53 (m, 6H), 2.96 – 2.83 (m, 3H), 2.70 – 2.59 (m, 3H), 1.43 (dd, *J* = 15.1, 9.9 Hz, 3H), 1.11 (dd, *J* = 15.1, 6.0 Hz, 3H), -0.02 (s, 27H); **^{13}C NMR** (100 MHz $CDCl_3$) :δ 149.70, 141.46, 134.15, 129.09, 128.89, 126.88, 126.00, 125.81, 118.02, 115.92, 55.27, 42.13, 26.68, 25.66, 0.98; **FTIR** (ν/cm^{-1}, neat): 3274, 3063, 2950, 2898, 1597, 1492, 1376, 1246, 1025, 922, 849, 746, 691.

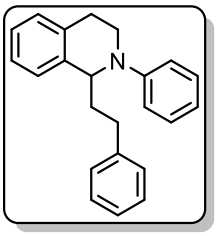

1-phenethyl-2-phenyl-1,2,3,4-tetrahydroisoquinoline 4.19n

Yield 10%, Yellow oil; **HRMS** [M+H] calculated for [$C_{23}H_{23}N$ + H] 314.1909 observed 314.1904; **^{1}H NMR** (400 MHz, cdcl$_3$) δ 7.30 – 7.10 (m, 11H), 6.83 (d, *J* = 8.1 Hz, 2H), 6.71 (t, *J* = 7.2 Hz, 1H), 4.67 (t, *J* = 7.0 Hz, 1H), 3.64 (dd, *J* = 7.0, 5.3 Hz, 2H), 3.05 (ddd,

J = 23.1, 14.5, 7.2 Hz, 2H), 2.88 – 2.66 (m, 3H), 2.35 – 2.21 (m, 1H), 2.12 – 1.97 (m, 1H); **^{13}C NMR** (101 MHz, cdcl$_3$) δ 149.64, 141.89, 138.76, 134.99, 129.19, 128.62, 128.46, 128.32, 127.24, 126.45, 125.79, 117.25, 114.15, 58.40, 41.81, 38.33, 32.88, 26.77.

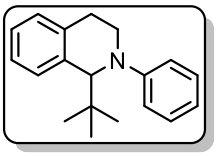

1-(tert-butyl)-2-phenyl-1,2,3,4-tetrahydroisoquinoline 4.19o

Yield 28%, blue-purple oil; **HRMS** [M+H] calculated for [$C_{19}H_{23}N$ + H] 266.1909 observed 266.1929; **^{1}H NMR** (400 MHz, CDCl3):δ 7.23 – 7.08 (m, 6H), 6.91 (d, *J* = 7.7 Hz, 2H), 6.66 (t, *J* = 7.0 Hz, 1H), 4.66 (s, 1H), 3.92 – 3.82 (m, 1H), 3.58 – 3.41 (m, 1H), 3.01 (dt, *J* = 16.4, 9.5 Hz, 2H), 1.02 (s, 9H); **^{13}C NMR** (100 MHz, cdcl$_3$) δ 135.40, 128.93, 128.71, 128.30, 126.53, 125.01, 116.60, 114.15, 66.00, 43.98, 39.13, 29.17, 27.28; **FTIR** (ν/cm^{-1}, neat):3060, 3023, 2969, 2955, 2930, 2868, 1640, 1595, 1502, 1394, 1294, 1213 1033, 929, 766, 747, 693.

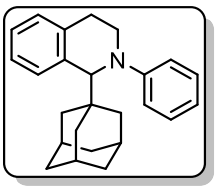

1-((3r,5r,7r)-adamantan-1-yl)-2-phenyl-1,2,3,4-tetrahydroisoquinoline 4.19p

Yield 45%, blue oil; **HRMS** [M+H] calculated for [$C_{25}H_{29}N$ + H] 344.2334 observed 344.23354; **^{1}H NMR** (400 MHz, CDCl3):δ 7.16 (dt, *J* = 14.7, 6.4 Hz, 6H), 6.93 (d, *J* = 8.2 Hz, 2H), 6.66 (t, *J* = 7.1 Hz, 1H), 4.54 (s, 1H), 3.96 – 3.83 (m, 1H), 3.46 (dd, *J* = 19.3, 8.0 Hz, 1H), 3.16 (dt, *J* = 15.8, 7.7 Hz, 1H), 2.99 – 2.87 (m, 1H), 1.92 (s, 3H), 1.74 (d, *J* = 11.8 Hz, 3H), 1.59 (q, *J* = 12.2 Hz, 10H); **^{13}C NMR** (100 MHz CDCl$_3$) :δ 27.94, 28.98,

36.96, 40.99, 41.49, 45.30, 67.10, 113.89, 116.42, 125.12, 126.75, 128.19, 129.04, 129.23, 135.68, 136.40, 151.36; **FTIR** (ν/cm^{-1}, neat): 2904, 2850, 1536, 1493, 1449, 1279, 1204, 1155, 1105, 1082, 849, 747, 693, 661.

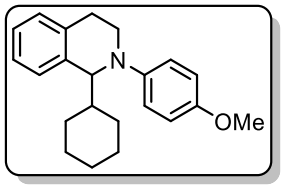

1-cyclohexyl-2-(4-methoxyphenyl)-1,2,3,4-tetrahydroisoquinoline 4.20a

yield 62%; **HRMS** [M+H] calculated for [$C_{22}H_{27}NO$ + H] 322.21708 observed 322.2189; **^{1}H NMR** (400 MHz, CDCl3):δ 7.19 – 7.05 (m, 4H), 6.80 (s, 4H), 4.24 (d, *J* = 8.0 Hz, 1H), 3.79 – 3.64 (m, 4H), 3.44 (dt, *J* = 12.5, 6.4 Hz, 1H), 3.02 – 2.84 (m, 2H), 2.01 (d, *J* = 12.0 Hz, 1H), 1.77 – 1.61 (m, 5H), 1.20 – 0.98 (m, 5H); **^{13}C NMR** (100 MHz $CDCl_3$) :δ 151.47, 144.97, 137.75, 135.28, 128.45, 128.37, 126.36, 124.99, 115.32, 114.59, 64.49, 55.73, 43.96, 43.43, 30.96, 30.72, 26.84, 26.67, 26.45; **FTIR** (ν/cm^{-1}, neat): 2924, 2850, 1508, 1449, 1242, 1181, 1035, 934, 812, 748, 661.

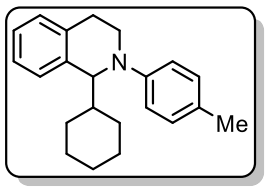

1-cyclohexyl-2-(p-tolyl)-1,2,3,4-tetrahydroisoquinoline 4.20b

yield 63%; **HRMS** [M+H] calculated for [$C_{22}H_{27}N$ + H] 306.22217 observed 306.2309; **^{1}H NMR** (400 MHz, CDCl3):δ 7.18 – 6.99 (m, 6H), 6.77 (d, *J* = 8.5 Hz, 2H), 4.35 (d, *J* = 8.1 Hz, 1H), 3.71 (dt, *J* = 12.3, 6.2 Hz, 1H), 3.50 – 3.41 (m, 1H), 2.97 (t, *J* = 6.5 Hz, 2H), 2.23 (s, 3H), 2.00 (s, 1H), 1.67 (dd, *J* = 38.3, 6.3 Hz, 5H), 1.19 – 1.02 (m, 5H); **^{13}C NMR** (100 MHz $CDCl_3$) :δ 148.13, 138.00, 135.47, 129.75, 128.52, 128.37, 126.58,

125.66, 125.19, 113.48, 64.04, 44.21, 43.17, 34.64, 31.08, 30.83, 27.32, 26.80, 26.58, 20.32; **FTIR** (ν/cm^{-1}, neat): 2920, 2850, 1617, 1515, 1448, 1391, 1317, 1199, 1150, 935, 795, 749.

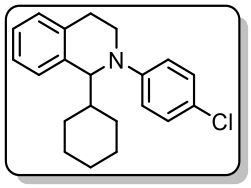

2-(4-chlorophenyl)-1-cyclohexyl-1,2,3,4-tetrahydroisoquinoline 4.20c

yield 52%; **HRMS** [M+H] calculated for [$C_{21}H_{24}NCl$ + H] 326.16755 observed 326.1730; **^{1}H NMR** (400 MHz, $CDCl_3$) δ 7.19 – 7.09 (m, 5H), 7.09 – 7.03 (m, 1H), 6.75 (d, *J* = 9.1 Hz, 2H), 4.34 (d, *J* = 8.3 Hz, 1H), 3.69 (dt, *J* = 11.9, 6.0 Hz, 1H), 3.40 (ddd, *J* = 12.0, 8.0, 6.4 Hz, 1H), 3.08 – 2.90 (m, 2H), 1.92 (d, *J* = 12.3 Hz, 1H), 1.78 – 1.57 (m, 5H), 1.19 – 0.95 (m, 5H); **^{13}C NMR** (100 MHz $CDCl_3$) :δ 148.65, 137.63, 135.11, 128.95, 128.40, 128.34, 126.88, 125.44, 114.22, 64.10, 44.19, 43.39, 31.08, 30.81, 27.38, 26.73, 26.49, 26.47; **FTIR** (ν/cm^{-1}, neat):2924, 2851, 1595, 1495, 1449, 1327, 805, 753.

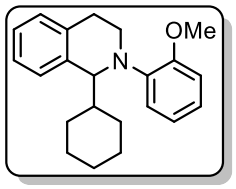

1-cyclohexyl-2-(2-methoxyphenyl)-1,2,3,4-tetrahydroisoquinoline 4.20d

yield 62%; **HRMS** [M+H] calculated for [$C_{22}H_{27}NO$ + H] 322.21708 observed 322.2169; **^{1}H NMR** (400 MHz, CDCl3):δ 7.16 – 6.99 (m, 4H), 6.85 (m, 2H), 6.78 – 6.70 (m, 2H), 4.08 (d, *J* = 8.1 Hz, 1H), 3.84 (s, 3H), 3.68 – 3.58 (m, 2H), 2.83 (dt, *J* = 17.0, 8.6 Hz, 1H), 2.68 (dt, *J* = 16.7, 4.2 Hz, 1H), 2.11 (d, *J* = 12.5 Hz, 1H), 1.70 (m, 5H), 1.23 – 1.00 (m,

5H); **^{13}C NMR** (100 MHz $CDCl_3$) :δ 152.70, 141.79, 138.30, 135.19, 128.93, 128.50, 125.99, 124.70, 121.67, 121.24, 120.96, 112.23, 64.99, 55.72, 43.17, 42.79, 31.23, 31.05, 26.97, 26.69, 26.58, 26.44; **FTIR** (ν/cm^{-1}, neat): 2921, 2850, 1592, 1498, 1450, 1236, 1177, 1113, 1029, 933, 743, 663.

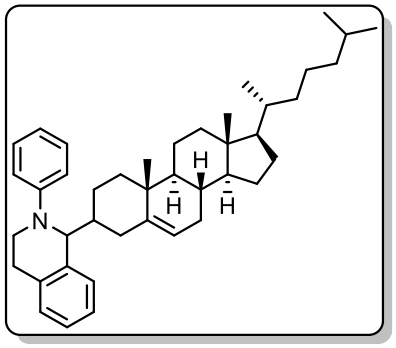

1-((8S,9S,10R,13R,14S,17R)-10,13-dimethyl-17-((R)-6-methylheptan-2-yl)-2,3,4,7,8,9,10,11,12,13,14,15,16,17-tetradecahydro-1H-cyclopenta[a]phenanthren-3-yl)-2-phenyl-1,2,3,4-tetrahydroisoquinoline 4.22

Yield 33%, Yellow Oil; **HRMS** [M+H] calculated for [$C_{42}H_{59}N$ + H] 578.4726 observed 578.4704; **^{1}H NMR** (400 MHz, cdcl$_3$) δ 7.23 – 7.02 (m, 11H), 6.90 – 6.83 (m, 4H), 6.64 (ddd, *J* = 14.5, 12.2, 7.2 Hz, 2H), 5.56 – 5.27 (m, 1H), 5.18 – 5.03 (m, 1H), 4.67 (dd, *J* = 20.5, 10.8 Hz, 1H), 4.44 (dd, *J* = 11.3, 8.3 Hz, 1H), 3.82 – 3.63 (m, 3H), 3.57 – 3.43 (m, 1H), 3.16 – 3.03 (m, 1H), 3.02 – 2.93 (m, 2H), 2.86 – 2.71 (m, 1H), 2.48 – 2.24 (m, 2H), 2.24 – 2.03 (m, 4H), 2.01 – 0.79 (m, 85H), 0.69 (d, *J* = 3.7 Hz, 3H), 0.66 (s, 2H).

Stern-Volmer Quenching Experiments

Fluorescence quenching experiments were conducted on a Varian Cary Eclipse fluorescence spectrophotometer. Experiments were conducted with $[Ir(ppy)_2(dtbbpy)]PF_6$ (0.1mM) in methanol with quencher at varied concentrations. Experiments were carried out with an excitation wavelength of 454nm

Formation of Ir-2 species

The emission spectrum of a degassed solution of $[Ir(ppy)_2(dtbbpy)]PF_6$ (0.1mM) and **4.9** (50 mM) in methanol was measured with an excitation wavelength of 454nm and scanning between 465-650nm. The same solution was then taken and re-sparged by lightly bubbling N_2 for 10 minutes. The Ir-THIQ solution was irradiated with a 14W blue light source for 30 minutes under a blanket of nitrogen before scanning the emission spectrum again- revealing the transformation to **Ir-2**.

Quenching of Ir-2 species with iodopropane

A solution of $[Ir(ppy)_2(dtbbpy)]PF_6$ (0.1mM) and DIPEA (50 mM) in methanol was sparged lightly for 10 minutes, this solution was then under a blacket of N_2 gas irradiated for 1 minute and the emission spectra measured with a an excitation wavelength of 454nm and scanning between 465-650nm. Upon scanning 5µL of iodopropane was injected with a microsyringe into the Ir-DIPEA solution and the measurement of emission spectra was repeated. Successive multiples of 5µL of iodopropane were injected into the Ir-DIPEA solution and the emission spectra was again measured, the data was recorded and Stern-Volmer quenching was plotted.

Cyclic Voltammetry

Cyclic Voltammetry experiments were conducted on a Potentiostat 466 using Ag/AgCl, Carbon and platinum electrodes as the reference, working and auxiliary electrodes respectively. Tetrabutylammoniumhexafluorophosphate was used as an electrolyte being dissolved in acetonitrile as solvent as a with a 0.1mol concentration. Analyte was added to the electrolyte solution to make a 5mmol.

Radical trapping with methyl vinyl ketone

To a 4mL vial with inbuilt rubber septa lid, **4.9** (0.225 mmol, 47mg), K_2HPO_4 (0.450 mmol, 87mg) and $[Ir(ppy)_2(dtbbpy)]PF_6$ (0.00561 mmol, 5.14mg) were added. 2mL of methanol and stirrer bar was added to the vial along with 0.338mmol (43.7µL) of cyclohexyl iodide. The following solution was then lightly sparged with nitrogen to degas. Methyl vinyl ketone (0.675mmol 56.3µL) was then injected into the reaction vial and then closed off with parafilm and Teflon tape. The reaction mixture was then stirred under irradiation by 14W blue light for 44 hours. The crude reaction mixture was then taken, and solids were filtered, the remaining solution was evaporated to dryness. The crude reaction mixture was then purified via preparatory thin layered chromatography to give the radical trapped product **4.30** in 53%.

5.0 Conclusions

Throughout this thesis, three new methodologies for the synthesis and functionalisation of amines were developed. Each protocol exploits the photogeneration of α-amino radicals as key intermediates to pursue underexplored reaction pathways. Initially, a methodology for the visible-light mediated transfer hydrogenation of diarylimines catalysed by $[Ir(ppy)_2(dtbbpy)]PF_6$ was established. This procedure is achieved via a reductive quenching cycle which utilises triethylamine as both a sacrificial reductant and hydrogen source. The key step in this procedure involves the single electron reduction of an imine facilitated by PCET to the corresponding α-amino radical, with subsequent hydrogen abstraction from triethylamine conferring the desired diphenylmethamine. This methodology provides mild conditions for the synthesis of the diphenylmethamine scaffold, exhibiting excellent yields and chemoselectivity. A flow protocol provided reduced reaction times while simultaneously presenting an attractive method towards scaling this process whilst retaining chemoselectivity. Further studies in the Polyzos group revealed this methodology proceeds via a tandem photocatalytic process, conferring the ability to access reduction potentials beyond that $[Ir(ppy)_2(dtbbpy)]PF_6$ can theoretically access.

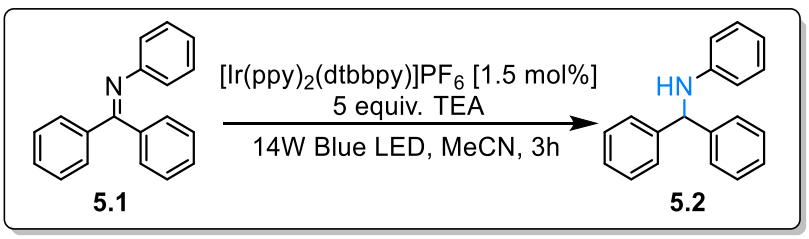

Figure 5.1: Summary of the visible-light mediated transfer hydrogenation of diarylimines

Next, a protocol for the decarboxylative α-alkylation of amines was developed, this methodology employed NHP esters as alkyl radical precursors, coupling with α-amino radicals via a redox-neutral process. The addition of co-reductant, $HNPh_2$ is hypothesised to provide an alternative mode of reactivity for α-amino radical generation, this pathway proceeds simultaneously and enables improved yields. A flow protocol was then established, allowing for: further enhanced yields, reduced reaction times and the reduction in equivalents of both NHP ester and $HNPh_2$. Upon optimisation, a variety of potentially biologically active substrates were synthesised in typically good yields.

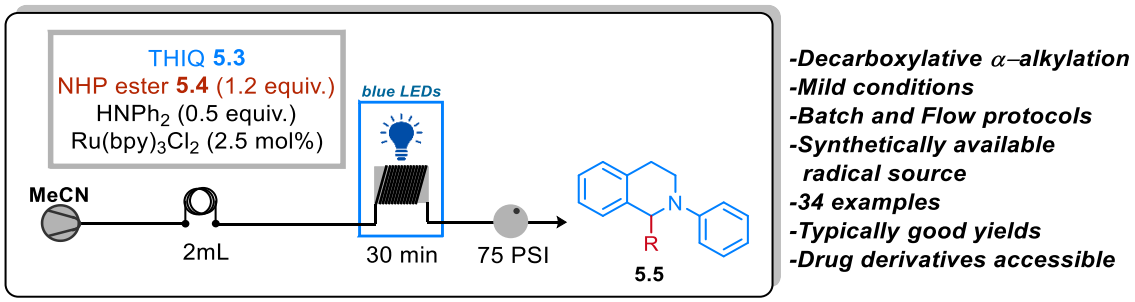

Figure 5.2: Summary of the decarboxylative α-alkylation of THIQ derivatives via radical-radical coupling in flow

Having realised that the transfer hydrogenation of diarylimines proceeds via a tandem catalytic cycle, accessing a highly reducing species, further exploration of this system towards the α-alkylation of THIQ derivatives was conducted. Energy demanding alkyl halides were used as cross-coupling partners. The tandem photocatalytic cycle permitted the single electron reduction of alkyl halides, substrates with theoretical reduction potentials beyond that accessible by photocatalyst $[Ir(ppy)_2(dtbbpy)PF_6$. Thorough quenching studies indicate that both the single electron reduction of alkyl halides as well as a radical-radical coupling process proceeds to impart carbon-carbon bond formation. This transformation enabled the α-alkylation of THIQ derivatives in typically good yields and represents a pathway for the synthesis of potentially biologically active molecules from commercially available substrates.

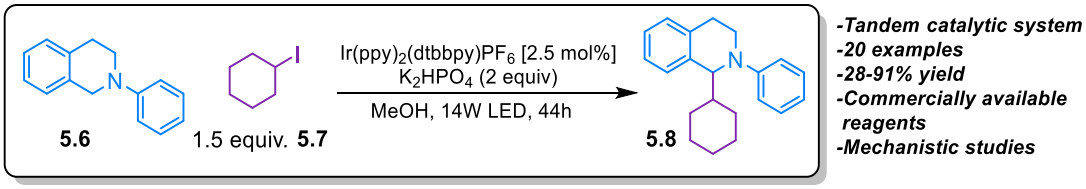

Figure 5.3: Summary of the α-alkylation of THIQ derivatives accessed by the tandem catalytic cycle.

This thesis explored the generation of α-amino radicals via visible light mediated catalysis and investigated their reactivity towards lesser examined reaction pathways. Three methodologies were developed which access α-amino radicals and their reactivity via: the single electron reduction of imines, radical-radical coupling and a tandem photocatalytic pathway. Upon optimization, each of these processes were successfully transferred to a flow protocol substantially enhancing each reaction's conditions.

Appendix 1: General Methods

Materials and Methods

Commercially available starting materials and reagents were purchased at the highest quality and used without further purification unless stated otherwise. Solvents were commercially purchased at reagent grade or greater. $[Ir(ppy)_2(dtbbpy)]PF_6$ was prepared according to the method of Tordera and Baranoff.[1] Flash chromatography was performed with silica gel (Merck Kieselgel 60, 0.040-0.063 mm) according to the method of Still *et al.*[2] Analytical thin-layer chromatography (TLC) was performed on Merck Kieselgel 60F254 aluminium backed plates and visualized using a 254 nM UV lamp and a combination of vanillin stain and heat Preparatory thin layered chromatography plates were conducted using Analtech silica gel matrix preparative TLC plates (1.00 mm)

Analytical Information

NMR spectroscopy was recorded on a Varian MR-400 instrument at 400.13 MHz for ^{1}H nuclei and at 100.61 MHz for ^{13}C nuclei. Samples were recorded in deuterated solvent as specified, and data was acquired at 25 °C. Chemical shifts are reported as δ values in parts per million (ppm). In reporting spectral data, the following abbreviations have been used: s, singlet; br s, broad singlet; d, doublet; t, triplet; q, quartet; quint., quintet; m, multiplet.

High resolution mass spectrometry analysis was performed on an Agilent 6520 Quadrupole Time of Flight (Q-TOF) mass spectrometer coupled to an Agilent 1100 autosampler system and controlled via MassHunter software package B.05.01. ESI solutions (~5 ppm) were prepared in HPLC grade acetonitrile and transferred to the electrospray source by an autosampler. For each analysis, 1 µL of sample was injected into the carrier solvent stream of 0.1% formic acid in 70% acetonitrile at a flow rate of 0.3 mL per minute. Recorded m/z data were corrected using a reference mass by a dual-

spray electrospray ionization source and using the factory-defined calibration pressure. Mass spectrometer conditions: drying gas flow rate, 7 L min–1; nebulizer pressure, 40 psi; drying gas temperature, 300 °C; capillary voltage, 4000 V; skimmer voltage, 65 V; Oct Rf, 750 V; scan range acquired, 100-1000 m/z.

Infrared spectra were recorded neat on a Perkin Elmer Spectrum 100 FT-IR in attenuated total reflectance (ATR) mode. Spectra were obtained between 4000 and 400 cm-1 using 8 scans.

Steady-state emission quenching experiments were recorded using a Varian Cary Eclipse Fluorescence Spectrophotometer.

All continuous flow reactions were performed using a Syrris Asia syringe pump module with a Syrris sample loop injector and standard 1/16" PFA tubing. Images of experimental flow setups can be seen in figures 2.27 and 3.17, while a typical continuous flow method can be observed in figure 3.20.

Transient absorption spectroscopy (TAS) measurements were performed using an Edinburgh Instruments LP900 spectrometer coupled with a nanosecond pulsed Nd3+YAG laser (Quantel, Brio), operating at 355 nm and 10 Hz repetition rate as the excitation source. The solution was deoxygenated immediately prior to measurement by bubbling with argon for approximately 6 min.

Cyclic Voltammetry experiments were conducted on an Edaq Potentiostat 466 using controlled by Echem software. Ag/AgCl, Carbon and platinum electrodes were utilised as the reference, working and auxiliary electrodes respectively. A 0.1 mol solution of Tetrabutylammoniumhexafluorophosphate was used as an electrolyte, dissolved in acetonitrile as solvent. Analytes were typically added to the electrolyte solution to make approximately 5mmol.

LED Photoreactors

All photoredox reactions were performed using a either a 40W PR160 Kessel lamp, or a custom-built blue LED photoreactor (Figure S1). The custom reactor was comprised of a square metal frame (100 mm × 110 mm) with 14 blue LEDs (2 × SP-02-V4 LED assembly, each consisting of 7 LXML-PR02-A900 Royal-Blue LUXEON Rebel ES LEDs; www.luxeonstar.com). The photoreactor was fitted with computer cooling fans and heat sinks for temperature control (internal temperature of the reactor typically reaches 27 ± 5 °C overnight). The power of the light source can be varied using an intensity control.

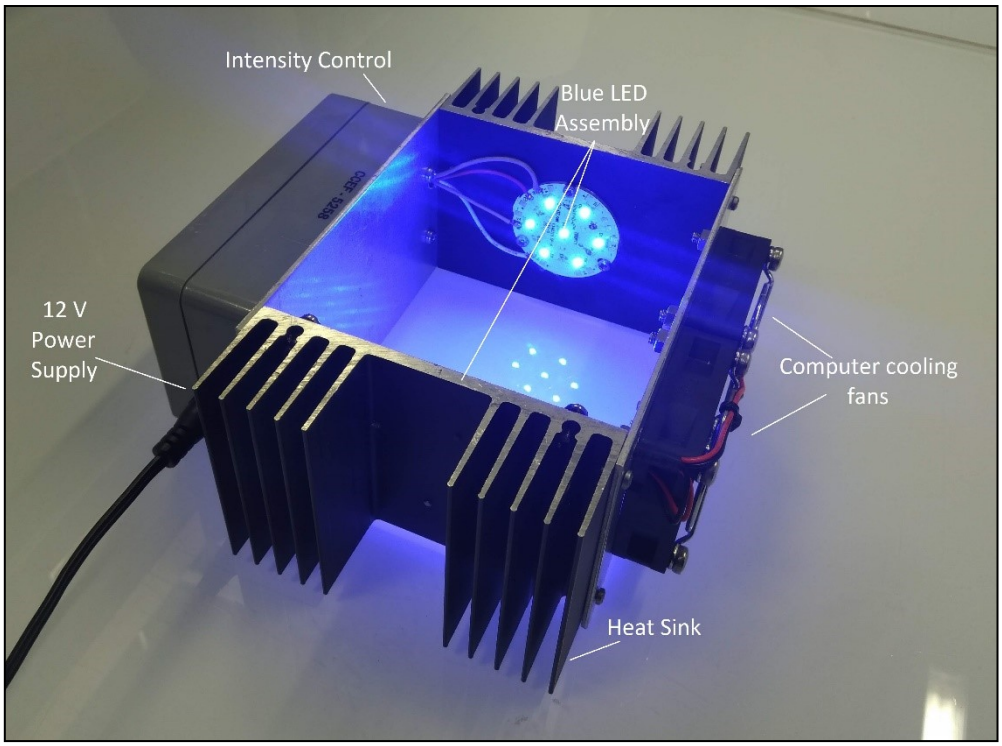

Figure S1: Annotated photo of custom built photoreactors

Appendix 2: Papers Published During this PhD

This page is left intentionally blank

Papers are attached on the following page

Organic LETTERS

Letter

Cite This: Org. Lett. 2018, 20, 905−908

pubs.acs.org/OrgLett

Photocatalytic and Chemoselective Transfer Hydrogenation of Diarylimines in Batch and Continuous Flow

Dean J. van As,[†] Timothy U. Connell,[‡] Martin Brzozowski,[†,§] Andrew D. Scully,[§] and Anastasios Polyzos*[,†,§]

[†]School of Chemistry, The University of Melbourne, Parkville, VIC 3010, Australia

[‡]School of Science, RMIT University, Melbourne, VIC 3000, Australia

[§]CSIRO Manufacturing, Clayton, VIC 3068, Australia

Supporting Information

ABSTRACT: A visible-light photocalytic method for the chemoselective transfer hydrogenation of imines in batch and continuous flow is described. The reaction utilizes Et_3N as both hydrogen source and single-electron donor, enabling the selective reduction of imines derived from diarylketimines containing other reducible functional groups including nitriles, halides, esters, and ketones. The dual role of Et_3N was confirmed by fluorescence quenching measurements, transient absorption spectroscopy, and deuterium-labeling studies. Continuous-flow processing facilitates straightforward scale-up of the reaction.

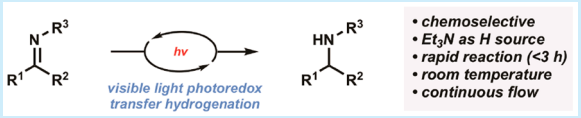

The ubiquity of aliphatic amines in nature has engendered this structural motif with prominence throughout families of biologically active molecules. The importance of this structural class to human health is evidenced by a wealth of pharmaceuticals, natural products, and agrochemicals exhibiting a broad spectrum of bioactivities including antibiotic, anticancer, and antiviral properties.[1] The prevalence of amines in biologically relevant small molecules necessitates the development of new, chemoselective methods for their preparation.

Photoredox catalysis has contributed to a renaissance in radical-based methods in organic synthesis. Building upon seminal studies in photocatalysis,[2] Yoon, MacMillan, and Stephenson demonstrated that visible light could be harnessed to access a range of new catalytic transformations.[3] These pioneering studies have led to a host of novel amine α-C(sp^3)−H functionalization reactions based on the oxidative formation of iminium ions and their subsequent trapping with (pro)-nucleophiles.[4] Alternatively, a reverse polarity reaction manifold is also accessible by intercepting the transient α-amino radical intermediate prior to iminium formation and coupling this species with electron-deficient olefins.[5] Examples of such umpolung amine functionalization are less common in comparison to the oxidative iminium approach due to the propensity of the α-amino radical to undergo overoxidation to the iminium ion. Within this context, single-electron reduction of imines has been investigated as an alternative means of generating α-amino radicals in a controlled fashion. Several groups have recently disclosed that imine substrates can be engaged in photoredox chemistry to affect dimerization,[6] alkylation,[7] allylation,[8] and aminomethylation[9] transformations.

Given the propensity for imines to undergo selective single-electron transfer (SET) reduction, we hypothesized that a visible-light-mediated, chemoselective imine transfer hydrogenation could be achieved using a photoredox catalysis manifold. Such a transformation would putatively exhibit high chemoselectivity for imines in the presence of functional groups typically susceptible to reduction under traditional hydrogenation conditions. Given the propensity of tertiary amines to undergo single-electron oxidation with mild oxidants ($E_{1/2}$ = +0.6−0.8 V),[10] together with the ability of the aminium radical cation to undergo facile hydrogen atom transfer (BDE = ∼42 kcal/mol),[11] we postulated that simple amine additives could serve the dual role of hydrogen source and single-electron oxidant (Scheme 1). Herein, we describe the development of a mild, chemoselective transfer hydrogenation reaction of diarylimines under visible-light irradiation in batch and continuous flow. The resulting benzhydrylamines are key structural motifs in δ opioid receptor agonists,[12] dopamine transporter ligands,[13] and histamine H_1 antagonists.[14]

Scheme 1. Mechanistic Hypothesis for Photoredox-Transfer Hydrogenation Reaction

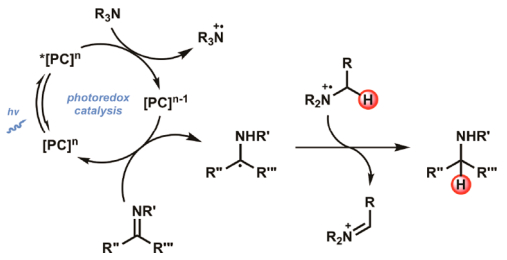

Preliminary optimization studies were conducted using ketimine **1a** and Et_3N in DMF (Table 1) with photocatalyst

Received: November 16, 2017
Published: January 30, 2018

DOI: 10.1021/acs.orglett.7b03565
Org. Lett. 2018, 20, 905−908

Table 1. Selected Optimization Experiments[a,b]

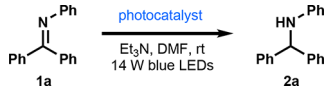

entry	deviation from above conditions	yield (%)[c]
1	$[Ru(bpy)_3]Cl_2.6H_2O$	39
2	fluorescein	26
3	Eosin Y	25
4	$Ir(ppy)_3$	25
5	$[Ir\{dF(CF_3)ppy\}_2(dtbbpy)]PF_6$	52
6	**$[Ir(ppy)_2(dtbbpy)]PF_6$**	**97**
7	$[Ir(ppy)_2(dtbbpy)]PF_6$, 2 equiv Et_3N	79
8	$[Ir(ppy)_2(dtbbpy)]PF_6$, 1 equiv Et_3N	39
9	**$[Ir(ppy)_2(dtbbpy)]PF_6$, MeCN, 3 h**	**>98**

[a]Reactions performed with imine (0.45 mmol), photocatalyst (1.5 mol %), Et_3N (5 equiv), DMF, 16 h, 14 W blue LEDs unless specified otherwise. [b]bpy = 2,2′-bipyridine; ppy = 2-phenylpyridine; $dF(CF_3)$-ppy = 2-(2,4-difluorophenyl)-5-(trifluoromethyl)pyridine; dtbbpy = 4,4′-di-*tert*-butyl-2,2′-bipyridine. [c]Yields were determined by ^1H NMR analysis using 2,5-dimethylfuran as internal standard.

selection guided by analysis of the electrochemical reduction potentials. Pleasingly, our design plan was promptly verified when irradiation of the reaction components and archetypal photocatalyst $[Ru(bpy)_3]Cl_2$ with 14 W blue LEDs for 16 h afforded the desired product **2a** in 39% yield (entry 1). Organic dyes fluorescein and Eosin Y exhibit similar oxidizing potential (E^0 [$*PC^n/PC^{n-1}$] ≈ + 0.8 V vs SCE)[15] relative to $[Ru(bpy)_3]Cl_2$ (E^0 [$*Ru^{II}/Ru^{I}$] = +0.77 V vs SCE in MeCN)[16] and should undergo reductive quenching in the presence of Et_3N (E^0 = +0.66 V vs $AgNO_3$ in MeCN). Both fluorescein and Eosin Y gave low yields of **2a** (entries 2 and 3), presumably due to diminished reducing power from the PC^{n-1} state (−1.22 and −1.08 V, respectively). The strongly reducing photocatalyst $Ir(ppy)_3$ (E^0 [Ir^{II}/Ir^{III}] = −2.19 V)[17] also gave a low yield of 25% (entry 4), which is rationalized by the excited state species being a comparatively weaker oxidant (E^0 [$*Ir^{III}/Ir^{II}$] = +0.31 V) than $[Ru(bpy)_3]Cl_2$.

The strongly oxidizing and reducing heteroleptic iridium complex $[Ir\{dF(CF_3)ppy\}_2(dtbbpy)]PF_6$ furnished a 52% yield of **2a** (entry 5). Near-quantitative yields were achieved using the analogous desfluorinated complex $[Ir(ppy)_2(dtbbpy)]PF_6$ (entry 6), which is also a potent reductant from the Ir(II) state (E^0 [Ir^{II}/Ir^{III}] = −1.51 V).[18] The reaction tolerated a range of different amine donors, with n-Bu_3N, i-Pr_2NEt, and triethanolamine each facilitating effective reduction of **1a**.[19] Stoichiometry investigations revealed that lowering the Et_3N loading from 5 to 1 equiv resulted in a significant decrease in reaction efficiency (entries 7 and 8). Polar, aprotic solvents were most effective, with MeCN giving quantitative conversion by ^1H NMR spectroscopic analysis within 90 min.[20] The optimal reaction conditions were selected as 1.5 mol % $[Ir(ppy)_2(dtbbpy)]PF_6$ photocatalyst and 5 equiv of Et_3N in MeCN with 3 h of visible light irradiation (entry 9). Control experiments showed that the reaction product was not formed in the absence of photocatalyst, visible light, or Et_3N.

With optimal reaction conditions established, we sought to evaluate the scope of *N*-aryl and *N*-alkyl substrates amenable to the transfer hydrogenation reaction (Scheme 2). The reaction proceeded in high yield with both electron-rich (**1a−e**) and electron-deficient (**1f−k**) *N*-aryl substrates. Unprotected phenol groups (**2e**) were viable, as were chloro and trifluoromethyl substituents (**2g,i**). Aryl iodide product **2h** could be isolated in

Scheme 2. Evaluation of *N*-Aryl and *N*-Alkyl Substrates[a]

[a]Reaction conditions: imine (0.45 mmol), photocatalyst (1.5 mol %), Et_3N (5 equiv), MeCN, 3 h, rt, 14 W blue LEDs. [b]Reaction time of 5 min.

91% yield with careful reaction monitoring. ^1H NMR spectroscopy studies revealed that imine **1h** was converted quantitatively to amine **2h** within 5 min and then protodeiodination occurred slowly over 100 min. Excellent chemoselectivity for imine reduction was observed in the presence of ketone (**2j**) and ester (**2k**) functional groups as well as nitrile group (**2f**), which typically undergo reduction when subjected to transfer hydrogenation or hydrosilylation conditions.[21] *N*-Alkylimines were also competent substrates, giving access to *N*-benzyl- or *N*-allyl-protected amines (**2l−m**) as well as saturated *N*-alkylamine products (**2n**).

Further substrate evaluation focused on differing the substitution pattern of the diaryl ketimine group (Scheme 3).

Scheme 3. Evaluation of Diarylketimine Groups[a]

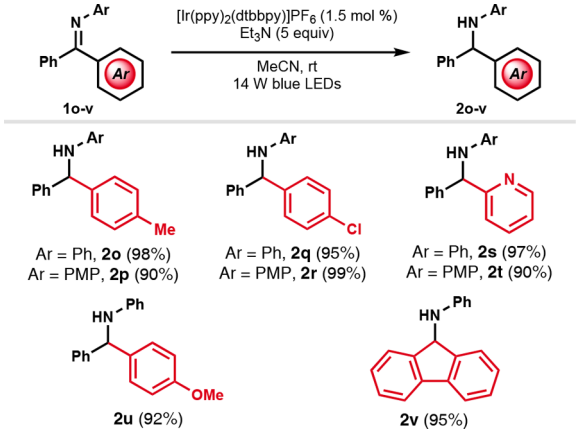

[a]Reaction conditions: imine (0.45 mmol), photocatalyst (1.5 mol %), Et_3N (5 equiv), MeCN, 3 h, rt, 14 W blue LEDs. PMP = *p*-methoxyphenyl.

The transfer hydrogenation reaction was found to be insensitive to electronic effects with both electron-rich and electron-deficient systems proceeding in high yields. Notably, pyridine-substituted ketimines (**2s,t**) were readily reduced, as were *N*-PMP-protected imines (**2p,r,t**).

We next turned to flow chemistry as a means of enabling effective scale-up and improving the efficiency of light penetration of the liquid medium.[22] The continuous flow setup consisted of a 5 mL reactor coil irradiated in a custom built 14 W blue LED photoreactor (Figure S1). A selection of diaryl ketimines were submitted to transfer hydrogenation under continuous-flow conditions (Scheme 4). The continuous-flow process afforded the corresponding amines in comparable yields to the batch methods with a significant reduction in reaction time and inherent scalability offered by flow approaches. To demonstrate the scalability of this protocol, 1 g of imine **1a** afforded 96% isolated yield of **2a** without modification of the

DOI: 10.1021/acs.orglett.7b03565
Org. Lett. 2018, 20, 905−908

Scheme 4. Continuous Flow Photoredox Transfer Hydrogenation

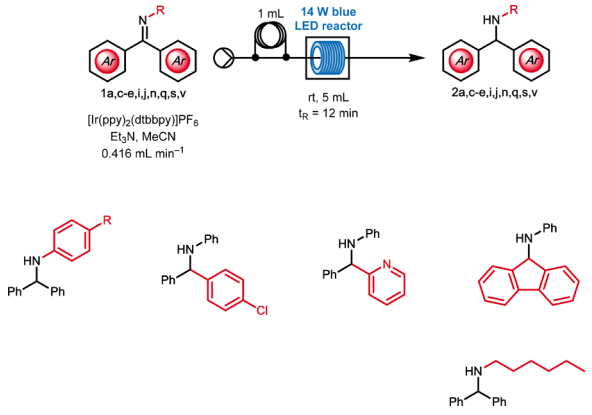

Reaction conditions: [a]imine (0.09 mmol), photocatalyst (1.5 mol %), Et_3N (5 equiv), MeCN, rt, 12 min, 14 W blue LEDs. [b]**1a** (3.89 mmol), photocatalyst (1.5 mol %), Et_3N (5 equiv), MeCN, rt, 12 min, 14 W blue LEDs.

method, highlighting the robustness and practicality of the flow process.

We performed mechanistic and control experiments to probe the reaction mechanism. Deuterium labeling studies confirmed that Et_3N was indeed functioning in the dual role of hydrogen atom source and single electron donor. When the reaction was conducted under standard conditions with Et_3N-d_{15}, 75% deuterium incorporation was observed at the amine α-position (Scheme 5). No deuterium incorporation was observed with

Scheme 5. Deuterium Incorporation Studies

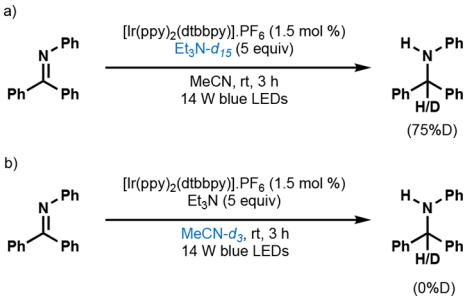

MeCN-d_3 as the reaction solvent. Radical-trapping experiments with radical scavengers (TEMPO, BHT, 1,1-diphenylethylene) did not afford the expected α-amino radical derived adducts presumably due to steric hindrance at the diphenylmethylene position.

Steady-state luminescence quenching experiments showed that phosphorescence intensity from the photocatalyst [Ir^{III}(ppy)$_2$(dtbbpy)]PF$_6$ was quenched in the presence of Et_3N. The linearity of the Stern–Volmer plot (Figure 1A) indicates the absence of static quenching, and that quenching involves only a reaction between the emitting state of the photocatalyst and Et_3N. Negligible quenching of photocatalyst phosphorescence was observed in the presence of imine **1a**. Transient absorption spectroscopy measurements were conducted to elucidate the nature of the quenching reaction. The differential absorption spectrum of [Ir^{III}(ppy)$_2$(dtbbpy)]PF$_6$ in solution displays strong transient absorption bands centered at around 380, 480, and 800 nm (Figure S6) and closely resembles

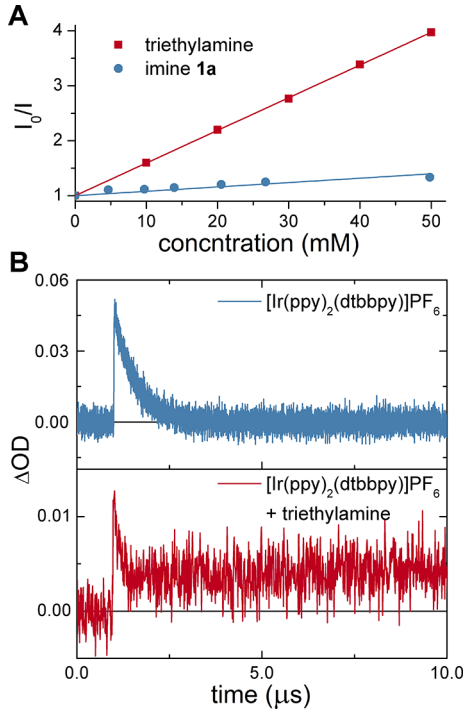

Figure 1. Mechanistic elucidation experiments. **A)** Stern–Volmer plot for quenching of [Ir(ppy)$_2$(dtbbpy)]PF$_6$ phosphorescence intensity by triethylamine (■) and imine **1a** (●). **B)** Transient absorption decay profiles (λ_{meas} = 380 nm) of [Ir(ppy)$_2$(dtbbpy)]PF$_6$ (0.1 mM, blue line) and in the presence of triethylamine (50 mM, orange line). Solutions were prepared using acetonitrile, and sparged with argon (6 min) before measurement, λ_{ex} = 355 nm (Figure S7).

the reported excited state absorption spectrum of similar heteroleptic iridium complexes.[23] Consequently, the transient absorbing species is assigned to a triplet metal-to-ligand charge-transfer (^{3}MLCT) excited state in which an electron is transferred from iridium to the dtbbpy ancillary ligand. The lifetime of this ^{3}MLCT excited state, [Ir^{IV}(ppy)$_2$(dtbbpy$^{\bullet-}$)]^{3,*} was determined to be 0.58 μs from the transient absorption decay profile at 380 nm shown in Figure 1B. The decay profile measured at 380 nm is very different when measured in the presence of Et_3N (50 mM); in this case, the decay is much shorter, consistent with the steady-state phosphorescence quenching measurements, together with an absorption signal that persists for the time scale of this measurement.

Further measurements indicate that this absorption displays no sign of decay even on a 100 μs time scale (Figure S7). This result confirms the generation of a new chemically distinct species upon excitation of the photocatalyst in the presence of Et_3N. Based on the persistence of the characteristic dtbbpy$^{\bullet-}$ absorption at 380 nm, this new species is assigned as the reduced photocatalyst [Ir^{III}(ppy)$_2$(dtbbpy$^{\bullet-}$)]^0. These results provide compelling evidence for a reductive quenching photocatalyst cycle which is consistent with the proposed electron-transfer mechanism. Further evidence for formation of the long-lived reduced photocatalyst and its properties are the subject of ongoing investigation.

In summary, a method for the facile and chemoselective photoredox transfer hydrogenation of imines in batch and flow is reported. With Et_3N in the dual role of hydrogen source and single-electron donor, high chemoselectivity for imines in the presence of other reducible functional groups was achieved. Comprehensive spectroscopic investigations into the reaction

DOI: 10.1021/acs.orglett.7b03565
Org. Lett. 2018, 20, 905–908

mechanism are currently underway and will be reported in due course.

■ ASSOCIATED CONTENT

Supporting Information

The Supporting Information is available free of charge on the ACS Publications website at DOI: 10.1021/acs.orglett.7b03565.

Experimental procedures, mechanistic studies, compound characterization data, and NMR spectra for all compounds (PDF)

■ AUTHOR INFORMATION

Corresponding Author

*E-mail: anastasios.polyzos@unimelb.edu.au.

ORCID

Anastasios Polyzos: 0000-0003-1063-4990

Notes

The authors declare no competing financial interest.

■ ACKNOWLEDGMENTS

D.J.v.A. acknowledges the University of Melbourne, Melbourne Research Scholarship (MRS). A.P. acknowledges the University of Melbourne and CSIRO for the joint Establishment Grant.

■ REFERENCES

(1) Vitaku, E.; Smith, D. T.; Njardarson, J. T. *J. Med. Chem.* **2014**, *57*, 10257−10274.

(2) Hedstrand, D. M.; Kruizinga, W. M.; Kellogg, R. M. *Tetrahedron Lett.* **1978**, *19*, 1255−1258.

(3) (a) Ischay, M. A.; Anzovino, M. E.; Du, J.; Yoon, T. P. *J. Am. Chem. Soc.* **2008**, *130*, 12886−12887. (b) Nicewicz, D. A.; MacMillan, D. W. C. *Science* **2008**, *322*, 77−80. (c) Narayanam, J. M. R.; Tucker, J. W.; Stephenson, C. R. J. *J. Am. Chem. Soc.* **2009**, *131*, 8756−8757.

(4) (a) Condie, A. G.; González-Gómez, J. C.; Stephenson, C. R. J. *J. Am. Chem. Soc.* **2010**, *132*, 1464−1465. (b) Rueping, M.; Zhu, S.; Koenigs, R. M. *Chem. Commun.* **2011**, *47*, 12709−12711. (c) DiRocco, D. A.; Rovis, T. *J. Am. Chem. Soc.* **2012**, *134*, 8094−8097.

(5) Kohls, P.; Jadhav, D.; Pandey, G.; Reiser, O. *Org. Lett.* **2012**, *14*, 672−675.

(6) Nakajima, M.; Fava, E.; Loescher, S.; Jiang, Z.; Rueping, M. *Angew. Chem., Int. Ed.* **2015**, *54*, 8828−8832.

(7) (a) Hager, M.; MacMillan, D. W. C. *J. Am. Chem. Soc.* **2014**, *136*, 16986−16989. (b) Jeffrey, J.; Petronijević, F. R.; MacMillan, D. W. C. *J. Am. Chem. Soc.* **2015**, *137*, 8404−8407. (c) Patel, N. R.; Kelly, C. B.; Siegenfeld, A. P.; Molander, G. A. *ACS Catal.* **2017**, *7*, 1766−1770.

(8) (a) Qi, L.; Chen, Y. *Angew. Chem., Int. Ed.* **2016**, *55*, 13312−13315. (b) Fuentes de Arriba, A. L.; Urbitsch, F.; Dixon, D. *Chem. Commun.* **2016**, *52*, 14434−14437.

(9) (a) Uraguchi, D.; Kinoshita, N.; Kizu, T.; Ooi, T. *J. Am. Chem. Soc.* **2015**, *137*, 13768−13771. (b) Fava, E.; Millet, A.; Nakajima, M.; Loescher, S.; Rueping, M. *Angew. Chem., Int. Ed.* **2016**, *55*, 6776−6779.

(10) Chow, Y. L.; Danen, W. C.; Nelsen, S. F.; Rosenblatt, D. H. *Chem. Rev.* **1978**, *78*, 243−274.

(11) Beatty, J. W.; Stephenson, C. R. J. *Acc. Chem. Res.* **2015**, *48*, 1474−1484.

(12) (a) Barn, D. R.; Bom, A.; Cottney, J.; Caulfield, W. L.; Morphy, J. R. *Bioorg. Med. Chem. Lett.* **1999**, *9*, 1329−1334. (b) Delorme, D.; Berthelette, C.; Lavoie, R.; Roberts, E. *Tetrahedron: Asymmetry* **1998**, *9*, 3963−3966.

(13) (a) Dutta, A. K.; Xu, C.; Reith, M. E. A. *J. Med. Chem.* **1998**, *41*, 3293−3297. (b) Zhang, Y.; Joseph, D. B.; Bowen, W. D.; Flippen-Anderson, J. L.; Dersch, C. M.; Rothman, R. B.; Jacobson, A. E.; Rice, K. C. *J. Med. Chem.* **2001**, *44*, 3937−3945.

(14) Opalka, C. J.; D'Ambra, T. E.; Faccone, J. J.; Bodson, G.; Cossement, E. *Synthesis* **1995**, *1995*, 766−768.

(15) Romero, N. A.; Nicewicz, D. A. *Chem. Rev.* **2016**, *116*, 10075−10166.

(16) Juris, A.; Balzani, V.; Belser, P.; von Zelewsky, A. *Helv. Chim. Acta* **1981**, *64*, 2175−2181.

(17) Flamigni, L.; Barbieri, A.; Sabatini, C.; Ventura, B.; Barigelletti, F. *Top. Curr. Chem.* **2007**, *281*, 143−203.

(18) Lowry, M. S.; Goldsmith, J. I.; Slinker, J. D.; Rohl, R.; Pascal, R. A.; Malliaras, G. G.; Bernhard, S. *Chem. Mater.* **2005**, *17*, 5712−5719.

(19) The reduction potentials of these tertiary amines are favourable for exergonic electron transfer to the *[Ir] species. For tributylamine, E^0 = + 0.62 V vs $AgNO_3$ in MeCN. See: ref 9. For *N*,*N*-diisopropylethylamine, E^0 = + 0.65 V vs SCE in MeCN; see: Chatterjee, T.; Iqbal, T.; You, Y.; Cho, E. J. *Acc. Chem. Res.* **2016**, *49*, 2284−2294. For triethanolamine, E^0 = + 0.52 V vs SCE in MeCN. Value vs SCE calculated from literature value reported vs normal hydrogen electrode (NHE); see: Kalyanasundaram, K.; kiwi, J.; Grätzel, M. *Helv. Chim. Acta* **1978**, *61*, 2720−2730.

(20) See the Supporting Information for further details.

(21) For reviews of transfer hydrogenation see: (a) Brieger, G.; Nestrick, T. *Chem. Rev.* **1974**, *74*, 567−580. (b) Wang, D.; Astruc, D. *Chem. Rev.* **2015**, *115*, 6621−6686 For examples of nitrile and ketone hydrosilylation, see:. (c) Gutsulyak, D. V.; Nikonov, G. I. *Angew. Chem., Int. Ed.* **2010**, *49*, 7553−7556. (d) Pérez, M.; Qu, Z.-W.; Caputo, C. B.; Podgorny, V.; Hounjet, L. J.; Hansen, A.; Dobrovetsky, R.; Grimme, S.; Stephan, D. W. *Chem. - Eur. J.* **2015**, *21*, 6491−6500.

(22) Tucker, J. W.; Zhang, Y.; Jamison, T. F.; Stephenson, C. R. J. *Angew. Chem., Int. Ed.* **2012**, *51*, 4144−4147.

(23) Ichimura, K.; Kobayashi, T.; King, K. A.; Watts, R. J. *J. Phys. Chem.* **1987**, *91*, 6104−6106.

DOI: 10.1021/acs.orglett.7b03565
Org. Lett. 2018, 20, 905−908

doi:10.2533/chimia.2019.823 Chimia 73 (2019) 823–827

A Chemoselective and Scalable Transfer Hydrogenation of Aryl Imines by Rapid Continuous Flow Photoredox Catalysis

Rowan L. Pilkington[a], Nikolai P. Rossouw[a], Dean J. van As[a], and Anastasios Polyzos*[ab]

Abstract: The chemoselective reduction of diaryl imines in the presence of competitively reducible groups is uniquely accessed through precise control of reaction and irradiation time by continuous flow visible light photoredox catalysis. The method enables the mild and efficient transfer hydrogenation of diaryl imines in the presence of sensitive functionality including halides, ester, ketone, and cyano groups. The flow protocol is efficient, rapid (>98% conversion within 9 min) and readily scaled to deliver multigram quantities of amine products in high purity.

Keywords: Flow chemistry · Imines · Photoredox · Radicals · Transfer hydrogenation

Rowan L. Pilkington was born in England before moving to Australia in later life. He studied Science (Chemistry) at the the University of Melbourne, working in his final year under the supervision of Dr. A. Polyzos on photoredox carbonylation in flow. He has completed an MSc in the same group, with research interests in the development of novel photoredox processes and their application in flow processing.

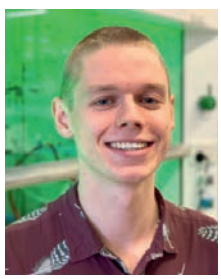

Nikolai P. Rossouw was born in Richards Bay, South Africa, before immigrating to Australia. He graduated with a BSc (Chemistry) from the University of Melbourne, working on photoredox thiolation in flow and synthesis of organic photoredox catalysts with Dr. A. Polyzos. He is continuing a MSc with the Polyzos laboratory developing natural product total synthesis in flow.

Dean J. van As grew up in Melbourne, Australia. He obtained an MSc from the chemistry department at the University of Melbourne in 2015 under the supervision of Dr. W. Wong. He is currently completing his PhD studies at the University of Melbourne under the supervision of Dr. A. Polyzos in photoredox catalysis. His areas of interest involve the development of new visible light photocatalytic methods for the synthesis and functionalization of amines in batch and flow.

Anastasios Polyzos was awarded his PhD in 2005 from La Trobe University and appointed to Research Fellow at the Australian national science agency, CSIRO in the same year. In 2008 he pursued post-doctoral research at University of Cambridge under guidance of Professor Steven V. Ley FRS. In 2011 he returned to Australia to lead the flow chemistry and catalysis group at CSIRO in Australia. He established an independent research career with appointment to Senior Lecturer within the School of Chemistry, University of Melbourne in 2015. His research interests include the development of new methods and enabling technologies for organic synthesis, photocatalysis, C–H reaction discovery, and the development of sustainable industrial process chemistry. Anastasios currently serves as Director of the Australian Research Council Industrial Transformation Training Centre for Chemical Industries.

The ubiquity of aryl amines in pharmaceutical, agrochemical and industrial products has fostered the development of methods enabling their straightforward and scalable production.[1] Innumerous protocols for the synthesis of aryl amines exist, encompassing S_NAr of aryl fluorides,[2] Ulmann, Buchwald-Hartwig and Chan-Evans-Lam coupling,[3] and hydrogen borrowing.[4] One of the most robust and well-established methods is reductive amination by heterogeneous catalytic hydrogenation of imines on platinum and palladium metal. Whilst catalytic hydrogenation is scalable and generally economically viable, chemoselectivity is challenged by the presence of multiple unsaturated bonds or other reducible groups on the intermediates and products.[5] The development of methods for reductive amination under mild conditions with requisite chemoselectivity and functional group tolerance remains a focus in industrial, and academic laboratories.[6] These requirements become progressively important when reductive amination is required in the late-stage functionalisation of targets with increasing complexity, including bioactive lead molecules and natural products. Mild hydride transfer agents

*Correspondence: Dr. A. Polyzos[ab], E-mail: anastasios.polyzos@unimelb.edu.au
[a]School of Chemistry, The University of Melbourne, Parkville, VIC 3010, Australia; [b]CSIRO Manufacturing, Clayton, VIC 3068, Australia

Scheme 1. Continuous flow processing enabling the scalable, chemoselective photoredox transfer hydrogenation of imines. FG = functional group.

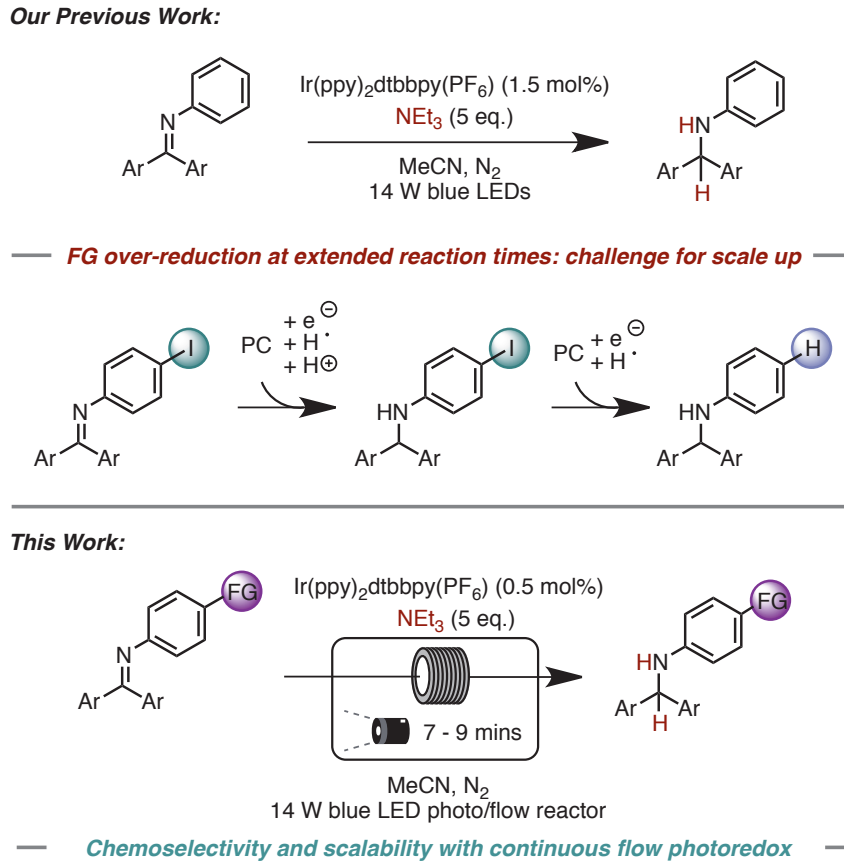

including $NaCNBH_4$ and $NaBH(OAc)_3$ offer opportunities for chemoselective reduction of imines, however a dependence on acidic conditions, solvent polarity and imine electrophilicity impedes application to a broader selection of substrates.[7] Furthermore, the requirement for stoichiometric hydride transfer reagent and the formation of cyanide by-products (in the case of $NaCNBH_4$) may limit the translation of these methods beyond laboratory preparation.[6]

We recently disclosed a visible light photoredox method for the catalytic transfer hydrogenation of diaryl-ketimines (Scheme 1).[8] The process utilises triethylamine as a highly economical single source of electron, proton and hydrogen atom. The reaction was characterised by high product yields, fast reaction times and visible light as the solitary energy source. Based on literature reports,[9] our mechanistic hypothesis (Scheme 2) was centralised on the direct single electron reduction of the diaryl-ketimine moiety (**I**) to the corresponding α-aminyl radical anion species (**II**) by the photoredox catalyst, followed by subsequent protonation and hydrogen atom transfer (HAT) from triethylamine radical cation (**IV**) and triethylamine (**III**) respectively to afford the hydrogenated diaryl amine (**VI**).

Through the course of these investigations, we observed that imines bearing an aryl-iodo substituent underwent competitive protodehalogenation with extended reaction times. To address this limitation, we reasoned that the different rates of single electron transfer (SET) to the imine moiety relative to the aryl halide, could be exploited to furnish chemoselectivity that was dependent on reaction time. Continuous flow photochemistry methods[10] offer the temporal and spacial resolution necessary to enable the kinetically favoured reduction of the imine whilst minimising unwanted protodehalogenation. This selectivity mode can be readily achieved by establishing a finely-tuned set of reaction conditions that impede the time-dependent over-reduction of the aryl halide and can be extended to other reducible substituents. Furthermore, improved photocatalytic activity can be expected since greater light permittivity is effected over the smaller pathlength in tubular

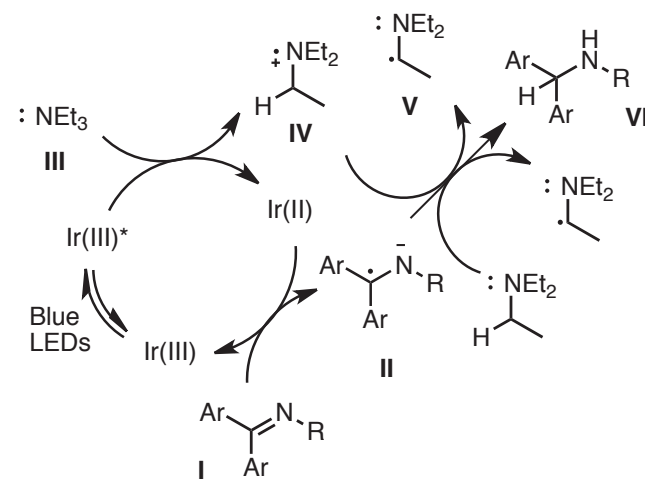

Scheme 2. Proposed mechanism of photoredox-catalysed transfer hydrogenation.

flow reactors compared to standard reaction glassware,[11] and the continuous nature of flow chemistry could be leveraged to efficiently scale the photocatalytic chemoselective reduction.[12]

We initiated the study by assembling a flow platform consisting of a commercially available syringe pumping system (Syrris Asia) fitted with an injection port and sample loop (any commercially available system is suitable for this application). A bespoke tubular photoreactor was fitted, consisting of two 7 W 447 nm LED arrays and a coiled perfluoralkoxy alkane (PFA) tube (3 mL, 0.75 mm i.d.). The system was pressurised by a back pressure regulator, rated to 40 PSI (Fig.1) and the solvent reservoir was continually sparged with nitrogen.

The photoredox transfer hydrogenation of the aryl iodide bearing imine **1a** was investigated and studies to establish conditions for the quantitative production of iodoamine **1b** over the protodehalogenated product **1c** were undertaken. Following

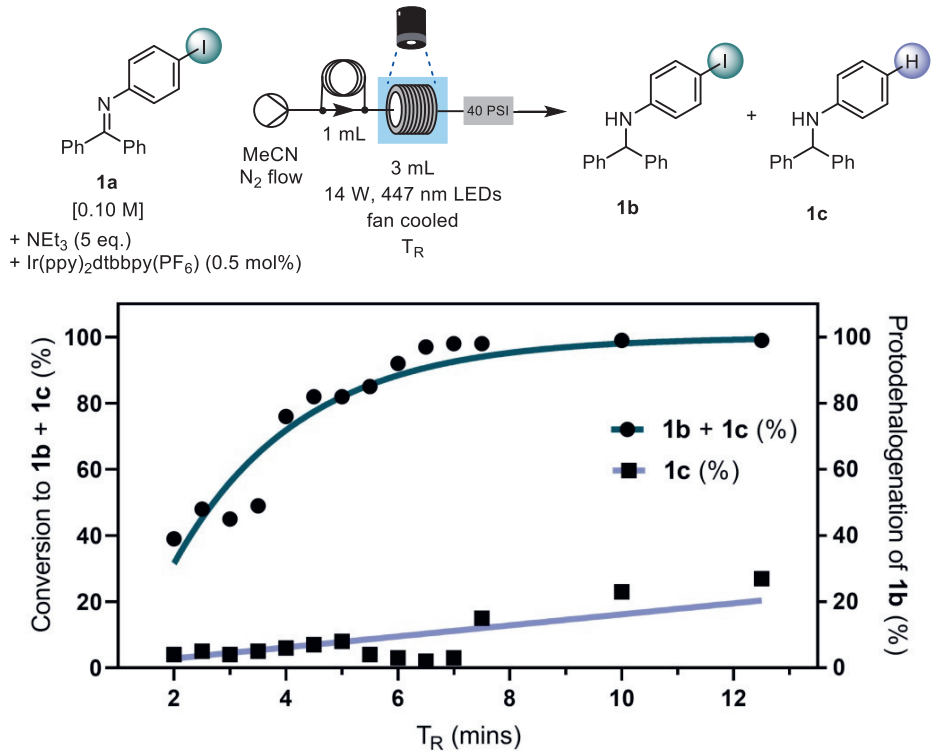

Fig. 1. Reaction time screening for substrate **1a**. Conversions determined by ^{1}H NMR analysis of the crude reaction mixture. Performed on a 0.10 mmol scale.

optimisation of residence time (Fig. 1) excellent conversions (>97%) of the substituted imine **1a** were achieved with rapid T_R as low as 7 min. Incomplete conversion of **1a** was observed at T_R below 6.5 min, indicating that the transfer hydrogenation was incomplete at faster flow rates. Slower flow rates resulting in T_R more than 7 min increased protodeiodination of **1b** to **1c**. Background dehalogenation by photodissociation under blue light irradiation was not detected when the photocatalyst was omitted from the reaction. With the optimised reaction time (T_R = 7 min) in hand, the preparation of iodoamine **1c** was successfully scaled to 0.4 mmol and isolated in 87% yield.

To demonstrate practicality and scalability of the method, we embarked on a multi-gram preparation of **1b** (Fig. 2). The flow reactor configuration was modified to accommodate the processing of larger volumes of reagent and solvent . The sample loops were removed and the reagents were delivered from a single flask under an N_2 atmosphere. FlowIR™ infra-red (FTIR) spectroscopic monitoring was utilised to monitor the reaction mixture in-line to provide real-time information on the progress of the continuous run (9 h).[13] The establishment of steady-state conditions was readily identified by in-line FTIR and the reaction product stream was collected when a steady-state was observed. The reaction front and tail (non-steady-state reaction plug) was diverted away from the collection flask to ensure unreacted material and by-products generated by dispersion effects were not collected. The desired amine **1b** was isolated in 77% (7.68

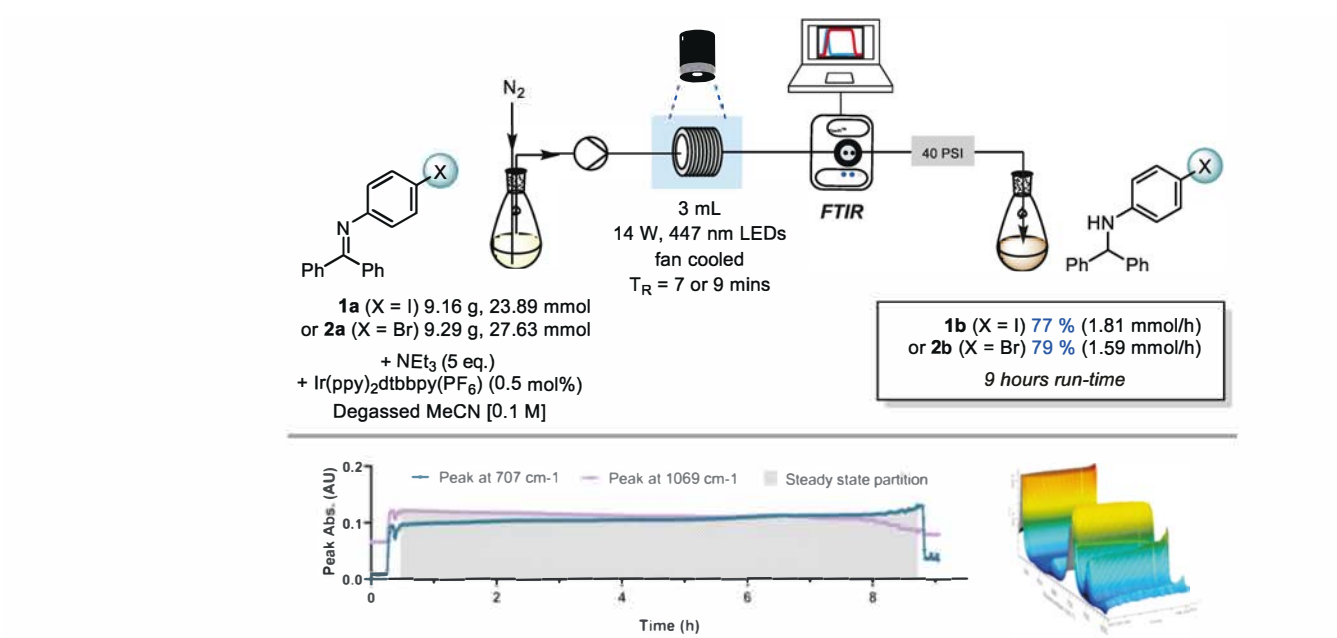

Fig. 2. Large-scale continuous flow photoredox transfer hydrogenation of iodo- and bromo- substituted aryl imines. In-line FTIR trace and peak absorption of diagnostic IR bands used to partition the reaction mixture at steady state (for **1b**).

g) with a space-time yield (STY) of 1.81 mmol/h. Parasitic protodehalogenation of **1b** was minimised comparably to the smaller scale reaction, with < 4% conversion to **1c** detected in the crude residue by ^{1}H-NMR.

We next addressed the 4-bromo substituted diphenyl aryl imine **2a** which, according to cyclic voltammetry and unpublished experimental data, is also reducible under our photoredox system.[14] The T_R was extended to 9 min to effect complete transfer hydrogenation, affording **2b** in 84% isolated yield at 0.40 mmol scale. The bromo-substituted imine **2a** was submitted to the scaled procedure with in-line FTIR monitoring, providing 6.44 g of the corresponding amine in 79% yield, with a space-time yield of 1.59 mmol/h. Notably, the scaled reaction products could be isolated in high purity by simple filtration through silica and trituration with hexanes from the crude reaction mixture.

Substrates with cyano, aryl ketone and ester substituents on the diphenylimine scaffold were investigated as other potentially reducible groups under the reaction conditions (Scheme 3).[14] The functional groups were well tolerated with preferential reduction of the imine and with complete conversions to the corresponding amine at 0.4 mmol scale. A nitro-substituted imine did not afford the product **2f** under the optimised reaction conditions, most likely due to preferential electron transfer to the electron deficient aryl ring.

To validate the effectiveness of the flow procedure, the rate of conversion and protodehalogenation of **1a** was examined under batch photoredox conditions (Scheme 4A). The reduction of **1a** on 1 mmol scale proceeded as expected with 99% conversion of the starting imine effected after 3 h of irradiation with TLC monitoring, however 64% protodehalogenation was observed by ^{1}H NMR analysis. A traditional reduction with $NaBH_4$ (Scheme 4B) did not effect complete conversion to **1b** even after 24 h. Finally, the halogenated product **1b** prepared *via* the chemoselective photocatalytic reduction protocol was submitted to a representative Sonogashira coupling reaction[15] with phenylacetylene to afford a further functionalised alkynyl product in 82% yield (Scheme 4C).

In summary, a versatile flow system for the photoredox transfer hydrogenation of sensitive imines was developed, uniquely facilitating the scalable synthesis of substituted diaryl amines with time-dependent retention of functionality. Further studies are underway to implement and scale this photoredox transfer hydrogenation protocol in new multistage flow systems.

Supplementary Information

Supplementary information is available on *https://www.ingentaconnect.com/content/scs/chimia*

Scheme 3. Selected scope of imines with sensitive functional groups. Isolated yields are shown and reactions were performed on 0.40 mmol scale. FG = functional group.

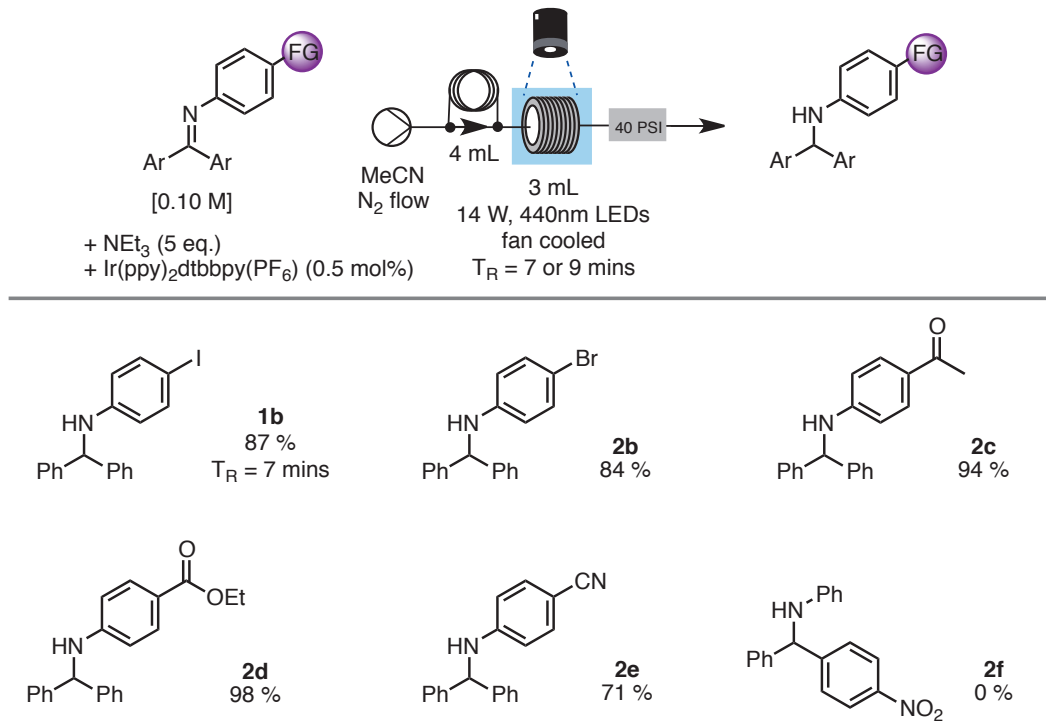

Scheme 4. A) Protodehalogenation behaviour under standardised batch photoredox conditions. Progress was monitored by TLC. B) Transfer hydrogenation of diaryl ketimine with $NaBH_4$. C) Further transformation of the chemoselectively reduced iodo-amine.[16] # = Determined by ^{1}H NMR analysis of the crude reaction mixture.

Acknowledgements

The authors acknowledge Mr Vir H. Ghandi who assisted RLP with the experimental procedures and Professor Paul Francis (Deakin University) for the kind loan of the Syrris Asia syringe pump system. DvA acknowledges the University of Melbourne, Melbourne Research Scholarship (MRS). AP acknowledges the University of Melbourne and CSIRO for the joint Establishment Grant.

Received: May 8, 2019

[1] a) E. Vitaku, D. T. Smith, J. T. Njardarson, *J. Med. Chem.* **2014**, *57*, 10257, doi: 10.1021/jm501100b; b) M. Baumann, I. R., Baxendale, *Beilstein J. Org. Chem.* **2013**, *9*, 2265, doi:10.3762/bjoc.9.265; c) S. D., Roughley, A. M. Jordan, J. Med. Chem. 2011, 54, 3451, doi: 10.1021/jm200187y.

[2] J. March, 'Advanced Organic Chemistry: Reactions, Mechanisms, and Structure', Wiley, New York, **1992**, 641.

[3] a) C. Sambiago, S. P. Marsden, A. J. Blacker, P. C. McGowan, *Chem. Soc. Rev.* **2014**, *43*, 3525, doi: 10.1039/C3CS60289C; b) K. Okano, H. Tokuyama, T. Fukuyama, *Chem. Commun.* **2015**, *50*, 13650, doi: 10.1039/C4CC03895A; c) M. Carril, R. SanMartin, E. Dominguez, *Chem. Soc. Rev.* **2008**, *37*, 639, doi: 10.1039/B709565C; d) J. F. Hartwig, *Nature* **2008**, *455*, 314, doi: 10.1038/nature07369.

[4] a) B. G. Reed-Berendt, K. Polidano, L. C. Morril, *Org. Biomol. Chem.* **2019**, *17*, 1595, doi: 10.1039/C8OB01895B; b) A. Corma, J. Navas, M. J. Sabater, *Chem. Rev.* **2018**, *118*, 1410, doi: 10.1021/acs.chemrev.7b00340; c) K. O. Marichev, J. M. Takacs, *ACS Catal.* **2016**, *6*, 2205, doi: 10.1021/acscatal.6b00175.

[5] A. F. Abdel-Magid, K. G. Carson, B. D. Harris, C. A. Maryanoff, R. D. Shah, *J. Org. Chem.* **1996**, *61*, 3849, doi: 10.1021/jo960057x.

[6] a) D. C. Blakemore, L. Castro, I. Churcher, D. C. Rees, A. W. Thomas, D. M. Wilson, A. Wood, *Nature Chem*. **2018**, *10*, 383, doi: 10.1038/s41557-018-0021-z; b) T. Cernak, K. D. Dykstra, S. Tyagarajan, P. Vachal, S. W. Krska, *Chem. Soc. Rev*. **2016**, *45*, 546, doi: 10.1039/c5cs00628g.

[7] R. F. Borch, M. D. Bernstein, H. D. Durst, *J. Am. Chem. Soc*. **1971**, *93*, 2897, doi: 10.1021/ja00741a013.

[8] D. J. van As, T. U. Connell, M. Brzozowski, A. D. Scully, A. Polyzos, *Org. Lett.* **2018**, *20*, 905, doi: 10.1021/acs.orglett.7b03565.

[9] a) L. R. E. Pantaine, J. A. Milligan, J. K. Matsui, C. B. Kelly, G. A. Molander, *Org. Lett*. **2019**, *21*, 2317, doi: 10.1021/acs.orglett.9b00602; b) R. Wang, M. Ma, X. Gong, G. B. Panetti, X. Fan, P. J. Walsh, *Org. Lett.* **2018**, *20*, 2433, doi: 10.1021/acs.orglett.8b00778; c) R. Wang., M. Ma, X. Gong, X. Fan, P. J. Walsh, *Org. Lett.* **2019**, *21*, 27, doi: 10.1021/acs.orglett.8b03394; d) X. Fan, X. Gong, M. Ma, R. Wang, P. J. Walsh, *Nature Commun.* **2018**, 9; e) Z. W. Xi, L. Yang, D. Y. Wang, C. D. Pu, Y. M. Shen, C. D. Wu, X. G. Peng, *J. Org. Chem.* **2018**, *83*, 11886, doi: 10.1021/acs.joc.8b01651; f) M. Nakajima, E. Fava, S. Loescher, Z. Jiang, M. Rueping, *Angew. Chem., Int. Ed.* **2015**, *54*, 8828, doi: 10.1002/anie.201501556. g) A. L. Fuentes de Arriba, F. Urbitsch, D. J. Dixon, *Chem. Commun.* **2016**, *52*, 14434, doi: 10.1039/c6cc09172e; h) T. Rossolini, J. A. Leitch, R. Grainger, D. J. Dixon, *Org. Lett.* **2018**, *20*, 6794, doi: 10.1021/acs.orglett.8b02923; i) J. Rong, P. H. Seeberger, K. Gilmore, *Org. Lett.* **2018**, *20*, 4081, doi: 10.1021/acs.orglett.8b01637; j) M. Hager, D. W. C. MacMillan, *J. Am. Chem. Soc.* **2014**, *136*, 16986, doi: 10.1021/ja5102695; k) L. Qi, Y. Chen, *Angew. Chem., Int. Ed.* **2016**, *55*, 13312, doi: 10.1002/anie.201607813.

[10] a) Y. Su, N. J. W. Straathof, V. Hessel, T. Noel, *Chem. Eur. J.* **2014**, *20*, 10562, doi: 10.1002/chem.201400283; b) Z. J. Garlets, J. D. Nguyen, C. R. J. Stephenson, *Isr. J. Chem.* **2014**, *54*, 351, doi: 10.1002/ijch.201300136.

[11] a) F. Lima, M. A. Kabeshov, D. N. Tran, C. Battilocchio, J. Sedelmeier, G. Sedelmeier, B. Schenkel, S. V. Ley, *Angew. Chem. Int. Ed.* **2016**, *55*, 14085, doi: 10.1002/anie.201605548; b) F. Lima, L. Grunenberg, H. B. A. Rahman, R. Labes, J. Sedelmeier, S. V. Ley, *Chem. Commun.* **2018**, *54*, 5606, doi: 10.1039/c8cc02169d; c) L. D. Elliot, J. P. Knowles, P. J. Koovits, K. G. Maskill, M. J. Ralph, G. Lejeune, L. J. Edwards, R. I. Robinson, I. R. Clemens, B. Cox, D. D. Pascoe, G. Koch, M. Eberle, M. B. Berry, K. I. Booker-Milburn, *Chem. Eur. J.* **2014**, *20*, 15226, doi: 10.1002/chem.201404347; d) J. W. Tucker, Y. Zhang, T. F. Jamison, C. R. J. Stephenson, *Angew. Chem., Int. Ed*. **2012**, *51*, 4144, doi: 10.1002/anie.201200961; e) K. C. Harper, E. G. Moschetta, S. V. Bordawekar, S. J. Wittenberger, *ACS Cent. Sci.* **2019**, *5*, 109, doi: 10.1021/acscentsci.8b00728.

[12] a) J. W. Beatty, J. J. Douglas, R. Miller, R. C. McAtee, K. P. Cole, C. R. J. Stephenson, *Chem*. **2016**, *1*, 456, doi 10.1016/j.chempr.2016.08.002; b) D. Cambie, C. Bottecchia, N. J. W. Straathof, V. Hessel, T. Noël, *Chem. Rev.* **2016**, *116*, 10276, doi: 10.1021/acs.chemrev.5b00707.

[13] a) D. Musio, E. Gala, S. V. Ley, *ACS Sustainable Chem. Eng.* **2018**, *6*, 1489, doi: 10.1021/acssuschemeng.7b04012 b) D. E. Fitzpatrick S.V. Ley, *Tetrahedron* **2018**, *74*, 3087, doi: 10.1016/j.tet.2017.08.050

[14] See supplementary information for cyclic voltammetry data of all imine substrates.

[15] D. Q. Wu, Z. Y. Guan, Y. Peng, J. Sun, C. Zhong, Q. H. Deng, *Adv. Synth. Catal.* **2018**, *360*, 4720, doi: 10.1002/adsc.201800810.